TECHNISCHE UNIVERSITÄT MÜNCHEN

Institut für Maschinen- und Fahrzeugtechnik – Lehrstuhl für Maschinenelemente

Efficiency Determination and Synthesis of Complex-Compound Planetary Gear Transmissions

Franz Kurth

Vollständiger Abdruck der von der Fakultät für Maschinenwesen der Technischen Universität München zur Erlangung des akademischen Grades eines

Doktor-Ingenieurs

genehmigten Dissertation.

Vorsitzender:		Univ.-Prof. Dr.-Ing. U. Lindemann
Prüfer der Dissertation:	1.	Univ.-Prof. Dr.-Ing. B.-R. Höhn, i.R.
	2.	Prof. A. Kahraman, Ph.D., Ohio State University, USA
	3.	Univ.-Prof. Dr.-Ing. K. Stahl

Die Dissertation wurde am 23.05.2012 bei der Technischen Universität München eingereicht und durch die Fakultät für Maschinenwesen am 19.07.2012 angenommen.

Vorwort / Preface

Die vorliegende Arbeit entstand während meiner Tätigkeit als wissenschaftlicher Mitarbeiter am Lehrstuhl für Maschinenelemente und Forschungsstelle für Zahnräder und Getriebebau (FZG) der Technischen Universität München. Grundlage dieser Arbeit bildete das von der Deutschen Forschungsgemeinschaft (DFG) geförderte Vorhaben „Entwicklung eines Auslegungs- und Berechnungsverfahrens für reduzierte Planetenkoppelgetriebe mit beliebiger Leistungsführung“.

Ich danke allen, die zum Gelingen meiner Dissertation beigetragen haben, insbesondere

meinem Doktorvater, Herrn Prof. Dr.-Ing. Bernd-Robert Höhn, für die fachliche Begleitung meiner Arbeit, die vielen Inspirationen, die konstruktiven und ideenreichen Diskussionen, die Möglichkeit zur Promotion an der FZG und zur Mitwirkung an zahlreichen Projekten sowie die damit verbundene Vorbereitung auf mein weiteres Berufsleben. Er wird mir immer ein großes Vorbild im beruflichen und privaten Sinne sein.

Herrn Prof. Ahmet Kahraman für die bereitwillige Übernahme des Co-Referats, für die wichtigen Gespräche und Anregungen zum Inhalt meiner Arbeit, im Speziellen für die Anstrengungen in Zusammenhang mit meiner Promotionsprüfung sowie im Allgemeinen für die wohlwollende Unterstützung und das freundschaftliche Verhältnis. Auch er wird mir immer ein Vorbild in beruflicher und menschlicher Hinsicht sein.

Herrn Prof. Dr.-Ing. Karsten Stahl für die bereitwillige Übernahme des Co-Referats und die wohlgesonnene Unterstützung in der Endphase meiner Arbeit.

Herrn Prof. Dr.-Ing. Udo Lindemann für die Übernahme des Prüfungsvorsitzes.

meinem Forschungsgruppenleiter, Herrn Dr.-Ing. Klaus Michaelis, für die Betreuung und Führung in der Anfangsphase meiner Tätigkeit an der FZG sowie speziell für die motivierenden Diskussionen und die beispielhafte Arbeitsatmosphäre.

meinem Forschungsgruppenleiter und Freund, Herrn Dr.-Ing. Christian Wirth, der mir den Weg zur FZG bereitet hat, mich über die Jahre hinweg begleitet und gefördert hat und mir aufgezeigt hat, wie eine erfolgreiche Promotion verlaufen kann. Für sein Entgegenkommen und seine Freundschaft werde ich ihm stets zutiefst verbunden sein.

meinem Bürokollegen und Freund, Herrn Michael Hombauer, für den glücklichen Umstand, miteinander arbeiten zu dürfen, für die unzähligen Fachdiskussionen und die gemeinsamen, unvergesslichen Erlebnisse. Die hierbei entstandene Freundschaft und der mir von ihm entgegengebrachte Rückhalt haben wesentlich zum Erfolg meiner Promotion beigetragen.

meinem ehemaligen Kollegen und Freund, Herrn Dr.-Ing. Nick Bretl, für die hilfreichen Gespräche, die gemeinsamen Aktivitäten, die Kameradschaft, seinen Beitrag zum einem besonderen Arbeitsklima und die oftmals nötige Ablenkung.

meinem Nachfolger und Freund, Herrn Johannes Geiger, für die Unterstützung vor allem in der Anfangshase meiner Tätigkeit an der FZG und die wertvollen beruflichen und privaten Unterhaltungen und Unternehmungen.

meinem Nachfolger, Herrn Philipp Gwinner, für die wichtige Mitwirkung an den durchgeführten Forschungsvorhaben, welche für das Gelingen der Arbeit von unschätzbarem Wert war.

allen Kolleginnen und Kollegen, im Besonderen Herrn Dr.-Ing. Michael Wirth, Herrn Dr.-Ing. Andreas Ziegler, Herrn Johann-Paul Stemplinger, Herrn Gero Bansemir, Herrn Stefan Schurer, Herrn Ivan Boiadjiev sowie Herrn Michael Ernstorfer für die vielen beruflichen und privaten Gespräche und die gewachsene Freundschaft.

allen Studentinnen und Studenten, die im Rahmen von Diplom- und Semesterarbeiten sowie als wissenschaftliche Hilfskräfte zur erfolgreichen Durchführung der Vorhaben beigetragen haben. Besonderer Dank gilt hierbei Herrn Andreas Sing.

den Mitarbeiterinnen und Mitarbeitern aus den Bereichen Sekretariat, Werkstatt, Prüffeld, Labor und E-Labor für die Unterstützung im beruflichen und privaten Umfeld.

meiner Familie, meinen Geschwistern Robert und Britta sowie meinen Freunden aus der Heimat für den Zusammenhalt und den Ausgleich im privaten Umfeld, was für die Anfertigung dieser Arbeit von entscheidender Bedeutung war.

meinen Eltern Walter und Hortense für die liebevolle Erziehung, die prägenden und wichtigen Ratschläge, die stete Zuwendung, die nötige Strenge und die Freiheiten, welche ich genießen durfte und letztlich für den Weg, den ich eingeschlagen habe. Mein Vater wird mir immer das größte Vorbild sein.

Nürnberg, im November 2012

Contents

Abbreviations

CCPGT	Complex-compound planetary gear transmission
DFG	Deutsche Forschungsgemeinschaft
DOF	Degree of freedom
FZG	Forschungsstelle für Zahnräder und Getriebebau / Gear Research Centre
ICE	Internal combustion engine
PGT	Planetary gear transmission

1 Introduction

1.1 Objective of the study

Amongst others, planetary gear transmissions offer more options for generating transmissions ratios, more compact, space and weight saving design, noise reduction, higher efficiency, more favorable load distribution and higher load carrying capacity in comparison to conventional transmissions. Complex-compound planetary gear transmissions are classified as special types among the general group of planetary gear transmissions. They feature more than three shafts, which can be connected to the periphery, and a single planet carrier. Complex-compound planetary gear transmissions are frequently used as simple speed reduction gears or within multi-speed transmissions. A typical representative is shown in **Figure 1-1** which occurs both in dated and modern automated transmission concepts. Complex-compound planetary gear transmissions feature particular characteristics and advantages in addition to the general ones:

- High number of available transmission ratios
- Use of multiple inputs and outputs
- Expanded operating range in terms of power summation and power partition
- High efficiency in combination with high transmission ratios
- Low number of parts and low number of special parts (planet carrier)
- Low material inventory and low designed space
- High power density, low weight and costs

The kinematics and statics as well as the operating behavior of complex-compound planetary gear transmissions are rather complex. Most of the existing analysis methods are non-transparent, often subject to mistakes or computationally demanding. In many cases, a limitation on few selected designs and operating conditions is needed in order to handle the diversity. The objective of the present study is to develop easy, plausible and computationally manageable analysis and synthesis methods that are suitable for the use of designers in early conceptual design phases. These methods are envisioned to be general such that they can handle any arbitrary design and operating conditions.

Figure 1-1: Complex-compound planetary gear transmission of the Ravigneaux type [6_RAV38]

1.2 Method of solution

The first part of the study focuses on the analysis and efficiency calculation of complex-compound planetary gear transmissions. For this purpose, the external and internal power flow behaviors are examined in detail. By means of graph theory, the decisive parts and physical interrelationships within the complex-compound planetary gear transmission are identified. Existing and effective mathematical algorithms are adapted. Furthermore, a well-established method using Wolf symbols is augmented for being capable to analyze any kind of planetary gear transmission. Special cases and operating conditions such as self-locking are treated. Moreover, an efficiency approximation method is proposed to analyze transmission concepts without knowing their complete design details.

The second part of the study is dedicated to the synthesis of complex-compound planetary gear structures. A dual approach is presented. On the one hand, an abstract lever analogy being detached from design aspects is utilized to define desired operating conditions. On the other hand, a reference transmission representative of the most complicated structure allowed is specified. By means of the efficiency approximation method mentioned above, the lever model is detailed. A systematic matching process combining the lever model and the reference transmission generates definite transmission structures. The proposed synthesis method avoids creating all possible combinations of solutions but generates only those solutions satisfying the desired operating conditions. Finally, a limited, manageable amount of feasible and practicable structure variants is disclosed.

2 Basics and terminology

Various terms have evolved over time to describe parts, designs, operating conditions and physical interrelationships of or within planetary gear transmissions. For a clear terminology a short overview of commonly used planetary gear transmission designs with frequently used terms and abbreviations is given. Further, basic formulas, physical values, sign conventions, matrix notations and degrees of freedom are discussed.

2.1 Single planetary gear transmissions

The most important component inside a single planetary gear transmission (single PGT) is a mechanism providing a transmission ratio between two rotating shafts with a housing assumed as being fixed, a so-called *basic train*. The transmission ratio of this basic train is most often generated using spur or helical gears which will be focused in this work. It can alternatively be provided using bevel gears, chain or belt drives, hydrostatic transmissions, friction wheels, etc.. An example conventional, geared transmission is shown in **Figure 2-1** as schematic representation. It is also known as planetary gear in star arrangement.

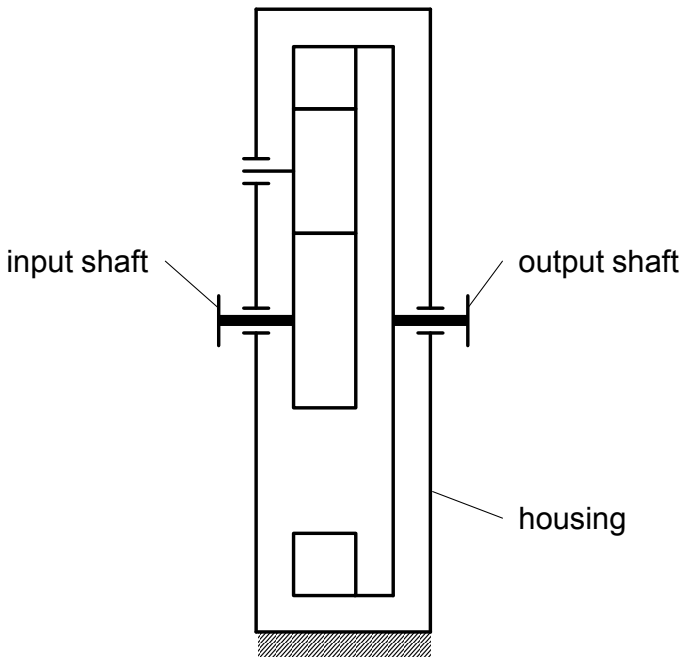

Figure 2-1: Example conventional transmission

The single PGT is developed from an arbitrary conventional transmission by pivoting the housing around a common central axis of rotation as additional shaft. Thus, the single PGT features exactly three shafts connected to the periphery (**Figure 2-2**).

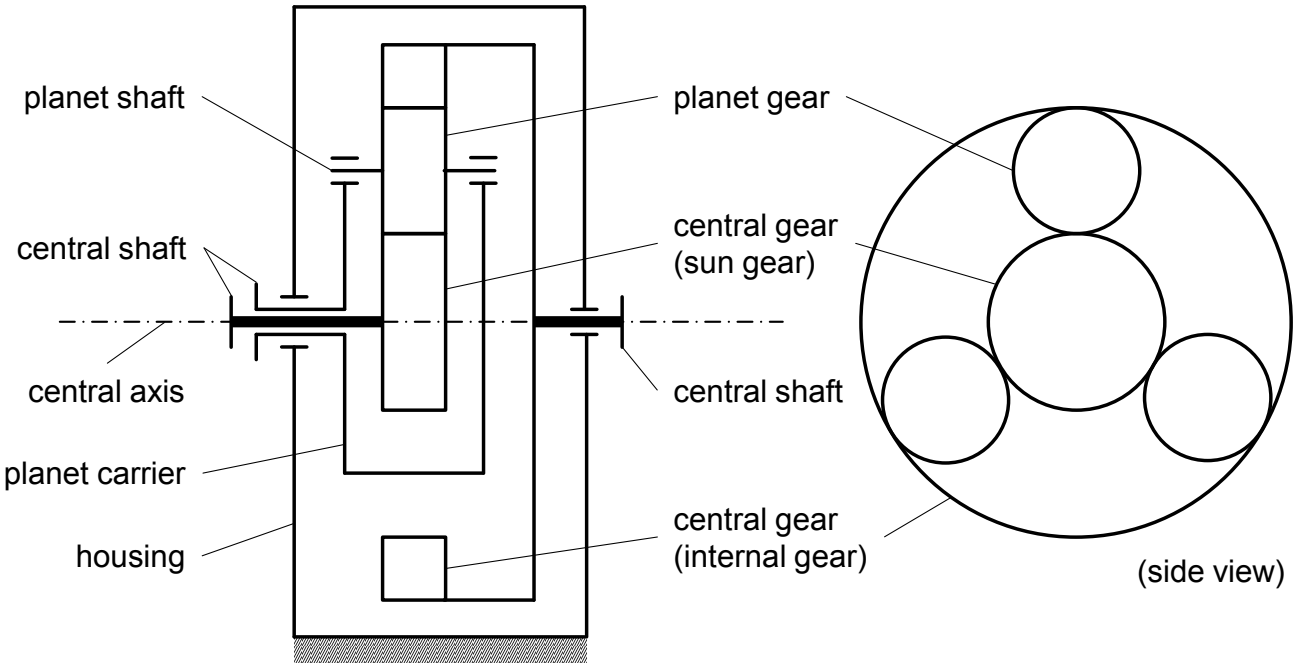

Figure 2-2: Example simple PGT

If the axis of rotation of a gear is the *central axis*, the gear is referred to as *central gear*. Other gears feature a center distance to the central axis and are called *planet gears* or *planets*. The planets are mounted on *planet shafts* which are supported by the *planet carrier*. Alternatively, the planets can be directly supported on a *planet pin*, which is fixed to the carrier. The shafts connected to the central gears and the carrier are called *central shafts*. Mostly, several identical planets are equally spaced around the sun gear in order to achieve a favorable load sharing amongst the planets. Schematic representations show only one of the planets. A single PGT is termed *simple* PGT if its planets are single, intermediate gearwheels directly connected to the central gears.

A planet of a PGT does not have to be performed by only one gearwheel. PGTs can also contain *stepped planets* or multiple *meshing planets* or rather *planet pairs* (**Figure 2-3**). These PGTs are named *compound* PGTs, since their planets are compound of multiple gearwheels. In respect of meshing planet pairs, each planet can also be of the stepped type, but usually not more than two planets are arranged within a PGT due to lack of space for the planets themselves and for the carrier.

If a PGT features two central gears, the PGT is referred to as *reverted* PGT, since the gear chain of the basic train from one central gear to the other leads back to the same axis of rotation, the central axis. The planets do not have a direct link to the periphery. Otherwise, if the input and output of the basic train do not share a common axis of rotation, the PGT is referred to as *open* PGT. This type of PGT is seldom used for special applications due to the eccentric movement of at least one shaft. An open PGT can also be converted into a

reverted PGT by inserting a universal joint or mechanical feedback (**Figure 2-4**). By reason of the increased construction effort and torque fluctuations created by the universal joint, this type of PGT is not taken into consideration within the course of this work.

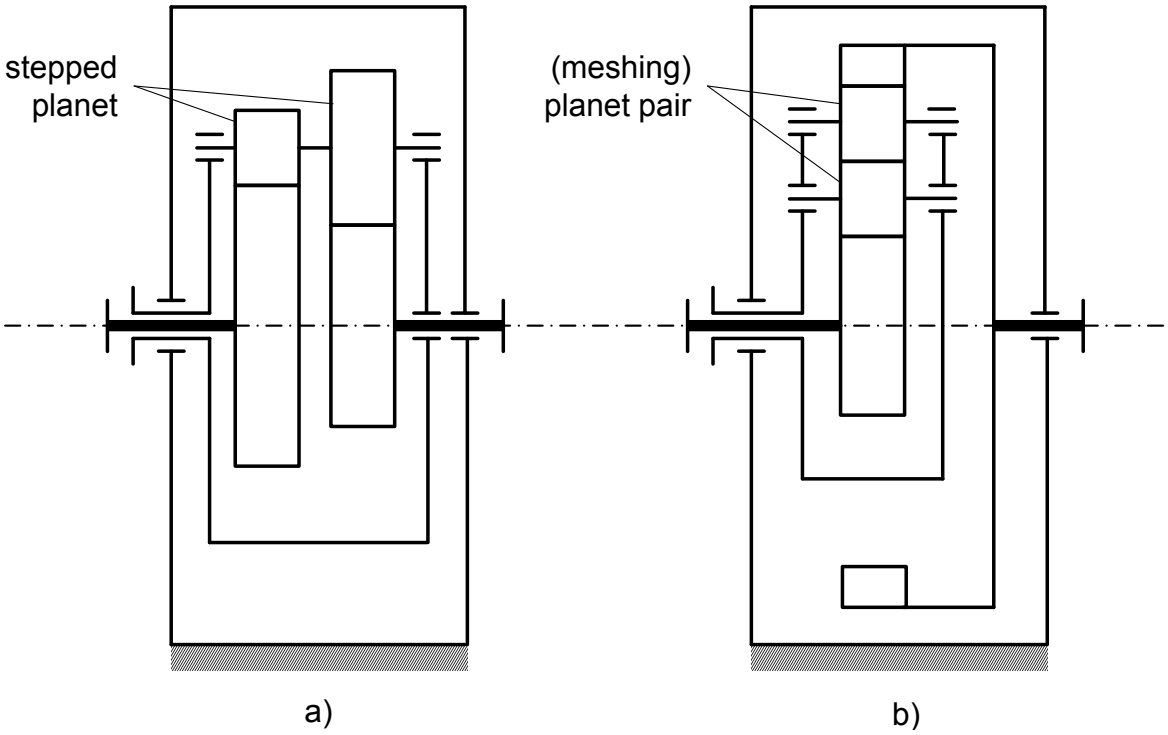

Figure 2-3: Example compound PGT with a) stepped planet, b) meshing planet pair

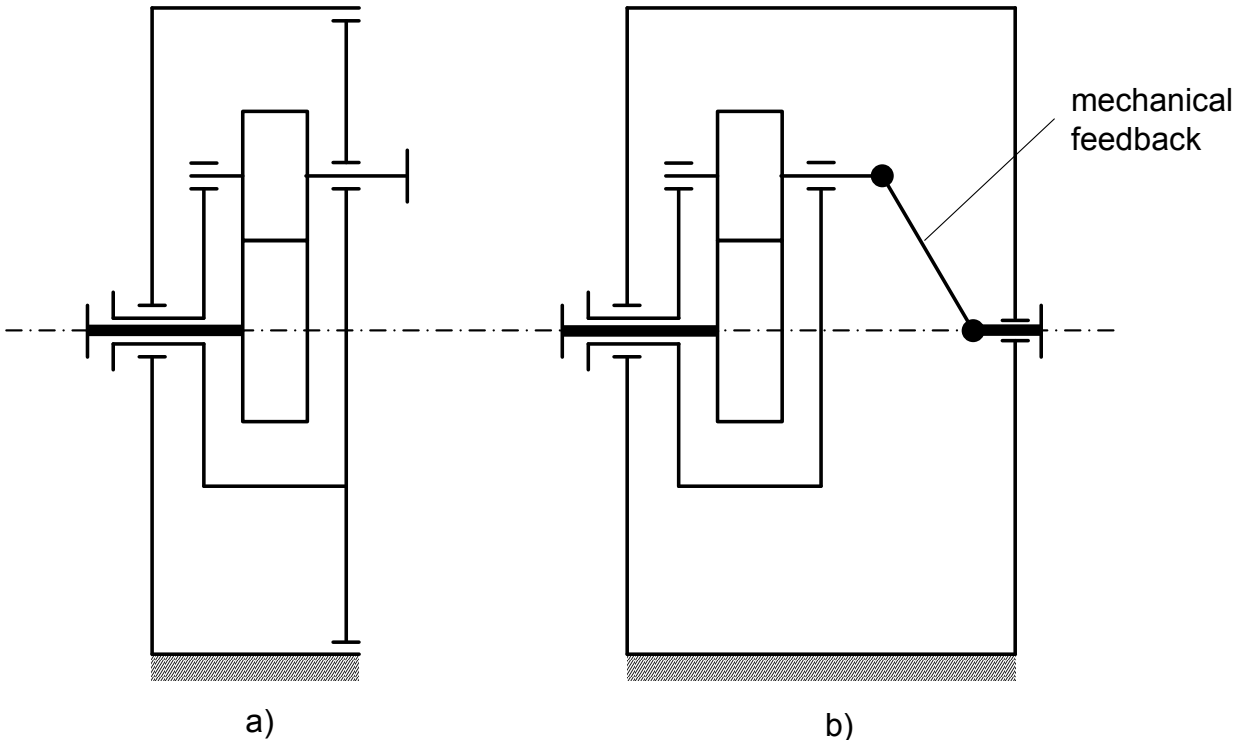

Figure 2-4: Example a) open PGT, b) reverted PGT with mechanical feedback

2.2 Complex-compound planetary gear transmissions

By connecting more than two central gears to a compound planet of a PGT, a so-called *complex-compound* PGT (CCPGT) is achieved. Theoretically, the number of planet gearwheels and thus the number of central gears is not limited. CCPGTs are distinguished by their number of central shafts. **Figure 2-5** shows an example 5-shaft CCPGT. This kind of PGT is also known as double-planet system.

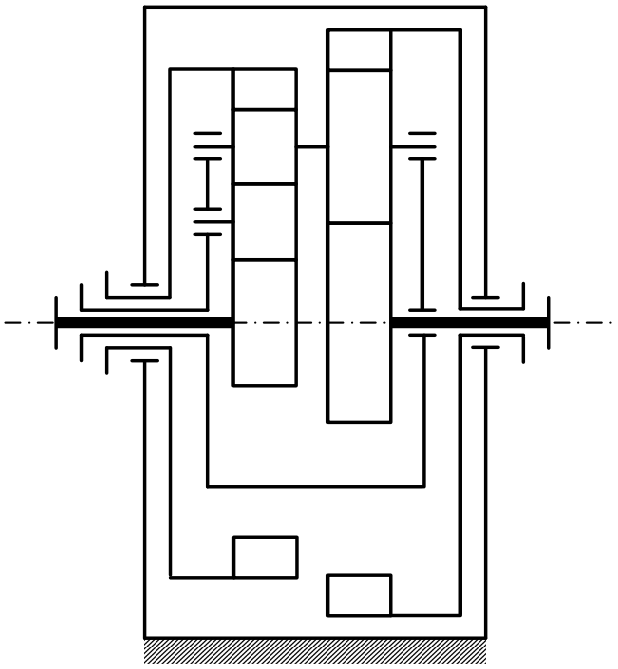

Figure 2-5: Example 5-shaft CCPGT

The CCPGT always features a single planet carrier. Every two central gears are indirectly connected via a chain of planet gears. Therefore, multiple sets of single PGTs are included in every CCPGT.

In comparison to single PGTs, CCPGTs offer a larger number of inputs and outputs, a higher static degree of freedom (Section 2.6), a larger number of transmission ratios and thus an advanced operating range regarding the power flow. Also, CCPGTs are often used as high ratio transmissions by only connecting three central shafts to the periphery. In this case, the efficiency can be much higher and the designed space can be significantly smaller, respectively.

In many cases, CCPGTs are advantageous compared to coupled PGTs (Section 2.3) due to less number of parts, higher efficiency, lower construction effort, lower weight and their naturally very compact design. On the other hand, disadvantages in respect of manufacturing complexity, load sharing, stiffness and noise are to be accepted depending on the final design.

2.3 Coupled planetary gear transmissions

Coupled PGTs contain multiple sets of single PGTs and/or CCPGTs. At least one central shaft of every PGT included is either permanently or temporarily connected to a central shaft of another PGT. As the number of connections is not strictly prescribed, PGTs can be coupled in various ways. An example coupled PGT is shown in **Figure 2-6**. In contrast to CCPGTs, coupled PGTs always feature multiple planet carriers (which can be connected).

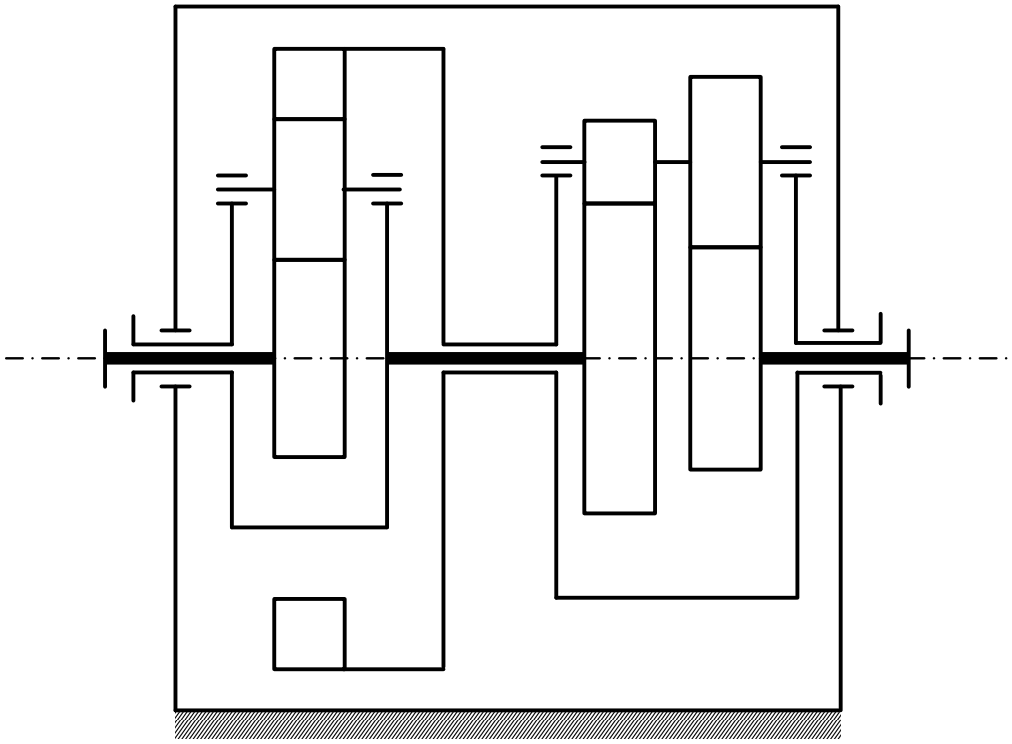

Figure 2-6: Example coupled PGT

As a function of the number of couplings, coupled PGTs increase the kinematic **and** static degree of freedom. Complex designs of single PGTs and CCPGTs can be avoided using coupled PGTs consisting of multiple sets of simple PGTs. It is also possible to gain higher transmission ratios while increasing the efficiency or ensuring a favorable load sharing among the PGTs included. Applying clutches and brakes, coupled PGTs offer multiple gear speed ratios between certain input and output members.

2.4 Basic formulas and sign conventions

In the context of PGT efficiency calculation, the basic physical parameters are angular speeds, torques, power as well as certain efficiency factors and power losses, respectively. In the following, basic formulas for the kinematics and statics analyses are derived assuming **loss-free** conditions. Sign conventions are defined. The efficiency calculation itself will be treated from Chapter 3 on.

2.4.1 Kinematics analysis

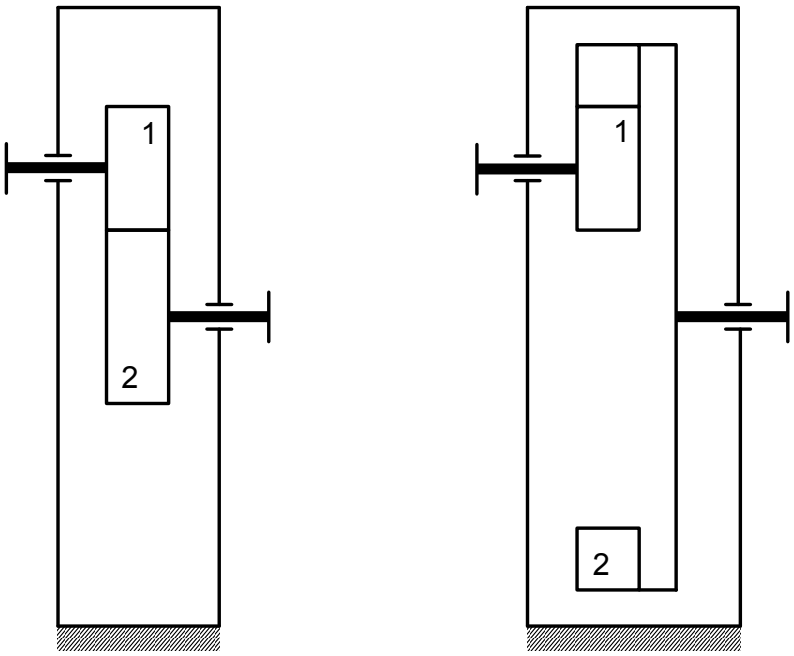

Figure 2-7: Basic gearings

The transmission ratio of basic gearings shown in **Figure 2-7** is defined by the ratio of the angular or rotational speeds of its members 1 and 2:

$$i_{1\,2} = \frac{n_1}{n_2} = \frac{\omega_1}{\omega_2} = -\frac{z_2}{z_1} = -\frac{d_2}{d_1} = -\frac{d_{w2}}{d_{w1}} = -\frac{d_{b2}}{d_{b1}} \qquad (2.1)$$

i	[-]	transmission ratio	d	[mm]	diameter of reference circle
n	[1/s]	rotational speed	d_w	[mm]	diameter of pitch circle
ω	[rad/s]	angular speed	d_b	[mm]	diameter of base circle
z	[-]	number of teeth			

It is simultaneously defined by the ratio of the numbers of teeth, the diameters of the reference circles, the pitch circles or the base circles. Numbers of teeth and diameters are to be inserted as positive values for external gears and as negative values for internal gears, respectively.

A member's direction of rotation is to be taken into account by a positive or negative sign for its speed. In this regard, it does not matter which direction is defined as positive or negative, but the definition has to be maintained for the whole system. According to this definition, external gearings provide negative transmission ratios, whereas internal gearings provide positive transmission ratios.

2.4.1.1 Single planetary gear transmissions

If the basic gearings in **Figure 2-7** are converted into open PGTs (**Figure 2-4**) by adding a carrier s, the motion of the members 1 and 2 relative to the carrier is still characterized by their basic transmission ratio:

$$i^{s}_{1\,2} = \frac{n'_1}{n'_2} = \frac{n_1 - n_s}{n_2 - n_s} \quad \Rightarrow \quad n_1 - i^{s}_{1\,2} \cdot n_2 + (i^{s}_{1\,2} - 1) \cdot n_s = 0 \qquad (2.2)$$

i	[-]	transmission ratio	n	[1/s]	absolute rotational speed
			n'	[1/s]	rotational speed relative to the carrier

This equation is formally known as *Willis Equation* [4_WIL41]. The subscripts of the transmission ratio i indicate the members of the considered gearing whereas the superscript indicates the fixed element or the element imagined as being fixed, respectively. A reverted, single PGT contains minimum two basic gearings. Thus, for every gearing a Willis Equation can be formulated. If the speed of the planets is not of relevance, but only the speeds of the central shafts, the single transmission ratios of the basic gearings can be multiplied and merged to a single transmission ratio of the whole basic train, called *basic ratio* (**Figure 2-8**). If the basic ratio of a single PGT is negative, it is referred to as *negative-ratio drive*, otherwise it is a *positive-ratio drive*.

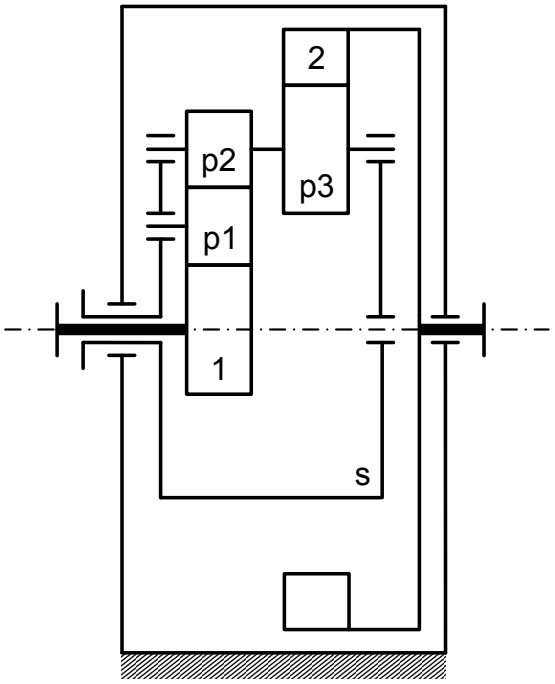

Figure 2-8: Speed equations for an example single PGT

$$i^{s}_{1\,p1} = \frac{n'_1}{n'_{p1}} = \frac{n_1 - n_s}{n_{p1} - n_s}$$

$$i^{s}_{p1\,p2} = \frac{n'_{p1}}{n'_{p2}} = \frac{n_{p1} - n_s}{n_{p2} - n_s}$$

$$i^{s}_{p3\,2} = \frac{n'_{p3}}{n'_2} = \frac{n_{p3} - n_s}{n_2 - n_s} \qquad (2.3)$$

$$n_{p2} = n_{p3}\,;\; n'_{p2} = n'_{p3}$$

$$\Rightarrow \quad i^{s}_{1\,2} = i^{s}_{1\,p1} \cdot i^{s}_{p1\,p2} \cdot i^{s}_{p3\,2} = \frac{n_1 - n_s}{n_2 - n_s}$$

i	[-]	transmission ratio
n	[1/s]	absolute rotational speed
n'	[1/s]	rotational speed relative to the carrier

The motion of a central gear or planet gear can always be interpreted as a combined motion relative and equal to the carrier:

$$n_1 = (n_1 - n_s) + n_s = n'_1 + n_s$$

$$n_2 = (n_2 - n_s) + n_s = n'_2 + n_s \qquad (2.4)$$

$$n_{p1} = (n_{p1} - n_s) + n_s = n'_{p1} + n_s\,;\; n_{p2} = \cdots$$

n	[1/s]	absolute rotational speed	n'	[1/s]	rotational speed relative to the carrier

A relative motion of the gears to the carrier causes meshing. Therefore, the state of motion with the carrier being fixed and the gears rotating is termed *meshing case*. If the whole

PGT rotates as a block, meaning that all parts are running with the same speed, no relative motion occurs. This case of motion is called *coupling case*. Every general state of motion of a single PGT, with all three central shafts running with different speeds, can be distinguished as a superposition of these two special cases, the meshing and the coupling case. In this context, the speed of a gear relative to the carrier is termed *meshing speed*, as the speed of the carrier is termed *coupling speed*.

Other special states of motion are caused by means of a kinematic or rather epicyclic inversion, if not the carrier, but a central gear is fixed, for example central gear 1:

$$\begin{aligned} & n_1 = 0 \\ \Longrightarrow \quad & -i_{1\,2}^{s} \cdot n_2 + (i_{1\,2}^{s} - 1) \cdot n_s = 0 \\ \Longrightarrow \quad & \frac{n_2}{n_s} = i_{2\,s}^{1} = 1 - \frac{1}{i_{1\,2}^{s}} \end{aligned} \qquad (2.5)$$

i	[-]	transmission ratio	n	[1/s]	absolute rotational speed

Since every central shaft of a single PGT can be used as input, output or fixed element, four definite transmission ratios are derived analogically: $i_{1\,s}^{2}$, $i_{s\,1}^{2}$, $i_{2\,s}^{1}$ and $i_{s\,2}^{1}$. These transmission ratios with the carrier acting as input or output are termed *epicyclc ratios*. In combination with the basic ratio $i_{1\,2}^{s}$ and its direct inverse $i_{2\,1}^{s}$, every arbitrary, single PGT features four positive basic or epicyclic ratios and two negative ones. If any of these ratios is given, all the others can be identified due to their interdependency. Furthermore, none of these ratios can have a value of 0 or 1.

2.4.1.2 Complex-compound planetary gear transmissions

In respect of the kinematics of a CCPGT, the basics of a single PGT are still valid. According to the number of basic gearings, Willis Equations are formed (**Figure 2-9**). The transmission ratios can be merged to basic ratios, if the speed of the planets is not of relevance. In this regard, every two central gears are part of a basic train. Thus, three basic ratios are derived for the given 4-shaft CCPGT. Not all of these basic ratios are needed for a complete system of equations, since a basic ratio does not give additional information if it can be derived from other basic ratios, e.g. $i_{1\,3}^{s}$ from $i_{1\,2}^{s}$ and $i_{2\,3}^{s}$.

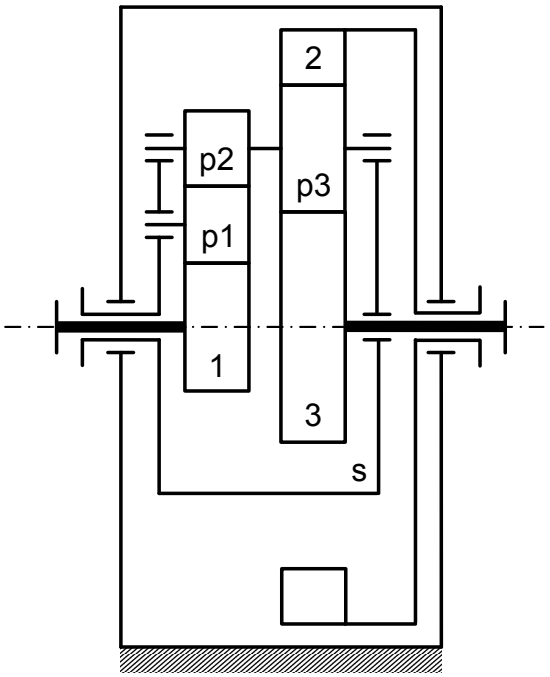

Figure 2-9: Speed equations for an example 4-shaft CCPGT

$$i^{s}_{1\,p1} = \frac{n'_1}{n'_{p1}} = \frac{n_1 - n_s}{n_{p1} - n_s}$$

$$i^{s}_{p1\,p2} = \frac{n'_{p1}}{n'_{p2}} = \frac{n_{p1} - n_s}{n_{p2} - n_s}$$

$$i^{s}_{p3\,2} = \frac{n'_{p3}}{n'_2} = \frac{n_{p3} - n_s}{n_2 - n_s}$$

$$i^{s}_{p3\,3} = \frac{n'_{p3}}{n'_3} = \frac{n_{p3} - n_s}{n_3 - n_s} \qquad (2.6)$$

$$n_{p2} = n_{p3}\ ;\ n'_{p2} = n'_{p3}$$

$$\Rightarrow \quad i^{s}_{1\,2} = i^{s}_{1\,p1} \cdot i^{s}_{p1\,p2} \cdot i^{s}_{p3\,2} = \frac{n_1 - n_s}{n_2 - n_s}$$

$$\Rightarrow \quad i^{s}_{1\,3} = i^{s}_{1\,p1} \cdot i^{s}_{p1\,p2} \cdot i^{s}_{p3\,3} = \frac{n_1 - n_s}{n_3 - n_s}$$

$$\Rightarrow \quad i^{s}_{2\,3} = \frac{1}{i^{s}_{p3\,2}} \cdot i^{s}_{p3\,3} = \frac{n_1 - n_s}{n_3 - n_s}$$

i	[-]	transmission ratio
n	[1/s]	absolute rotational speed
n'	[1/s]	rotational speed relative to the carrier

Besides basic ratios and epicyclic ratios, CCPGTs offer further definite transmission ratios among two central gears x and y, if a third central gear z is fixed instead of the carrier s. This ratio is termed *compound ratio* and can be interpreted as two series-coupled epicyclic ratios:

$$i^{z}_{x\,y} = i^{z}_{x\,s} \cdot i^{z}_{s\,y} = \frac{1 - i^{s}_{x\,z}}{1 - i^{s}_{y\,z}} \qquad (2.7)$$

i	[-]	transmission ratio

The number of definite transmission ratios of a CCPGT is calculated as follows as a function of the number of central gears or central shafts:

$$BR = 2 \cdot \binom{CG}{2} = 2 * \binom{CS - 1}{2}$$

$$ER = 4 \cdot \binom{CG}{2} = 4 * \binom{CS - 1}{2} \qquad (2.8)$$

$$CR = 6 \cdot \binom{CG}{3} = 6 * \binom{CS - 1}{3}$$

BR	[-]	number of basic ratios	CG	[-]	number of central gears
ER	[-]	number of epicyclic ratios	CS	[-]	number of central shafts
CR	[-]	number of compound ratios			

An overview of transmissions ratios included in a single PGT or CCPGT is provided in **Table 2-1**. For each single PGT or CCPGT one-third of all definite transmission ratios are negative and two-thirds are positive.

CS	3	4	5	6	7	8	9	10	11
BR	2	6	12	20	30	42	56	72	90
ER	4	12	24	40	60	84	112	144	180
CR	0	6	24	60	120	210	336	504	720
Σ	**6**	**24**	**60**	**120**	**210**	**336**	**504**	**720**	**990**

BR [-] number of basic ratios
ER [-] number of epicyclic ratios
CR [-] number of compound ratios
CS [-] number of central shafts

Table 2-1: Number of definite transmission ratios of a CCPGT

2.4.1.3 Coupled planetary gear transmissions

Analogically, Willis Equations are formulated for each PGT included in a coupled PGT (**Figure 2-10**). In addition, the speeds of coupled shafts are equalized.

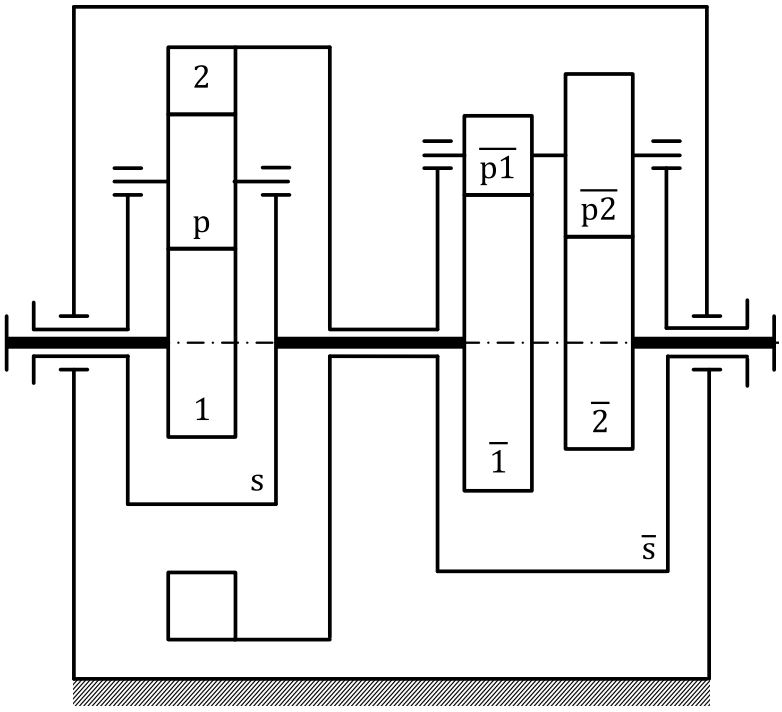

Figure 2-10: Speed equations for an example coupled PGT

$$i^{s}_{1\,2} = \frac{n'_1}{n'_2} = \frac{n_1 - n_s}{n_2 - n_s}$$

$$i^{\bar{s}}_{\bar{1}\,\bar{2}} = \frac{n'_{\bar{1}}}{n'_{\bar{2}}} = \frac{n_{\bar{1}} - n_{\bar{s}}}{n_{\bar{2}} - n_{\bar{s}}} \qquad (2.9)$$

$$n_2 = n_{\bar{s}}$$

$$n_s = n_{\bar{1}}$$

i	[-]	transmission ratio
n	[1/s]	absolute rotational speed
n'	[1/s]	rotational speed rel. to the carrier

2.4.2 Statics analysis

For a better differentiation regarding the statics analysis, *external* and *internal torques* are distinguished. External torques are applied on the central shafts from the periphery. Internal torques are the ones acting on the gears due to mesh forces and balance the external torques inside the transmission (**Figure 2-11**). A torque is defined to be positive if its effective direction is equal to the direction of rotation defined as positive and vice versa.

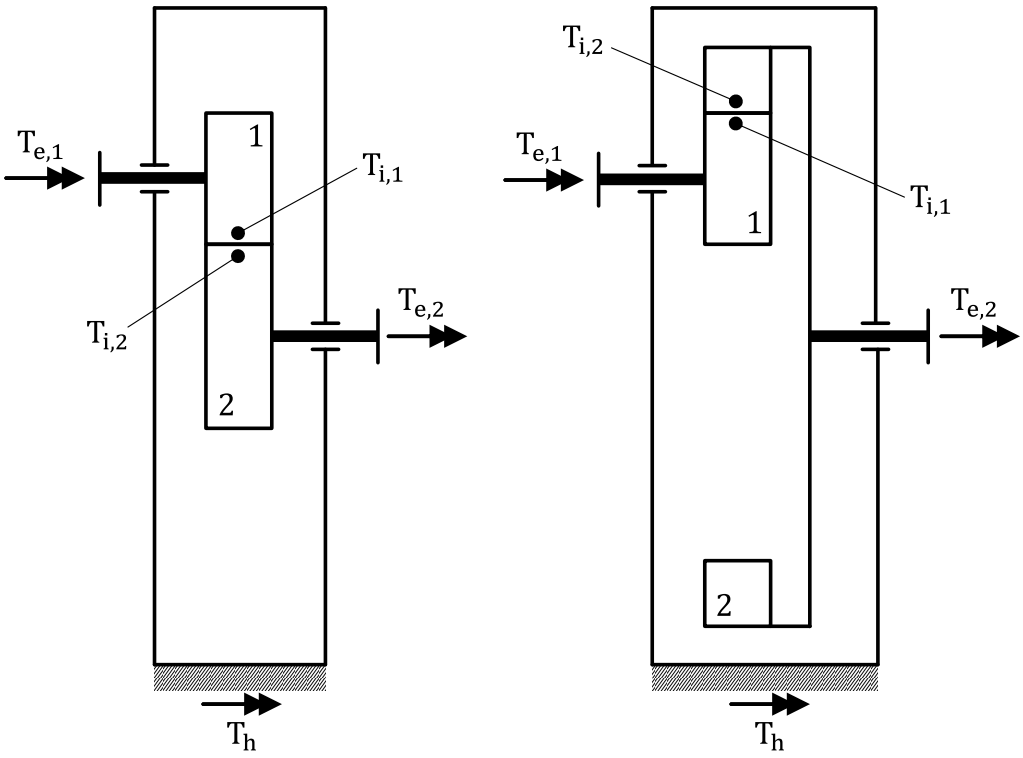

Figure 2-11: Internal and external torques acting on basic gearings

In respect of static operating conditions, torques acting on each part must be balanced. This is also true for all external torques acting on the gear train system:

$$T_{e,1} + T_{i,1} = 0 \;;\; T_{e,2} + T_{i,2} = 0$$
$$T_{e,1} + T_{e,2} + T_h = 0 \qquad (2.10)$$

T_e	[Nm]	external torque	T_h	[Nm]	external torque acting on the housing
T_i	[Nm]	internal torque			

For loss-free conditions, the input and output power of a gear mesh are to be balanced, too:

$$P_{i,1} + P_{i,2} = 0$$
$$\Rightarrow \frac{P_{i,1}}{P_{i,2}} = -1 = \frac{T_{i,1} \cdot n_1}{T_{i,2} \cdot n_2} = \frac{T_{i,1}}{T_{i,2}} \cdot i_{1\,2} \qquad (2.11)$$
$$\Rightarrow \frac{T_{i,2}}{T_{i,1}} = \frac{T_{e,2}}{T_{e,1}} = -i_{1\,2} = \frac{z_2}{z_1}$$

P_i	[W]	internal power	T_e	[Nm]	external torque
i	[-]	transmission ratio	T_i	[Nm]	internal torque
n	[1/s]	rotational speed	z	[-]	number of teeth

Thus, the ratio of the external and internal torques of a basic gearing is given by the numbers of teeth and the transmission ratio respectively as a function of the geometry.

2.4.2.1 Single planetary gear transmissions

Neglecting power losses, e.g. churning losses, corresponding external and internal torques are equal except their sign. Therefore, mainly external torques are used as operands. In the following, internal torques are denoted by subscript ‘i’ explicitly, whereas external torques are not marked with an ‘e’ any longer.

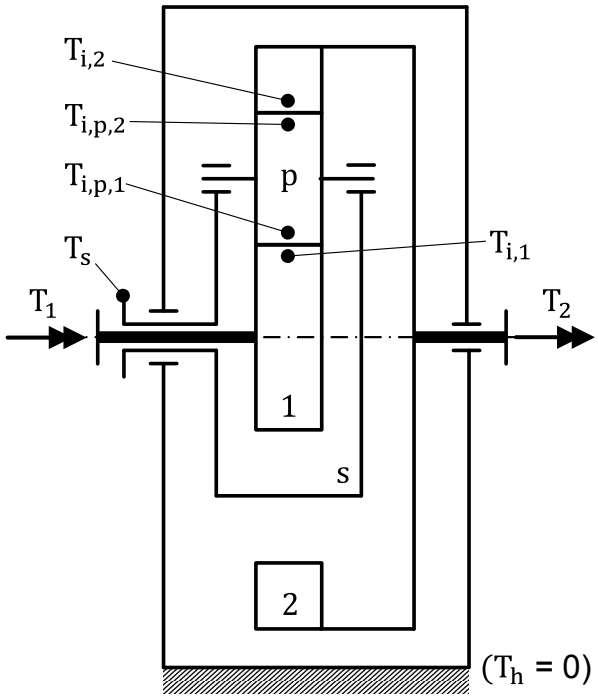

Figure 2-12: Internal and external torques acting on a simple PGT

In the absence of a loaded housing, the sum of external torques of a single PGT including the carrier must equal zero. The torque ratio of the central gears is given by the basic ratio. In this regard, the planet(s) can be seen as the torque balance for the central gears:

$$\frac{T_{p,1}}{T_{i,1}} = -i_{1\,p}^{s}\ ;\ \frac{T_{i,2}}{T_{p,2}} = -i_{p\,2}^{s}\ \text{(basic gearings)}$$

$$T_{i,p,1} + T_{i,p,2} = 0\ \text{(planet)} \qquad (2.12)$$

$$T_1 + T_{i,1} = 0\ ;\ T_2 + T_{i,2} = 0\ \text{(central shafts)}$$

$$\Rightarrow\ \frac{T_2}{T_1} = -i_{1\,2}^{s}\ ;\ \frac{T_s}{T_1} = i_{1\,2}^{s} - 1\ ;\ \frac{T_s}{T_2} = \frac{1}{i_{1\,2}^{s}} - 1\ ;\ T_1 + T_2 + T_s = 0$$

T	[Nm]	external torque	i	[-]	basic ratio
T_i	[Nm]	internal torque			

One of the external torques of the three central shafts must be the largest. Its sign is opposite to the smaller torques. The central shaft charged with the largest torque is termed *summation shaft*, the other two central shafts are termed *difference shafts*. The summation shaft of every negative-ratio drive is the central shaft connected to the carrier. In case of positive-ratio drives, it depends on the indexing. The summation shaft is either the central shaft connected to central gear 1, if the basic ratio is smaller than 1, or the central shaft connected to central 2, if the basic ratio is larger than 1.

2.4.2.2 Complex-compound planetary gear transmissions

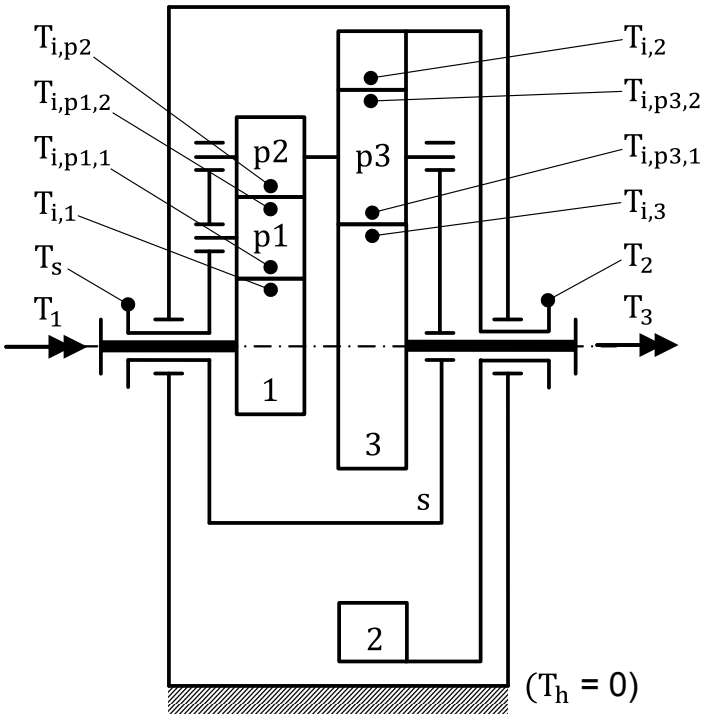

Figure 2-13: Internal and external torques acting on an example 4-shaft CCPGT

For the example shown in **Figure 2-13** the complete system of equations is formed:

$$\frac{T_{i,p1,1}}{T_{i,1}} = -i^s_{1\,p1}\ ;\ \frac{T_{i,p2}}{T_{i,p1,2}} = -i^s_{p1\,p2}\ ;\ \frac{T_{i,p3,1}}{T_{i,2}} = -i^s_{2\,p3}\ ;\ \frac{T_{i,p3,2}}{T_{i,3}} = -i^s_{3\,p3}\ \text{(basic gearings)}$$

$$T_{i,p1,1} + T_{i,p1,2} = 0\ ;\ T_{i,p2} + T_{i,p3,1} + T_{i,p3,2} = 0\ \text{(planets)} \qquad (2.13)$$

$$T_1 + T_{i,1} = 0\ ;\ T_2 + T_{i,2} = 0\ ;\ T_3 + T_{i,3} = 0\ \text{(central shafts)}$$

$$\Rightarrow\ i^s_{1\,p1} \cdot i^s_{p1\,p2} \cdot T_1 + i^s_{2\,p3} \cdot T_2 + i^s_{3\,p3} \cdot T_3 = 0\ ;\ T_1 + T_2 + T_3 + T_s = 0$$

T	[Nm]	external torque	i	[-]	transmission ratio
T_i	[Nm]	internal torque			

In contrast to single PGTs, CCPGTs feature minimum one planet which meshes with at least three mating gears (e.g. stepped planet in **Figure 2-13**), since minimum three central gears are connected via planets by definition. The torque equilibrium for this planet in combination with the external torque equilibrium results in a set of only two conditional equations for the external torques. Thus, for this example, two external torques are required to determine the other two. For this reason, a definite summation shaft and difference shafts or definite torque ratios cannot be identified as a function of the geometry. It depends on the operating conditions.

2.4.2.3 Coupled planetary gear transmissions

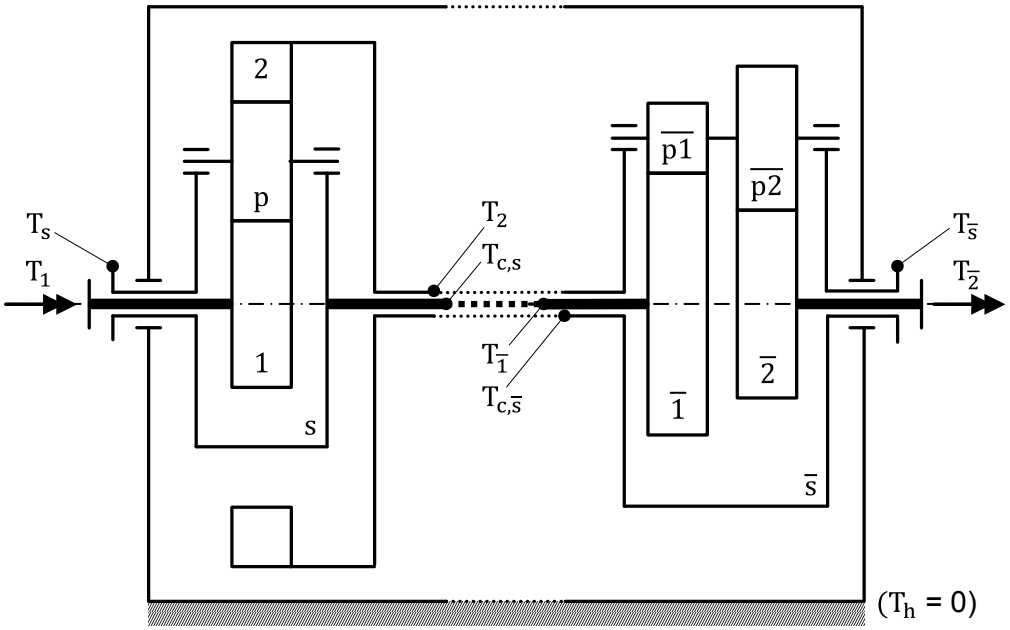

Figure 2-14: Internal and external torques acting on an example coupled PGT

In terms of coupled PGTs, the torque equilibria at the cut-free couplings are to be considered in addition to the system of equations for each PGT included (**Figure 2-14**):

$$\frac{T_2}{T_1} = -i^{s}_{1\,2} \;;\; \frac{T_{\bar{2}}}{T_{\bar{1}}} = -i^{\bar{s}}_{\bar{1}\,\bar{2}} \quad \text{(basic trains, internal torques included)}$$

$$T_2 + T_{c,\bar{s}} = 0 \;;\; T_{\bar{1}} + T_{c,s} = 0 \quad \text{(couplings)} \qquad (2.14)$$

$$T_1 + T_2 + T_s + T_{c,s} = 0 \;;\; T_{\bar{1}} + T_{\bar{2}} + T_{\bar{s}} + T_{c,\bar{s}} = 0 \quad \text{(central shafts)}$$

$$\Rightarrow \; (1 - i^{s}_{1\,2}) \cdot T_1 + T_s + \frac{1}{i^{\bar{s}}_{\bar{1}\,\bar{2}}} \cdot T_{\bar{2}} = 0 \;;\; T_1 + T_s + T_{\bar{2}} + T_{\bar{s}} = 0$$

T	[Nm]	external torque	i	[-]	basic ratio
T_c	[Nm]	coupling torque			

2.4.3 Power transfer

The absolute power transmitted at a certain link is equal to the acting torque multiplied with the absolute angular speed. If the power shows a positive sign, the link works as a power input, otherwise as a power output:

$$P = T \cdot \omega = 2 \cdot \pi \cdot T \cdot n \qquad (2.15)$$

P	[W]	power	ω	[rad/s]	(absolute) angular speed
T	[Nm]	torque	n	[1/s]	(absolute) rotational speed

Neglecting power losses, the power sum of all external inputs and outputs of a single or complex-compound PGT must be equalized:

$$\Sigma P = P_1 + P_2 + P_3 + \cdots + P_s = 0 \qquad (2.16)$$

P	[W]	(absolute) power of external in- or output

This is also true for all external torques:

$$\Sigma T = T_1 + T_2 + T_3 + \cdots + T_s = 0 \qquad (2.17)$$

T	[Nm]	external torque

According to Section 2.4.1, the absolute power of a central gear (as well as of a planet) can be grouped into *meshing power* and *coupling power* by inserting equation (2.4) and (2.15) into (2.16):

$$\begin{aligned} &T_1 \cdot n_1 + T_2 \cdot n_2 + T_3 \cdot n_3 + \cdots + T_s \cdot n_s = \\ &= T_1 \cdot (n_1 - n_s) + T_1 \cdot n_s + T_2 \cdot (n_2 - n_s) + T_2 \cdot n_s + \\ &\qquad + \underbrace{T_3 \cdot (n_3 - n_s)}_{\text{meshing power}} + \underbrace{T_3 \cdot n_s}_{\text{coupling power}} + \cdots + T_s \cdot n_s = 0 \end{aligned} \qquad (2.18)$$

n	[1/s]	(absolute) rotational speed	T	[Nm]	external torque

In the context of efficiency calculation, meshing and coupling power are of special importance. If power is transmitted as meshing power, load-dependent power losses are induced due to relative motion and friction contacts. If power is transmitted as coupling power, no load-dependent power losses are induced due to no relative motion. The meshing and coupling power of a central gear can be smaller or larger than the absolute power depending on the present speeds.

Inserting equation (2.17) into (2.18), power balances both for meshing and coupling are gained:

$$\begin{aligned} &T_1 \cdot n_s + T_2 \cdot n_s + T_3 \cdot n_s + \cdots + T_s \cdot n_s = 0 \qquad \text{(coupling power)} \\ &T_1 \cdot (n_1 - n_s) + T_2 \cdot (n_2 - n_s) + T_3 \cdot (n_3 - n_s) + \cdots = 0 \qquad \text{(meshing power)} \end{aligned} \qquad (2.19)$$

n	[1/s]	(absolute) rotational speed	T	[Nm]	external torque

In terms of single PGTs with three running central shafts, one of the central shafts has to transmit the total input power in case of power division, or the total output power in case of power summation. This shaft is termed *total-power shaft*, the other two shafts are called *partial-power shafts*. The total-power shaft does not have to be the summation shaft. CCPGTs or coupled PGTs do not necessarily feature a total-power shaft, if more than three central shafts are involved in the power transfer.

2.5 Matrix notations

The solving of conditional equations in respect of speeds and torques for loss-free operating conditions is a linear problem. In order to maintain linearity, power losses, and hence, their corresponding calculation equations must show a linear dependency on acting torques (Chapter 3). For computer-based calculation purposes, the use of matrix notations is advantageous. Different matrix notations are possible depending on the indexing and enumeration of relevant transmission elements and depending on the states of interest.

2.5.1 Kinematics

The kinematics system of equations can be written as follows:

$$\mathbf{S} \cdot \vec{n} = \overrightarrow{e_n} \qquad (2.20)$$

S	[-]	basic speed coefficient matrix	$\overrightarrow{e_n}$	[1/s]	basic speed solution / preset vector
$\vec{n}$	[1/s]	basic speed state vector			

A possibility of a universal notation is achieved, if every single element is given its own number and own speed state in the state vector respectively, e.g. used by Stangl [4_STA07]. Besides the Willis Equations for basic gearing, the speeds of rigidly coupled elements have to be equalized for each element belonging to a connected body by means of a separate conditional equation. Thus, a relatively large system of equations is formed.

The shortest notation for smallest matrix dimension is achieved, if only the states which are possibly different are used exclusively, i.e. a whole connected body is given a number or rather state, which is appropriate for every belonging element. In any case, an assignment table specifies the relationship of elements and bodies, respectively.

In general, every basic gearing g features a first geared member x, a mating geared member y and a supporting member, the carrier s or the housing. The basic gearing is characterized by its transmission ratio i_{xy}^{s}. Every member may only appear once in a certain basic gearing. **Figure 2-15** shows an example configuration including enumeration of all connected bodies b.

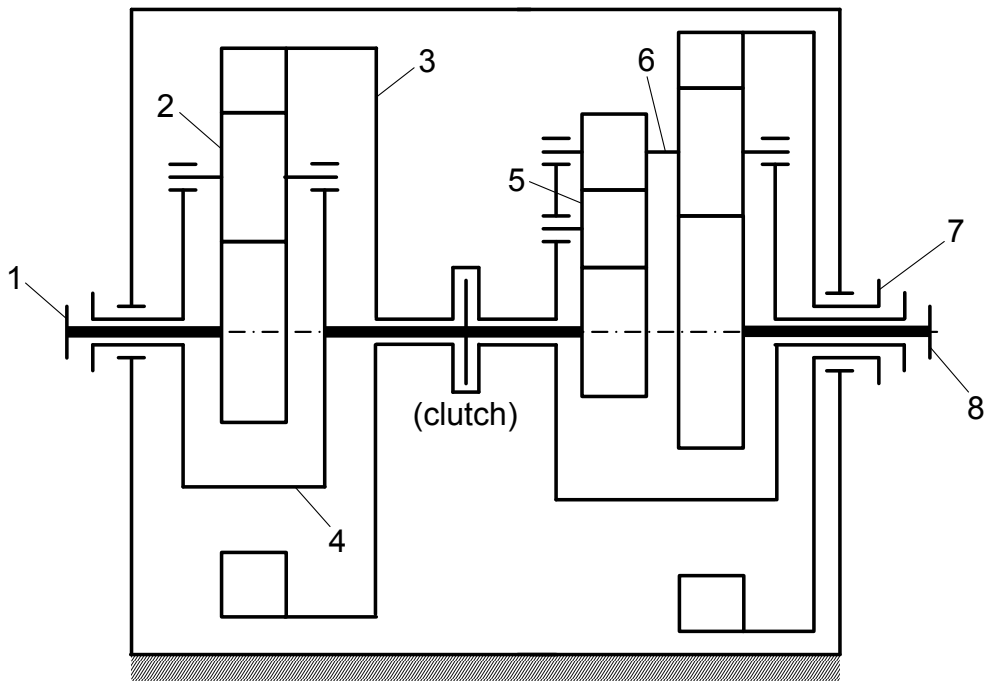

Figure 2-15: Example coupled PGT with enumeration of bodies

The corresponding table contains the functional assignments of bodies to each basic gearing:

basic gearing g	member x	member y	member s	transmission ratio $i^{s}_{x\,y}$
1	1	2	4	$i^{4}_{1\,2}$
2	2	3	4	$i^{4}_{2\,3}$
3	4	5	3	$i^{3}_{4\,5}$
4	5	6	3	$i^{3}_{5\,6}$
5	6	7	3	$i^{3}_{6\,7}$
6	6	8	3	$i^{3}_{6\,8}$

Table 2-2: Basic gearing assignment table for Figure 2-15

The speed state vector $\vec{n}$ contains the speeds of all bodies:

$$\vec{n} = \begin{bmatrix} n_1 \\ \vdots \\ n_b \\ \vdots \\ n_B \end{bmatrix} \qquad (2.21)$$

$\vec{n}$	[1/s]	speed state vector	B	[-]	total number of bodies
n_b	[1/s]	rotational speed of body b			

The entries for the basic speed coefficient matrix are derived from the Willis Equations for each basic gearing:

$$\boxed{1} \cdot n_x \boxed{-i^{s}_{x\,y}} \cdot n_y \boxed{+\left(i^{s}_{x\,y} - 1\right)} \cdot n_s = 0 \qquad (2.22)$$

i	[-]	transmission ratio	n_x	[1/s]	rotational speed of member x

Thus, the basic speed matrix contains G rows according to the total number of basic gearings and B columns according to the total number of bodies:

$$\mathbf{S} = \begin{pmatrix} s_{1,1} & \cdots & s_{1,b} & \cdots & s_{1,B} \\ \vdots & \ddots & \vdots & \ddots & \vdots \\ s_{g,1} & \cdots & s_{g,b} & \cdots & s_{g,B} \\ \vdots & \ddots & \vdots & \ddots & \vdots \\ s_{G,1} & \cdots & s_{G,b} & \cdots & s_{G,B} \end{pmatrix} \text{ with } s_{g,b} = \begin{cases} 1 & \text{if } b = x \text{ of } g \\ -i^{s}_{x\,y} & \text{if } b = y \text{ of } g \\ \left(i^{s}_{x\,y} - 1\right) & \text{if } b = s \text{ of } g \\ 0 & \text{else} \end{cases} \qquad (2.23)$$

S	[-]	basic speed coefficient matrix	B	[-]	total number of bodies
s	[-]	speed coefficient	G	[-]	total number of basic gearings
i	[-]	transmission ratio			

The basic speed preset vector contains G entries of zeros:

$$\overrightarrow{e_n} = \begin{bmatrix} 0_1 \\ \vdots \\ 0_G \end{bmatrix} \qquad (2.24)$$

$\overrightarrow{e_n}$	[1/s]	basic speed solution/preset vector

In respect of the given example, the whole system of equations reads as follows (housing not relevant here):

$$\begin{pmatrix} 1 & -i_{1\,2}^{4} & 0 & i_{1\,2}^{4}-1 & 0 & 0 & 0 & 0 \\ 0 & 1 & -i_{2\,3}^{4} & i_{2\,3}^{4}-1 & 0 & 0 & 0 & 0 \\ 0 & 0 & i_{4\,5}^{3}-1 & 1 & -i_{4\,5}^{3} & 0 & 0 & 0 \\ 0 & 0 & i_{5\,6}^{3}-1 & 0 & 1 & -i_{5\,6}^{3} & 0 & 0 \\ 0 & 0 & i_{6\,7}^{3}-1 & 0 & 0 & 1 & -i_{6\,7}^{3} & 0 \\ 0 & 0 & i_{6\,8}^{3}-1 & 0 & 0 & 1 & 0 & -i_{6\,8}^{3} \end{pmatrix} \cdot \begin{bmatrix} n_1 \\ n_2 \\ n_3 \\ n_4 \\ n_5 \\ n_6 \\ n_7 \\ n_8 \end{bmatrix} = \begin{bmatrix} 0 \\ 0 \\ 0 \\ 0 \\ 0 \\ 0 \end{bmatrix} \qquad (2.25)$$

i	[-]	transmission ratio	n_x	[1/s]	rotational speed of body x

Because of missing preset values, the basic speed coefficient matrix is rectangular as the system of equations is under-determined (G < B). By choosing an appropriate number of preset values as a function of the kinematic degree of freedom, the resulting speed coefficient matrix is made quadratic (Section 2.6.1).

As a special case, a closed clutch rigidly connects two members x and y, e.g. bodies 3 and 4 in **Figure 2-15**. Analogically, an assignment table is written:

clutch cl	member x	member y	constraint
1	3	4	$n_x - n_y = 0$

Table 2-3: Clutch assignment table for Figure 2-15

Further, the basic speed coefficient matrix is expanded by additional rows:

$$\mathbf{S} = \begin{pmatrix} s_{1,1} & \cdots & s_{1,b} & \cdots & s_{1,B} \\ \vdots & \ddots & \vdots & \ddots & \vdots \\ s_{g,1} & \cdots & s_{g,b} & \cdots & s_{g,B} \\ \vdots & \ddots & \vdots & \ddots & \vdots \\ s_{G,1} & \cdots & s_{G,b} & \cdots & s_{G,B} \\ s_{1+G,1} & \cdots & s_{1+G,b} & \cdots & s_{1+G,B} \\ \vdots & \ddots & \vdots & \ddots & \vdots \\ s_{cl+G,1} & \cdots & s_{cl+G,b} & \cdots & s_{cl+G,B} \\ \vdots & \ddots & \vdots & \ddots & \vdots \\ s_{CL+G,1} & \cdots & s_{CL+G,b} & \cdots & s_{CL+G,B} \end{pmatrix} \quad \text{with } s_{cl+G,b} = \begin{cases} 1 & \text{if b = x of cl} \\ -1 & \text{if b = y of cl} \\ 0 & \text{else} \end{cases} \qquad (2.26)$$

S	[-]	basic speed coefficient matrix	B	[-]	total number of bodies
s	[-]	speed coefficient	G	[-]	total number of basic gearings
			CL	[-]	total number of (closed) clutches

For the sake of completeness, it is mentioned that the speed of the housing is not considered as a state in this example, since it is kinematically isolated from other bodies in respect of rotation. If a member were to be coupled to the housing permanently or temporarily, this would be necessary.

2.5.2 Statics

Likewise, the statics system of equations reads as follows:

$$\mathbf{T} \cdot \vec{t} = \vec{e_t} \qquad (2.27)$$

T	[-]	basic torque coefficient matrix	$\vec{e_t}$	[Nm]	basic torque solution / preset vector
$\vec{t}$	[Nm]	basic torque state vector			

In terms of a basic gearing the torques of the central shafts are depending on each other (Section 2.4.2). Thus, one of these torques is sufficient as state for the torque state vector, e.g. the inner torque of member x. The states are marked with an additional index g to identify the concerning basic gearing:

$$\begin{aligned} T_{i,x,g} &= \boxed{1} \cdot T_{i,x,g} \\ T_{i,y,g} &= \boxed{-i^s_{x\,y}} \cdot T_{i,x,g} \\ T_{i,s,g} &= \boxed{(i^s_{x\,y} - 1)} \cdot T_{i,x,g} \end{aligned} \qquad (2.28)$$

i	[-]	transmission ratio	$T_{i,x,g}$	[Nm]	internal torque of member x of basic gearing g

Hence, the torque state vector features as many entries as basic gearings occur:

$$\vec{t} = \begin{bmatrix} T_{i,x,1} \\ \vdots \\ T_{i,x,g} \\ \vdots \\ T_{i,x,G} \end{bmatrix} \qquad (2.29)$$

$\vec{t}$	[Nm]	basic torque state vector	$T_{i,x,g}$	[Nm]	internal torque of member x of basic gearing g
G	[-]	total number of basic gearings			

In respect of the torque coefficient matrix, its coefficients are derived from equation (2.28). Each row of the matrix summates the acting torques on a certain body:

$$\mathbf{T} = \begin{pmatrix} t_{1,1} & \cdots & t_{1,g} & \cdots & t_{1,G} \\ \vdots & \ddots & \vdots & \ddots & \vdots \\ t_{b,1} & \cdots & t_{b,g} & \cdots & t_{b,G} \\ \vdots & \ddots & \vdots & \ddots & \vdots \\ t_{B,1} & \cdots & t_{B,g} & \cdots & t_{B,G} \end{pmatrix} \text{ with } t_{b,g} = \begin{cases} 1 & \text{if b = x of g} \\ -i^s_{x\,y} & \text{if b = y of g} \\ (i^s_{x\,y} - 1) & \text{if b = s of g} \\ 0 & \text{else} \end{cases} \qquad (2.30)$$

T	[-]	basic torque coefficient matrix	B	[-]	total number of bodies
t	[-]	torque coefficient	G	[-]	total number of basic gearings
i	[-]	transmission ratio			

The torque constraint vector contains B entries of zeros:

$$\vec{e_t} = \begin{bmatrix} 0_1 \\ \vdots \\ 0_B \end{bmatrix} \qquad (2.31)$$

$\vec{e_t}$	[Nm]	basic torque solution/preset vector

By means of **Table 2-2** the statics system of equations according to **Figure 2-15** is formed:

$$\begin{pmatrix} 1 & 0 & 0 & 0 & 0 & 0 \\ -i_{1\,2}^{4} & 1 & 0 & 0 & 0 & 0 \\ 0 & -i_{2\,3}^{4} & i_{4\,5}^{3}-1 & i_{5\,6}^{3}-1 & i_{6\,7}^{3}-1 & i_{6\,8}^{3}-1 \\ i_{1\,2}^{4}-1 & i_{2\,3}^{4}-1 & 1 & 0 & 0 & 0 \\ 0 & 0 & -i_{4\,5}^{3} & 1 & 0 & 0 \\ 0 & 0 & 0 & -i_{5\,6}^{3} & 1 & 1 \\ 0 & 0 & 0 & 0 & -i_{6\,7}^{3} & 0 \\ 0 & 0 & 0 & 0 & 0 & -i_{6\,8}^{3} \end{pmatrix} \cdot \begin{bmatrix} T_{i,1,1} \\ T_{i,2,2} \\ T_{i,4,3} \\ T_{i,5,4} \\ T_{i,6,5} \\ T_{i,6,6} \end{bmatrix} = \begin{bmatrix} 0 \\ 0 \\ 0 \\ 0 \\ 0 \\ 0 \\ 0 \\ 0 \end{bmatrix} \qquad (2.32)$$

i	[-]	transmission ratio	$T_{i,x,g}$	[Nm]	internal torque of member x of basic gearing g

In contrast to the kinematics system of equations, the rectangular form of the torque coefficient matrix leads to an over-determined statics system (B > G). Due to missing known and unknown external torques which are to be added to the concerning bodies, the basic torque state vector lacks of states according to the static degree of freedom (Section 2.6.2).

In case of closed clutches, the coupling torques of the involved members x and y are of the same absolute value, but directed oppositely (**Table 2-3**). Thus, one of both torques is sufficient as extension for the basic torque state vector:

$$\vec{t} = \begin{bmatrix} T_{i,x,1} \\ \vdots \\ T_{i,x,g} \\ \vdots \\ T_{i,x,G} \\ T_{c,x,1} \\ \vdots \\ T_{c,x,cl} \\ \vdots \\ T_{c,x,CL} \end{bmatrix} \qquad (2.33)$$

$\vec{t}$	[Nm]	basic torque state vector	$T_{c,x,cl}$	[Nm]	coupling torque of member x of clutch cl
$T_{i,x,g}$	[Nm]	internal torque of member x of basic gearing g	G	[-]	total number of basic gearings
			CL	[-]	total number of clutches

Additionally, the basic torque coefficient matrix is expanded by additional columns:

$$\mathbf{T} = \begin{pmatrix} t_{1,1} & \cdots & t_{1,g} & \cdots & t_{1,G} & t_{1,1+G} & \cdots & t_{1,cl+G} & \cdots & t_{1,CL+G} \\ \vdots & \ddots & \vdots & \ddots & \vdots & \vdots & \ddots & \vdots & \ddots & \vdots \\ t_{b,1} & \cdots & t_{b,g} & \cdots & t_{b,G} & t_{b,1+G} & \cdots & t_{b,cl+G} & \cdots & t_{b,CL+G} \\ \vdots & \ddots & \vdots & \ddots & \vdots & \vdots & \ddots & \vdots & \ddots & \vdots \\ t_{B,1} & \cdots & t_{B,g} & \cdots & t_{B,G} & t_{B,1+G} & \cdots & t_{B,cl+G} & \cdots & t_{B,CL+G} \end{pmatrix} \qquad (2.34)$$

$$\text{with } t_{b,cl+G} = \begin{cases} 1 & \text{if b = x of cl} \\ -1 & \text{if b = y of cl} \\ 0 & \text{else} \end{cases}$$

T	[-]	basic torque coefficient matrix	B	[-]	total number of bodies
t	[-]	torque coefficient	G	[-]	total number of basic gearings
			CL	[-]	total number of (closed) clutches

Comparing equations (2.22) and (2.28) or (2.26) and (2.34), it is noted that the basic speed and torque coefficient matrices are transposes of each other:

$$\mathbf{T} = \mathbf{S}^{\mathrm{T}} \;;\; t_{ij} = s_{ji} \qquad (2.35)$$

T	[-]	basic torque coefficient matrix	t	[-]	torque coefficient
S	[-]	basic speed coefficient matrix	s	[-]	speed coefficient

The same conclusion was also stated by Sanger [4_SAN75] or del Castillo [4_DEL02b]. Once further constraints and unknown states are inserted (Section 2.6), this relation between T and S no longer applies, but depends on the type of constraints.

Regardless of the enumeration method (element by element or body by body), the transpose equivalence of both basic matrices can be obtained, if the states are chosen in the manner shown above. Therefore, the basic system of equations has to be set up only once.

2.6 Degree of freedom

The (operating) degree of freedom (DOF_{op}) of a system is defined as the number of independently and arbitrarily presettable parameters or states for a definite operating condition. In this context, presettable speeds and torques exist. According to Mueller [2_MUL01] the operating DOF of a PGT equals the sum of its kinematic and static DOF:

$$DOF_{op} = DOF_{kin} + DOF_{stat} \qquad (2.36)$$

DOF_{op}	[-]	operating DOF	DOF_{kin}	[-]	kinematic DOF
			DOF_{stat}	[-]	static DOF

2.6.1 Kinematic degree of freedom

The Kutzbach criterion [4_KUT27] reveals that the kinematic DOF of a system or mechanism is equal to the kinematic DOF of each body involved minus the number of constraints due to joints:

$$DOF_{kin} = \lambda \cdot (B - 1) - \Sigma c_j \qquad (2.37)$$

DOF_{kin}	[-]	kinematic DOF	λ	[-]	degree of freedom of a body
c_j	[-]	number of constraints of joint j	B	[-]	total number of bodies (with housing)

The degree of the freedom λ of a body is on the one hand a function of the space in which the mechanism is intended to work and on the other hand a function of the motions that are of interest for the viewer. For instance, λ equals six in case of spatial mechanisms or three in case of planar mechanisms such as PGTs according to Tsai [5_TSA01]. Often, only one rotational, kinematic DOF is of interest in terms of PGTs. Then, λ can be reduced to one. The number of bodies B in equation (2.37) is diminished by one as the housing, which is also assumed as a separate body, does not feature any kinematic degrees of freedom.

Tsai postulates that the bodies of PGTs are linked by only two basic groups of joints, revolute joints R and gear pair joints G. Revolute joints allow two elements to rotate with respect to one another about a common axis of the joint whereas all other relative motions

are blocked. Here, a gear pair is defined as a joint constraining the relative rotation of member x compared to member y about their own axes as a function of the transmission ratio. By means of this definition, the number of constraints of a joint yields:

$$c_R = \begin{cases} 5 \text{ if } \lambda = 6 \\ 2 \text{ if } \lambda = 3 \\ 0 \text{ if } \lambda = 1 \end{cases} ; \; c_G = \begin{cases} 1 \text{ if } \lambda = 6 \\ 1 \text{ if } \lambda = 3 \\ 1 \text{ if } \lambda = 1 \end{cases} \quad (2.38)$$

c_R	[-]	number of constraints of revolute joints	λ	[-]	degree of freedom of a body
c_G	[-]	number of constraints of gear pair joints			

Assuming the absence of closed clutches, substituting equation (2.37) into (2.38) for λ equal to one leads to:

$$\mathrm{DOF}_{\mathrm{kin}} = \mathrm{B} - \mathrm{G} - 1 \quad (2.39)$$

DOF_{kin}	[-]	kinematic DOF	B	[-]	total number of bodies (with housing)
			G	[-]	total number of basic gearings

Thus, the kinematic DOF of a basic gearing equals two as it consists of three bodies whereof two are linked by a gear pair joint. It should be noted that the set of identic planets used in the gear set are referred to as a single body within this context.

2.6.1.1 Single planetary gear transmissions

A reverted, simple PGT contains two basic gearings and four bodies (compare **Figure 2-2**). The kinematic DOFs equal two. Inserting additional planets (**Figure 2-3b**) the number of bodies is likewise increased as the number of basic gearings. The kinematic DOF remains two in any case.

From another perspective, the kinematic DOF of a single PGT must be two just as well, since the rotational motion of the three central shafts is only constrained by one conditional Willis Equation (2.3). For instance, a meshing and coupling speed of a member might be available as preset values to define the operating condition (Section 2.4.1.1).

2.6.1.2 Complex-compound planetary gear transmissions

The kinematic DOF of a CCPGT does not differ from that of a single PGT. For every additional central gear, the number of bodies as well as the number of basic gearings is increased by one (**Figure 2-5**). Likewise, the number of independent Willis Equations and basic ratios respectively (cf. Section 2.4.1.2) is increased for which reason equation (2.39) can also be written as:

$$\mathrm{DOF}_{\mathrm{kin}} = \mathrm{CS} - \mathrm{BR}_{\mathrm{ind}} \; (= 2) \quad (2.40)$$

DOF_{kin}	[-]	kinematic DOF	CS	[-]	total number of central shafts
			BR_{ind}	[-]	total number of independent basic ratios

Analogical to single PGTs, the meshing speed of one central gear predicts the meshing speed of the other central gears, since all central gears are connected via planets (Section 2.2), and a coupling speed can be superimposed.

2.6.1.3 Coupled planetary gear transmissions

The kinematic DOF of a coupled PGT can be derived directly from the dimension of the basic speed coefficient matrix (2.26). Additionally, each closed clutch provides a conditional equation. In this case, equation (2.39) is expanded as follows:

$$\mathrm{DOF_{kin}} = \mathrm{B} - \mathrm{G} - \mathrm{CL} - 1 \qquad (2.41)$$

$\mathrm{DOF_{kin}}$	[-]	kinematic DOF	B	[-]	total number of bodies
CL	[-]	total number of (closed) clutches/brakes	G	[-]	total number of basic gearings

Alternatively, one can imagine that two kinematic DOFs are provided by every PGT included and a permanent or temporary paired shaft coupling provides a constraint. According to Mueller [2_MUL01] the kinematic DOF of a coupled PGT is calculated as:

$$\mathrm{DOF_{kin}} = 2 \cdot \mathrm{PGT} - \mathrm{CL} \qquad (2.42)$$

$\mathrm{DOF_{kin}}$	[-]	kinematic DOF	CL	[-]	total number of permanent / temporary couplings (or closed clutches/brakes)
PGT	[-]	total number of PGTs included			

Equations (2.41) and (2.42) indicate that the number of simultaneously closed clutches in a shiftable transmission is to be kept constant to maintain a constant kinematic DOF.

To add presets to the system of equations (2.26), the basic speed coefficient matrix is expanded by additional lines and the preset values themselves are attached to the speed preset vector:

$$\begin{pmatrix} & & \mathbf{S} & & \\ s_{1,1} & \cdots & s_{1,b} & \cdots & s_{1,B} \\ \vdots & \ddots & \vdots & \ddots & \vdots \\ s_{pr,1} & \cdots & s_{pr,b} & \cdots & s_{pr,B} \\ \vdots & \ddots & \vdots & \ddots & \vdots \\ s_{\mathrm{DOF_{kin}},1} & \cdots & s_{\mathrm{DOF_{kin}},b} & \cdots & s_{\mathrm{DOF_{kin}},B} \end{pmatrix} \cdot \vec{n} = \begin{bmatrix} \overrightarrow{e_n} \\ n_{pr,1} \\ \vdots \\ n_{pr,\mathrm{DOF_{kin}}} \end{bmatrix} \qquad (2.43)$$

$$\text{with } s_{pr,b} = \begin{cases} 1 & \text{if } n_b = n_{pr} \\ 0 & \text{else} \end{cases}$$

S	[-]	basic speed coefficient matrix	B	[-]	total number of bodies
s	[-]	speed coefficient	$\mathrm{DOF_{kin}}$	[-]	kinematic degree of freedom^
n_b	[1/s]	rotational speed of body b	n_{pr}	[1/s]	speed preset value

Hence, the speed coefficient matrix is made quadratic and of full order in case of a reasonably defined system and reasonably chosen presets.

2.6.2 Static degree of freedom

In conformity with Mueller [2_MUL01], the operating DOF of a transmission must equal the total number of connections to the periphery. In theory, a body and a shaft respectively can feature an arbitrary number of load application points. Therefore, it makes sense to restrict the number of external torques on a shaft to one. Further, the planets of a reverted PGT are not connected to the periphery, so each central shaft can and does feature one external torque. Modifying equation (2.36) yields:

$$\mathrm{DOF_{op}} = \mathrm{DOF_{kin}} + \mathrm{DOF_{stat}} = \mathrm{B} - \mathrm{P} - 1 = \mathrm{CS} \qquad (2.44)$$

$\mathrm{DOF_{op}}$	[-]	operating DOF	B	[-]	total number of bodies
$\mathrm{DOF_{kin}}$	[-]	kinematic DOF	P	[-]	total number of planets
$\mathrm{DOF_{stat}}$	[-]	static DOF	CS	[-]	total number of central shafts

Substituting equation (2.41) or (2.42) into (2.44) leads to:

$$\mathrm{DOF_{stat}} = \mathrm{B} - \mathrm{P} - 1 - \mathrm{B} + \mathrm{G} + 1(+\mathrm{CL}) = \mathrm{G} - \mathrm{P}\ (+\mathrm{CL}) \qquad (2.45)$$

$\mathrm{DOF_{stat}}$	[-]	static DOF	B	[-]	total number of bodies
CL	[-]	total number of (closed) clutches	P	[-]	total number of planets
			G	[-]	total number of basic gearings

2.6.2.1 Single planetary gear transmissions

As for single PGTs, the static DOF is always one, since the number of central shafts is limited to three and the kinematic DOF is two:

$$\mathrm{DOF_{stat}} = \mathrm{B} - \mathrm{P} - 1 - \mathrm{DOF_{kin}} = \mathrm{CS} - 2 = \mathrm{G} - \mathrm{P} = 1 \qquad (2.46)$$

$\mathrm{DOF_{stat}}$	[-]	static DOF	B	[-]	total number of bodies
$\mathrm{DOF_{kin}}$	[-]	kinematic DOF	P	[-]	total number of planets
G	[-]	total number of basic gearings	CS	[-]	total number of central shafts

This also corresponds to the number of central shafts less the number of independent conditional equations (2.12).

2.6.2.2 Complex-compound planetary gear transmissions

CCPGTs feature a number of static DOFs depending on the number of central shafts. There are always two conditional equations for the external torques (2.13):

$$\mathrm{DOF_{stat}} = \mathrm{B} - \mathrm{P} - 1 - \mathrm{DOF_{kin}} = \mathrm{CS} - 2 = \mathrm{G} - \mathrm{P} \qquad (2.47)$$

$\mathrm{DOF_{stat}}$	[-]	static DOF	B	[-]	total number of bodies
$\mathrm{DOF_{kin}}$	[-]	kinematic DOF	P	[-]	total number of planets
G	[-]	total number of basic gearings	CS	[-]	total number of central shafts

2.6.2.3 Coupled planetary gear transmissions

Term (G – P) in equation (2.45) points out that the static DOF is not influenced by permanent couplings of central shafts since the number of basic gearings and planets remains unchanged. The static DOF can also be expressed by substituting equation (2.42) into (2.44):

$$\mathrm{DOF_{stat}} = \mathrm{CS} - \mathrm{DOF_{kin}} = \mathrm{CS} + \mathrm{CL} - 2 \cdot \mathrm{PGT} \qquad (2.48)$$

$\mathrm{DOF_{kin}}$	[-]	kinematic DOF	CS	[-]	total number of central shafts
$\mathrm{DOF_{stat}}$	[-]	static DOF	CL	[-]	total number of (closed) clutches
			PGT	[-]	total number of PGTs included

If as many external torques are to be predefined as the number of static DOFs, as many external torques are unknowns as available kinematic DOFs. The unknown external torques are attached to the torque state vector as states. Further, the torque coefficient matrix is expanded by additional columns to add the unknown external torques to the body which they are acting on. The basic torque coefficient matrix is made quadratic as follows:

$$\begin{pmatrix} & \mathrm{t_{1,1}} & \cdots & \mathrm{t_{1,u}} & \cdots & \mathrm{t_{1,DOF_{kin}}} \\ & \vdots & \ddots & \vdots & \ddots & \vdots \\ \mathbf{T} & \mathrm{t_{b,1}} & \cdots & \mathrm{t_{b,u}} & \cdots & \mathrm{t_{b,DOF_{kin}}} \\ & \vdots & \ddots & \vdots & \ddots & \vdots \\ & \mathrm{t_{B,1}} & \cdots & \mathrm{t_{B,u}} & \cdots & \mathrm{t_{B,DOF_{kin}}} \end{pmatrix} \cdot \begin{bmatrix} \vec{\mathrm{t}} \\ \\ \mathrm{T_{e,b,1}} \\ \vdots \\ \mathrm{T_{e,b,u}} \\ \vdots \\ \mathrm{T_{e,b,DOF_{kin}}} \end{bmatrix} = \vec{\mathrm{e_t}} \qquad (2.49)$$

$$\text{with } \mathrm{t_{b,u}} = \begin{cases} 1 & \text{if } \mathrm{T_e} \text{ of b is unknown} \\ 0 & \text{else} \end{cases}$$

T	[-]	basic torque coefficient matrix	B	[-]	total number of bodies
t	[-]	torque coefficient	$\mathrm{DOF_{kin}}$	[-]	kinematic DOF
$\vec{\mathrm{t}}$	[Nm]	basic torque state vector	$\mathrm{T_{e,b,u}}$	[Nm]	external, unknown torque of body b
$\vec{\mathrm{e_t}}$	[Nm]	basic torque solution/preset vector			

In order to add preset values, it is possible to attach all known external torques as states to the torque state vector. Then, additional columns are required for the speed coefficient matrix to sum the external torques to the corresponding bodies according to (2.49). Further, additional rows are needed to actually equalize the known states with the preset values attached to the basic torque preset vector. Hereby, the dimension of the system of equation is increased by $\mathrm{DOF_{stat}}$.

To keep the system dimension as small as possible, it makes sense to directly add the known external torques to the appropriate body by modifying the basic torque preset vector. The zero entry at the b-th position of the basic torque state vector is replaced by the known, negative preset value:

$$\vec{\mathrm{e_t}} = \begin{bmatrix} -\mathrm{T_{e,b,1}} \\ \vdots \\ -\mathrm{T_{e,b,pr}} \\ \vdots \\ -\mathrm{T_{e,B,DOF_{stat}}} \end{bmatrix} \text{ with } \mathrm{T_{e,b,pr}} \mathrel{\widehat{=}} \begin{cases} \text{preset value} & \text{if } \mathrm{T_e} \text{ of b is known} \\ 0 & \text{else} \end{cases} \qquad (2.50)$$

$\vec{\mathrm{e_t}}$	[Nm]	torque solution/preset vector	$\mathrm{T_{e,b,pr}}$	[Nm]	external, known torque of body b
$\mathrm{DOF_{stat}}$	[-]	static DOF			

3 State of the art

3.1 Power losses and available calculation methods

Power losses in transmissions are caused by different components and physical phenomena. As a rough classification, the origin of friction power can be deduced from lubricated and loaded contacts of solid bodies rolling and sliding with respect to each other, e.g. in the gear mesh, as well as from contacts of spinning solid bodies with surrounding fluids leading to windage, churning and pumping effects.

The overall power loss can be subdivided into component-specific portions and further into load-dependent and load-independent portions depending on whether they vary only with the speed or also with the load. According to Niemann, Winter and Hoehn [1_NIE03], the classification of power losses reads as follows:

$$P_L = P_{LGP} + P_{LG0} + P_{LBP} + P_{LB0} + P_{LS} + P_{LX} \quad (3.1)$$

P_L	[W]	overall power loss	P_{LBP}	[W]	load-dependent bearing power loss
P_{LGP}	[W]	load-dependent gear power loss	P_{LB0}	[W]	load-independent bearing power loss
P_{LG0}	[W]	load-independent gear power loss	P_{LX}	[W]	(load-independent) power losses of other components
P_{LS}	[W]	(load-independent) seal power loss			

Various calculation methods, mostly of empirical but also of analytical nature, exist for determining the power loss of each component. A small selection is discussed here.

3.1.1 Gear power losses

3.1.1.1 Load-dependent gear power losses

A significant number of studies attend to the determination and calculation of load-dependent gear power losses. This sort of power loss occurs due to rolling and sliding in the loaded gear mesh. Most studies try to separate the influences into geometry-based and tribology-based factors. According to Niemann [1_NIE03] the gear power loss reads:

$$P_{LGP} = \mu_m \cdot H_V \cdot P_{in} \quad (3.2)$$

P_{LGP}	[W]	load-dependent gear power loss	μ_m	[-]	(average) coefficient of friction
P_{in}	[W]	input power to the gear mesh	H_V	[-]	tooth loss factor

Several authors, like e.g. Ohlendorf [3_OHL58], Volmer [2_VOL90], Tuplin [1_TUL62], Merritt [1_MER46], Klein [2_KLE62], Pickard [2_PIC81] or Poppinga [2_POP49], only take into account sliding effects. Other authors, like e.g. Anderson and Loewenthal [3_AND80b and 3_AND83] and Gackstetter [3_GAC68] also consider rolling friction. Based on the

work of Ohlendorf, Wimmer [3_WIM06] specifies the tooth loss factor, which rates the specific sliding, as a function of the number of teeth and the transverse contact ratio:

$$H_V = \frac{\pi \cdot (u+1)}{z_1 \cdot u \cdot \cos\beta_b} \cdot (a_0 + a_1 \cdot |\varepsilon_1| + a_2 \cdot |\varepsilon_2| + a_3 \cdot |\varepsilon_1| \cdot \varepsilon_1 + a_4 \cdot |\varepsilon_2| \cdot \varepsilon_2) \quad (3.3)$$

H_V	[-]	tooth loss factor	β_b	[°]	helix angle at base circle
u	[-]	ratio of numbers of teeth (z_2/z_1)	$\varepsilon_{1/2}$	[-]	tip contact ratio
$z_{1/2}$	[-]	number of teeth of gear / mating gear	$a_{1...4}$	[-]	coefficients depending on contact ratio

As the balance of forces changes before and behind the pitch point along the line of action as the friction force changes the orientation due to bracing and pulling sliding, Duda [3_DUD71] recognizes the power loss unbalance of spur gears.

The average coefficient of friction is often assumed as being constant for every contact point of the engagement region within a range of approximately 0,03 to 0,08. Eiselt [3_EIS66], Michaelis [3_MIC88] and Schlenk [3_SCH95] account for more determining factors such as oil parameters, sum velocity, normal force, line load, radii of curvature, surface roughness and so on. For instance, the coefficient of friction according to Schlenk is:

$$\mu_m = 0{,}048 \cdot \left(\frac{F_{bt}}{b} \cdot \frac{1}{v_{\Sigma C} \cdot \rho_{redC}}\right)^{0,2} \cdot \eta_{oil}^{-0,05} \cdot Ra^{0,25} \cdot X_L \quad (3.4)$$

μ_m	[-]	(average) coefficient of friction	ρ_{redC}	[mm]	radius of curvature at the pitch point
F_{bt}	[N]	circumferential force at base circle	η_{oil}	[mPas]	dynamic oil viscosity
b	[mm]	tooth width	Ra	[µm]	arithmetic surface roughness
$v_{\Sigma C}$	[m/s]	sum velocity at pitch point	X_L	[-]	lubricant factor

More accurate results are achieved if test rig measurements are available. Doleschel [3_DOL02] proposes an approach which extrapolates based on measured values. Solid and EHD friction are distinguished.

Figure 3-1 illustrates the simplified assumptions of the methods mentioned above. Advanced methods try to compute the instantaneous operating conditions by making use of higher sophisticated program tools and physical models in respect of the load distribution, EHL and surface roughness models, e.g. Mihailidis [3_MIH02].

Wimmer [3_WIM06] proposes a local tooth loss factor taking into account elastic deformations and tooth flank modifications. **Figure 3-2** shows an example line load distribution of a corrected helical gear pair. Wimmer proves deviations of 30% compared to (3.3) for some worked samples. He also believes that the instantaneous friction coefficient is higher at the beginning of contact due to unfavorable lubrication conditions (**Figure 3-3**).

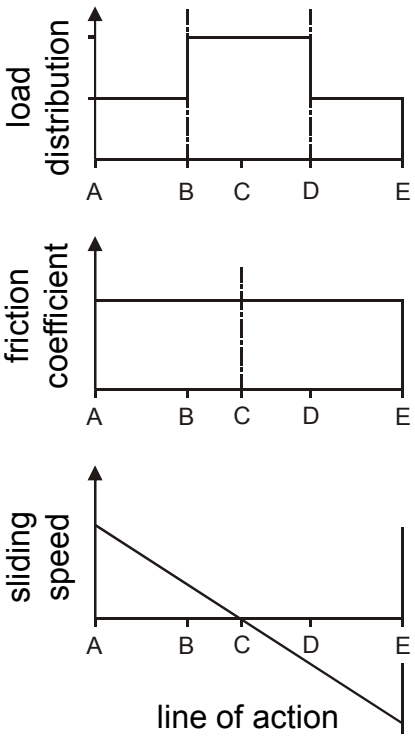

Figure 3-1: Simplified load distribution, friction coefficient and sliding speed [3_WIM06]

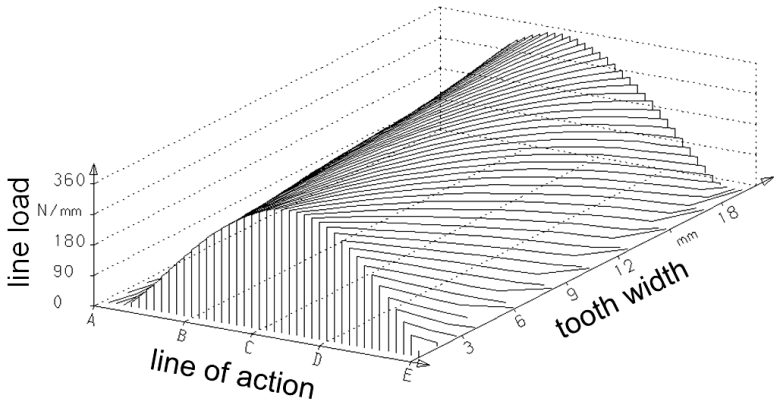

Figure 3-2: Line load distribution of an example corrected helical gear pair [3_WIM06]

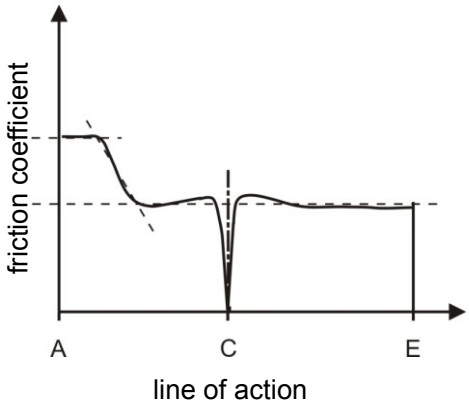

Figure 3-3: Instantaneous friction coefficient acc. to [3_WIM06]

Xu and Kahraman [3_KAH07] introduce a new friction coefficient model using a validated, rough-surface, thermal EHL model in conjunction with a multiple regression analysis. By making use of a gear contact model, the basic gear geometry, tooth modifications, operating load and speed as well as surface finish and manufacturing or assembly errors are or can be taken into account. The authors point out that the model predictions are within 0,1% deviation in respect of the measured values (**Figure 3-4**). The results are also included in an overall efficiency model for manual transmissions by Seetharaman et al. [3_ROS08].

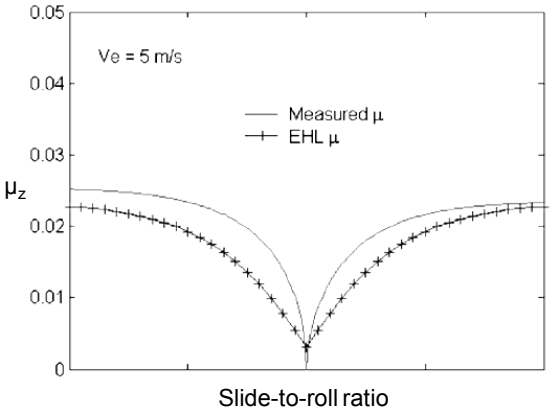

Figure 3-4: Measured and computed friction coefficients acc.to [3_KAH07]

3.1.1.2 Load-independent gear power losses

Load-independent gear power losses, also called spin power losses, of gears are related to churning or windage effects as well as to oil squeezing and pumping in the gear mesh. In case of jet lubrication, impact power losses can also occur. Various studies tried to quantify these losses and identify the key parameters including basic lubricant and air parameters, circumferential speed, depth of immersion, geometry parameters and distance to the housing and other parts, alignment and direction of rotation of the gears or tip and flank clearances. In most cases, results are obtained from empirical investigations using an enclosed spur gear pair, e.g. Anderson and Loewenthal [3_AND80a and 3_AND81], Boness [3_BON89], Butsch and Ariura [3_BUT89], Changenet and Velex [3_CHA06 and 3_CHA07], Dawson [3_DAW84 and 3_DAW88], Greiner [3_GRE90], Jaufmann [JAU94], Maurer [3_MAU94], Mauz [3_MAU87], Townsend [3_MIZ89], Strasser [3_STR05] and Walter [3_WAL82]. Otto [3_OTT09 and 3_HOH07] proposes a lubrication factor to rate the effects of minimized lubrication on the temperature of the gears, which influences the load

carrying capacity again. Kettler [4_KET01] modifies the equations of Mauz to comprise load-independent gear power losses of simple planetary gear sets.

Other authors like Marchesse, Changenet, Ville and Velex [3_MAR09] or Gratz [3_GRA99] actually try to model these power losses e.g. by using CFD simulations. Seetharaman and Kahraman [3_SEE09a and 3_SEE09b] come up with a physics-based and validated fluid mechanics model to predict spin power losses of gear pairs. In terms of dip-lubrication, churning power losses are subdivided into drag power losses on the periphery and on the faces of the gears, oil pocketing power losses from squeezing oil out of the cavities of the gear mesh and root filling power losses from filling the tooth spaces with oil when gears are partially immersed. In case of jet-lubrication, the windage power losses are related to drag and pocketing power losses.

3.1.2 Bearing power losses

To provide a brief overview, **Figure 3-5** qualitatively shows the overall bearing drag torque and corresponding friction coefficient depending on the load according to [3_BRA95]. Naturally, bearing power losses increase with increasing speed and load.

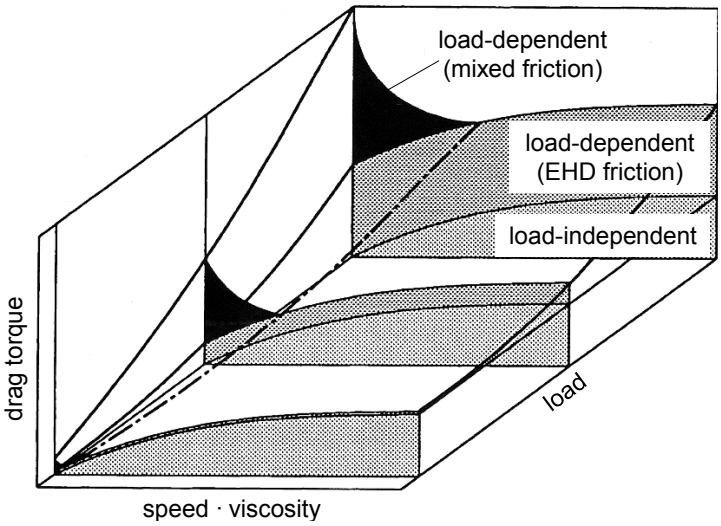

Figure 3-5: Drag torque of roller bearings [3_BRA95]

A widely recognized calculation method for determining load-dependent and load-independent bearing power losses is based on investigations by Palmgren [3_PAL56 and 3_PAL59], which were employed by other investigators such as by Dahlke [3_DAH94] or Braendlein et al. [3_BRA95]. Further, the method was published in several roller bearing catalogues of different manufacturers, such as FAG [3_FAG99] or SKF [3_SKF94]. Hereafter, the two portions are calculated as function of few application parameters:

$$T_0 = 10^{-7} \cdot f_0 \cdot (\nu \cdot n)^{\frac{2}{3}} \cdot d_m^3 \quad \text{for} \quad (\nu \cdot n) \geq 2000$$

$$T_0 = 160 \cdot 10^{-7} \cdot f_0 \cdot d_m^3 \quad \text{for} \quad (\nu \cdot n) < 2000 \qquad (3.5)$$

$$T_1 = f_1 \cdot P_1^a \cdot d_m^b$$

T_0	[Nm]	load-independent drag torque	T_1	[Nm]	load-dependent drag torque
f_0	[-]	lubrication and bearing type factor	P_1	[N]	decisive bearing load
v	[mm²/s]	kinematic viscosity of lubricant	d_m	[mm]	middle bearing diameter
n	[rpm]	rotational speed of bearing	a,b	[-]	exponents depending on bearing type

Additional drag torques are to be considered for axially loaded roller bearings and sealed bearings. The INA bearing catalogue [INA08] modifies the lubrication factor f_0 as a function of the depth of immersion.

Harris [3_HAR01] proposes a more precise subdivision of bearing power losses by separating losses due to elastic hysteresis, rolling and deformation, sliding friction for the raceway and rolling element contact as well as for the cage and rolling element contact, viscous drag and so on. The SKF catalogue of 2004 [3_SKF04] introduces a higher sophisticated method which distinguishes the drag torque components as a function of their origin:

$$T_{LB} = \phi_{ish} \cdot \phi_{rs} \cdot T_{rr} + T_{sl} + T_{seal} + T_{drag} \qquad (3.6)$$

T_{LB}	[Nm]	bearing drag torque	T_{drag}	[Nm]	drag torque due to splashing and churning in case of splash lubrication
T_{rr}	[Nm]	rolling drag torque			
T_{sl}	[Nm]	sliding drag torque	Φ_{ish}	[-]	lubricant film thickness factor
T_{seal}	[Nm]	seal drag torque	Φ_{rs}	[-]	lubricant displacement factor

3.1.3 Power losses of seals and other components

Seal power losses are load-independent and can be estimated using ISO norms [3_ISO01a and 3_ISO01b] or equations provided by seal manufacturers, such as Simrit. Only the shaft speed and diameter as well as the seal type are used as input values.

Power losses of other components are for instance power losses of planet carriers. For this, only very few calculation approaches exist. Kettler [4_KET01] provides an approximation equation for different designs of planet carriers of simple planetary gears.

Further power losses, e.g. of shafts, synchronizers, multi-disc or free-wheel clutches and other spinning components, are completely neglected, require more significant methods of determination or test rig measurements in most cases.

3.1.4 Approximate quantification of power losses

An allotment of power losses occurring in transmissions shows a predominant role of load-dependent gear power losses for nominal load and speed. Only when applying low torques and high speeds respectively the load-independent gear and bearing power losses overbalance, according to Niemann [1_NIE03] (**Figure 3-6**). Power losses of seals and other components almost vanish in comparison.

Using the FZG efficiency calculation program WTplus [3_KUR08], a prediction of power losses of an example 6-speed manual transmission for automotive applications is disclosed by Kurth [3_KUR09] in **Figure 3-7**. Mueller [2_MUL01] states that load-independent power losses are only of relevance for planetary gears below approximately 10% of the nominal input power (**Figure 3-8**). Kettler [4_KET01] indicates that more than 85% of all power losses of an example two-stage compound planetary gear transmission are related to load-dependent effects for nominal operating conditions.

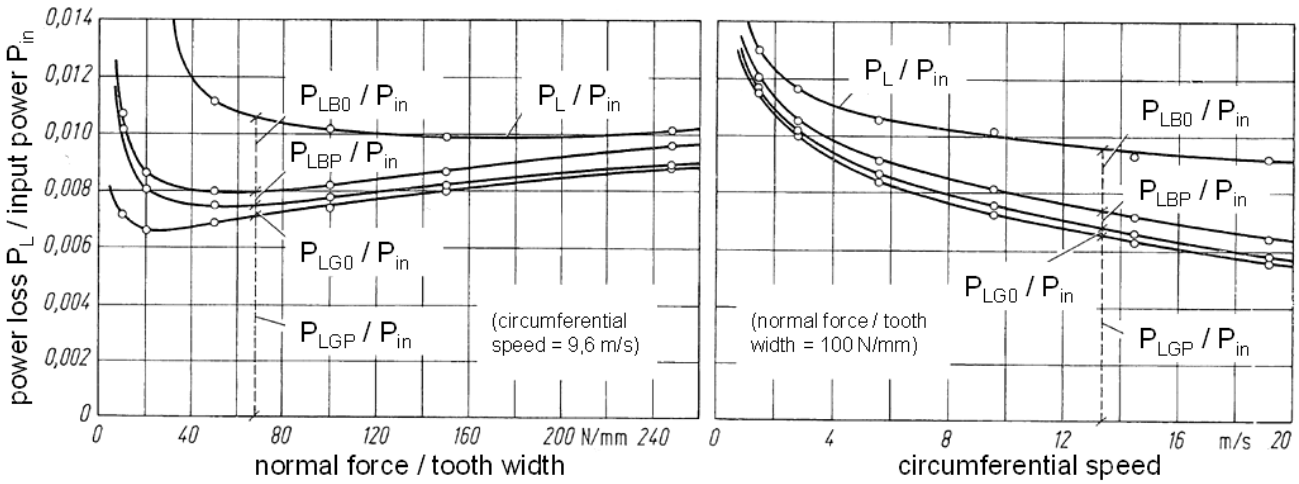

Figure 3-6: Power losses of an example spur gear pair [1_NIE03]

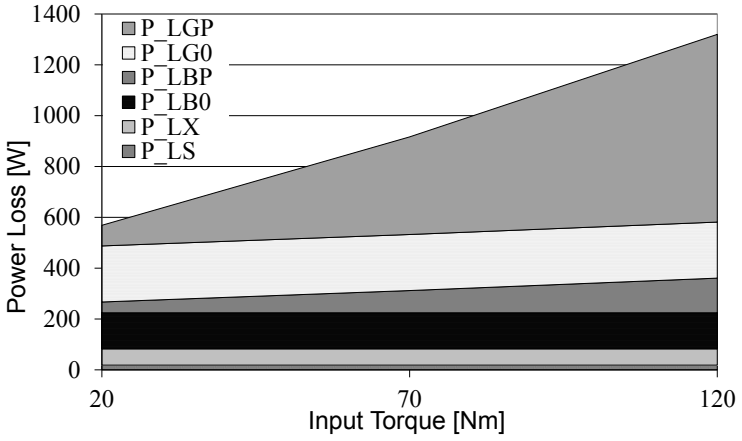

Figure 3-7: Predicted power loss of an example 6-speed manual transmission [3_KUR09]

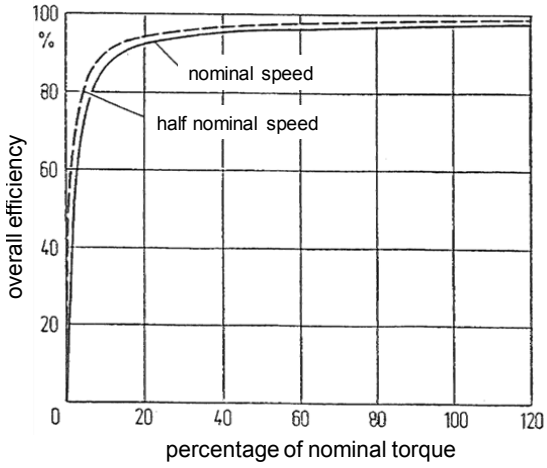

Figure 3-8: Approximate power loss of planetary gear set [2_MUL01]

For the purpose of power loss prediction in early design stages when only a few parameters are known, it is generally accepted to merge all power loss portions to an approximate efficiency factor multiplied with the input power of the gear set or the basic train. Hardy [4_HAR60] chooses an overall basic train efficiency factor of 98% to 99% for his calculations. Dudley [1_DUD94] indicates a power loss of 0,5% to 3% per mesh of spur and helical gears. Mueller [2_MUL01] proposes an efficiency of 99% for external gears and 99,5% for internal gears as a good approximation:

$$\eta_0 = \prod \eta_{e/i} \qquad (3.7)$$

η_0	[-]	basic train efficiency	$\eta_{e/i}$	[-]	efficiency of external/internal basic gearing included in the basic train

Looman [1_LOO96] as well as the VDI norm 2157 [4_VDI78] specify power loss factors of 99% for every loaded gear mesh and 99% to 99,5% for the bearings altogether appearing in the basic train. Neussel [4_NEU62] even comes to the conclusion that 99,2% to 99,8% is an appropriate value as basic efficiency depending on the gear type included. Load-

independent power losses are assumed to be included in these efficiency factors whereupon they are hard to determine without having a complete set of detailed parameters available.

3.2 Representation and abstraction methods

Different representation and abstraction methods were used for simplifying the structural analysis of PGTs in general and especially of coupled PGTs. Some methods are suitable for the purpose of synthesis and/or allow a check of the designability or the isomorphism in respect to similar designs.

3.2.1 Wolf symbolism

The Wolf symbolism is a widely-used abstraction method and is to be traced back to the work of its eponym Wolf [4_WOL49 and 2_WOL58]. An elementary Wolf symbol consists of a circle representing a single PGT and three edges connected to the circle which represent the central shafts (**Figure 3-9**). Often, but not necessarily, the summation shaft is marked as a double edge. The edge representing the central shaft of the carrier is extended into the circle. Then, positive-ratio and negative-ratio PGTs can easily be distinguished (cf. Section 0).

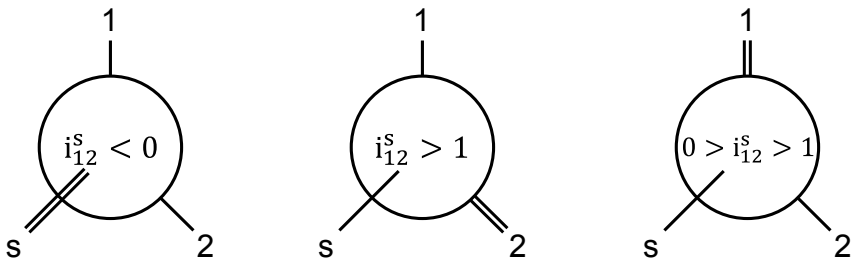

Figure 3-9: Elementary Wolf symbols for single PGTs with different basic ratios

Planets as well as design features do not appear in Wolf symbols. Thus, this representation is detached from geometry parameters and offers a clear overview of the structure and the internal couplings. As an example, **Figure 3-10** shows the Wolf symbol of the coupled PGT of **Figure 2-10**.

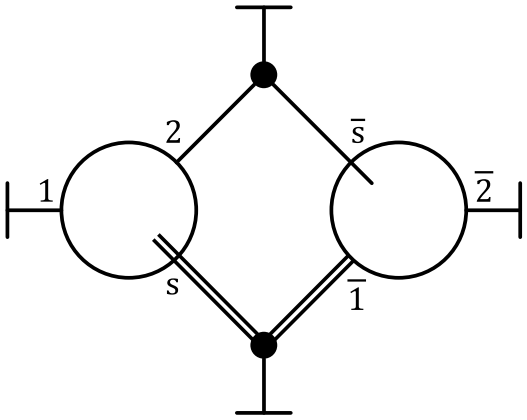

Figure 3-10: Wolf symbol of a coupled PGT consistent with Figure 2-10

According to Mueller [2_MUL01], coupled PGTs featuring the Wolf symbol structure of **Figure 3-10** are called *elementary coupled PGTs* and have a kinematic DOF of two. The high abstraction level of the Wolf symbolism leads to a hindered identification of the resulting transmission

ratios of coupled PGTs. Hence, Arnaudow [4_ARN96 and 4_ARN01] proposes to indicate the difference shaft, which is charged with the higher torque, with a thick edge. Then, a speed increase or reduction as well as a positive or negative ratio can intuitively be identified by means of torque ratios.

For a kinematics analysis, the basic ratio must be given for each Wolf symbol. The solving of kinematic relationships is carried out by using the methodology outlined in Section 2.4.1.3. In terms of statics analysis, the Wolf symbols can be cut free and treated similarly to Section 2.4.2. There is no special Wolf symbol with more than three central shafts known for CCPGTs.

3.2.2 Kutzbach and Helfer diagram

Both Kutzbach [4_KUT27] and Helfer [4_HEL66 and 4_HEL67] convert a PGT into an equivalent lever model using a lever analogy. Using this lever model, speeds and torques can be analyzed conveniently. The central shafts appear as nodes in the lever model (**Figure 3-11**). Translational (vertical) speeds of the nodes correspond to rotational speeds of the central shafts. Likewise, (vertical) forces at the nodes correspond to torques at central shafts. Therefore, the length of the lever arms is a function of the basic ratio.

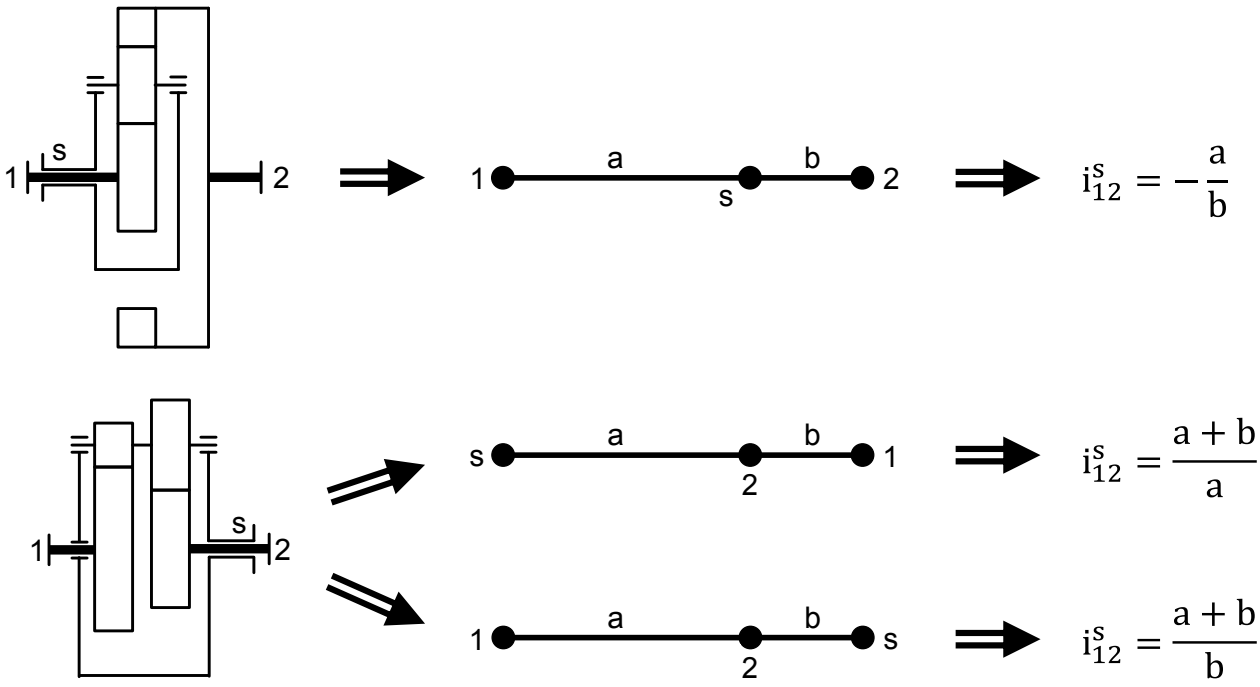

i	[-]	basic ratio	a, b	[mm]	length of lever arm

Figure 3-11: Representation of a single PGT by an equivalent lever

In respect of the speeds, it is easy to see whether the ratio is positive or negative and whether the speeds are high or low, respectively. **Figure 3-12** shows an example for an operating condition with three rotating shafts. Corresponding to the single PGT, the lever features two kinematic DOF for this model. A pure vertical translation corresponds to the coupling case, a pure rotation around the node s corresponds to the meshing case.

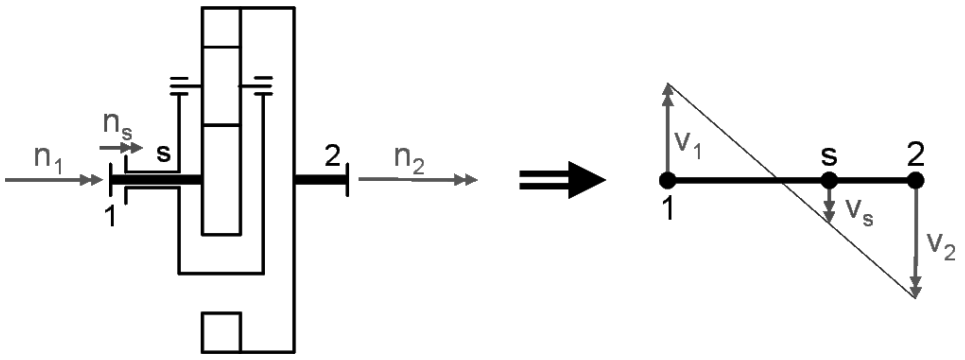

n	[1/s]	rotational speed	v	[m/s]	translational speed

Figure 3-12: Speed equivalency between PGT and lever model

Regarding the torque and force equivalency, it is noticed that the node representing the summation shaft must be located at the middle of the lever to fulfill the requirements concerning the force and torque balance.

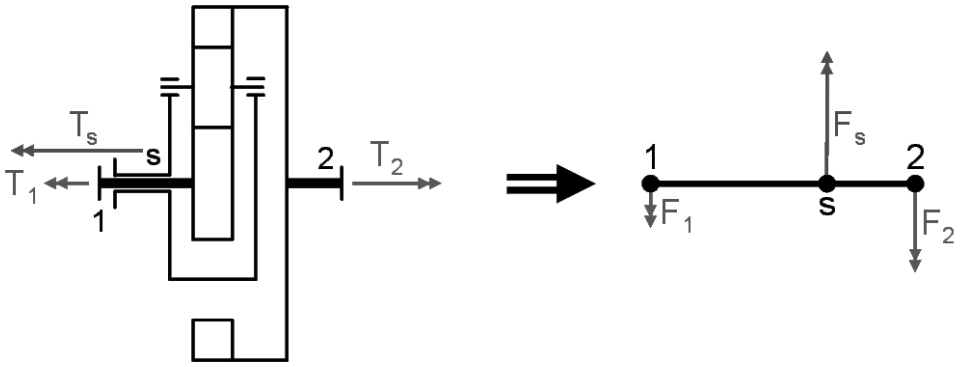

T	[Nm]	torque	F	[N]	force

Figure 3-13: Torque and force equivalency between PGT and lever model

Similarly, CCPGTs can also be converted into a lever model (**Figure 3-14**). The lever features the same number kinematic and static DOF. Therefore, the lever model offers a very clear illustration of the speed and torque ratios of a CCPGT.

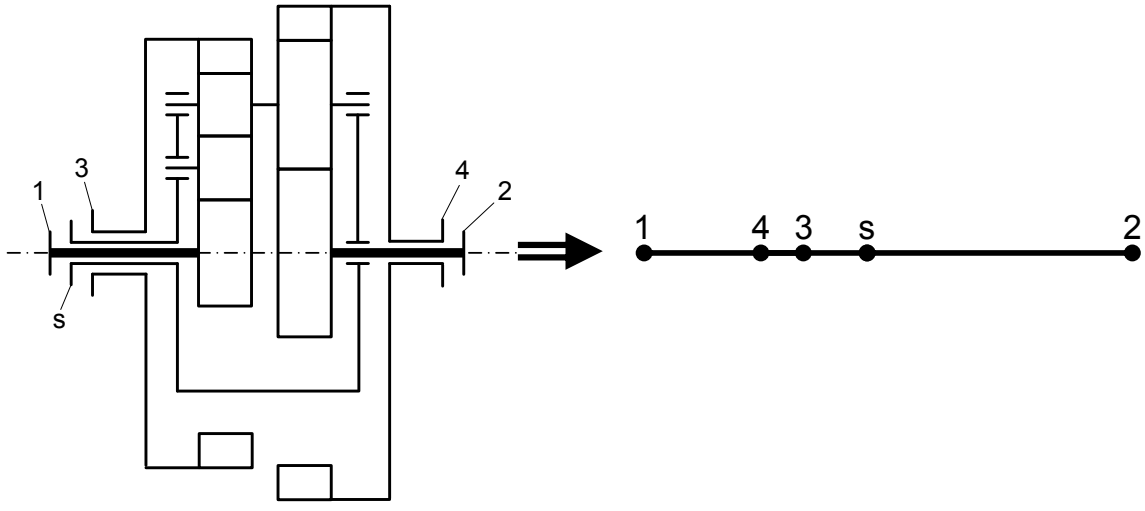

Figure 3-14: Representation of a CCPGT by an equivalent lever

3.2.3 Graph theory

The representation of PGTs by means of graph theory is a common utility for systematic structure and kinematics analysis. First derivations of PGT graphs are related to Buchsbaum and Freudenstein [4_BUC70]. The authors show that different graph illustrations exist, whereupon the most accepted one is discussed here. Tsai published a detailed description of graph theory for PGTs amongst other things in [5_TSA01]. Hsieh and Tsai [4_HSI96b], Olson, Erdman and Riley [4_OLS91], Liu, Chen and Chang [4_LIU04], as well as Wojnarowski and Lidwin [4_WOJ75] use graph theory for structure and kinematics analysis of PGTs.

According to the authors mentioned above, a PGT consists of bodies interacting with each other by means of links. The relevant links are revolute joints R and gear pair joints G (cf. Section 2.6.1). A graph features vertices representing the bodies and edges representing the links which connect the vertices in pairs. Frequently, a thick edge acts for a gear pair joint and a thin edge stands for a revolute joint. Furthermore, a unique graph representation can be achieved by a canonical graph. In a canonical graph representation, the housing vertex is denoted as the root. In addition, the thin edges are marked with an identifier standing for the level of the axis of rotation and the center distance, respectively. **Figure 3-15** shows an example.

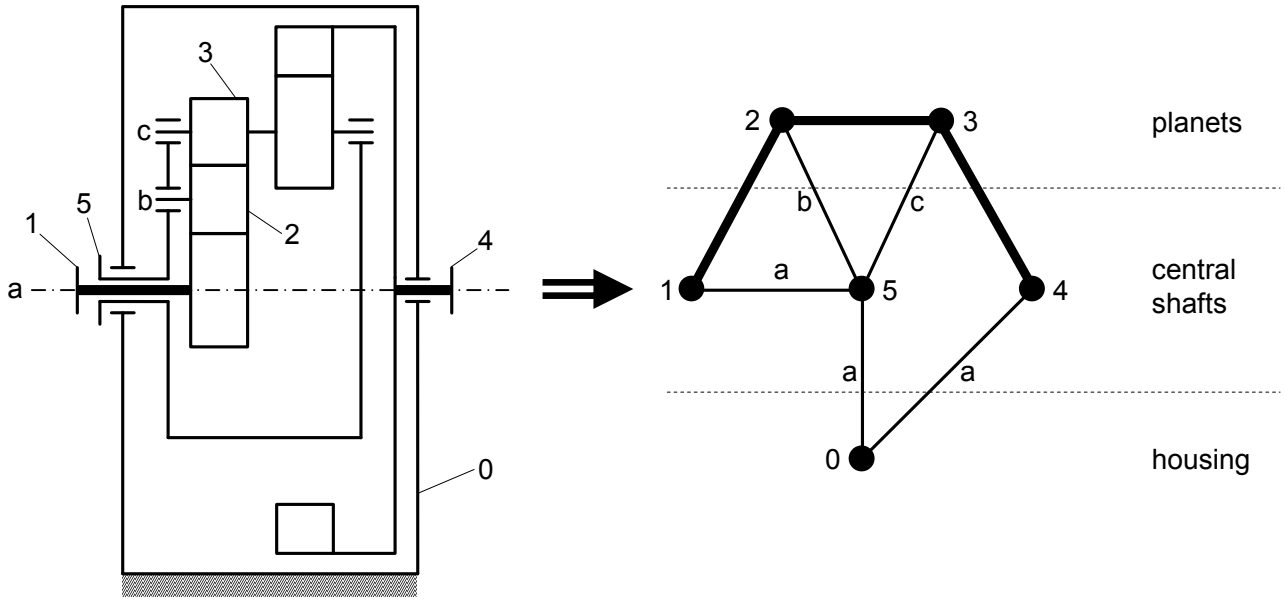

Figure 3-15: Canonical graph of an example single PGT

PGTs belong to the group of planar mechanisms according to Tsai. He postulates several theorems characterizing the graph of a PGT. The graph obtained by removing all geared edges from the graph is a tree (which is a graph without circuits) containing all vertices of the original graph. Thus, the number of rotating pairs is equal to the number of vertices minus one. Further, all thin edges of the same level in combination with their end vertices form a tree. The kinematic DOF is equal to number of rotating pairs minus the number of gear pairs.

Instead of drawing the graph of a PGT, a matrix representation is useful for computer-based calculation steps. Different matrix representations exist. Common ones are the adjacency matrix A and the incidence matrix B. The adjacency matrix is symmetric, with a dimension that is equal to the number of vertices. Its elements are either 1 if vertex i is directly connected to vertex j or 0. The incidence matrix relates the vertices and edges. It features as many rows as vertices exist and as many columns as edges occur. If vertex i is an end vertex of edge j the matrix element is 1, otherwise it is 0. Both matrices constitute a unique description of a given graph. Algorithms are known e.g. to find the shortest trace between vertices, to check planarity or isomorphism.

3.3 Direct efficiency calculation methods

By direct efficiency calculation methods, methods which require a kinematics and statics analysis to determine the power flow and its direction are meant. The calculations are carried out taking into account a realistic transmission model.

To consider power losses according to Section 3.1, different methods exist which are to be distinguished in respect of complexity and calculation effort. Here, it is always assumed that power losses affect torque ratios only, but not the speeds at least for steady-state operating conditions.

Simple methods only consider load-dependent power losses. Load-dependent power losses occur if meshing power is existent. According to Mueller [2_MUL01] the basic efficiency of single PGTs is defined as the negative power ratio the output and input meshing power of the basic train depending on the direction of the meshing power flow:

$$\eta^{s}_{1\,2} = -\frac{P_{m2}}{P_{m1}} = -\frac{T_2 \cdot (n_2 - n_s)}{T_1 \cdot (n_1 - n_s)} = -\frac{T_2}{T_1} \cdot \frac{1}{i^{s}_{1\,2}} \quad \text{for } P_{m1} > 0 \; and \; P_{m2} < 0$$
$$\eta^{s}_{2\,1} = -\frac{P_{m1}}{P_{m2}} = -\frac{T_1 \cdot (n_1 - n_s)}{T_2 \cdot (n_2 - n_s)} = -\frac{T_1}{T_2} \cdot i^{s}_{1\,2} \quad \text{for } P_{m1} < 0 \; and \; P_{m2} > 0 \qquad (3.8)$$

$\eta^{s}_{1\,2}, \eta^{s}_{2\,1}$	[-]	basic efficiency	$i^{s}_{1\,2}$	[-]	basic ratio
P_{mx}	[W]	meshing power of central shaft x	T	[Nm]	(external) torque
n	[1/s]	speed			

Although, η^{s}_{12} and η^{s}_{21} are not equal in general, this slight difference is often neglected as these variables are merged to η_0. Then, the torque ratio can be written as:

$$\frac{T_2}{T_1} = -i^{s}_{1\,2} \cdot \eta_0^{w1} \quad \text{with} \quad w1 = \begin{cases} +1 & \text{if } P_{m1} > 0 \\ -1 & \text{if } P_{m1} < 0 \\ 0 & \text{coupling case or loss} - \text{free case} \end{cases} \qquad (3.9)$$

η_0	[-]	basic train efficiency	w1	[-]	efficiency exponent
P_{m1}	[W]	meshing power of central shaft 1	T	[Nm]	torque
$i^{s}_{1\,2}$	[-]	basic ratio			

As a single PGT only features one static DOF, it is sufficient to know the kinematics as well as the inputs and outputs to calculate the overall efficiency. For every operating condition, the basic efficiency formula for single PGTs reads:

$$\eta = 1 - \frac{2 \cdot \pi \cdot T_1 \cdot (n_1 - n_s) \cdot (1 - \eta_0^{w1})}{\Sigma P_{in}} \qquad (3.10)$$

η	[-]	overall efficiency	η_0	[-]	basic train efficiency
T_1	[Nm]	torque of central gear 1	$w1$	[-]	efficiency exponent
n_1,n_s	[1/s]	speed of central gear 1 / carrier	P_{in}	[W]	(absolute) input power

Equation (3.10) shows that the overall efficiency is larger than the basic efficiency if the meshing power is smaller than the input power and vice versa. The meshing power can only be larger than the input power in the presence of certain operating conditions for positive-ratio drives.

Many authors like e.g. Brandenberger [4_BRA29], Chen and Angeles [4_CHE07], Foerster [4_FOR69], Hock [4_HOC65], Jakobsson [4_JAK66], Krause [4_KRA61], Pennestri and Freudenstein [4_PEN93b] and Pasquier [4_PAS94] proposed different formulations, which were all based on equation (3.10). Pennestri and Valentini provided an overview and comparison of formulas in [4_PEN03b]. Nikitin and Reschetow [4_NIK53] described an even more fundamental method using (friction) forces and lever arms.

In order to maintain linearity, the basic efficiency itself must not depend on the input power and torque respectively. Therefore, the basic efficiency is frequently set as a factor in the range of approx. 97% to 99% (cf. Section 3.1.4) for rough and simple calculations. For this, Hedman [4_HED88 and 4_HED93] describes a systematic procedure to generate the equation system for coupled PGTs containing further transmission elements.

For CCPGTs with more than one static DOF, Maegi [4_MAG74] proposed an analogical method by inserting efficiency factors into torque balance equations, not for an entire basic train, but for each basic gearing (cf. Section 2.4.2.2). To identify the direction of meshing power flow in each basic gearing a loss-free torque analysis is to be performed first. By means of loss-free torques and meshing speeds the power flow directions can be determined assuming that the direction of power flow does not change when power losses are considered. Duan [4_DUA01] proposed the same procedure for CCPGTs of the Wolfrom type [4_WOL12]. Due to the multitude of basic gearings, this procedure is cumbersome as it leads to a large number of somewhat confusing equations.

If all kind of power losses are to be considered also using non-linear equations, computer-based calculation methods are proposed by Pennestri and Mantriota [4_PEN03a] as well as by Stangl [4_STA07]. A converging iteration helps narrow down torques and load-dependent power losses.

As a special characteristic, Stangl [4_STA07] treats every power loss as an additional virtual brake acting on the appropriate body. In case of meshing power losses, a distinction is to be made by means of the meshing power flow direction (**Figure 3-16**). It is easy to see,

that the occurrence of power losses does not affect the static DOF, since for every power loss an additional conditional equation is to be added to the system.

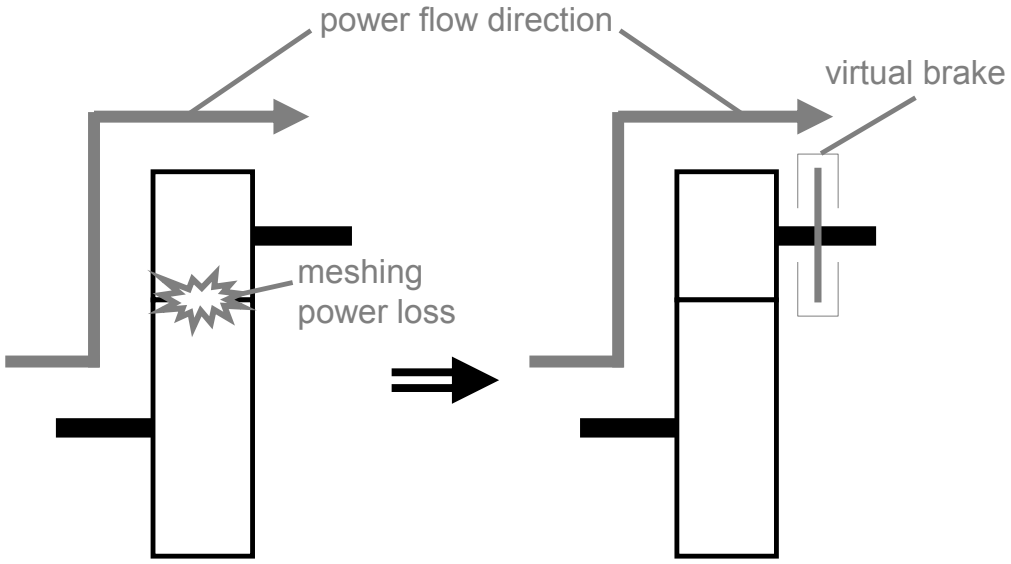

Figure 3-16: Principle of virtual brakes [4_STA07]

3.4 Indirect efficiency calculation methods

Indirect efficiency calculation methods differ from direct methods in respect of the identification of the meshing power flow or in respect of the structural representation.

Li [5_LI93] took into account coupled PGTs with one kinematic DOF and a single in- and output. He interpreted the inclusion of basic efficiency factors as a small alteration of the (torque) ratio of basic gearings, meaning that the basic ratio is to be multiplied or divided by the efficiency factor according to equation (3.9) depending on the meshing power flow direction. It is clear, that the absolute value of the output power has to be smaller compared to the loss-free case due to power losses. After accomplishing a kinematics analysis for loss-free operating conditions, a partial derivative of the output to input power ratio in respect of the basic ratio of each basic train or basic gearing reveals the meshing power flow direction in each basic train or basic gearing:

$$\frac{\partial \left| \frac{P_{output}}{P_{input}} \right|}{\partial i_{12}^{s}} \overset{!}{<} 0 \quad \Rightarrow \quad \text{distinction of cases: } w1 = +1/-1 \qquad (3.11)$$

i_{12}^{s}	[-]	basic ratio	w1	[-]	efficiency exponent
P_{output}	[W]	output power			

This distinction of cases can be reached only by forming the expression of the overall transmission ratio as a function of the basic ratios. Thus, a statics analysis is not necessary for determining the overall efficiency.

A more general expression was derived by Kreines [4_KRE43, 4_KRE47 and 4_KRE65], later Diaconescu and Duditza [4_DIA94a and 4_DIA94b] as well as del Castillo [4_DEL02b] arrive at the same conclusion. Regarding a transmission featuring one kinematic DOF and a single input and a single output, the ratio of the meshing power of a certain basic gearing or basic train to the input power is equal to the partial derivate of the overall transmission ratio in respect of the basic ratio multiplied by the quotient of the basic ratio and the overall ratio:

$$\frac{P_{m1}}{P_{input}} = \frac{\partial i_{in,out}}{\partial i^{s}_{1\,2}} \cdot \frac{i^{s}_{1\,2}}{i_{in,out}}$$

$$\Rightarrow \quad w1 = \operatorname{sgn}\left(\frac{\partial i_{in,out}}{\partial i^{s}_{1\,2}} \cdot \frac{i^{s}_{1\,2}}{i_{in,out}}\right) \qquad (3.12)$$

$i_{in,out}$	[-]	overall transmission ratio	w1	[-]	efficiency exponent
$i^{s}_{1\,2}$	[-]	basic ratio	P_{input}	[W]	input power
P_{output}	[W]	output power	P_{m1}	[W]	meshing power of central gear 1

This approach is not only valid for single PGTs, but also for coupled PGTs. As a strict precondition, the transmissions must not feature more than one static DOF. After determining the meshing power flow direction for each basic gearing or basic train, the statics analysis is to be performed according to Section 3.3.

Another indirect efficiency calculation method replaces the realistic transmission model of a CCPGT by a substitution figure using Wolf symbols and is traced back to Wolf [2_WOL58]. Thereby, the rather complex structure of a CCPGT is simplified and the system of equations is reduced. The method is suitable for determining the efficiency of compound ratios with only three loaded central gears, with the carrier being unloaded. First, the basic trains or single PGTs are identified within the CCPGT. Two single PGTs are necessary to form a substitution figure that is *kinematically-equivalent* to the CCPGT and featuring a kinematic DOF of two. Here, three solutions are obtained. Hence, a CCPGT is often regarded as being compound out of single PGTs sharing the carrier and a central gear. **Figure 3-17** shows a Ravigneaux type CCPGT and its kinematically-equivalent substitution figures.

Among the substitution figures, only one represents the internal power flow of the real CCPGT in a correct way as a superposition of power flows of each single PGT included. This substitution figure features one summation shaft pointing to the inside and one pointing to the outside of the structure and is termed *functionally-equivalent*. Since only three central shafts of the functionally-equivalent substitution figure are loaded, it can be treated just like a single PGT. The substitution basic ratio as well as the substitution basic efficiency is easily obtained as a function of the parameters of the single PGTs included if the shared central gear is imagined as being fixed.

Foerster [4_FOR69], Klein [4_KLE82], Looman [4_LOO88 and 4_LOO99] and Mueller [2_MUL01] all adopted this method. It offers a simple and clearly represented efficiency calculation procedure with a minimum of basic ratios to be considered. Nevertheless, all

authors limited themselves to a maximum of four shafts for a CCPGT. There is no substitution method defined for more than three shafts of a CCPGT being loaded.

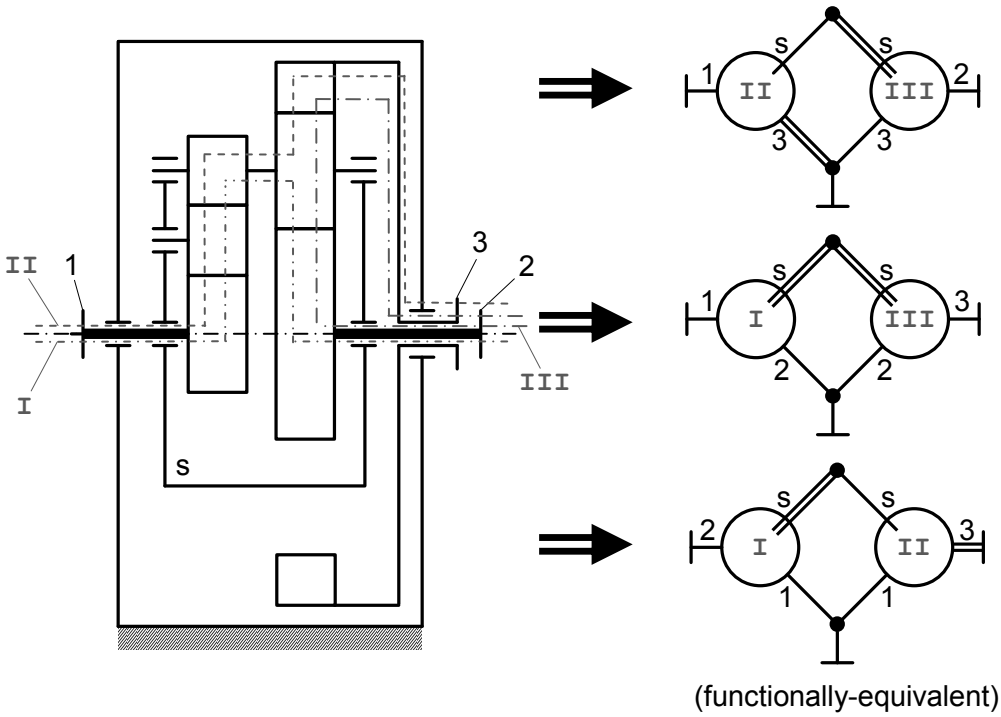

Figure 3-17: Kinematically-equivalent substitution figures for the Ravigneaux type CCPGT

3.5 Special operating conditions and self-locking

Single PGTs can show very high efficiency values if the coupling power is large in comparison to the meshing power. As a matter of fact, efficiency can also be very low in case of positive-ratio drives if the meshing power is explicitly larger than the external power. Further, idle power can occur in coupled PGTs reducing the efficiency e.g. according to Arnaudow [4_ARN04].

As a limit case, self-locking can occur with the whole transmission or at least one shaft being blocked. Self-locking was proved theoretically and experimentally for single PGTs by several authors like Jakobsson [4_JAK60], Mueller [4_MUL87], Ikejo et al. [4_IKE09]. Larsson, Carlsson and Jakobsson [4_LAR57] provide complete efficiency diagrams with shaded self-locking range for single PGTs with constant basic efficiency (**Figure 3-18**).

As for single PGTs, self-locking can only happen at the central shaft connected to the carrier if the basic ratio is within a range defined by the basic efficiency:

$$\eta_0 < i_{1\,2}^{s} < \frac{1}{\eta_0} \qquad (3.13)$$

η_0	[-]	basic efficiency	$i_{1\,2}^{s}$	[-]	basic ratio

Bouché [4_BOU88] proved that coupled PGTs can be self-locking in one direction whereas in the opposite direction the efficiency can be very high even in the absence of extreme transmission ratios. Neussel [4_NEU62] investigated the self-locking capability of coupled and complex-compound PGTs using Wolf symbols. Boettcher and Sierig [4_BOT69 and 4_SIE68] as well as Oernhagen [4_ORN63] demonstrated self-locking for the Wolfrom type CCPGT if it works as a speed increaser. In these references, only the operating conditions with a maximum of three loaded central shafts were taken into account.

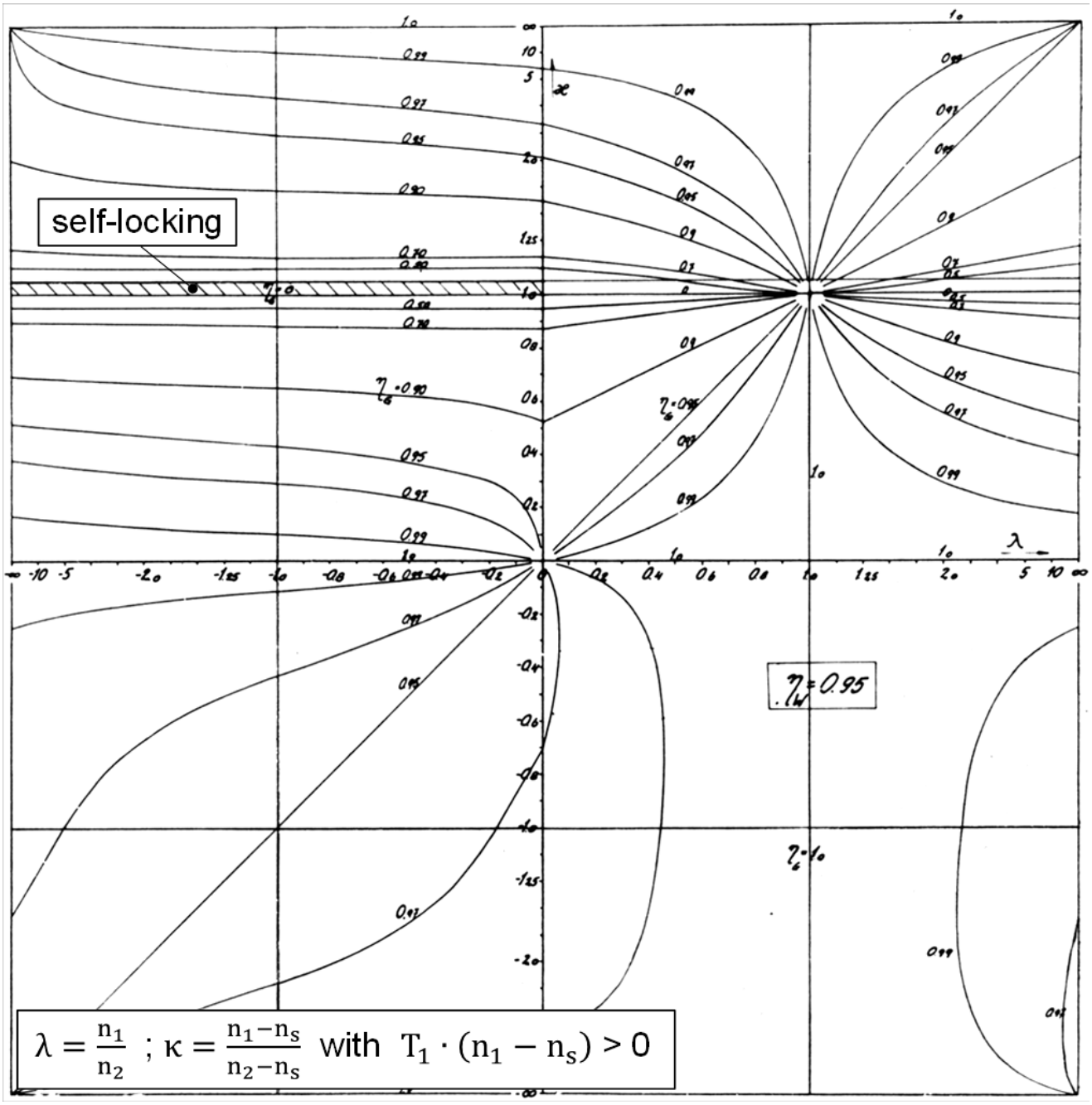

Figure 3-18: Efficiency diagram for single PGTs with 95% basic efficiency acc. to [4_LAR57]

3.6 Synthesis of planetary gear transmissions

The question of which PGT design is best for a certain application or how to combine PGTs in the right way is hard to answer. Very often, PGTs are designed based on experience and expert knowledge. Lists of PGT designs can be found in many standard works of such as Mueller [2_MUL01] or Volmer [2_VOL90]. Gibson and Kramer listed 22 essential single PGTs [5_GIB84]. Early references (e.g. by Altmann [5_ALT27b]) refer to numerous designs of single and coupled PGTs for different purposes.

If not taking advantage of computer-based calculations, graphical methods were employed. For instance, Pickard and Koepf [5_PIC76] tried to reverse the Kutzbach diagram (cf. Section 3.2.2) to find simple solutions for manageable problems. Other authors like Arnaudow and Karaivanov [5_ARN03, 5_ARN05a, 5_ARN05b and 5_ARN10] and Nitescu [5_NIT83 and 5_NIT86] used Wolf symbols for a systematic generation of different transmission structures up to a certain complexity level.

Frequently, synthesis methods are related to particular problems and applications. As CCPGTs, especially of the Wolfrom type [4_WOL12], are often used as high ratio drives, Gaunitz [5_GAU50], Mulzer [5_MUL09] and Loersch [5_LOR67] created several designs. Stahl and Mulzer [6_STA09] came up with a very simple design derived from the Wolfrom type CCPGT. Schnetz [5_SCH71 and 5_SCH76] presented a systematic synthesis and classification in terms of efficiency and designed space of high-ratio CCPGTs starting from chosen predefined designs. Likewise, Dreher [5_DRE83] presented a synthesis for coupled PGTs with up to two simple PGTs.

The problem of generating a reasonable automatic transmission is taken up by many engineers. An early application of a CCPGT in an automatic transmission of the Ford T is shown in **Figure 3-19**. Ott [5_OTT68] illustrated an entire synthesis of 3-speed automatic transmissions including up to two single PGTs featuring one plane of mesh engagement. Li [5_LI93] showed examples of synthesizing 4- and 5-speed automatic transmissions by means of graphical methods. Gumpoltsberger [5_GUM06] made use of computer-based combinatorics to create 7-, 8- and 9-speed automatic transmissions including exclusively simple PGTs. Here, graph theory is used to check the designability and isomorphism. Kahraman and Ligata [5_KAH04] published a procedure for creating structures of automatic transmission without limiting to certain PGT designs.

Graph theory constitutes another general possibility for PGT synthesis. Many authors such as An and Peiwen [5_AN01], Chen and Liu [5_CHE99], del Castillo [5_DEL02a], Hsu [5_HSU00], Shin and Krishnamurty [5_SHI93] or Tsai [5_TSA87] dedicated themselves to finding reasonable graphs for mechanism with different numbers of kinematic DOF, although, the conclusion to concrete transmission structures was missing or no technical problem was specified. Freudenstein [5_FRE71] or Chatterjee and Tsai [5_CHA96] presented first approaches of a systematic assembly of transmission structures based on graphs. Thereby, the generated solutions often lack of practical usability due to their complexity. Wojnarowski [5_WOJ06] provided a descriptive overview of PGT synthesis using

graph theory. In another context Domian [5_DOM01] applies graph theory for analyzing and generating structures of manual and dual clutch transmissions.

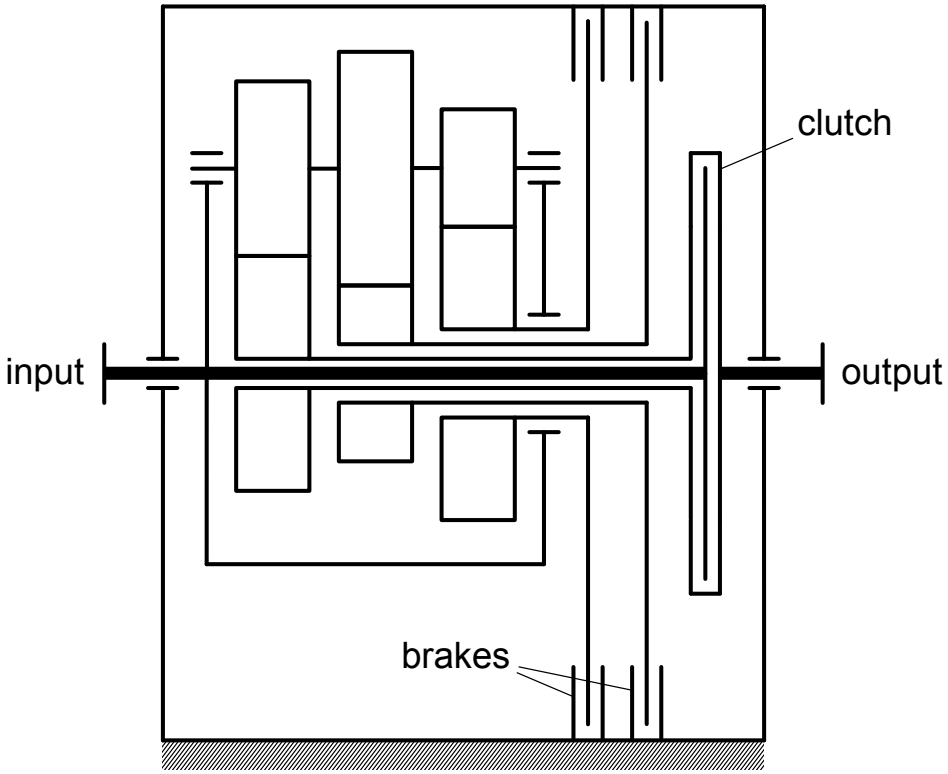

Figure 3-19: Structure of the automatic transmission of the Ford T acc. to [2_MUL01]

4 Efficiency determination for complex-compound planetary gear transmissions

4.1 Calculation by means of graph theory and graph representation

Graph representation offers a view on CCPGTs reduced to the essentials. By modeling a CCPGT as a graph, the relevant connections and interrelationships between bodies come forward. Also, the internal power flow considering power losses can be identified and calculated automatically using graph theory algorithms.

4.1.1 Graph representation of complex-compound planetary gear transmissions

According to equation (2.44) the number of bodies or vertices in a graph is a function of the number of central shafts and planets:

$$\mathrm{B} = \mathrm{CS} + \mathrm{P} + 1 \qquad (4.1)$$

B	[-]	total number of bodies	CS	[-]	total number of central shafts
P	[-]	total number of planets			

Substituting equation (4.1) into (2.47) yields:

$$\mathrm{G} = \mathrm{CS} + \mathrm{P} - 2 = \mathrm{B} - 3 \qquad (4.2)$$

G	[-]	total number of basic gearings	CS	[-]	total number of central shafts
B	[-]	total number of bodies	P	[-]	total number of planets

The number of basic gearings is identical to the number of geared edges in the graph. The number of geared members is equal to the sum of central gears and planets diminished by one:

$$\mathrm{G} = \mathrm{CS} + \mathrm{P} - 2 = \mathrm{CG} + \mathrm{P} - 1 \qquad (4.3)$$

G	[-]	total number of basic gearings	CS	[-]	total number of central shafts
CG	[-]	total number of central gears	P	[-]	total number of planets

Subtracting the number of geared members from the total number of bodies, it is clear that there are always two non-geared members in a CCPGT, the carrier and the housing:

$$B - CG - P = CS + P + 1 - CG - P = 2 \quad \Longrightarrow \quad CG + P = B - 2 \qquad (4.4)$$

B	[-]	total number of bodies	CS	[-]	total number of central shafts
G	[-]	total number of basic gearings	P	[-]	total number of planets
CG	[-]	total number of central gears			

Naturally, every geared member must be connected to a gear pair edge. Therefore, the number of gear pair edges is one less than the number of geared members which means that the subgraph of a single PGT or CCPGT consisting only of gear pair edges and their end vertices is a coherent tree. Likewise, according to Section 3.2.3, the subgraph obtained by removing all gear pair edges is also tree, but it contains all vertices of the original graph.

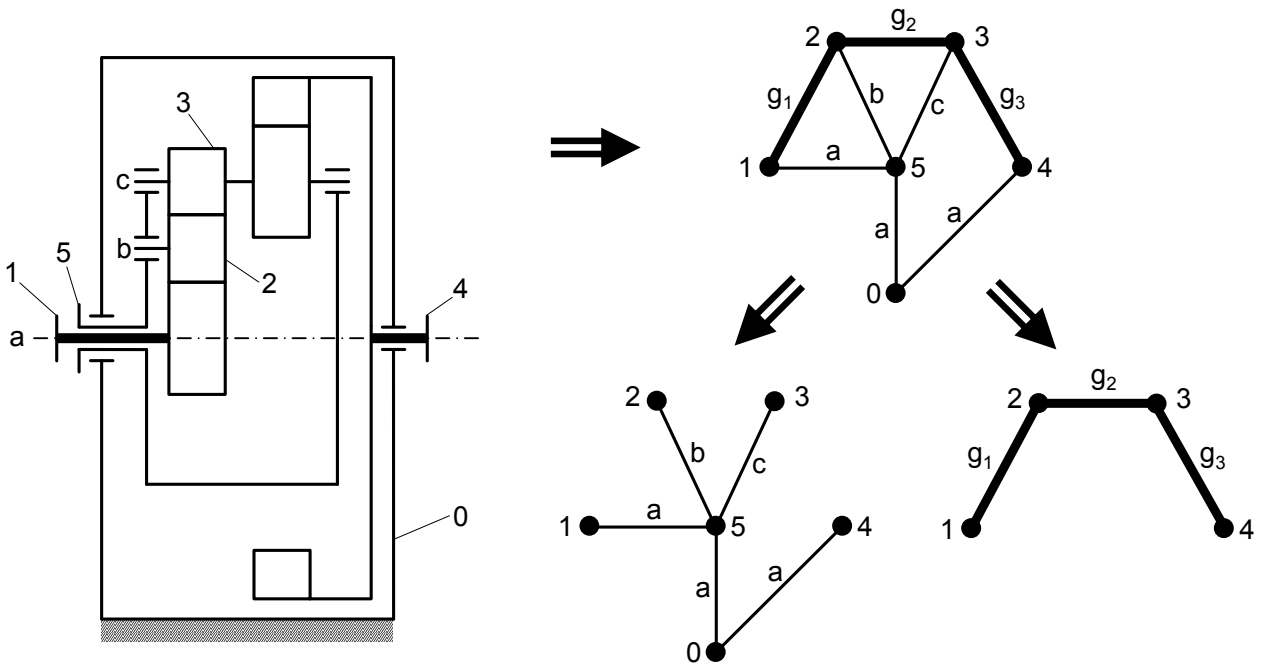

Figure 4-1: Example subdivision of a single PGT graph

The graph of the single PGT shown in **Figure 4-1** is subdivided into a tree of gear pair edges and a tree of turning pair edges. The gear pair edge tree is remarkable because of its chained structure representing the basic train. In accord with Section 2.1 the two central gears of a single PGT appearing in the gear pair edge subgraph are indirectly connected via the planets. Thus, the planets occur as binary vertices in the geared edge subgraph featuring exactly two incident gear pair edges, whereupon the number of planets is theoretically arbitrary.

In contrast, CCPGTs contain a least three central gears. Every two central gears are indirectly connected via chain of gear pair edges. This means that there exists at least one non-binary planet with at least three incident gear pair edges (**Figure 4-2**). Again, the number of planets is theoretically not limited as well as the number of central gears meshing with a planet. The shortest trace from one central gear to another represents the corresponding basic train.

Referred to the definition of a tree, the geared edge subgraph of a single PGT or CCPGT does not contain any circuits. Circuits consisting only of geared edges would represent a ring closure of transmission ratios which leads to blocking of the mechanism except for a ring transmission ratio of exactly +1. This characteristic is valid for PGTs if multiple, identical planets are equally spaced. These parts are usually not represented due to rotational symmetry and redundancy.

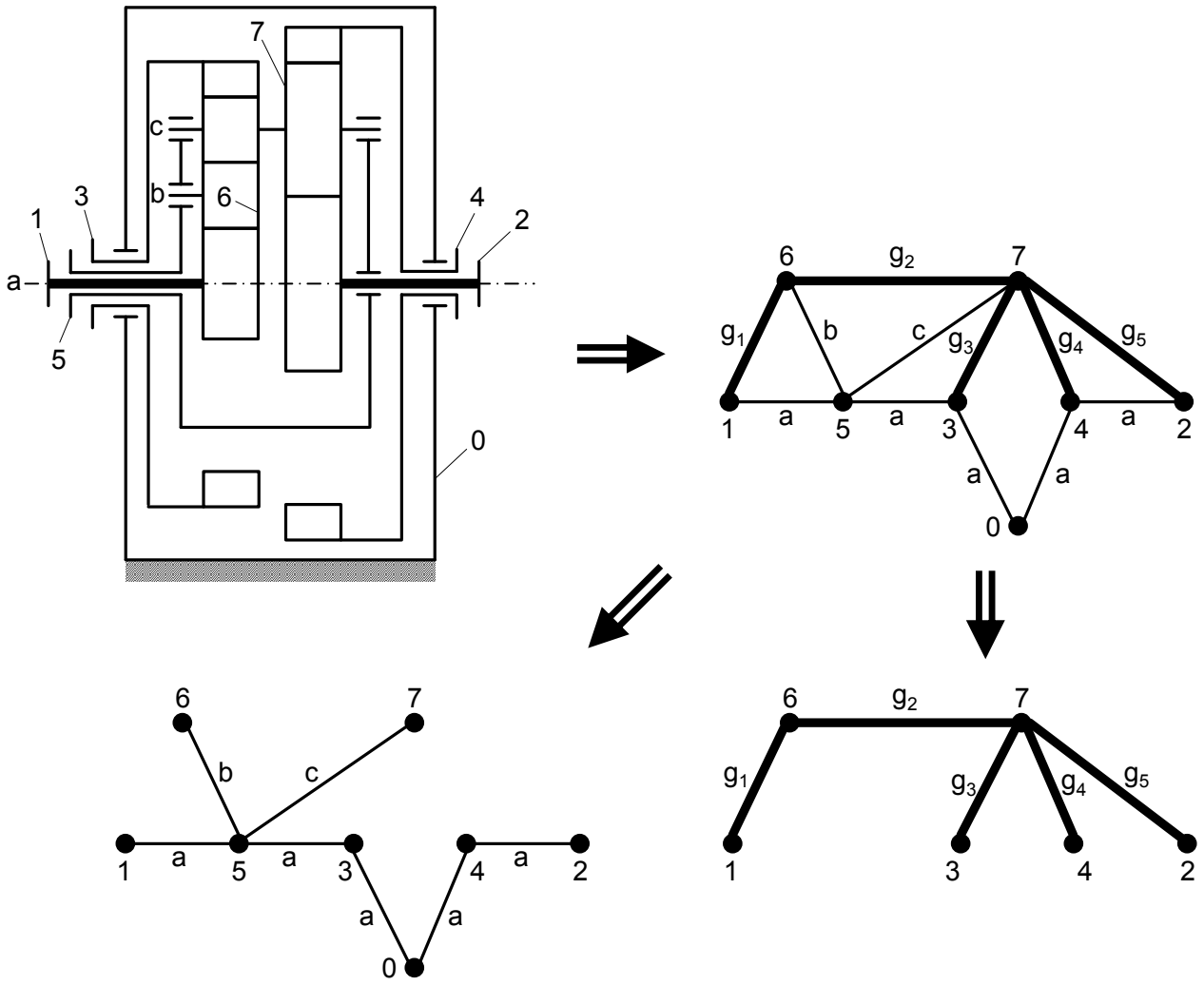

Figure 4-2: Example subdivision of a CCPGT graph

The corresponding matrix notation in terms of a symmetric adjacency matrix for the CCPGT shown in **Figure 4-2** containing a turning and a gear pair submatrix reads as follows:

$$\mathbf{A} = \begin{pmatrix} 0 & 0 & 0 & a & a & 0 & 0 & 0 \\ 0 & 0 & 0 & 0 & 0 & a & g_1 & 0 \\ 0 & 0 & 0 & 0 & a & 0 & 0 & g_5 \\ a & 0 & 0 & 0 & 0 & a & 0 & g_3 \\ a & 0 & a & 0 & 0 & 0 & 0 & g_4 \\ 0 & a & 0 & a & 0 & 0 & b & c \\ 0 & g_1 & 0 & 0 & 0 & b & 0 & g_2 \\ 0 & 0 & g_5 & g_3 & g_4 & c & g_2 & 0 \end{pmatrix} \quad (4.5)$$

A	[-]	adjacency matrix	a/b/c	[-]	turning pair edge of level a/b/c
			g	[-]	gear pair edge

4.1.2 Kinematics analysis

By means of the adjacency matrix, an automated derivation of the basic speed coefficient matrix is feasible. Every gear pair edge element of the adjacency matrix A is characterized by its basic transmission ratio $i^{s}_{x\,y}$ and connects the gear pair members x and y. To set up the speed coefficient matrix based on equation (2.23) the corresponding carrier element s has to be identified. In regards of a CCPGT, there is only one carrier present which is already known by means of the modeling process of its graph. However, there is a systematic identification method for the carrier. The end vertices of a gear pair edge are connected by a chain of turning pair edges. Since the subgraph of turning pair edges is a tree, there is only one trace of turning pair edges from one end vertex to the other end vertex of the focused gear pair edge. The circuit consisting of the turning pair trace and the gear pair edge is termed *fundamental circuit* e.g. by Hsieh and Tsai [4_HSI96b]. Within every fundamental circuit one and only one vertex functions as a so-called *transfer vertex* bridging the center distance of the gear pair members. This transfer vertex has to be the carrier vertex and is easily identified since the level of incident turning pair edges is different. For instance, the graph of **Figure 4-2** is decomposed into fundamental circuits in **Figure 4-3**. Obviously, vertex 5 is the transfer vertex of each fundamental circuit.

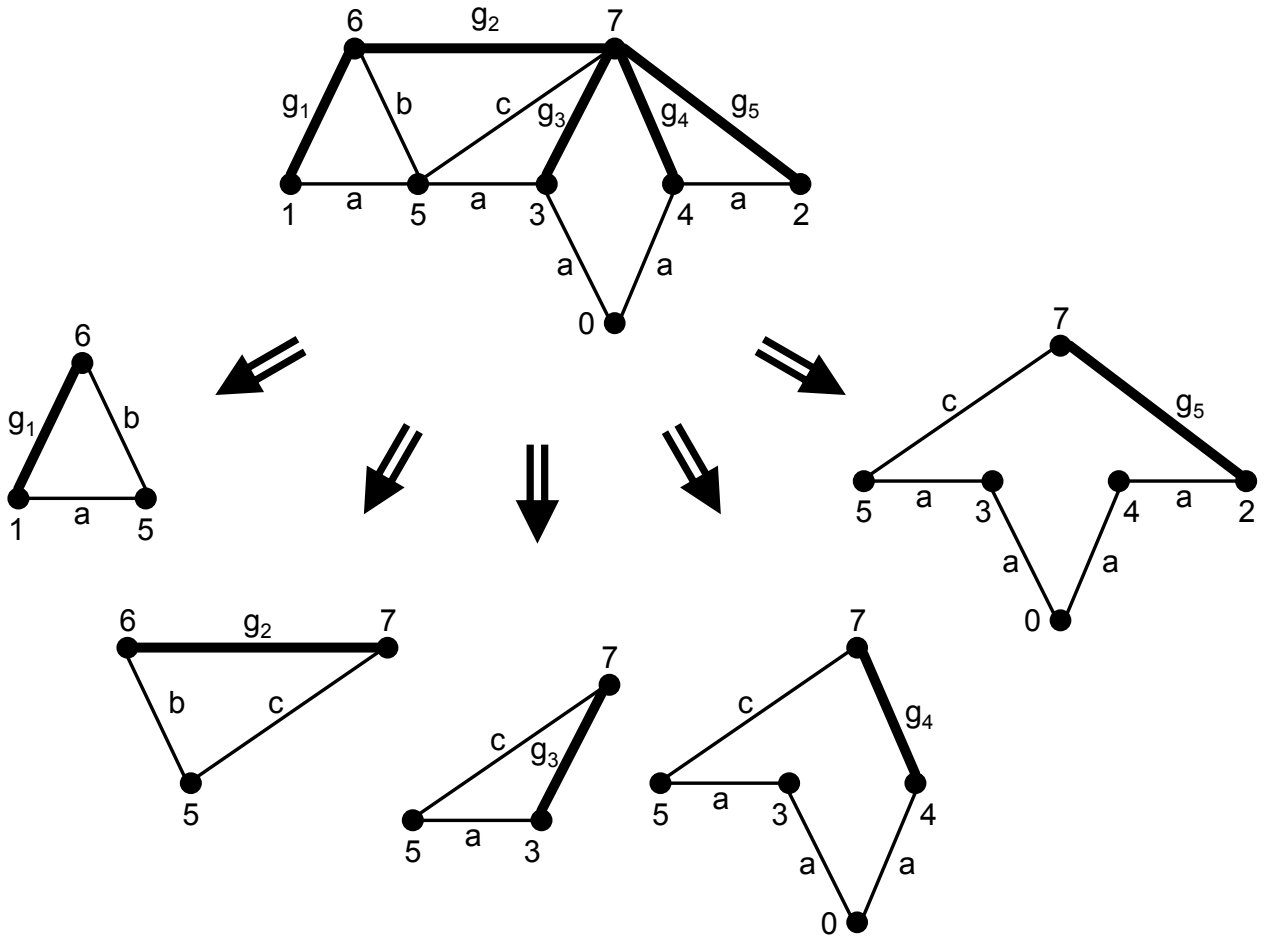

Figure 4-3: Example decomposition of a CCPGT graph into fundamental circuits

Since the adjacency matrix is symmetric, it is sufficient to analyze its upper triangle matrix row by row. For every gear pair edge element g, a row is written for the basic speed coefficient matrix with a 1 at the position x, a $(-\mathrm{i}_{\mathrm{x\,y}}^{\mathrm{s}})$ at the position y and a $(\mathrm{i}_{\mathrm{x\,y}}^{\mathrm{s}}-1)$ at the position of the carrier s of the corresponding fundamental circuit analogical to equation (2.22). Hence, the basic system of equations for the CCPGT in **Figure 4-2** reads:

$$\mathbf{A} = \begin{pmatrix} 0 & 0 & 0 & a & a & 0 & 0 & 0 \\ 0 & 0 & 0 & 0 & 0 & a & g_1 & 0 \\ 0 & 0 & 0 & 0 & a & 0 & 0 & g_5 \\ a & 0 & 0 & 0 & 0 & a & 0 & g_3 \\ a & 0 & a & 0 & 0 & 0 & 0 & g_4 \\ 0 & a & 0 & a & 0 & 0 & b & c \\ 0 & g_1 & 0 & 0 & 0 & b & 0 & g_2 \\ 0 & 0 & g_5 & g_3 & g_4 & c & g_2 & 0 \end{pmatrix}$$

$$\Rightarrow \begin{pmatrix} 0 & 1 & 0 & 0 & 0 & i_{1\,6}^{5} - 1 & -i_{1\,6}^{5} & 0 \\ 0 & 0 & 1 & 0 & 0 & i_{2\,7}^{5} - 1 & 0 & -i_{2\,7}^{5} \\ 0 & 0 & 0 & 1 & 0 & i_{3\,7}^{5} - 1 & 0 & -i_{3\,7}^{5} \\ 0 & 0 & 0 & 0 & 1 & i_{4\,7}^{5} - 1 & 0 & -i_{4\,7}^{5} \\ 0 & 0 & 0 & 0 & 0 & i_{6\,7}^{5} - 1 & 1 & -i_{6\,7}^{5} \end{pmatrix} \cdot \begin{bmatrix} n_0 \\ n_1 \\ n_2 \\ n_3 \\ n_4 \\ n_5 \\ n_6 \\ n_7 \end{bmatrix} = \begin{bmatrix} 0 \\ 0 \\ 0 \\ 0 \\ 0 \end{bmatrix} \quad (4.6)$$

A	[-]	adjacency matrix	i	[-]	basic transmission ratio of gear pair g
a/b/c	[-]	turning pair edge of level a/b/c	n_x	[1/s]	rotational speed of vertex/body x
g	[-]	gear pair edge			

As a CCPGT features two kinematic DOF, two presets are to be inserted (cf. Section 2.6.1). In addition, the speed of the housing vertex 0 has to be set to zero for this example since its rotation is kinematically decoupled from the CCPGT.

4.1.3 Statics analysis for loss-free operating conditions

Similar to the kinematics analysis, the statics systems of equations for loss-free operating conditions is derived in accordance with equations (2.28) and (2.30) for the CCPGT in **Figure 4-2**:

$$\begin{pmatrix} 0 & 0 & 0 & 0 & 0 \\ 1 & 0 & 0 & 0 & 0 \\ 0 & 1 & 0 & 0 & 0 \\ 0 & 0 & 1 & 0 & 0 \\ 0 & 0 & 0 & 1 & 0 \\ i_{1\,6}^{5} - 1 & i_{2\,7}^{5} - 1 & i_{3\,7}^{5} - 1 & i_{4\,7}^{5} - 1 & i_{6\,7}^{5} - 1 \\ -i_{1\,6}^{5} & 0 & 0 & 0 & 1 \\ 0 & -i_{2\,7}^{5} & -i_{3\,7}^{5} & -i_{4\,7}^{5} & -i_{6\,7}^{5} \end{pmatrix} \cdot \begin{bmatrix} T_{i,1,1} \\ T_{i,2,5} \\ T_{i,3,3} \\ T_{i,4,4} \\ T_{i,6,2} \end{bmatrix} = \begin{bmatrix} 0 \\ 0 \\ 0 \\ 0 \\ 0 \\ 0 \\ 0 \\ 0 \end{bmatrix} \quad (4.7)$$

i	[-]	basic transmission ratio of gear pair g	$T_{i,x,g}$	[Nm]	internal torque of vertex/body x of gear pair edge g

Every row of the basic torque coefficient matrix sums the acting torques on one vertex. In coincidence with Section 2.6.2, two external torques of central shafts are unknown, three external torques are to be provided and the housing torque is to be zeroed.

4.1.4 Power flow characteristics of complex-compound planetary gear transmissions

Three types of power are to be distinguished for the components of a CCPGT: absolute power, meshing power and coupling power. Considering only load-dependent power losses (cf. Section 3.1.4) the power balances read as follows:

$$\begin{aligned} \Sigma P &= P_1 + P_2 + P_3 + \cdots + P_s + P_L = 0 \\ \Sigma P_m &= P_{m1} + P_{m2} + P_{m3} + \cdots + P_L = 0 \\ \Sigma P_c &= P_{c1} + P_{c2} + P_{c3} + \cdots + P_s = 0 \\ P_i &= P_{m\,i} + P_{c\,i} \end{aligned} \qquad (4.8)$$

P	[W]	absolute (external) power of central shaft	P_m	[W]	meshing power of central shaft
P_L	[W]	overall (load-dependent) power loss	P_c	[W]	coupling power of central shaft

Herein, the meshing power of a gear pair is decisive, since its magnitude and direction determines the corresponding power loss (cf. Section 3.3). Naturally, meshing power can exclusively be transmitted by gear pair joints and gear pair edges, respectively. Thus, the gear pair subgraph illustrates feasible meshing power flow modes.

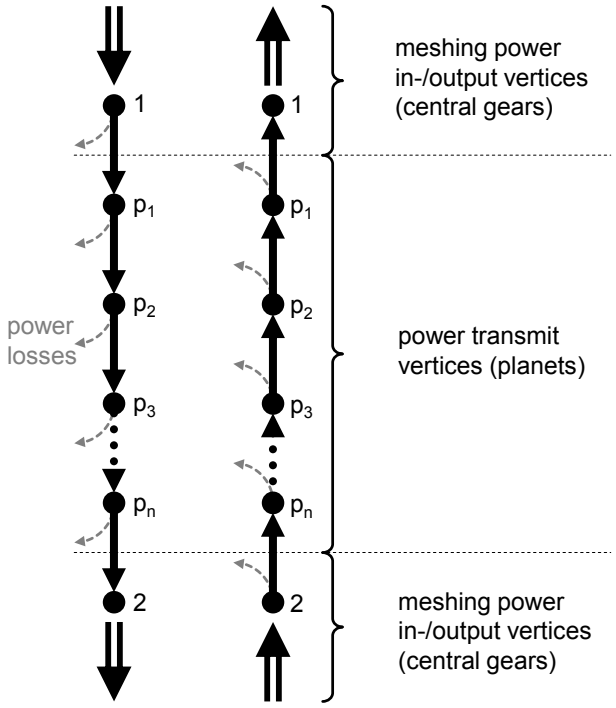

Figure 4-4: Meshing power modes of a single PGT

In terms of singles PGTs, the gear pair subgraph is a chain with the central gears as end vertices. The central gear vertices work as meshing power input and output whereas the intermediate planet vertices work as power transmitting elements without connection to the periphery (**Figure 4-4**). Considering meshing power flow directions, the gear pair subgraph adopts the form of a directed graph. Gear pair edges can only transmit meshing power in one direction. Otherwise, torque would be transmitted in both directions meaning that the working tooth flank as well as the opposite flank were loaded, which does not represent the intended operating behavior.

By contrast, the gear pair subgraph of a CCPGT is a branched tree. Every planet vertex can be connected to central gear vertices and other planet vertices. The planets connected to more than two further vertices work as power partition or summation elements, otherwise as power transmitting elements. Thus, the structure of the gear pair subgraph of a CCPGT can be generalized as follows (**Figure 4-5**):

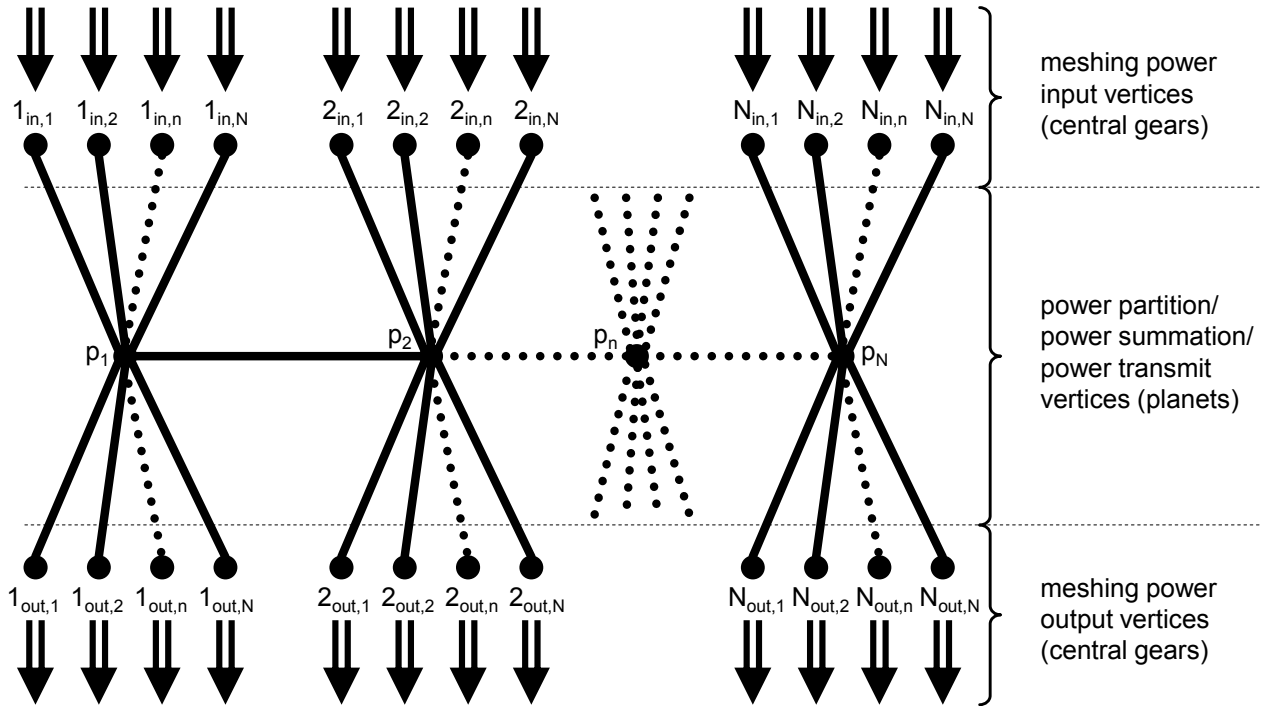

Figure 4-5: Generalized structure of the gear pair subgraph of a CCPGT

In this figure the edges are intentionally not directed. The edge directions, especially those of edges between planets, depend on the individual power inputs and outputs of the focused planet. Obviously, multiple operating conditions exist as a function of the number of central gears and planets but also as a function of the single quantities of power. Necessarily, at least one central gear vertex has to be a meshing power input and one has to be an output, respectively.

4.1.5 Efficiency calculation by iteration

An efficiency calculation can be performed by modifying the statics system of equations in Section 4.1.3. To determine the direction of the meshing power flow of each basic gearing and gear pair edge respectively, a kinematics and statics analysis for loss-free conditions have to be performed at first. Internal torques according to the nomenclature of Sections 2.4.2 and 4.1.3 are used to calculate the meshing power of a gear. If the meshing power of the focused gear is negative, it acts as power output of the body and as power input for the gear pair mesh, respectively, and vice versa. Thus, the basic ratios in the torque coefficient matrix are to be replaced by themselves multiplied or divided by the corresponding efficiency factors as a function of the sign of the related meshing power:

$$i^{s}_{x\,y} \Rightarrow i^{s}_{x\,y} \cdot \eta_0^{w1} \quad \text{with} \quad w1 = \begin{cases} +1 & \text{if } T_{i,x,g} \cdot (n_x - n_s) < 0 \\ -1 & \text{if } T_{i,x,g} \cdot (n_x - n_s) > 0 \\ 0 & \text{if } T_{i,x,g} \cdot (n_x - n_s) = 0 \end{cases} \qquad (4.9)$$

$i^{s}_{x\,y}$	[-]	basic ratio of gear pair g	$T_{i,x,g}$	[Nm]	internal torque of vertex/body x of gear pair edge g
η_0	[-]	basic efficiency of gear pair g			
$w1$	[-]	efficiency exponent	n_x	[1/s]	speed of body/vertex x
			n_s	[1/s]	speed of carrier/transfer vertex s

Considering power losses, the meshing power flow directions do not necessarily have to be identical to those of the loss-free case. A change of direction implicates the previous assumptions to be wrong, and hence, an incorrect modification of the statics system of equations. By means of an iteration, the direction of meshing power flows are checked and compared to those of the previous calculation step. If a change is noticed, then the efficiency exponent w1 is switched. The following flow chart illustrates the procedure in principle (**Figure 4-6**).

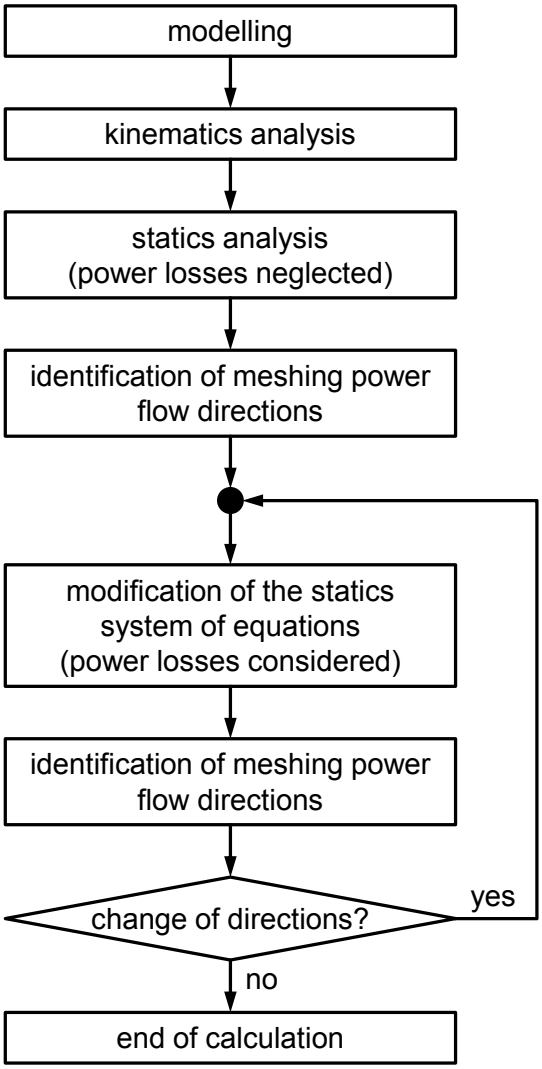

Figure 4-6: Flow chart for efficiency calculation by iteration

In case of an isolated CCPGT, the number of unknown meshing power flow directions is very limited. Due to the static DOF, there are only two external torques left to be determined. The other external torques are given as preset values, hence, the directions of the gear pair edges connected to these vertices are given from the beginning. In conclusion, only the directions of gear pair edges between planet vertices as well as between planet vertices and central gear vertices not being predefined are to be modified when indicated. Two cases can be distinguished. For the second case, the number of gear pair edge directions to be determined is one less in comparison to the first case:

1. The external torques of two central gear shafts are unknown.
2. The external torques of one central gear shaft and of the carrier shaft is unknown.

An iteration that does not converge represents an impossible operating condition. It will be discussed in Section 4.4.5.

Instead of choosing internal torques as states for the basic torque state vector, meshing and/or absolute power can be used. Then, the meshing power of a basic gearing does not have to be calculated separately. From Section 2.5.2, the meshing power of basic gearing member x is chosen as state. The meshing power of member y and the absolute power of the carrier result as a function of the meshing power of member x:

$$P_{m,x,g} = \boxed{1} \cdot P_{m,x,g}$$

$$P_{m,y,g} = \boxed{-\eta_{0,g}^{w1,g}} \cdot P_{m,x,g}$$

$$P_{s,g} = T_{s,g} \cdot \omega_s = \left(-T_{i,x,g} - T_{i,y,g}\right) \cdot \omega_s = \left(-\frac{P_{m,x,g}}{\omega_x - \omega_s} - \frac{P_{m,y,g}}{\omega_y - \omega_s}\right) \cdot \omega_s =$$

$$= \left(-\frac{P_{m,x,g}}{\omega_x - \omega_s} + \frac{\eta_{0,g}^{w1,g} \cdot P_{m,x,g}}{\omega_y - \omega_s}\right) \cdot \omega_s = \boxed{\left(\frac{\eta_{0,g}^{w1,g} \cdot \omega_s}{\omega_y - \omega_s} - \frac{\omega_s}{\omega_x - \omega_s}\right)} \cdot P_{m,x,g} \qquad (4.10)$$

$$\text{with} \quad w1,g = \begin{cases} +1 & \text{if} \quad P_{m,x,g} < 0 \\ -1 & \text{if} \quad P_{m,x,g} > 0 \\ 0 & \text{if} \quad P_{m,x,g} = 0 \end{cases}$$

$P_{m,x/y,g}$	[W]	meshing power of central gear x/y of basic gearing g	$T_{i,x/y,g}$	[Nm]	internal torque of central gear x/y of basic gearing g
$P_{s,g}$	[W]	absolute power of carrier s of basic gearing g	$T_{s,g}$	[Nm]	torque of carrier s of basic gearing g
$\omega_{x/y/s}$	[rad/s]	angular speed of central gear x/y or carrier s	$\eta_{0,g}$	[-]	basic efficiency of gear pair g
			$w1,g$	[-]	efficiency exponent of basic gearing g

Using this nomenclature, a preceding kinematics analysis is necessary to insert concerning speeds. Obviously, the absolute power of the carrier cannot be calculated for the coupling case as the meshing power of all central gears is zero and no relative speed occurs.

Due to closeness of the modeling to reality and the correct representation of the meshing power flow, both methods and nomenclatures allow a consideration of power losses for any number of input and output shafts and arbitrary operating conditions.

4.1.6 Efficiency calculation by simplex algorithm and network flows

Numerous solving algorithms for linear problems exist as alternative to the iteration procedure described in the previous section. A very popular and efficient one is the *simplex algorithm* according to Schrijver [7_SCH00]. The simplex algorithm is a tool for solving and optimizing linear problems. It either finds the optimum solution after a finite number of calculation steps or states unboundedness and incalculability. Vanderbei [7_VAN97] indicated that the simplex algorithm is capable of solving problems of the following form with a

target function to be maximized and a matrix-vector-system constraining the solution space:

$$\max \sum_{j=1}^{n} c_j \cdot x_j$$

$$\text{with} \sum_{j=1}^{n} a_{ij} \cdot x_j \leq b_i \quad \text{for} \quad i = 1,2,\dots,m \qquad (4.11)$$

$$\text{and} \qquad x_j \geq 0 \quad \text{for} \quad j = 1,2,\dots,n$$

x	[-]	variable	b	[-]	constraint value
a	[-]	constraint function coefficient	c	[-]	target function coefficient
n	[-]	number of variables	m	[-]	number of constraint functions

The constraint functions can both be given as inequalities or equations. Graphically, the solution space can be imagined as a polyhedron with peripheries defined by the constraint functions (**Figure 4-7**).

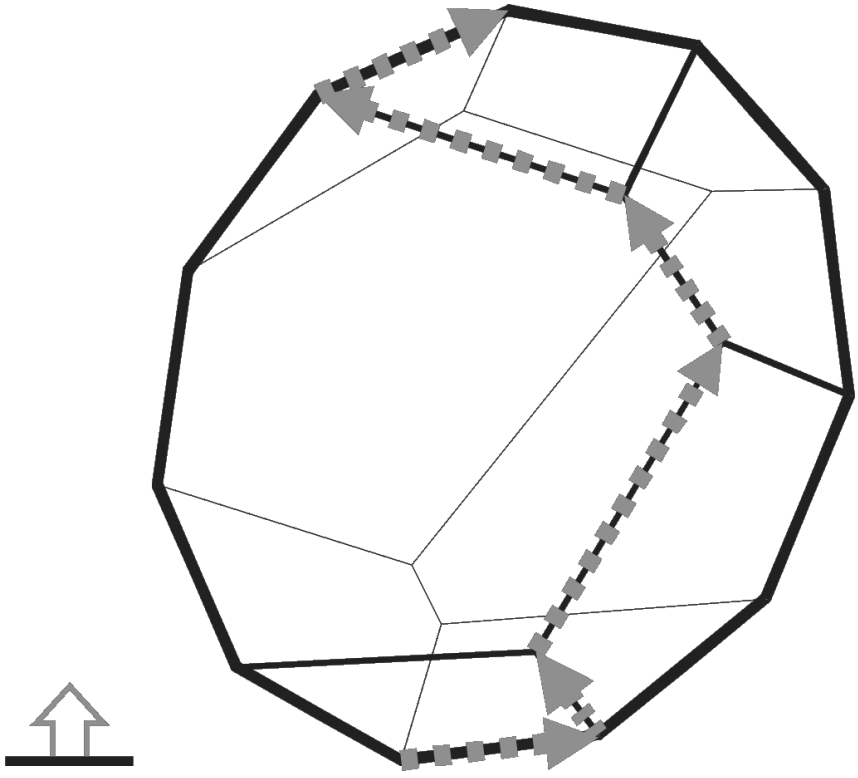

Figure 4-7: Simplex polyhedron and solution path

The simplex algorithm starts with an arbitrary, feasible solution. Subsequently, a single variable is systematically altered in a stepwise manner while freezing other variables after analyzing the system of equations. The solution path runs along the edges of the polyhedron until the top is reached (**Figure 4-7**).

The problem of calculating the efficiency and power flow respectively within a CCPGT is not a linear problem as the power loss depends on the direction of the meshing power flow from vertex to vertex. However, to avoid distinctions of cases, this problem can be trans-

formed into a linear optimization problem. For this purpose, the graph in **Figure 4-5** is modified as follows. Normally, every edge is capable of transferring meshing power in both directions. Therefore, each edge is split into two twin edges of opposite directions (**Figure 4-8**). Due to this transformation the gear pair subgraph is not a tree any longer and features several cycles.

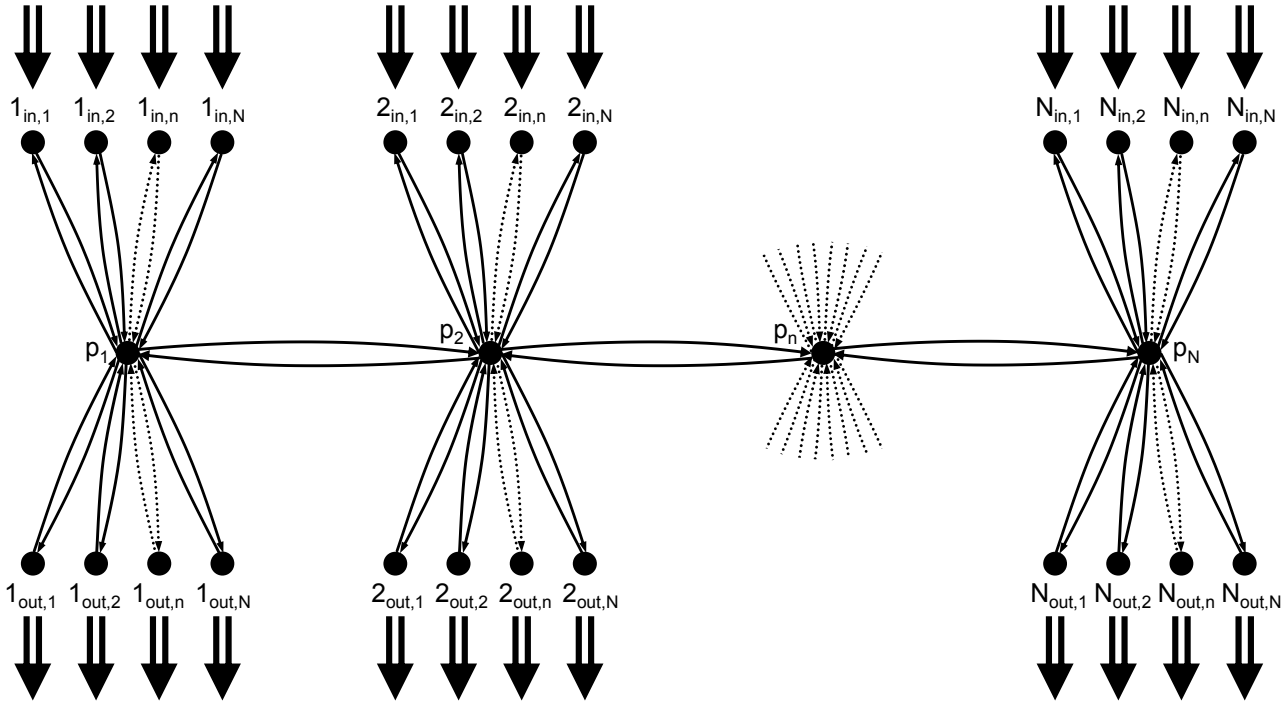

Figure 4-8: Transformed structure of the gear pair subgraph of a CCPGT for linear problem solving purposes

For this system a set of equations based on (4.11) is assembled with meshing power as variable. Each edge features an input and output meshing power and an efficiency factor. By definition, all meshing power values are positive:

$$P^{e}_{m,in} \cdot \eta^{e}_{0} = P^{e}_{m,out} \quad \text{for} \quad e = 1,2,\dots q \qquad (4.12)$$

$P^{e}_{m,in}$	[W]	input meshing power of edge e	η^{e}_{0}	[-]	efficiency factor of edge e
$P^{e}_{m,out}$	[W]	output meshing power of edge e	q	[-]	number of edges

Also, the meshing power for each vertex must be balanced:

$$\Sigma P^{v}_{m,int,in} - \Sigma P^{v}_{m,int,out} + P^{v}_{m,ext,in} - P^{v}_{m,ext,out} = 0 \quad \text{for} \quad v = 1,2,\dots p \qquad (4.13)$$

$P^{v}_{m,int,in}$	[W]	internal input meshing power of vertex v	$P^{v}_{m,ext,in}$	[W]	external input meshing power of vertex v
$P^{v}_{m,int,out}$	[W]	internal output meshing power of vertex v	$P^{v}_{m,ext,out}$	[W]	external output meshing power of vertex v
p	[-]	number of vertices			

According to the DOF of the system, external meshing power is to be preset as a constraint value. Naturally, planet vertices do not feature external meshing power. In case of only one external meshing power of a central gear is unknown, no further constraint functions are to be inserted. If the meshing power of two of central gears are unknown, but the torque of the carrier shaft is given, the torque balance of the whole system is the missing

constraint function. For this purpose, meshing power is converted into torque using the corresponding meshing speed:

$$\Sigma \frac{1}{\omega_v - \omega_s} \cdot P^v_{m,ext,in} - \Sigma \frac{1}{\omega_v - \omega_s} \cdot P^v_{m,ext,out} = -T_s \qquad (4.14)$$

$P^v_{m,ext,in}$	[W]	external input meshing power of vertex v	ω_v	[rad/s]	angular speed of central gear vertex v
$P^v_{m,ext,out}$	[W]	external output meshing power of vertex	ω_s	[rad/s]	angular speed of carrier s
			T_s	[Nm]	external torque of carrier s

With these constraint functions the simplex algorithm is supposed to minimize the power loss. Therefore, the term to be maximized reads:

$$\max \quad (-\Sigma P^e_{m,in} \cdot \eta^e_0) \quad \text{for} \quad e = 1,2,\dots q \qquad (4.15)$$

$P^e_{m,in}$	[W]	input meshing power of edge e	η^e_0	[-]	efficiency factor of edge e
			q	[-]	number of edges

As the minimum of power loss is gained if meshing power is not cycling, the twin edges vanish as at least one edge does not transfer meshing power in the end. Thus, the resulting subgraph is again a tree after removing all unloaded edges and the unknown values for the external meshing power are gained.

The presented problem is not only a linear problem but also a so-called *network flow* problem meaning that a certain entity is to be transported from one point to another via given routes. According to Ahuja et al. [7_AHU93], a popular and fundamental network flow problem is the minimum cost flow problem. Goods are to be transported from a number of suppliers to a number of consumers at which shipment costs arise. The shipment costs depend linearly on the amount of goods per transport. It is assumed that for the standard minimum cost flow problem the entity is neither consumed nor increased while transporting. This is not true for the given power flow problem as the meshing power decreases. Therefore, this problem belongs to the group of generalized flow problems whose edges are capable of reducing of increasing the transported entity. It can be compared e.g. to financial networks or electricity networks with edges featuring power losses.

Nevertheless, fast solving algorithms have been developed for network flow problems based on the simplex algorithm. Here, as many variables as possible are preset according to the DOF of the system. Thus, only one feasible solution can be achieved and the given problem is not a real optimization problem. It would, for example, also be possible to answer the question where to input power in order to satisfy a certain power demand for minimum power losses without initializing all DOFs.

4.1.7 Overall efficiency

In order to calculate the overall efficiency in the end, the overall input and output power is to be determined. The statics analysis considering power losses reveals the values for both unknown external torques. Other external torques are given as preset values. The formula for the overall efficiency reads:

$$P_{in} = 2 \cdot \pi \cdot \Sigma\left(T_{e,x} \cdot n_x\right) \quad \text{for} \quad T_{e,x} \cdot n_x > 0$$

$$P_{out} = 2 \cdot \pi \cdot \Sigma\left(T_{e,x} \cdot n_x\right) \quad \text{for} \quad T_{e,x} \cdot n_x < 0 \qquad (4.16)$$

$$\eta = -\frac{P_{out}}{P_{in}}$$

P_{in}	[W]	overall (absolute) input power	$T_{e,x}$	[Nm]	external torque of central shaft x
P_{out}	[W]	overall (absolute) output power	n_x	[1/s]	(absolute) speed of central shaft x
η	[-]	overall efficiency			

4.2 Calculation by means of Wolf symbols

Substitution figures composed of Wolf symbols offer a simplified and clear view on PGT structures (cf. Sections 3.2.1 and 3.4). As for single PGTs and coupled PGTs consisting only of single PGTs the Wolf symbol representation is unique. In terms of CCPGTs multiple Wolf symbol substitution figures may exist. In the following, the kinematics and statics analysis for operating conditions with and without power losses are discussed and differences between single/coupled PGTs and CCPGTs are identified.

4.2.1 Kinematics analysis and kinematically-equivalent substitution figures

4.2.1.1 Single and coupled planetary gears

A Wolf symbol corresponding to a single PGT or a coupled PGT derived from combining single PGTs strongly orientates on the real transmission structure. Instead of taking into account every basic gearing ratio, basic train ratios are used as parameters. Thus, information about planets and their rotational speeds and bearing power losses are lost. Apart from that, the Wolf symbol does not include any further simplification but illustrates the structural assembly in a concise way.

An example is given in **Figure 4-9**. It shows the Wolf symbol corresponding to the coupled PGT of **Figure 2-10** with adjusted numeration. **Table 4-1** provides the assignments of the members to the individual Wolf symbols and basic trains respectively. By means of the procedure of Section 2.5.1, the basic speed system of equations (4.17) is formed. Since the speeds of only four members occur as states instead of the speeds of six bodies of the realistic transmission model, the dimension of the system of equations is much smaller as a function of the number of contained planets.

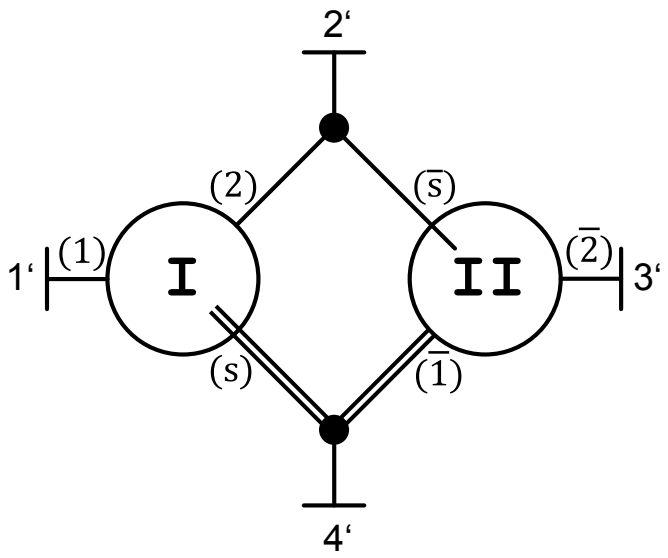

Figure 4-9: Wolf symbol of a coupled PGT consistent with Figure 2-10 with adjusted numeration

Wolf symbol	member x	member y	member s	transmission ratio $i^{s}_{x\,y}$
I	1’	2’	4’	$i_I = i^{s}_{1\,2}$
II	4’	3’	2’	$i_{II} = i^{\bar{s}}_{\bar{1}\,\bar{2}}$

Table 4-1: Basic train assignment table for Figure 4-9

$$\begin{pmatrix} 1 & -i_I & 0 & i_I - 1 \\ 0 & i_{II} - 1 & -i_{II} & 1 \end{pmatrix} \cdot \begin{bmatrix} n_{1'} \\ n_{2'} \\ n_{3'} \\ n_{4'} \end{bmatrix} = \begin{bmatrix} 0 \\ 0 \end{bmatrix} \qquad (4.17)$$

i	[-]	basic train ratio	n_x	[1/s]	rotational speed of member x

4.2.1.2 Complex-compound planetary gears

CCPGTs are often regarded as a composition of single PGTs sharing a common planet carrier and common central gears. A kinematically-equivalent substitution figure is built out of single PGTs contained in the CCPGT and features the same number of kinematic DOF of the CCPGT. The number of central shafts is identical as well as their speeds. Every single PGT added to the substitution figure provides three central shafts. The final number of central shafts is discounted by the number of permanent couplings:

$$CS = 3 \cdot PGT_{sub} - CL \qquad (4.18)$$

CS	[-]	total number of central shafts	PGT_{sub}	[-]	number of single PGTs contained in the substitution figure
CL	[-]	number of permanent paired shaft couplings			

As the number of kinematic DOF equals two, substituting equation (2.42) into (4.18) leads to:

$$\mathrm{PGT_{sub}} = \mathrm{CS} - 2$$
$$\mathrm{CL} = 2 \cdot \mathrm{CS} - 6 \qquad (4.19)$$

CS	[-]	total number of central shafts	$\mathrm{PGT_{sub}}$	[-]	number of single PGTs contained in the substitution figure
CL	[-]	number of permanent paired shaft couplings			

Thus, the substitution figure of a CCPGT consists of a definite number of single PGTs and permanent paired shaft couplings as a function of the number of central shafts. Per Section 2.4.1.2, a CCPGT contains multiple sets of single PGTs. Every two central gears of the CCPGT constitute a single PGT in combination with the carrier. Therefore, the number of single PGTs contained in a CCPGT equals:

$$\mathrm{PGT_{incl}} = \binom{\mathrm{CG}}{2} = \binom{\mathrm{CS}-1}{2} = \frac{(\mathrm{CS}-1)!}{2 \cdot (\mathrm{CS}-3)!} \qquad (4.20)$$

CS	[-]	total number of central shafts	$\mathrm{PGT_{incl}}$	[-]	number of single PGTs contained in a CCPGT
CL	[-]	number of permanent paired shaft couplings	CG	[-]	total number of central gears

Table 4-2 gives an overview of the number of single PGTs included in a CCPGT and the corresponding number of single PGTs contained in the substitution figure:

CS	**3**	**4**	**5**	**6**	**7**	**8**	**9**	**10**	**11**
$\mathrm{PGT_{incl}}$	1	3	6	10	15	21	28	36	45
$\mathrm{PGT_{sub}}$	1	2	3	4	5	6	7	8	9

CS	[-]	total number of central shafts	$\mathrm{PGT_{sub.}}$	[-]	number of single PGTs contained in the substitution figure
$\mathrm{PGT_{incl.}}$	[-]	number of single PGTs contained in a CCPGT			

Table 4-2: Number of single PGTs included in a CCPGT and corresponding number of single PGTs contained in the substitution figure

To ensure the same kinematic behavior of the substitution figure in relation to the CCPGT, it is not sufficient to select arbitrary single PGTs out of the multitude of single PGTs included. Since a CCPGT features a kinematic DOF of only two (the meshing and the coupling speed), every central gear must either be directly connected to another central gear via a basic train or at least via a kinematic chain of basic trains. Then, the meshing speed of one central gear dictates the meshing speeds of all other central gears. This means that all central gears must occur at least once in a PGT of the substitution figure. According to **Table 4-2,** (CS-2) basic trains are available to connect (CS-1) central gears kinematically. Thus, the structure of a virtual subgraph connecting all central gears via basic trains is a coherent tree. **Figure 4-10** shows a positive and negative example of a 5-shaft CCPGT transformed into a kinematically-equivalent and non-equivalent substitution figure and the related virtual subgraphs. Since the virtual subgraph of the negative example features a ring, it is not a tree and does not contain all central gears. Central gear shafts, being member of more than one Wolf symbol, are termed *central gear coupling shafts*.

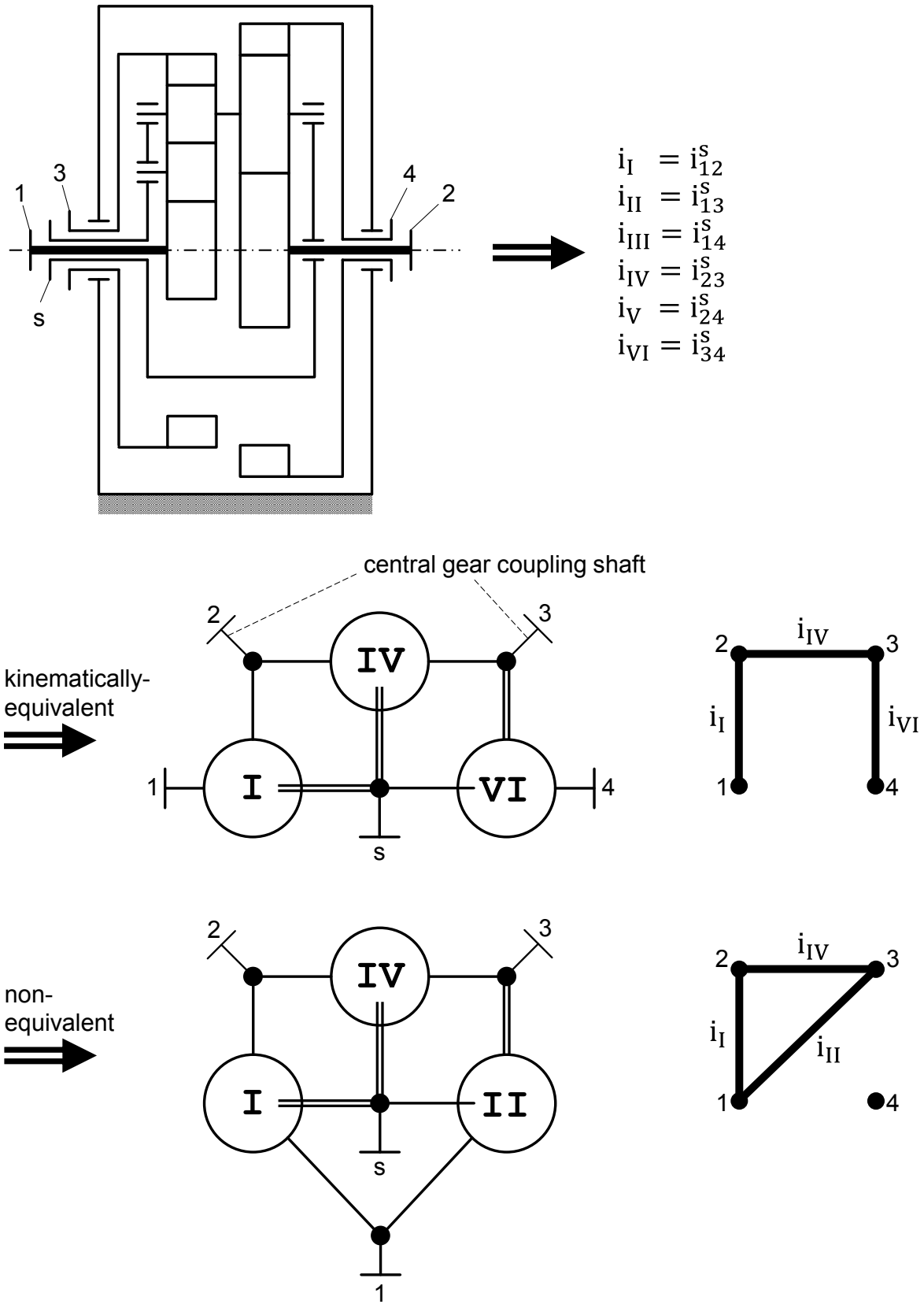

Figure 4-10: Kinematically-equivalent and non-equivalent substitution figure of an example 5-shaft CCPGT

Obviously, the total number of feasible substitution figures equals the total number of trees. According to Cayley [7_AIG10] the number of different trees connecting a certain number of vertices is given by the following equation:

$$\mathrm{SUB_{kin}} = \mathrm{CG}^{\mathrm{CG}-2} = (\mathrm{CS}-1)^{\mathrm{CS}-3} \qquad (4.21)$$

SUB_{kin}	[-]	total number kinematically-equivalent substitution figures	CS	[-]	total number of central shafts
			CG	[-]	total number of central gears

Table 4-3 provides the number of kinematically-equivalent substitution figures as a function of the number of central shafts. Due to the exponential growth, the number of kinematically-equivalent substitution figures is comparatively high even for small numbers of central shafts.

CS	**3**	**4**	**5**	**6**	**7**	**8**	**9**	**10**	**11**
SUB_{kin}	1	3	16	125	1.296	16.807	262.144	4.782.969	100.000.000

SUB_{kin}	[-]	total number kinematically-equivalent substitution figures	CS	[-]	total number of central shafts

Table 4-3: Number of kinematically-equivalent substitution figures

For computer-based generation of trees the Pruefer algorithm [7_PRU18, 7_WAN97 and 7_DEO01] can be utilized. For a given number of vertices all feasible trees are built iteratively. The Pruefer algorithm is fast as it avoids creating structures other than trees.

Referring to Section 4.2.1.1 the basic speed system of equations is derived for a given substitution figure. For example, the system of equations for the kinematically-equivalent substitution figure in **Figure 4-10** is written as:

$$\begin{pmatrix} 1 & -\mathrm{i_I} & 0 & 0 & \mathrm{i_I}-1 \\ 0 & 1 & -\mathrm{i_{IV}} & 0 & \mathrm{i_{IV}}-1 \\ 0 & 0 & 1 & -\mathrm{i_{VI}} & \mathrm{i_{VI}}-1 \end{pmatrix} \cdot \begin{bmatrix} \mathrm{n_1} \\ \mathrm{n_2} \\ \mathrm{n_3} \\ \mathrm{n_4} \\ \mathrm{n_s} \end{bmatrix} = \begin{bmatrix} 0 \\ 0 \\ 0 \end{bmatrix} \qquad (4.22)$$

i	[-]	basic train ratio	n_x	[1/s]	rotational speed of member x

Naturally, the dimension of the system is smaller since it features only five states instead of seven for the number of bodies of the transmission. In coincidence to the number of kinematic DOF, three Willis Equations are used for the description of the kinematics of the CCPGT and two preset values are necessary to complete the system of equations.

4.2.2 Statics analysis for loss-free operating conditions

4.2.2.1 Single and coupled planetary gears

The statics analysis discussed in Section 2.4.2 can be applied to Wolf symbol models accordingly. For this purpose, it is reasonable to cut free each Wolf symbol and mark the shafts ends with internal and external torques. The corresponding torque values of cut-free shaft ends have opposite signs. As an example, the Wolf symbol of **Figure 4-9** is modified in **Figure 4-11**:

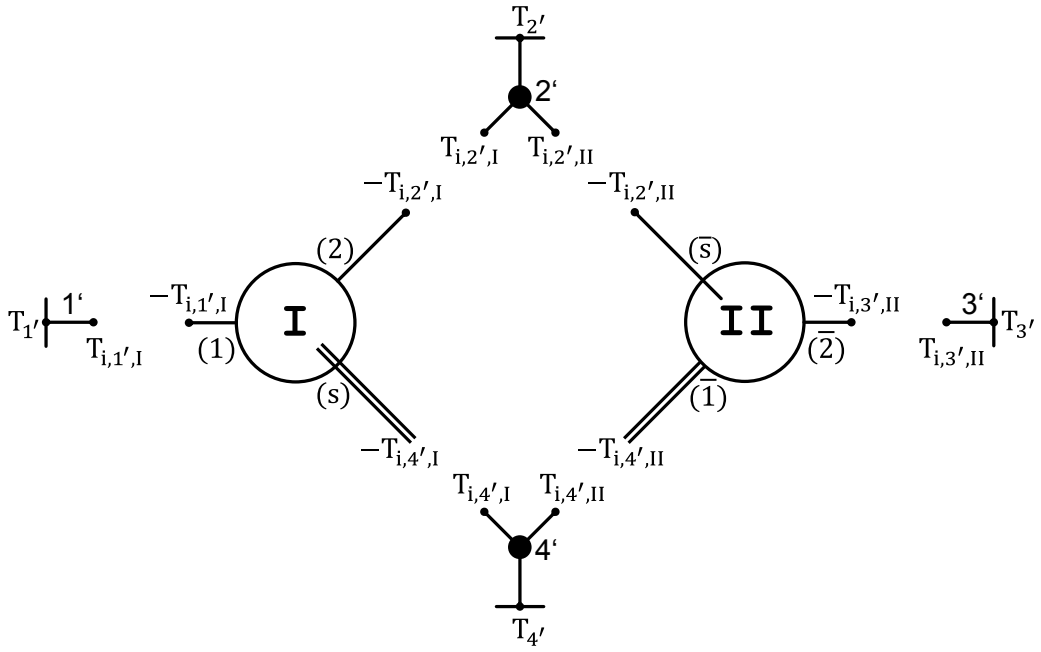

Figure 4-11: Wolf symbol of a coupled PGT consistent with Figure 2-10 and cut-free elements

In accordance with **Table 4-1**, the basic torque system of equations is set up as:

$$\begin{pmatrix} 1 & 0 \\ -i_I & i_{II}-1 \\ 0 & -i_{II} \\ i_I-1 & 1 \end{pmatrix} \cdot \begin{bmatrix} T_{i,1',I} \\ T_{i,4',II} \end{bmatrix} = \begin{bmatrix} 0 \\ 0 \\ 0 \\ 0 \end{bmatrix} \qquad (4.23)$$

i	[-]	basic train ratio	$T_{i,x,w}$	[Nm]	internal torque of member x of Wolf symbol / basic train w

By choosing the applied nomenclature, the basic torque coefficient matrix is the transpose of the basic speed coefficient matrix as stated in Section 2.5.

4.2.2.2 Complex-compound planetary gears

According to equation (2.48), the static DOF equals the number of central shafts having a connection to the periphery minus the kinematic DOF. Substituting equation (4.19) into (2.48) leads to:

$$DOF_{stat} = CS - DOF_{kin} = CS - 2 = PGT_{sub} \qquad (4.24)$$

DOF_{kin}	[-]	kinematic DOF	CS	[-]	total number of central shafts
DOF_{stat}	[-]	static DOF	PGT_{sub}	[-]	number of single PGTs contained in the substitution figure

Herein, the number of permanent paired shaft couplings is defined by equation (4.19) as well. Hence, a kinematically-equivalent substitution figure features the same static DOF as the corresponding CCPGT.

The statics of a CCPGT for loss-free operating conditions can be described using the formulations of equations (2.13) and (2.19). First, the sum for all external torques must equal zero:

$$\Sigma T = T_1 + T_2 + T_3 + \cdots + T_s = 0 \qquad (4.25)$$

T_x	[Nm]	external of central shaft x

Secondly, the sum of all meshing power amounts of the central shafts of a CCPGT must equal zero. Since the meshing speeds of all central shafts are kinematically coupled in pairs via the related basic train ratio, the sum of meshing power can be modified as follows:

$$\Sigma P_m = 2 \cdot \pi \cdot T_1 \cdot (n_1 - n_s) + 2 \cdot \pi \cdot T_2 \cdot (n_2 - n_s) + 2 \cdot \pi \cdot T_3 \cdot (n_3 - n_s) + \cdots = 0$$
$$\Rightarrow T_1 + T_2 \cdot \frac{n_2 - n_s}{n_1 - n_s} + T_3 \cdot \frac{n_3 - n_s}{n_1 - n_s} + \cdots = T_1 + T_2 \cdot \frac{1}{i_{12}^s} + T_3 \cdot \frac{1}{i_{13}^s} + \cdots 0 \qquad (4.26)$$

T_x	[Nm]	external of central shaft x	$n_{x/s}$	[1/s]	speed of central gear x / carrier s
P_m	[W]	meshing power	i	[-]	basic train ratio

The substitution figure features the same number of central shafts, and therefore the same number of connections to the periphery. Likewise, the sum of its external torques (4.25) must be zero. Since the substitution figure is arranged to have the same kinematic behavior as the CCPGT in terms of the central shaft speeds (cf. Section 4.2.1.2), equation (4.26) must be true for every substitution figure just as well. **Thus, every kinematically-equivalent substitution figure can be used to analyze the statics of a CCPGT for loss-free operating conditions. In this context, only the external torques of the substitution figure correspond to the real external shaft torques of the CCPGT. Due to the division of external torques to multiple Wolf symbols contained in the substitution figure, the internal torques do not necessarily equal the internal torques of the CCPGT and do not necessarily have a physical meaning.** As an example, the kinematically-equivalent substitution figure of **Figure 4-10** is cut free in **Figure 4-12**.

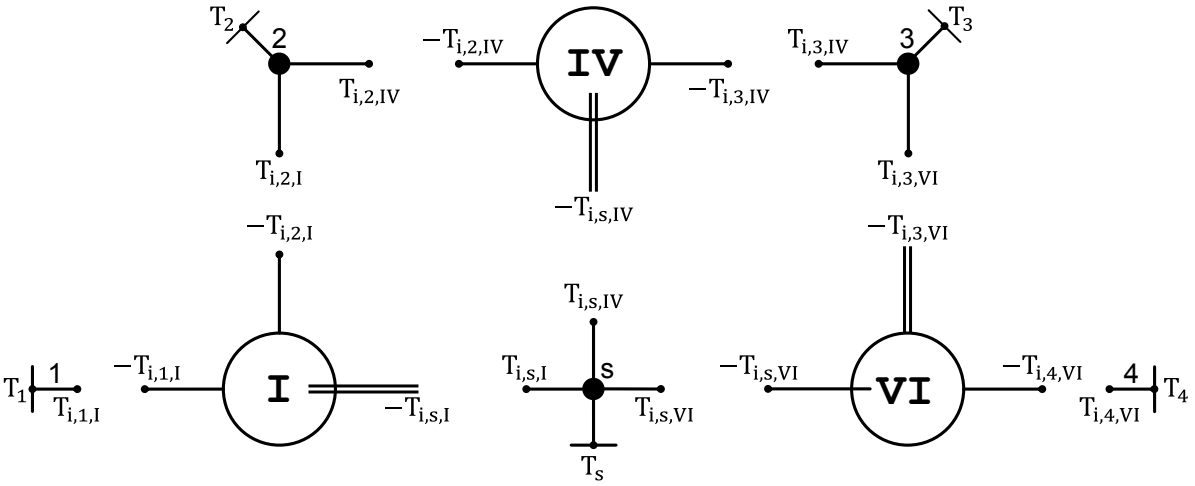

Figure 4-12: Kinematically-equivalent substitution figure consistent with Figure 4-10 and cut-free elements

The related basic statics system of equations reads:

$$\begin{pmatrix} 1 & 0 & 0 \\ -i_I & 1 & 0 \\ 0 & -i_{IV} & 1 \\ 0 & 0 & -i_{VI} \\ i_I - 1 & i_{IV} - 1 & i_{VI} - 1 \end{pmatrix} \cdot \begin{bmatrix} T_{i,1,I} \\ T_{i,2,IV} \\ T_{i,3,VI} \end{bmatrix} = \begin{bmatrix} 0 \\ 0 \\ 0 \\ 0 \\ 0 \end{bmatrix} \quad (4.27)$$

i	[-]	basic train ratio	$T_{i,x,w}$	[Nm]	internal torque of member x of Wolf symbol / basic train w

As stated before, the basic torque coefficient matrix is the transpose of the basic speed coefficient matrix by means of the applied nomenclature.

4.2.3 Efficiency calculation by functionally-equivalent substitution figures

4.2.3.1 Single and coupled planetary gears

As for single PGTs and coupled PGTs consisting of single PGTs, the efficiency calculation can be carried out based on the kinematics and statics analysis for loss-free operating conditions (Section 4.2.2.1). The basic train ratio is to be multiplied or to be divided by its corresponding efficiency factor appropriate to the meshing power flow direction in analogy to Sections 3.3 and 4.1.5. An iteration and alteration of the efficiency exponents are to be applied if necessary. The overall efficiency is calculated according to Section 4.1.7. Since no other methodical differences are to be mentioned, the procedure is not repeated here.

4.2.3.2 Definition of functionally-equivalent substitution figures for complex-compound planetary gear transmissions

By definition, a functionally-equivalent substitution figure must exhibit to show the same kinematic and static behavior as the corresponding CCPGT. The torques of central gears and central shafts, respectively, must be identical, even in case when power losses are included. Thus, the overall efficiency is supposed to be identical as well.

As shown in Sections 4.2.1.2 and 4.2.2.2, the structure of a gear pair subgraph of a CCPGT differs fundamentally from the structure of the corresponding virtual subgraph of a kinematically-equivalent substitution figure since planets are missing within the substitution figures. Therefore, the meshing power flow within substitution figures differs fundamentally from the meshing power flow within the CCPGT, too. In a CCPGT, meshing power can only be transferred from one central gear to another central gear via planets. Each central gear is part of only one gear pair. In contrast, the central gears are directly connected within the substitution figure. Central gears can be part of more than one Wolf symbol and basic train, respectively (**Figure 4-10**).

In order to generate a functionally-equivalent substitution figure, the planets are symbolically removed from the CCPGT gear pair subgraph. In other words, planets are omitted and central gear connections are replaced by direct gear pair edges between central gears. Hereby, the realistic meshing power flows are split into partial meshing power flows belonging to different basic trains and Wolf symbols respectively. To ensure the same

functional behavior the substitution figures must fulfill the following rules in respect of the corresponding CCPGT:

1. The substitution figure must be kinematically-equivalent.
2. The quantities of meshing power must be identical in sum.
3. Superimposing the partial meshing power flows of the substitution figure on the basis of the realistic CCPGT gear pair subgraph, all gear pair edges must feature meshing power flows in the same direction. Likewise, a gear pair edge must not feature partial meshing flows in opposite directions.
4. The partial meshing power flows of the substitution figure must be impacted by equivalent efficiency factors. For this purpose, the basic train efficiency of a certain Wolf symbol has to be identical to the efficiency of the corresponding path from one central gear to the other of the realistic CCPGT gear pair subgraph. Due to the fragmentation of meshing power flows, the efficiency factors must not feature any load dependency.

A simple example shown in **Figure 4-13** illustrates the relationship between a directed CCPGT gear pair subgraph and a corresponding functionally-equivalent substitution figure. Each gear pair edge features a certain efficiency factor. The efficiency factors of basic trains result as the product of related gear pair edge efficiency factors. The amounts of meshing power are chosen arbitrarily and charted as loss-free values for clarity purposes.

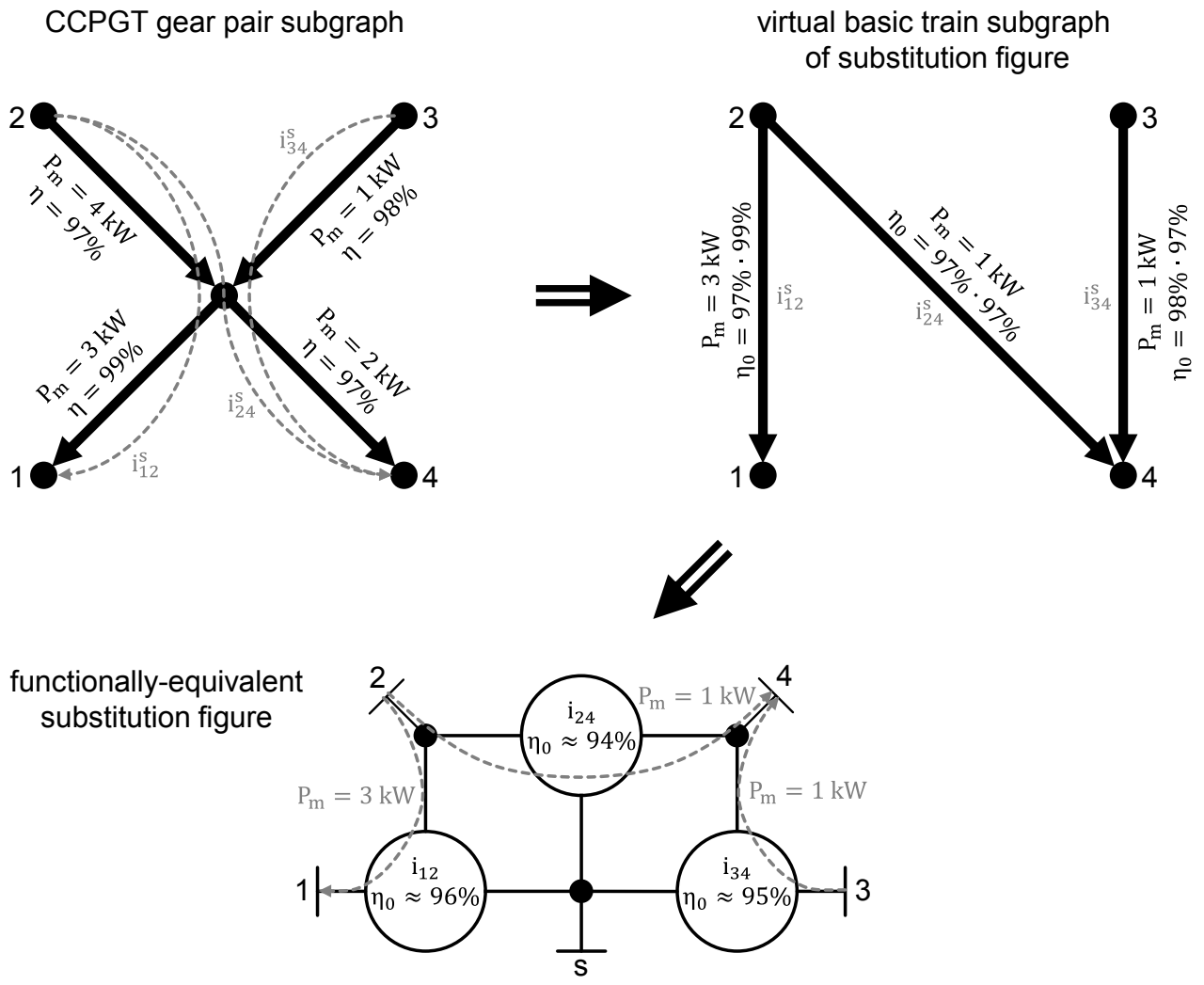

Figure 4-13: Example CCPGT gear pair subgraph and functionally-equivalent substitution figure

By compliance with the rules mentioned above, power losses and overall efficiency of the functionally-equivalent substitution figures are identical to those of the actual CCPGT. Due to this correspondence, the functionally-equivalent substitution figure cannot feature a better overall efficiency or lower power losses.

A better overall efficiency of a substitution figure can only be derived if rule 4 is violated meaning that basic train efficiency factors are chosen in an inconsistent way. Violation of either one of rules 2 or 3 results in higher meshing power and/or meshing power is impacted by too low efficiency factors. Both cases lead to much higher power loss and lower overall efficiency.

In the following, two negative examples highlight kinematically-equivalent but functionally-non-equivalent substitution figures. The first example in **Figure 4-14** shows a substitution figure with too much meshing power. The basic trains for the substitution figure are chosen in an inappropriate manner since meshing power is transferred from central gear 2 to central gear 3. Central gear 3 is a meshing power source and its external input meshing power is added to the meshing power delivered by central gear 2. Thus, the meshing power flow from central gear 3 to central 4 is larger than the external input meshing power provided

for central gear 3. In sum, too much meshing power is considered. Meshing power is transferred using detours instead of direct and short paths. To avoid detours, meshing power may only be transferred directly from meshing power source to meshing power sink. There must not exist any direct source to source or sink to sink connections. No central gear vertex and central gear coupling shaft respectively may feature meshing power flows of opposite directions. **Likewise, the sign of all inner torques belonging to one central gear coupling shaft must be identical.**

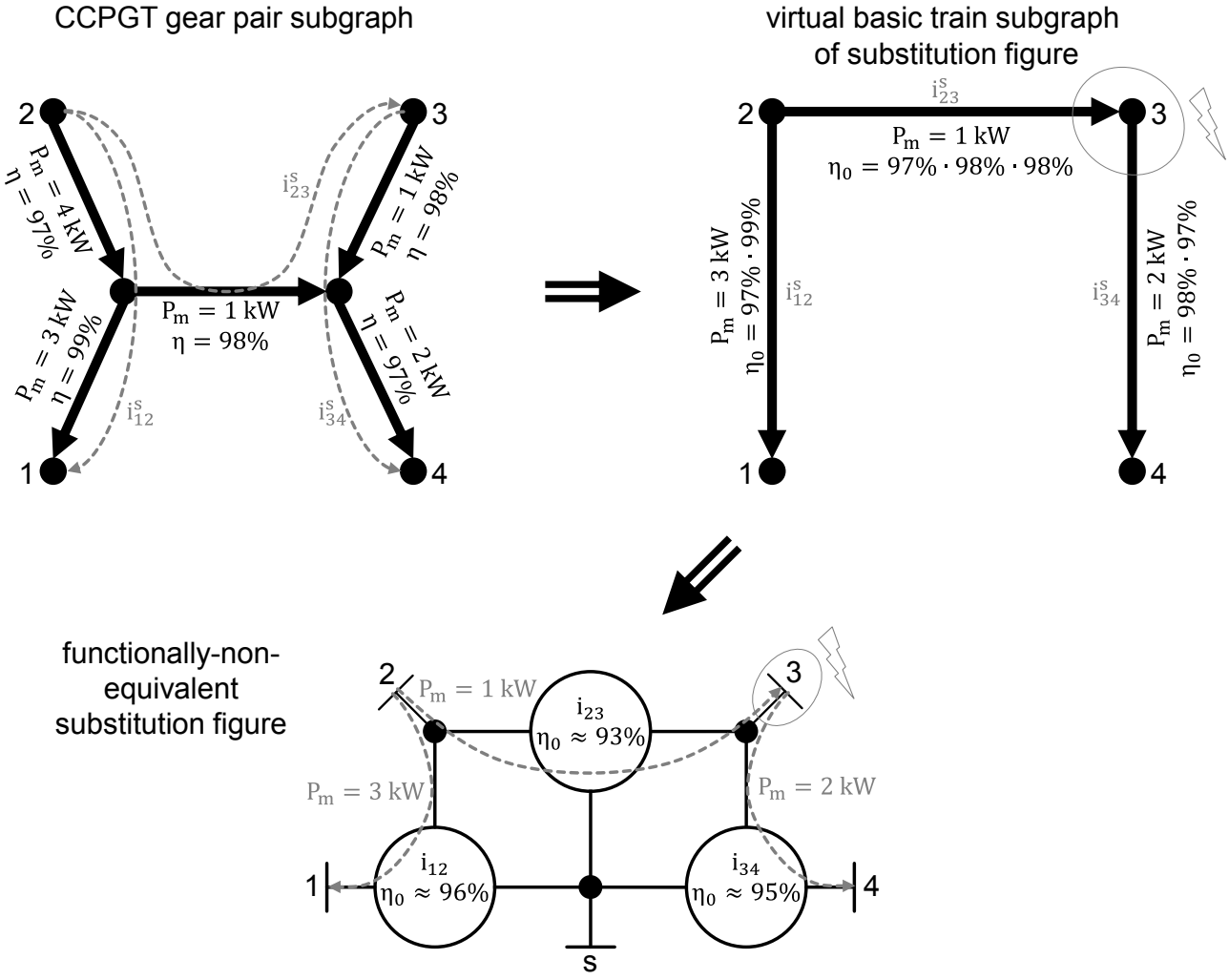

Figure 4-14: Negative example of functionally-non-equivalent substitution figure with too much meshing power

The second negative example in **Figure 4-15** demonstrates a substitution figure featuring too low basic train efficiency factors. Indeed, meshing power flows of all central gear coupling shafts are of equal direction but meshing power is transferred using too long paths. Superimposing all meshing power flows within the CCPGT gear pair subgraph, it becomes obvious that intersecting meshing power flows occur at the planet-planet edge. Due to missing information about planets, this case cannot to be recognized directly only by analyzing the substitution figure, but it results in too low overall efficiency values.

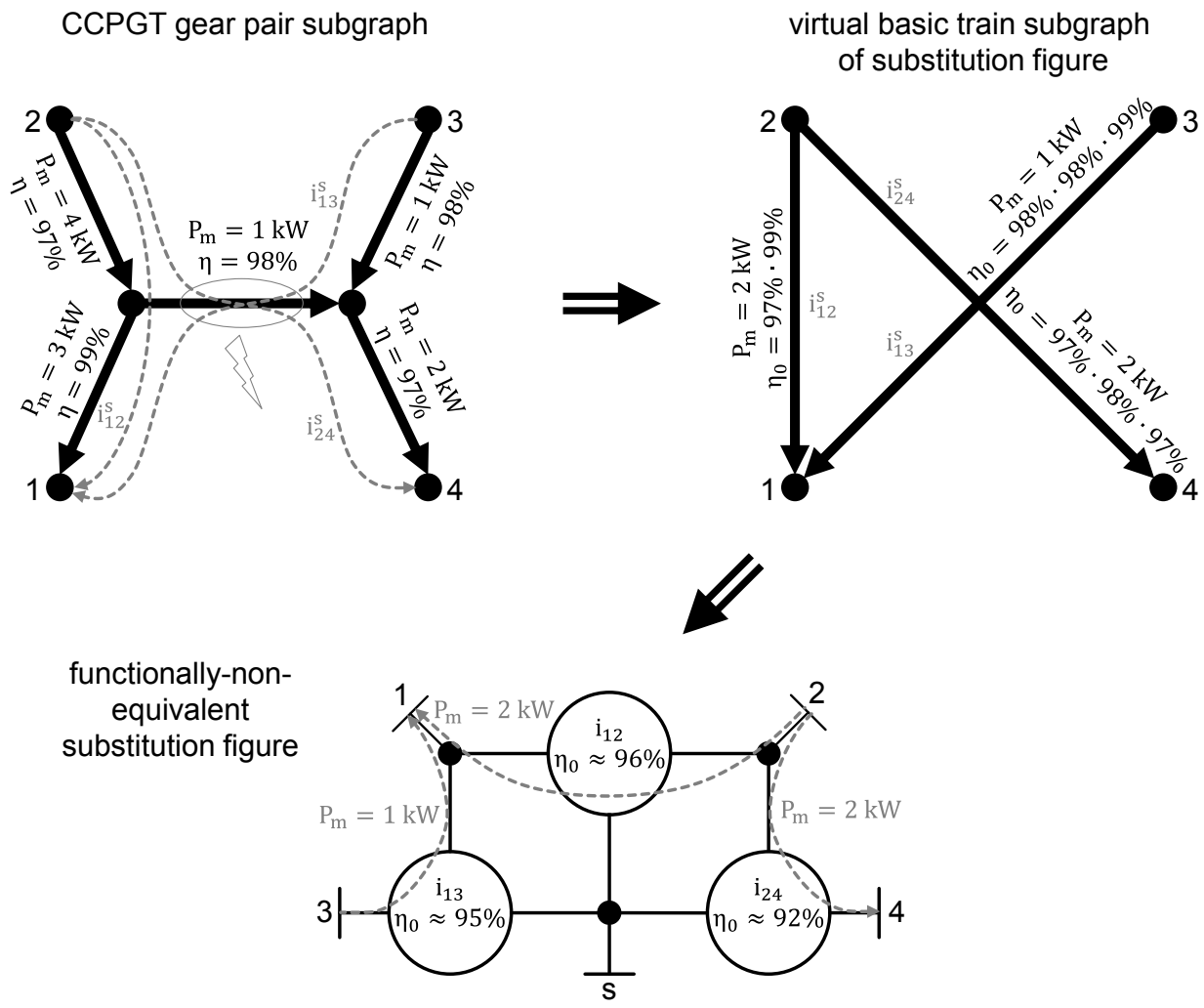

Figure 4-15: Negative example of functionally-non-equivalent substitution figure with too low basic train efficiency factors

In a more general sense, the central gear vertices can be grouped as a function of which planet they are belonging to (**Figure 4-5**). One can imagine that these groups are connected to each other via single planet-planet edges. Therefore, all meshing power flows from one group to another must be of the same direction to avoid intersecting meshing power flows at the planet-planet edges.

4.2.3.3 Systematic transformation of directed graphs into functionally-equivalent substitution figures

Directed CCPGT gear pair subgraphs can be transformed into virtual basic train subgraphs by means of a systematic procedure discussed as follows. Hence, a functionally-equivalent substitution figure can be found for any operating condition and any type of CCPGT. By applying this procedure the CCPGT gear pair subgraph G is dissembled as the virtual basic train subgraph G' is assembled. G consists of a set of meshing power source vertices Q, a set of meshing power sink vertices S, a set of planet vertices P and a set of edges E. Each edge $e \in E$ features a meshing power $P_m(e)$. G' consists of the corresponding set of meshing power source vertices Q', the corresponding set of meshing

power sink vertices S' and edges E'. An edge e' $\in$ E' features a meshing power $P_m(e')$. Naturally, G' does not contain planets.

Step 1: G is given. Set up the virtual subgraph G' with sources Q' and sinks S' without edges.

Step 2: Remove all edges from G with $P_m(e) = 0$.

Step 3: Choose a source q $\in$ Q and a sink s $\in$ S.

Step 4: Find the shortest path L between q and s and the involved edges e $\in$ L. If no path is found go to step 3.

Step 5: Check the directions of all edges e $\in$ L. Path L is feasible it leads from the source to the sink. If path L is not feasible go to step 3.

Step 6: Find the minimum meshing power $P_{m,min}$ of all edges e $\in$ L. Insert a new edge e' into G' from q' to s' with $P_m(e') = P_{m,min}$.

Step 7: Update G by subtracting $P_{m,min}$ from all edges e $\in$ L.

Step 8: Go to step 2 until all edges are removed from G.

Step 9: Insert further edges e' into G' to make the substitution figure kinematically-equivalent if necessary (→ optional).

Step 10: Build functionally-equivalent substitution figure.

The procedure works for operating conditions with or without power losses. When power losses are taken into account, one must consider in finding the minimum meshing power $P_{m.min}$ that the meshing power is decreasing along the path L.

With every full cycle of steps 2 to 8, at least one edge is removed from G until all edges are removed successively. Simultaneously, G' is assembled featuring edges between sources and sinks exclusively as required. As G is of the tree structure, it is cut into two further subtrees by every full cycle. Thus, the removed path can be interpreted as a missing edge connecting two trees. If two trees are connected by a single edge, the originated entire graph must be of the tree structure again. Hence, G' is a tree.

Figure 4-16 illustrates the transformation of a gear pair subgraph of an example 5-shaft CCPGT into a functionally-equivalent substitution figure. The procedure starts with vertex 2 as selected source and vertex 4 as selected sink. **Figure 4-17** shows the transformation of the same transmission with the same operating condition, but starting with vertex 1 as selected source and vertex 4 as selected sink. Both cases lead to functionally-equivalent but different substitution figures. Hence, the representation by means of functionally-equivalent substitution figures is neither definite nor unique. The question of how many

functionally-equivalent substitution figures exist depends on the structure of the CCPGT and on the operating condition itself. **In any case, at least one functionally-equivalent substitution figure must be available.**

Figure 4-18 shows another special case. The meshing power flow is on hand in such a manner that only two cycles of steps 2 to 8 are necessary to remove all edges from G. However, three basic trains are needed to generate a kinematically-equivalent substitution figure. Therefore, an additional (arbitrary) edge is added into G' by applying step 9. This edge does not feature any meshing power. Therefore, it does not influence the efficiency calculation, but it establishes a kinematic link.

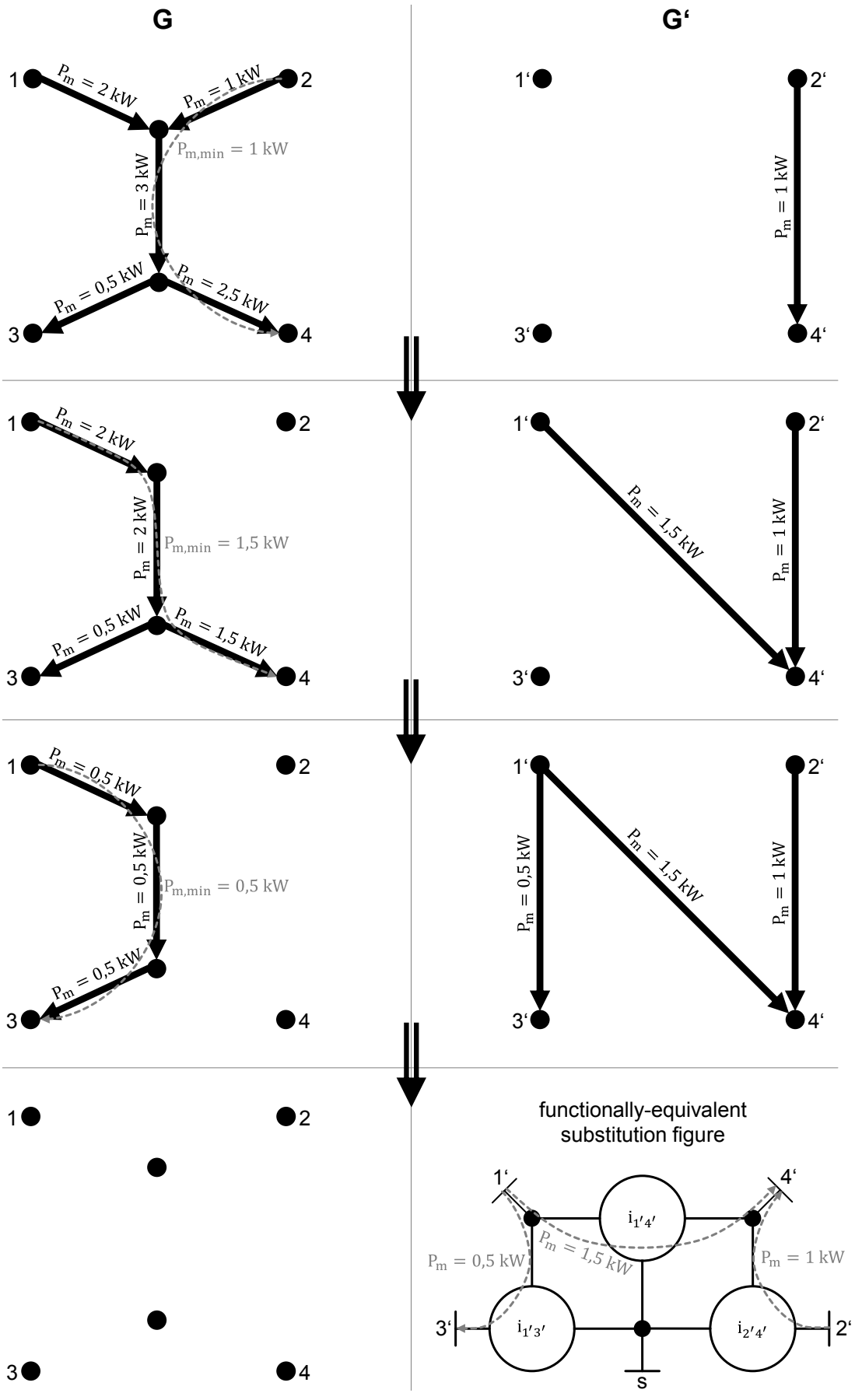

Figure 4-16: An example transformation of a CCPGT gear pair subgraph into a functionally-equivalent substitution figure

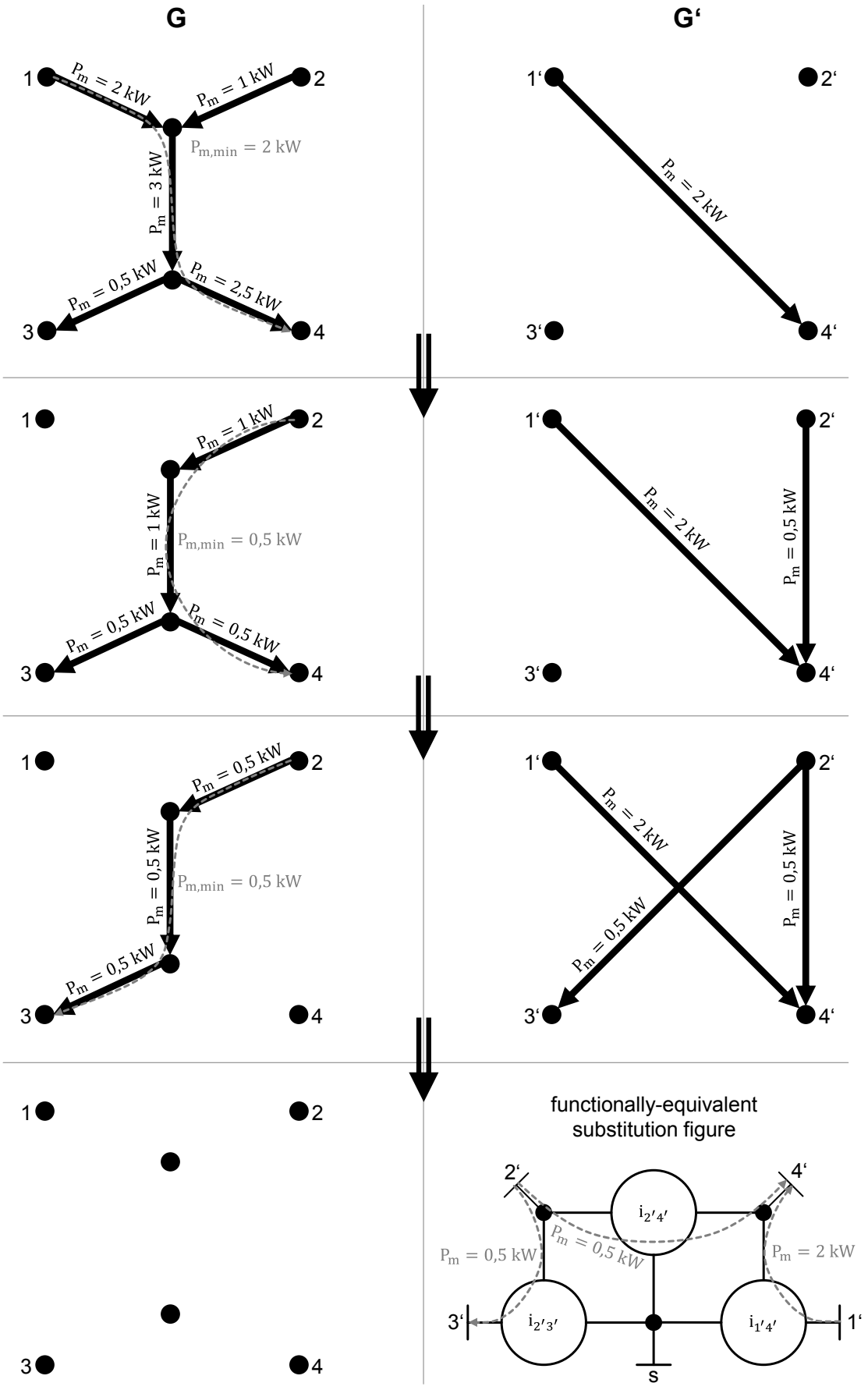

Figure 4-17: An example transformation of a CCPGT gear pair subgraph into a functionally-equivalent substitution figure

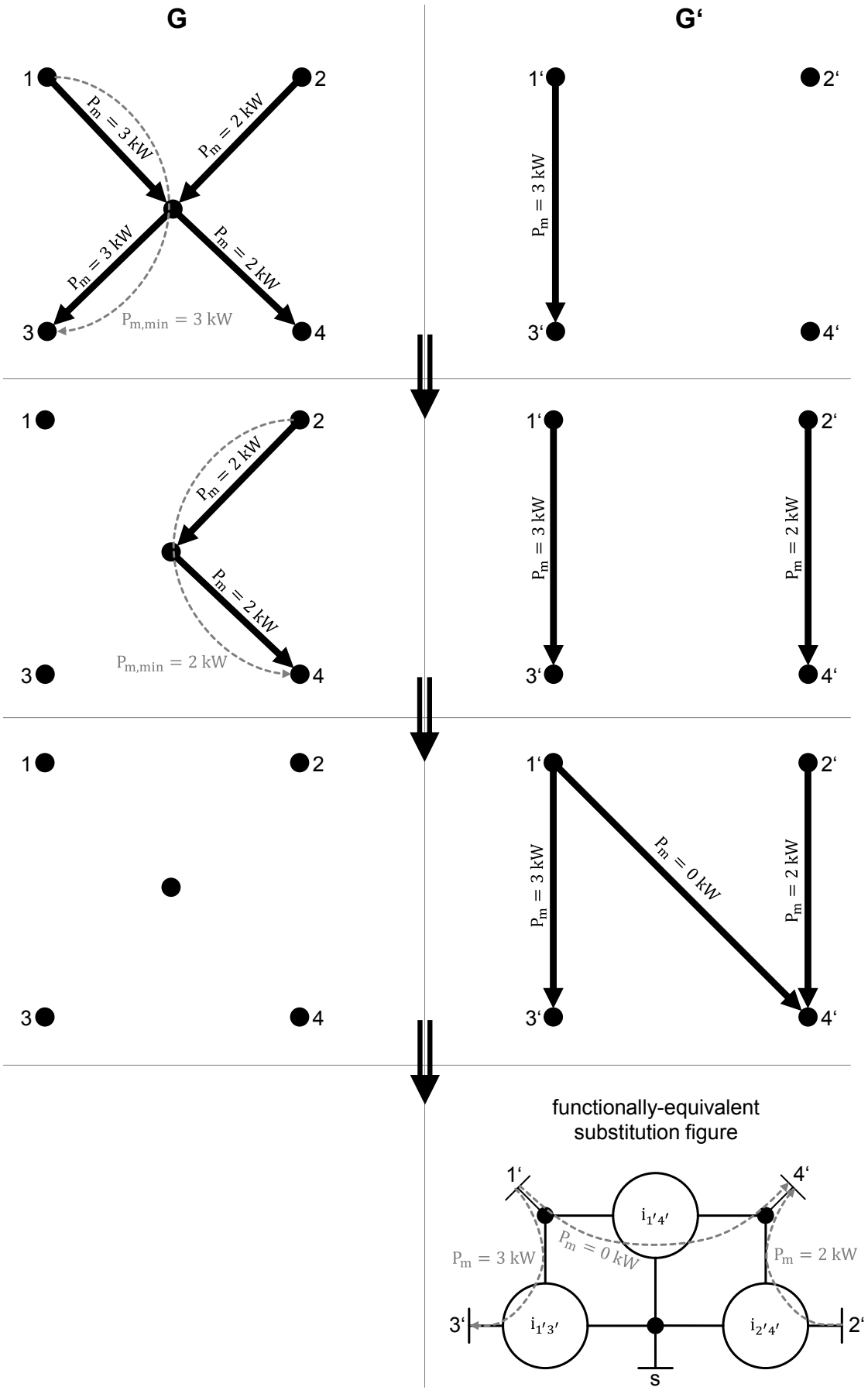

Figure 4-18: An example transformation of a CCPGT gear pair subgraph into a functionally-equivalent substitution figure

4.2.3.4 Identification of functionally-equivalent substitution figures among kinematically-equivalent substitution figures

Carrying out the procedure described in the previous Section 4.2.3.3 does not lead to a significant simplification of the efficiency calculation. The dimension of the statics system of equations for the functionally-equivalent substitution figure is slightly smaller than that of the realistic transmission model as the number of required basic trains is less than the number of basic gearings (cf. Sections 4.1.3 and 4.2.2.2). But at this, the transformation procedure results in extra computing time. However, the method of generating functionally-equivalent substitution figures does make sense if these figures are derived directly without performing a transformation procedure. For a limited number of central shafts, substitution figures constitute a clearly arranged and manually performable calculation tool.

A possible way to avoid the transformation procedure is to perform the efficiency calculation using kinematically-equivalent substitution figures which can be derived fast (Section 4.2.1.2). A kinematics and statics analysis for loss-free operating condition is to be performed first for each kinematically-equivalent substitution figure. After finding out the direction of meshing power flow for each basic train and Wolf symbol respectively, the basic ratios are to multiplied or divided by their basic efficiency factors within the statics system of equations. Using the nomenclature of Section 4.2.2.2 the calculation rule reads:

$$i_w \Rightarrow i_w \cdot \eta_0^{w1} \quad \text{with} \quad w1 = \begin{cases} +1 & \text{if } T_{i,x,w} \cdot (n_x - n_s) < 0 \\ -1 & \text{if } T_{i,x,w} \cdot (n_x - n_s) > 0 \\ 0 & \text{if } T_{i,x,w} \cdot (n_x - n_s) = 0 \end{cases} \qquad (4.28)$$

i_w	[-]	basic ratio of Wolf symbol w	$T_{i,x,w}$	[Nm]	internal torque of member x of Wolf symbol w
η_0	[-]	basic efficiency of Wolf symbol w			
$w1$	[-]	efficiency exponent	n_x	[1/s]	speed of member x
			n_s	[1/s]	speed of carrier s

As the direction of meshing power flow may change due to inclusion of power losses, an iteration is needed analogical to Section 4.1.5 and **Figure 4-6**. Through this, it is not possible to preselect potential functionally-equivalent substitution figures by checking the meshing power flow directions of central gear coupling shafts on the basis of the loss-free analysis. In other word, kinematically-equivalent substitution figures can turn into functionally-equivalent substitution figures after considering power losses due to a change of power flow directions. This case is discussed in detail within Section 4.4. Finally, the functionally-equivalent substitution figures are identified amongst the kinematically-equivalent substitution figures as they feature the best overall efficiency and the lowest overall power loss respectively according to Section 4.2.3.2.

Anyhow, due to the huge number of kinematically-equivalent substitution figures especially for large numbers of central shafts (cf. **Table 4-3**), a grouping of central shafts into meshing power sources and sinks is feasible after carrying out the statics analysis for loss-free operating conditions. It is known that the virtual subgraph of a functionally-equivalent substitution figure is a *bipartite tree* meaning that all vertices can be divided into two groups, here sources and sinks. Only those virtual subgraphs lead to adequate substitution figures

whose edges connect sources to sinks exclusively. For a given number of sources and sinks, the number of bipartite trees is much smaller than the number of arbitrary trees. According to [7_PAU04 and 7_HAJ10], the number of bipartite trees or the number of potential functionally-equivalent substitution figures is:

$$\mathrm{SUB_{bip}} = \mathrm{Q}^{\mathrm{S}-1} \cdot \mathrm{S}^{\mathrm{Q}-1} \qquad (4.29)$$

SUB_{bip}	[-]	total number of potential functionally-equivalent substitution figures gained from bipartite trees	Q	[-]	total number of meshing power sources
			S	[-]	total number of meshing power sinks

Table 4-4 lists the number of potential functionally-equivalent substitution figures in comparison to the number of kinematically-equivalent substitution figures. For a given number of central shafts, the worst case is assumed, meaning that the number of sources is preferably equal to the number of sinks. Naturally, at least one source and one sink has to exist.

CS	3	4	5	6	7	8	9	10	11
Q	1	2	2	3	3	4	4	5	5
S	1	1	2	2	3	3	4	4	5
SUB_{bip}	1	1	4	12	81	432	4.096	32.000	390.625
SUB_{kin}	1	3	16	125	1.296	16.807	262.144	4.782.969	100.000.000

SUB_{kin}	[-]	total number kinematically-equivalent substitution figures	SUB_{bip}	[-]	total number of potential functionally-equivalent substitution figures gained from bipartite trees
CS	[-]	total number of central shafts			
Q	[-]	total number of meshing power sources	S	[-]	total number of meshing power sinks

Table 4-4: Number of potential functionally-equivalent substitution figures

By way of example, normally only 12 substitution figures have to be analyzed instead of 125 for a 6-shaft CCPGT. This difference rises rapidly with the number of central shafts increasing (**Figure 4-19**). Using up to five central shafts, the division of central gears into meshing power sources and sinks becomes of special relevance and is discussed in detail within Section 4.2.5.

When considering power losses, sinks might become sources and vice versa in contrast to the loss-free analysis. Therefore, a change of direction of the meshing power in each basic train must be observed. If such a change of direction occurs, the previous assumptions regarding sources and sinks turns out to be incorrect and the bipartite trees do not lead to functionally-equivalent substitution figures. Thus, the grouping of central gear vertices into sources and sinks needs to be modified. According to the number of static DOF, only two central shaft torques are unknown. This means that either one central gear torque and the carrier shaft torque or two central gear torques are unknowns. As such, there are only two or four feasible groupings as most of the torques and meshing power flows are predefined. For the worst case, four groups of bipartite trees are to be calculated to find the functional-

ly-equivalent substitution figures. Still, the number of these trees is smaller than the number of all arbitrary trees. Also, it is not necessary to carry out a complete iteration for a substitution figure if a change of direction is observed as this substitution figure belongs to a wrong group. Naturally, it is much more efficient to use bipartite trees than to analyze all kinematically-equivalent substitution figures. Again, the functionally-equivalent substitution figures are identified among the substitution figures gained from bipartite trees as the ones featuring the best overall efficiency. Exemplarily, **Figure 4-20** illustrates one correct and two incorrect bipartite trees.

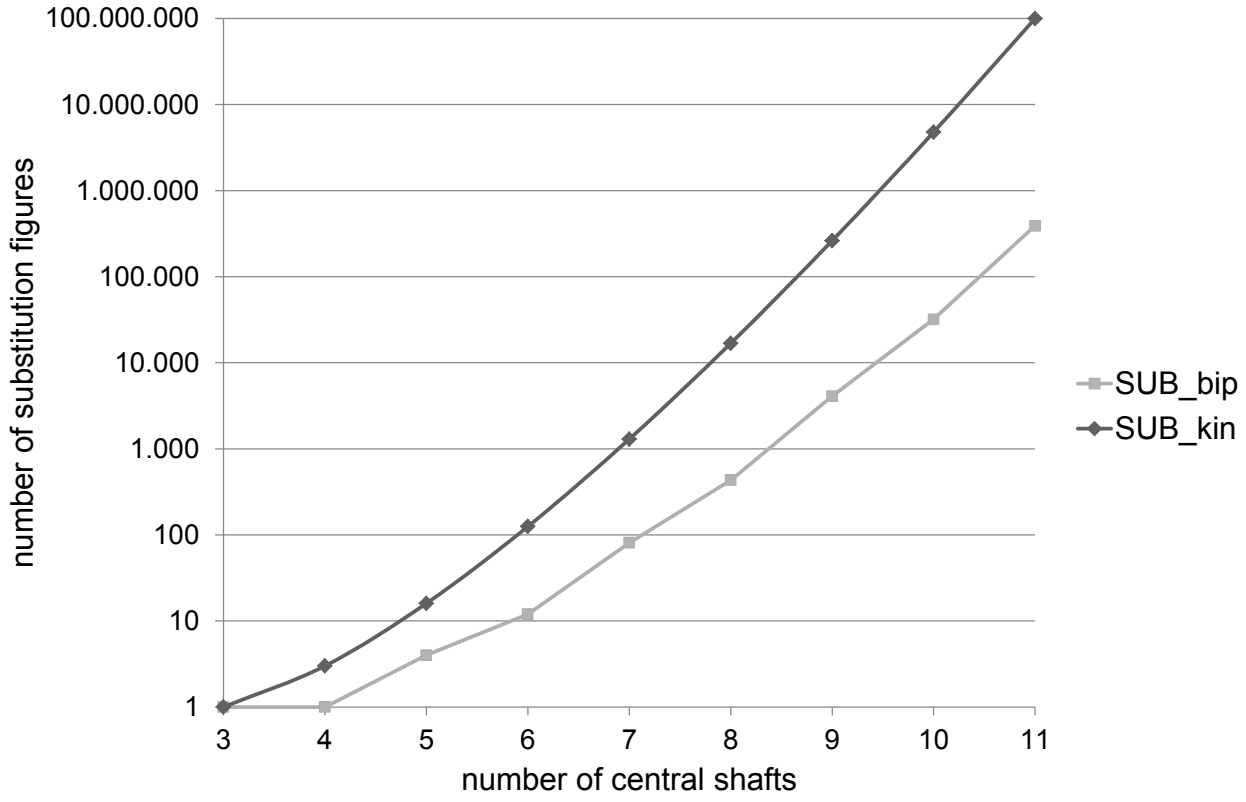

Figure 4-19: Number of kinematically-equivalent substitution figures SUB_kin and potential functionally-equivalent substitution figures SUB_bip

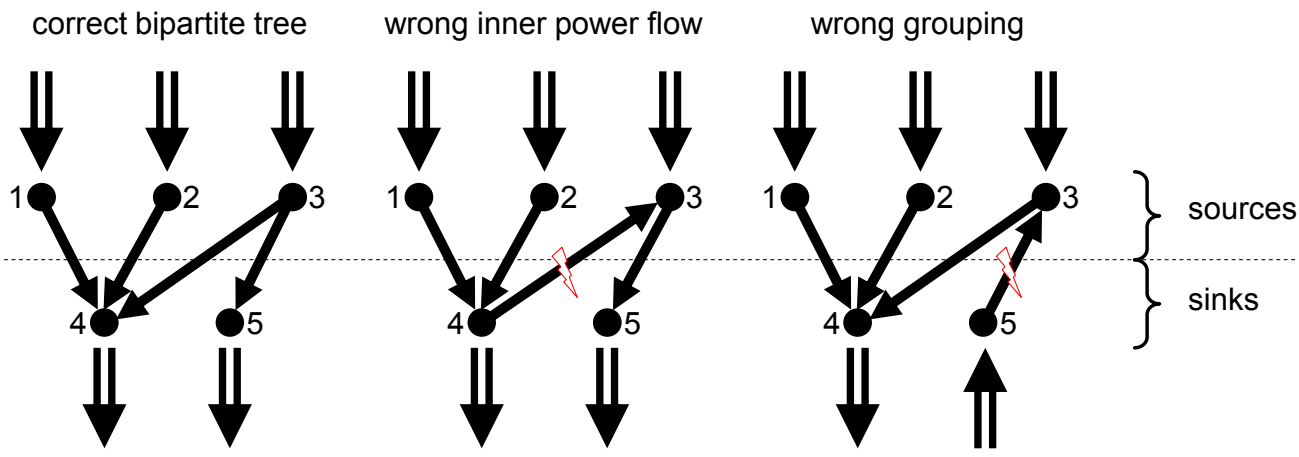

Figure 4-20: Examples of correct and incorrect directed bipartite trees

4.2.4 Overall efficiency

After performing a statics analysis considering power losses, the overall efficiency for a certain substitution figure is derived according to Section 4.1.7. Every row of the statics system of equations sums the torques acting on a central shaft (Section 4.2.2.2). Two external torques are unknown and to be found within the torque state vector. Other external torques given as preset values are inserted directly in the torque solution vector. The final expression for the overall efficiency is identical to (4.16).

4.2.5 Special cases for limited number of shafts

For a limited number of central shafts, only few operating conditions are to be distinguished. Also the number of possible substitution figures is limited. In the following, CCPGTs with up to five central shafts are discussed and the number of loaded central shafts is increased incrementally.

4.2.5.1 4-shaft CCPGT featuring three loaded shafts

The substitution figure for a 4-shaft CCPGT consists of two Wolf symbols according to equation (4.19). Three basic trains are contained within a 4-shaft CCPGT according to equation (4.20). Thus, three feasible and kinematically-equivalent substitution figures can be derived in reference to **Table 4-3**. An example is shown in **Figure 3-17**.

Often, CCPGTs are used as speed increasers or speed reducers with only three central shafts being loaded (epicyclic ratios or compound ratios). Those three shafts can either be two central gear shafts and the carrier shaft or three central gear shafts.

4.2.5.1.1 Operating conditions with two central gear shafts and the carrier shaft being loaded

The operating case with two central gear shafts and the carrier shaft being loaded is rather simple as the 4-shaft CCPGT works like a single PGT with one central gear shaft being unloaded. Then, the single PGT featuring the loaded shafts has to occur explicitly within the substitution figure. A second Wolf symbol is only needed to set up a kinematic link to the unloaded third central gear shaft. Therefore, two functionally-equivalent substitution figures exist (**Figure 4-21**). If the mentioned single PGT does not occur explicitly within the substitution figure unloaded shafts have to perform as loaded shafts (central gear 1 in **Figure 4-21**), causing a detour for the meshing power flow. This leads to too much meshing power. Thus, it is not allowed to substitute a single PGT by a set of PGTs featuring central gear shafts with no external load.

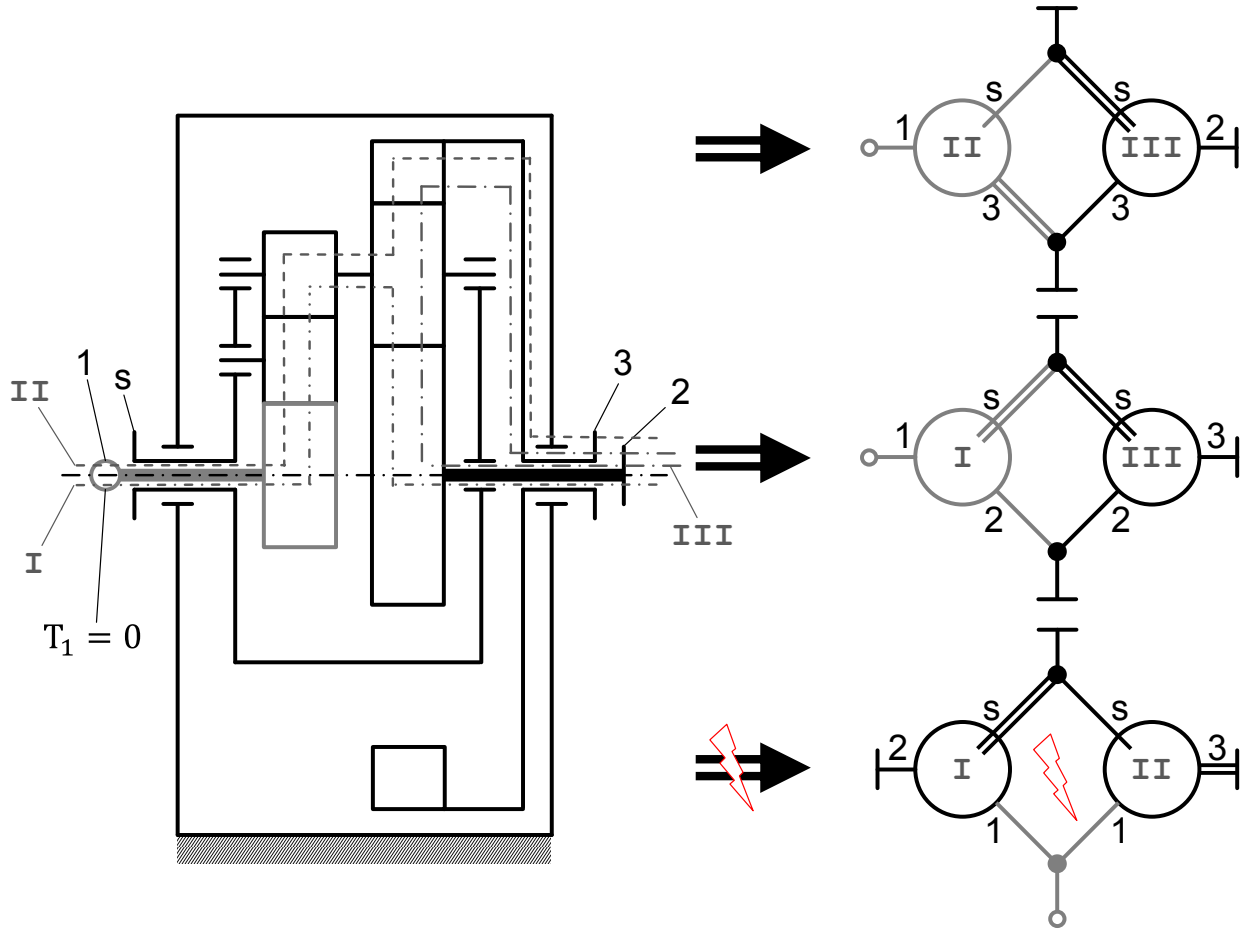

Figure 4-21: Functionally-equivalent substitution figures for a 4-shaft CCPGT with only two loaded central gear shafts and a loaded carrier shaft

Below, operating cases with unloaded central gear shafts will not be considered. In this case, additional Wolf symbols are to be added to the substitution figure to set up an appropriate kinematic link.

4.2.5.1.2 Operating conditions with three central gear shafts being loaded and the carrier shaft being unloaded

The case of an unloaded carrier shaft and three loaded central gear shafts means that all three central gears feature meshing power for the non-trivial case. With respect to the meshing power only, two operating conditions are possible: power partition or power summation. There are either two meshing power sources and one sink or one source and two sinks (**Figure 4-22**). Thus, only one substitution figure can be functionally-equivalent. Furthermore, a 4-shaft CCPGT features a static DOF of two. If the torque of the carrier shaft is set to be zero, the unknown torques of two central gears depend on only one central gear torque as preset value. Hence, the torque ratios do not change for one of the cases of **Figure 4-22**.

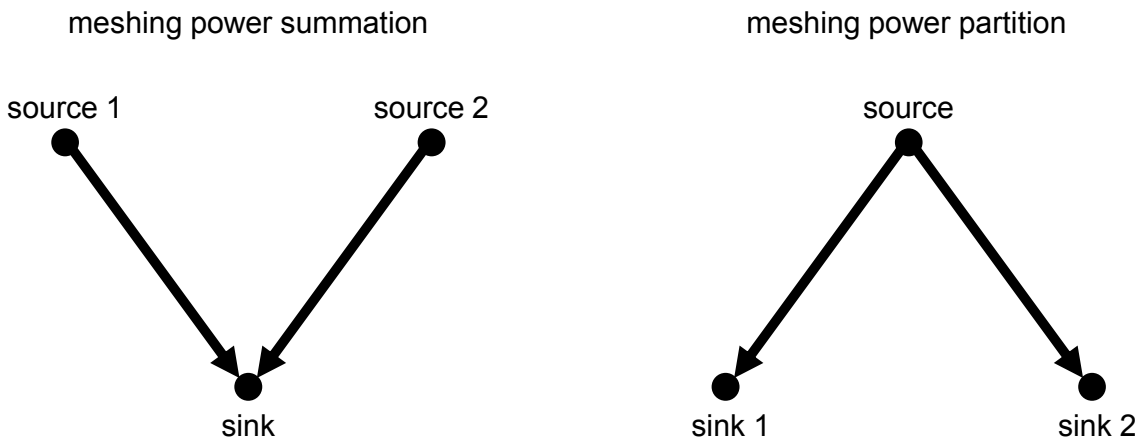

Figure 4-22: Virtual subgraphs of substitution figures for CCPGTs with three loaded central gear shafts

Among the kinematically-equivalent substitution figures, the one is to be found featuring inner torques with equal signs at the central gear coupling shaft (**Figure 4-23**). For this purpose, the basic structure is cut free. As the external torque of the carrier shaft is equal to zero, the signs of the inner torques of the carrier shaft are opposite. Finally, in order to get equal signs of the inner torques of the central gear coupling shaft, one Wolf symbol must provide a change of signs of its inner torques and the other Wolf symbol must provide equal signs. This can only be true if one summation shaft belongs to a coupling shaft and the other one does not. As a first result, two functionally-equivalent substitution figures are gained, which corresponds to the results of Mueller [2_MUL01]. One features a negative and a positive-ratio drive, the other one features two positive-ratio drives. Which one is feasible for which CCPGT depends on the design of the CCPGT.

The chain of basic train ratios with fixed carrier from central gear 1 to central gear 2 to central gear 3 and back to central gear 1 must equal +1. The three basic train ratios of a 4-shaft CCPGT can either be three positive-ratio drives or two negative-ratio drives and one positive-ratio drive.

Without loss of generality, a 4-shaft CCPGT shall contain two negative-ratio drives and a positive-ratio drive with a ratio range defined in **Figure 4-24**. Among the kinematically-equivalent substitution figures, only one can be identified as being functionally-equivalent according to **Figure 4-23** (bottom left). Also without loss of generality, another 4-shaft CCPGT shall contain three positive-ratio drives with a ratio range defined in **Figure 4-25**. Again, only one substitution figure can be identified as being functionally-equivalent according to **Figure 4-23** (bottom right). **In sum, for the operating condition with three loaded central gear shafts and an unloaded carrier shaft, a definite functionally-equivalent substitution figure can be identified which does not depend on further operating conditions.** Only two different solutions are possible as a function of the design of the CCPGT. Naturally, the central gear coupling shaft is always the *total-meshing-power* shaft and the other central gear shafts are *partial-meshing-power* shafts.

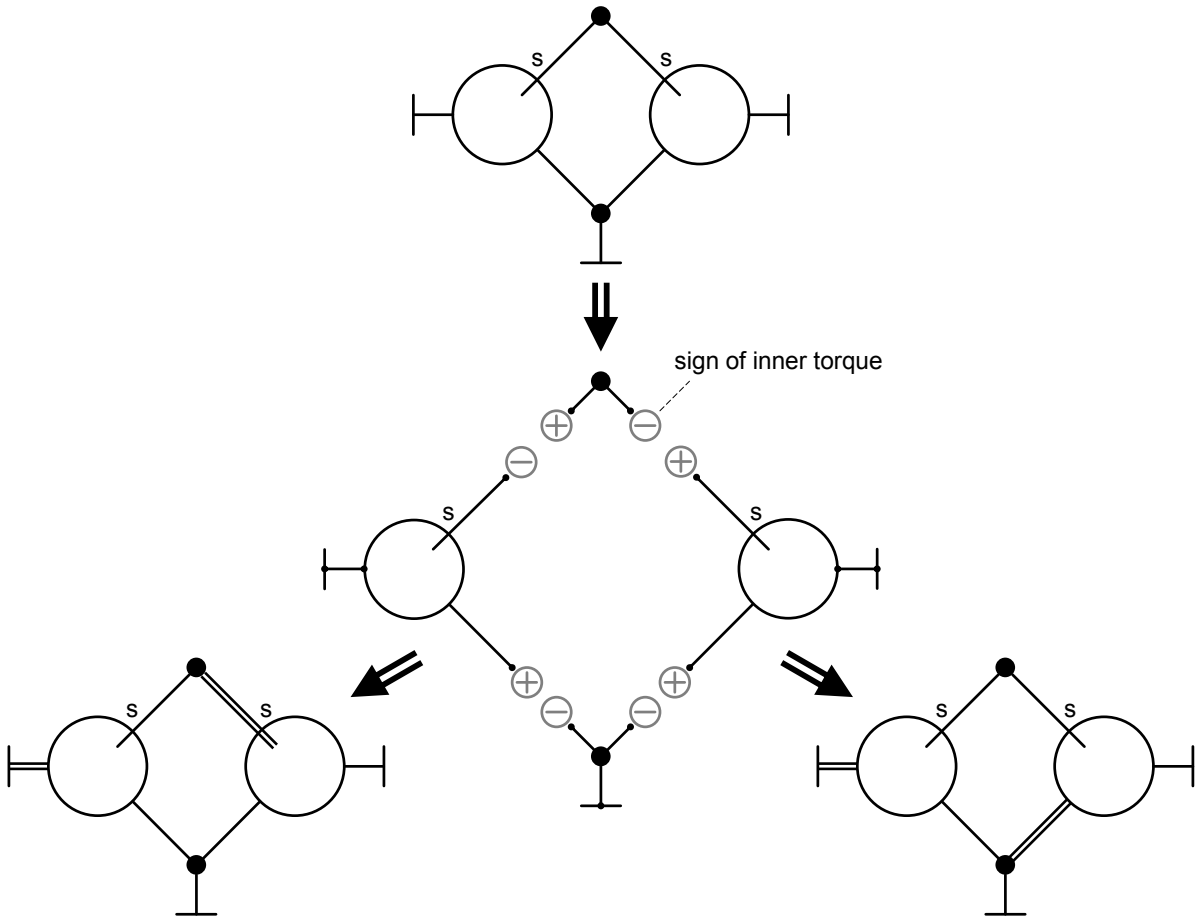

Figure 4-23: Functionally-equivalent substitution figures for CCPGTs with three loaded central gear shafts and unloaded carrier shaft

$$\underbrace{i_{12}^{s}}_{\substack{>0\\<1}} \cdot \underbrace{i_{23}^{s}}_{<0} \cdot \underbrace{i_{31}^{s}}_{<0} = +1$$

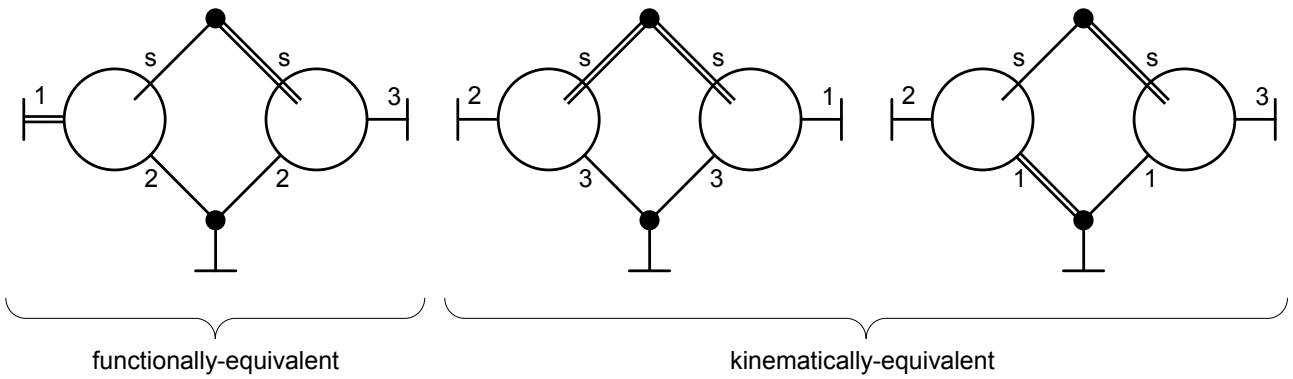

Figure 4-24: Functionally-equivalent substitution figure for 4-shaft CCPGTs with three loaded central gear shafts and unloaded carrier shaft containing two negative-ratio drives and one positive-ratio drive

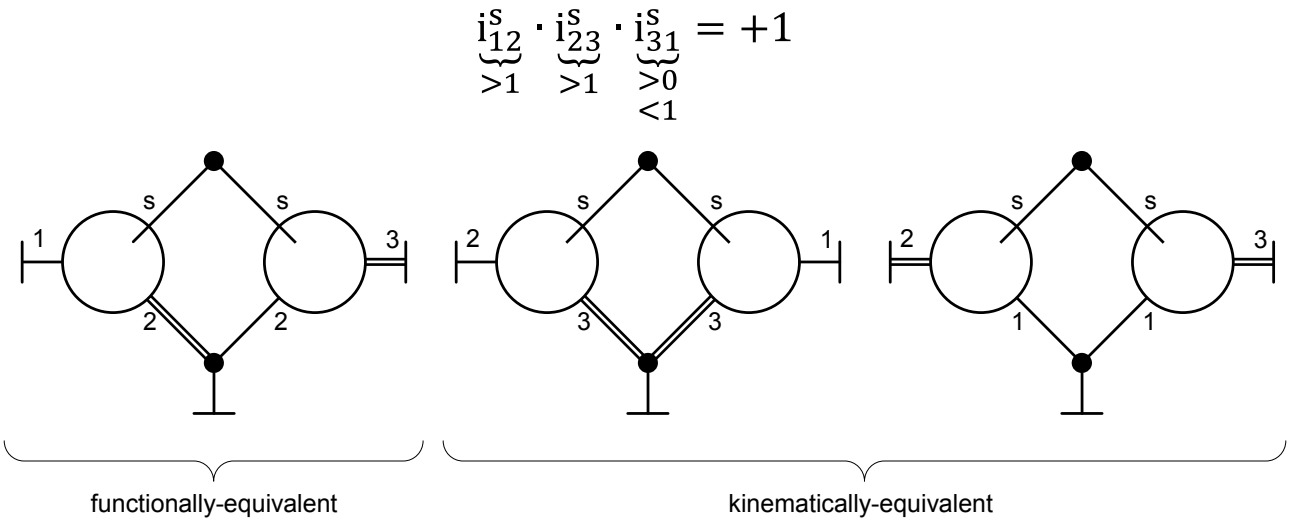

Figure 4-25: Functionally-equivalent substitution figure for CCPGTs with three loaded central gear shafts and unloaded carrier shaft containing three positive-ratio drives

As for the targeted operating condition, only three central shafts are connected to the periphery. As such, a further substitution helps simplify the efficiency calculation. For this purpose the functionally-equivalent substitution figure is replaced by a virtual 3-shaft single PGT (**Figure 4-26**).

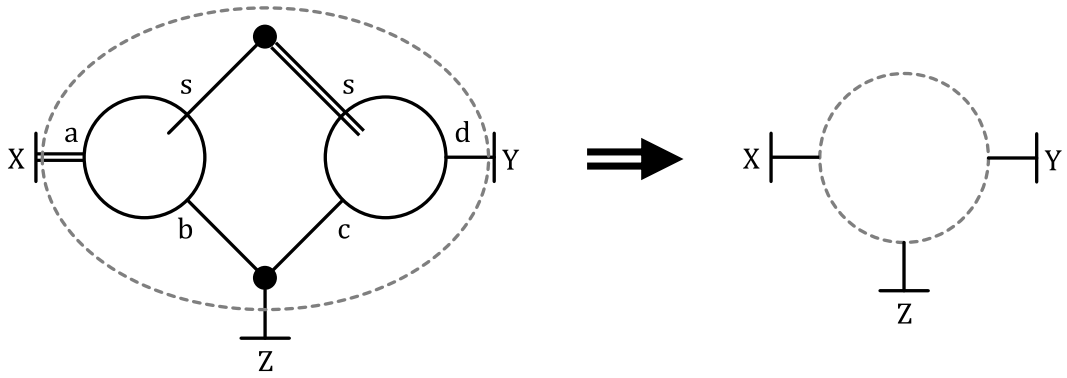

Figure 4-26: Example substitution of a functionally-equivalent substitution figure with three loaded central gear shafts and unloaded carrier shaft

Its virtual basic train ratio is easily obtained as the product of epicyclic ratios of contained Wolf symbols:

$$i_{XY}^{Z} = i_{as}^{b} \cdot i_{sd}^{c} \quad \text{or} \quad i_{YX}^{Z} = i_{ds}^{c} \cdot i_{sa}^{b} \qquad (4.30)$$

i_{XY}^{Z}/i_{YX}^{Z} [-]	virtual basic train ratio	$i_{as}^{b}/i_{sa}^{b}/i_{sd}^{c}/i_{ds}^{c}$ [-]	epicyclic ratio of Wolf Symbol

The virtual basic train efficiency is derived as the product of corresponding efficiency values of Wolf symbols for the focused operating condition:

$$\eta_{XY}^{Z} = \eta_{as}^{b} \cdot \eta_{sd}^{c} \quad \text{and} \quad \eta_{YX}^{Z} = \eta_{ds}^{c} \cdot \eta_{sa}^{b} \qquad (4.31)$$

$\eta_{XY}^{Z}/\eta_{YX}^{Z}$ [-]	virtual basic train efficiency	$\eta_{as}^{b}/\eta_{sa}^{b}/\eta_{sd}^{c}/\eta_{ds}^{c}$ [-]	epicyclic efficiency of Wolf Symbol

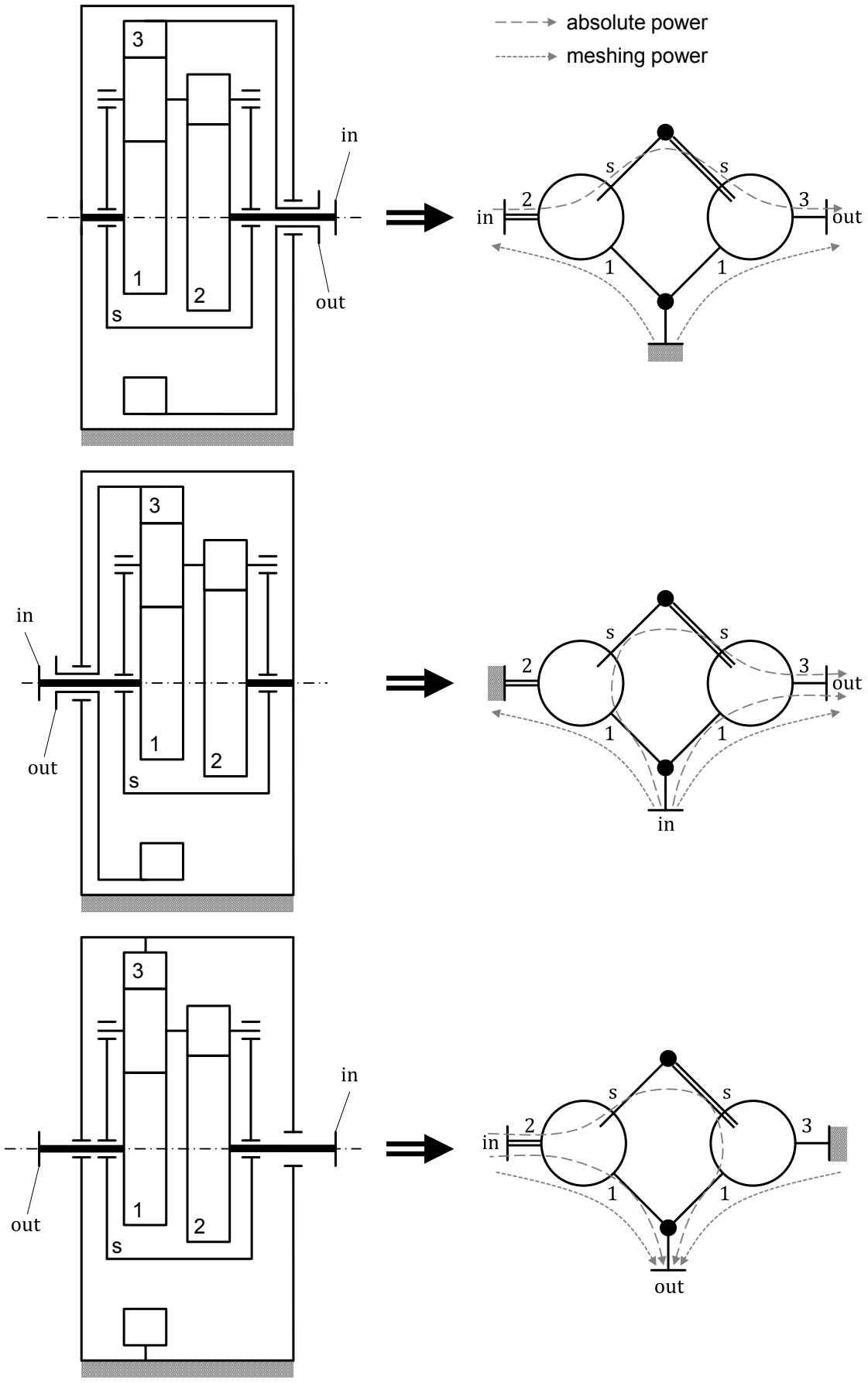

Figure 4-27: Example functionally-equivalent substitution figures for compound ratios of a 4-shaft CCPGT

Now, the 3-shaft PGT can be treated just like a real single PGT. But as the 3-shaft single PGT is only a virtual PGT, its basic train ratio is not related to a real basic train ratio with fixed carrier. The basic train ratio and also the basic efficiency are auxiliary quantities. Therefore, symmetry in respect of the basic efficiency values is not to be expected in general ($\eta^{Z}_{XY} \neq \eta^{Z}_{YX}$).

As an example, **Figure 4-27** shows operating conditions for three different compound ratios of a 4-shaft CCPGT. Within the functionally-equivalent substitution figures, a partition of the absolute power is monitored. This power partition does not occur in reality as the real CCPGT does not consist of separate basic trains. Also, the meshing power partition or summation is located at the planet in reality instead of the coupling shaft in the substitution figure (cf. **Figure 4-5**).

4.2.5.2 4-shaft CCPGT featuring four loaded shafts

For the case of three loaded central gear shafts and a loaded carrier shaft, possible operating conditions are slightly different to those of the previous section. First of all, there has to be more than one power input or output shaft. Yet, **Figure 4-22** is still valid since only three central gears feature meshing power. In contrast to the operating condition with the carrier shaft being unloaded, a total-meshing-power shaft cannot be identified without analyzing kinematics and statics. According to the static DOF, two external torques can be selected independently. Thus, the ratio and the signs of inner torques of the central gear coupling shaft are also a function of the external torques in addition to being a function of the basic train ratios. **Figure 4-28** shows all kinematically-equivalent substitution figures of a 4-shaft CCPGT. The shafts are marked with a superscript denoting which Wolf symbol they belong to.

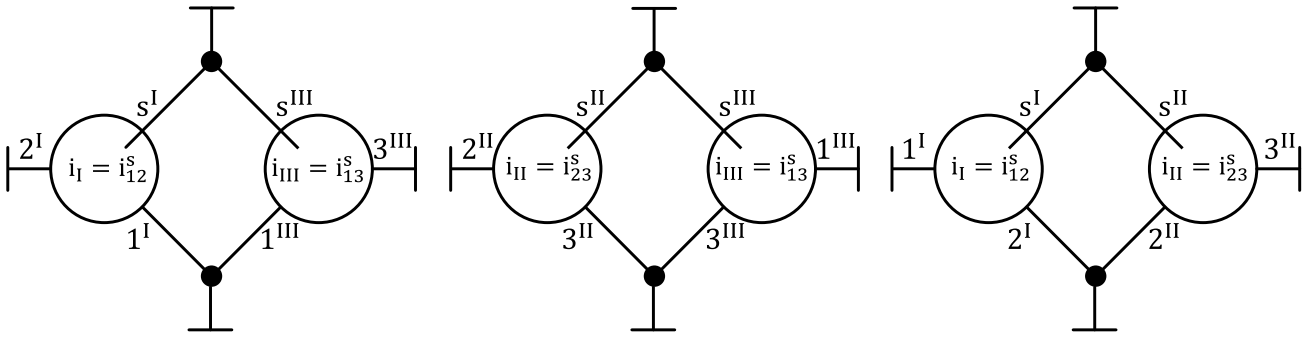

Figure 4-28: Kinematically-equivalent substitution figures for a 4-shaft CCPGT

Neglecting power losses, the ratio of inner torques of the coupling shaft can be derived for each substitution figure as a function of the basic train ratios and a ratio of external torques. Here, the external torques of central shaft 1 and the carrier central shaft s shall be given as presets without loss of generality:

$$v^* := \frac{T_1}{T_s}$$

$$\frac{T_{1^I}}{T_{1^{III}}} = v^I = -\frac{v^* - i_{III} + 1}{v^* - i_I + 1}$$

$$\frac{T_{2^I}}{T_{2^{II}}} = v^{II} = \frac{i_I - i_{III}}{v^* - i_I + 1} \qquad (4.32)$$

$$\frac{T_{3^{II}}}{T_{3^{III}}} = v^{III} = \frac{v^* - i_{III} + 1}{i_{III} - i_I}$$

T	[Nm]	internal torque	v	[-]	torque ratio
			i	[-]	basic train ratio

The correct functionally-equivalent substitution figures shows a positive torque ratio v^I, v^{II} or v^{III}. Isolating v^*, the torque ratios v^I, v^{II} and v^{III} can be expressed as a function of each other as:

$$v^I = -v^{II} - 1 = -\frac{v^{III}}{v^{III} + 1}$$

$$v^{II} = -v^I - 1 = -\frac{1}{v^{III} + 1} \qquad (4.33)$$

$$v^{III} = -\frac{v^I}{v^I + 1} = -\frac{v^{II} + 1}{v^{II}}$$

v	[-]	torque ratio

In **Figure 4-29**, the torque ratios v^{II} and v^{III} are drawn as a function of the torque ratio v^I. It can easily be seen that only one of these ratios can be positive at the same time. Naturally, this result complies with **Figure 4-22** since only one central gear shaft can represent the total-meshing-power shaft for a certain operating condition. To identify this shaft, a loss-free analysis is to be carried out first. Afterwards, the functionally-equivalent substitution figure can directly be derived. If change of direction of meshing power flows is monitored when the power losses are included, the assumption regarding meshing power sources and sinks is to be corrected (cf. Section 4.2.3.4).

The following definitive numerical example is intended to illustrate the calculation steps. **Figure 4-30** shows a 4-shaft CCPGT including basic train ratios and basic efficiency values. For each basic gearing, an efficiency of 99% is assumed. Furthermore, it is assumed that the speeds and external torques of central shaft 1 and 2 are predefined according to equation (4.34). Hence, for this example, central shaft 1 is a power input and central shaft 2 is a power output.

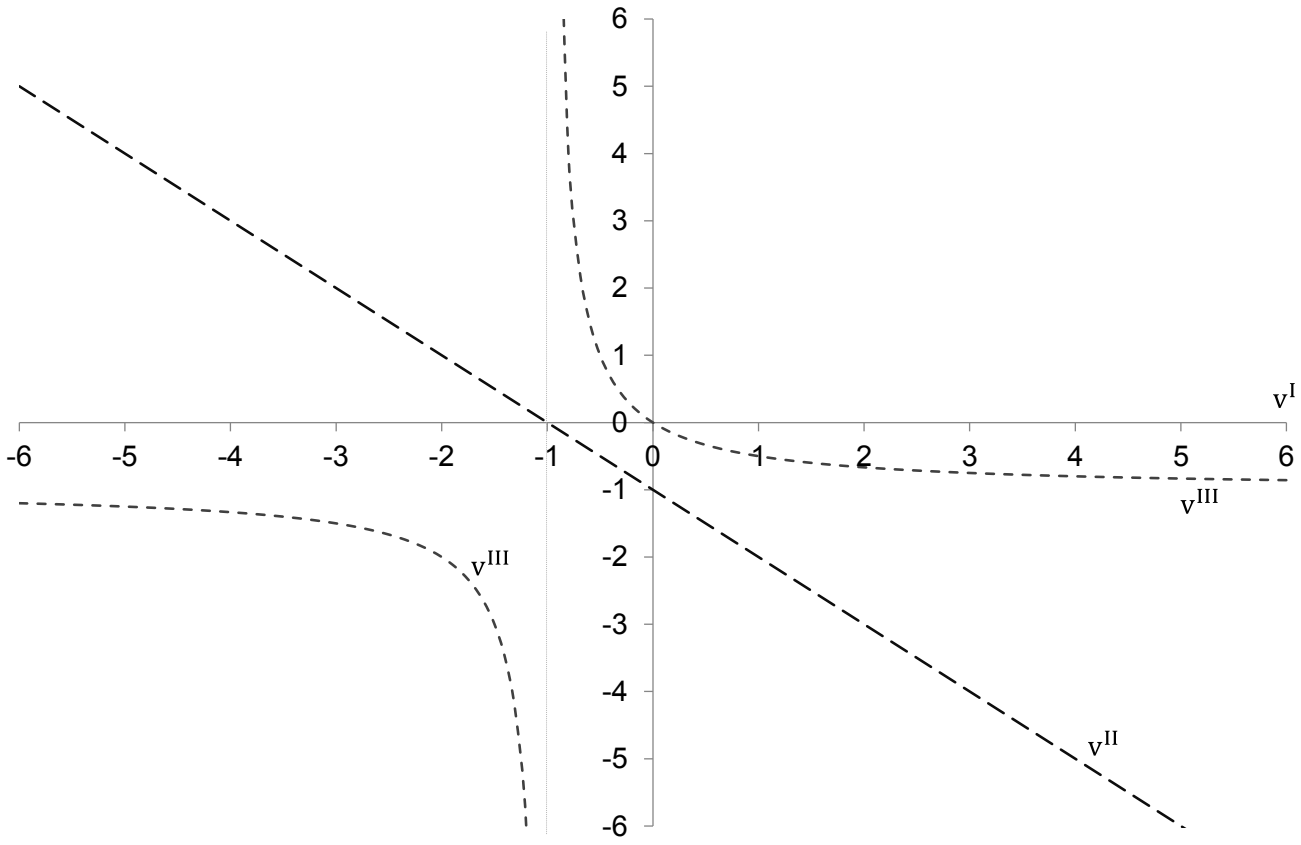

Figure 4-29: Ratios of inner torques of the central gear coupling shaft in kinematically-equivalent substitution figures for 4-shaft CCPGTs

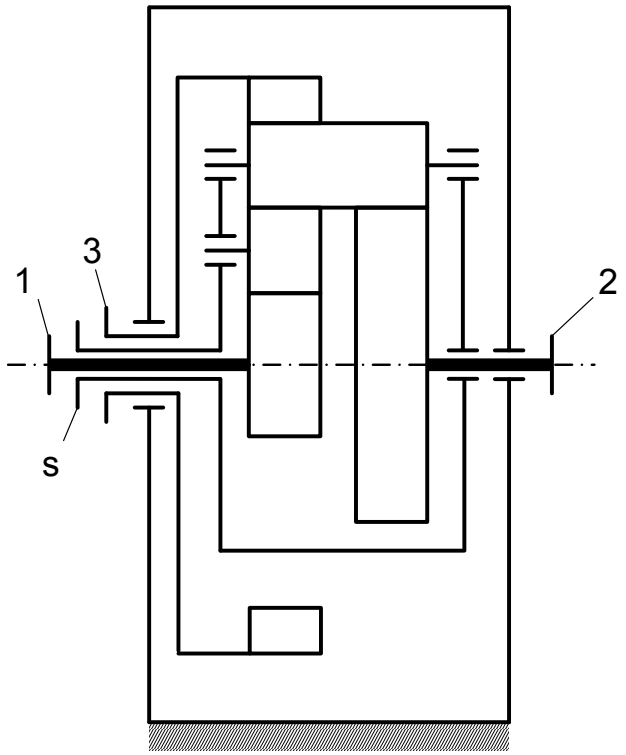

$$i_I = i_{12}^s = -2$$
$$i_{II} = i_{13}^s = +3$$
$$i_{III} = i_{23}^s = -1{,}5$$

$$\eta_{0,I} = 0{,}99^3 \approx 0{,}97$$
$$\eta_{0,II} = 0{,}99^3 \approx 0{,}97$$
$$\eta_{0,III} = 0{,}99^2 \approx 0{,}98$$

Figure 4-30: Example 4-shaft CCPGT with predefined values for basic train ratios and basic efficiencies

$$n_1 = 1000\ \text{rpm}\ ;\ T_1 = \quad 100\ \text{Nm}\ \Rightarrow\ P_1 = \quad 10472\ \text{W}$$
$$n_2 = 1500\ \text{rpm}\ ;\ T_2 = -200\ \text{Nm}\ \Rightarrow\ P_2 = -31416\ \text{W} \qquad (4.34)$$

n	[rpm]	absolute speed	T	[Nm]	external torque
			P	[W]	external (absolute) power

As the first step, a loss-free analysis is performed using Willis Equations for the kinematics as well as equations (4.25) and (4.26) for the statics:

$$n_s = 1333{,}3\ \text{rpm}\ ;\ T_s = \quad 700\ \text{Nm}\ \Rightarrow\ P_s = \quad 97736\ \text{W}$$
$$n_3 = 1222{,}2\ \text{rpm}\ ;\ T_3 = -600\ \text{Nm}\ \Rightarrow\ P_3 = -76793\ \text{W} \qquad (4.35)$$

n	[rpm]	absolute speed	T	[Nm]	external torque
			P	[W]	external (absolute) power

Here, the carrier shaft acts as an additional power input and central shaft 3 works as a power output. Next, meshing speeds and meshing powers are determined:

$$n_1' = -333{,}3\ \text{rpm}\ ;\ n_2' = +166{,}7\ \text{rpm}\ ;\ n_3' = -111{,}1\ \text{rpm}$$
$$P_{m1} = -3490\ \text{W}\ ;\ P_{m2} = -3491\ \text{W}\ ;\ P_{m3} = 6981\ \text{W} \qquad (4.36)$$

n'	[rpm]	meshing speed	P_m	[W]	meshing power

Consequently, central shaft 3 is the total-meshing-power shaft. The functionally-equivalent substitution figure for this operating condition is drawn in **Figure 4-31**.

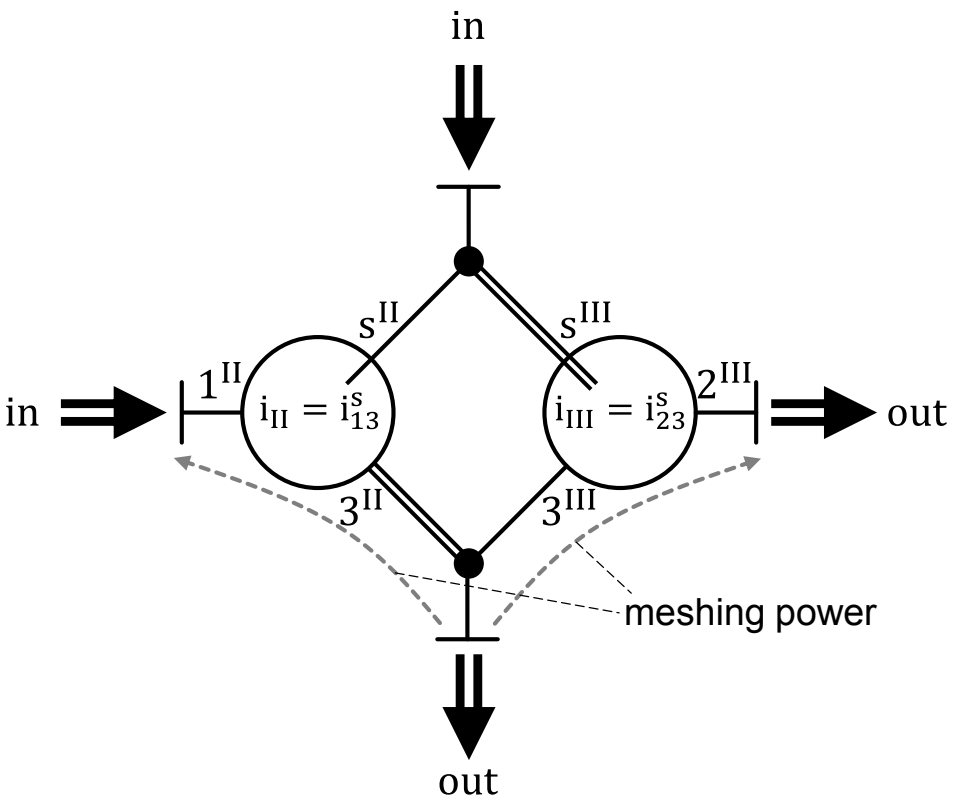

Figure 4-31: Functionally-equivalent substitution figure consistent with Figure 4-30

As the next step, power losses are taken into account by modifying the meshing powers by appropriate basic efficiency values. The meshing power of central gear is partitioned and flowing to central shafts 1 and 2. As a total-meshing-power shaft exists, the balance of meshing powers can easily be modified including basic efficiencies. Also, the sum of all external torques must equal zero:

$$\frac{P_{m1}}{\eta_{0,II}} + \frac{P_{m2}}{\eta_{0,III}} + P_{m3} = 0$$

$$\Rightarrow \frac{T_1 \cdot n_1'}{\eta_{0,II}} + \frac{T_2 \cdot n_2'}{\eta_{0,III}} + T_3 \cdot n_3' = 0 \Rightarrow \frac{T_1 \cdot i_{II}}{\eta_{0,II}} + \frac{T_2 \cdot i_{III}}{\eta_{0,III}} + T_3 = 0 \qquad (4.37)$$

$$T_1 + T_2 + T_3 + T_s = 0$$

n'	[rpm]	absolute speed	P_m	[W]	meshing power
T	[Nm]	external torque	η_0	[-]	basic train efficiency

Solving these statics equations again for central shaft 3 and carrier shaft s, the power loss conditions are derived:

$$T_s = 715{,}3\ \text{Nm} \Rightarrow P_s = 99872\ \text{W}$$

$$T_3 = -615{,}3\ \text{Nm} \Rightarrow P_3 = -78751\ \text{W};\ P_{m3} = 7159\ \text{W} \qquad (4.38)$$

T	[Nm]	external torque	P	[W]	external (absolute) power
			P_m	[W]	meshing power

Obviously, central shaft 3 is still the total-meshing-power shaft. Therefore, the substitution figure shown in **Figure 4-31** is valid. Finally, the overall efficiency is calculated as follows:

$$\eta = -\frac{P_2 + P_3}{P_1 + P_s} = 99{,}8\ \% \qquad (4.39)$$

η	[%]	overall efficiency	P	[W]	external (absolute) power

4.2.5.3 5-shaft CCPGT featuring five loaded shafts

Analogical to 4-shaft CCPGTs, the overall ratio of a closed loop of basic trains must equal +1. In **Figure 4-32**, the basic trains connecting two central gears in pairs are illustrated symbolically. Additionally, possible signs for the basic train ratios are shown. Every 'triangle' of basic trains can either contain three positive-ratio drives or two negative-ratio drives and one positive-ratio drive. A 'rectangle' of basic trains can contain four positive-ratio drives, two negative-ratio drives and two positive-ratio drives or four negative-ratio drives. In sum, a 5-shaft CCPGT consists out of six positive-ratio drives, three negative-ratio drives and three-positive-ratio drives or four negative-ratio drives and two positive-ratio drives. **Figure 4-33** shows example 5-shaft CCPGTs corresponding to **Figure 4-32**.

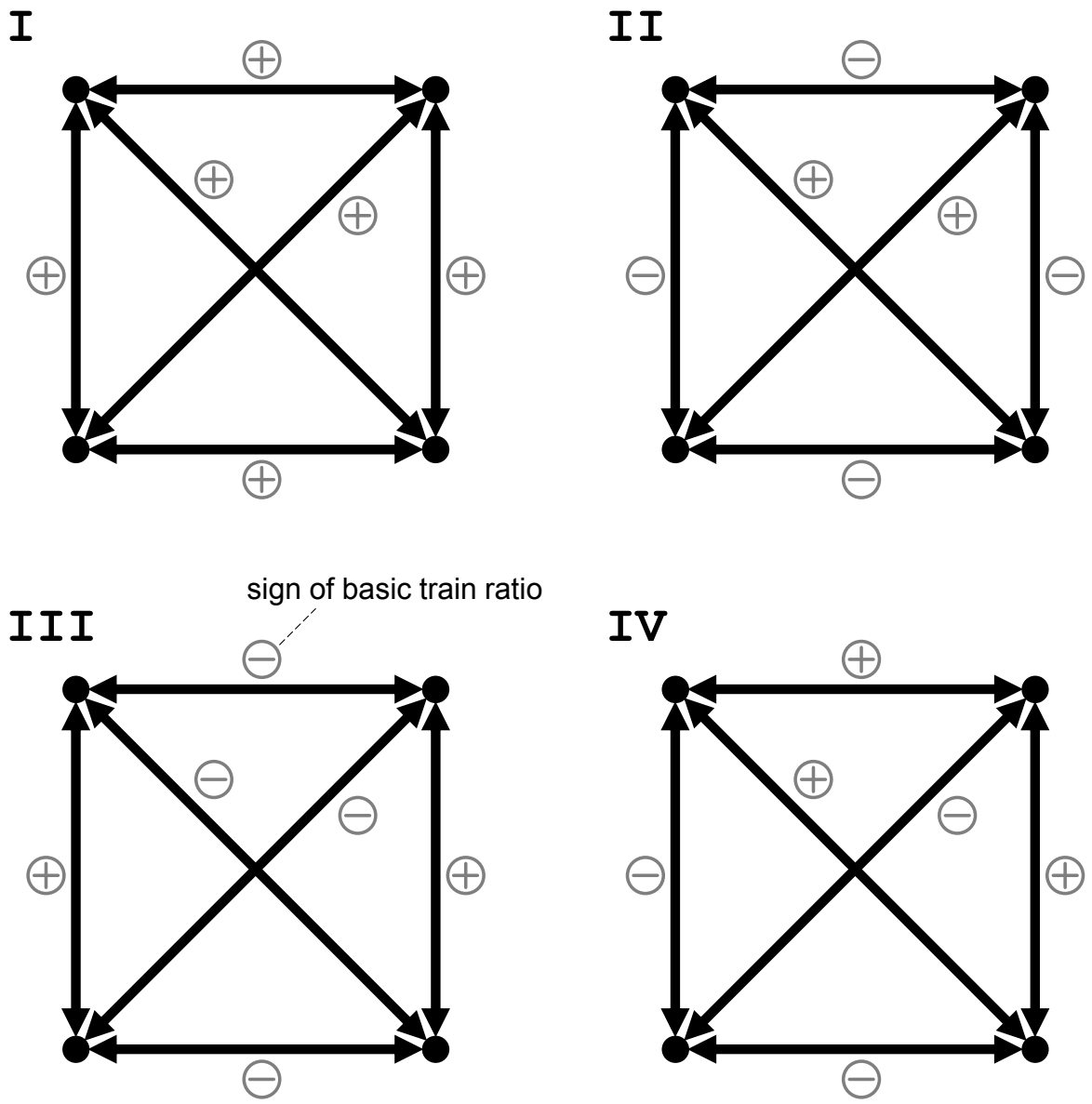

Figure 4-32: Signs of the basic train ratios of a 5-shaft CCPGT

For 5-shaft CCPGTs with four loaded central gear shafts, two categories of substitution figures are on hand. If a single meshing power source or sink occurs two virtual subgraphs of substitution figures are feasible (**Figure 4-34**). Thus, the functionally-equivalent substitution figure is definite and features a single central gear coupling shaft connected to three Wolf symbols (**Figure 4-35**).

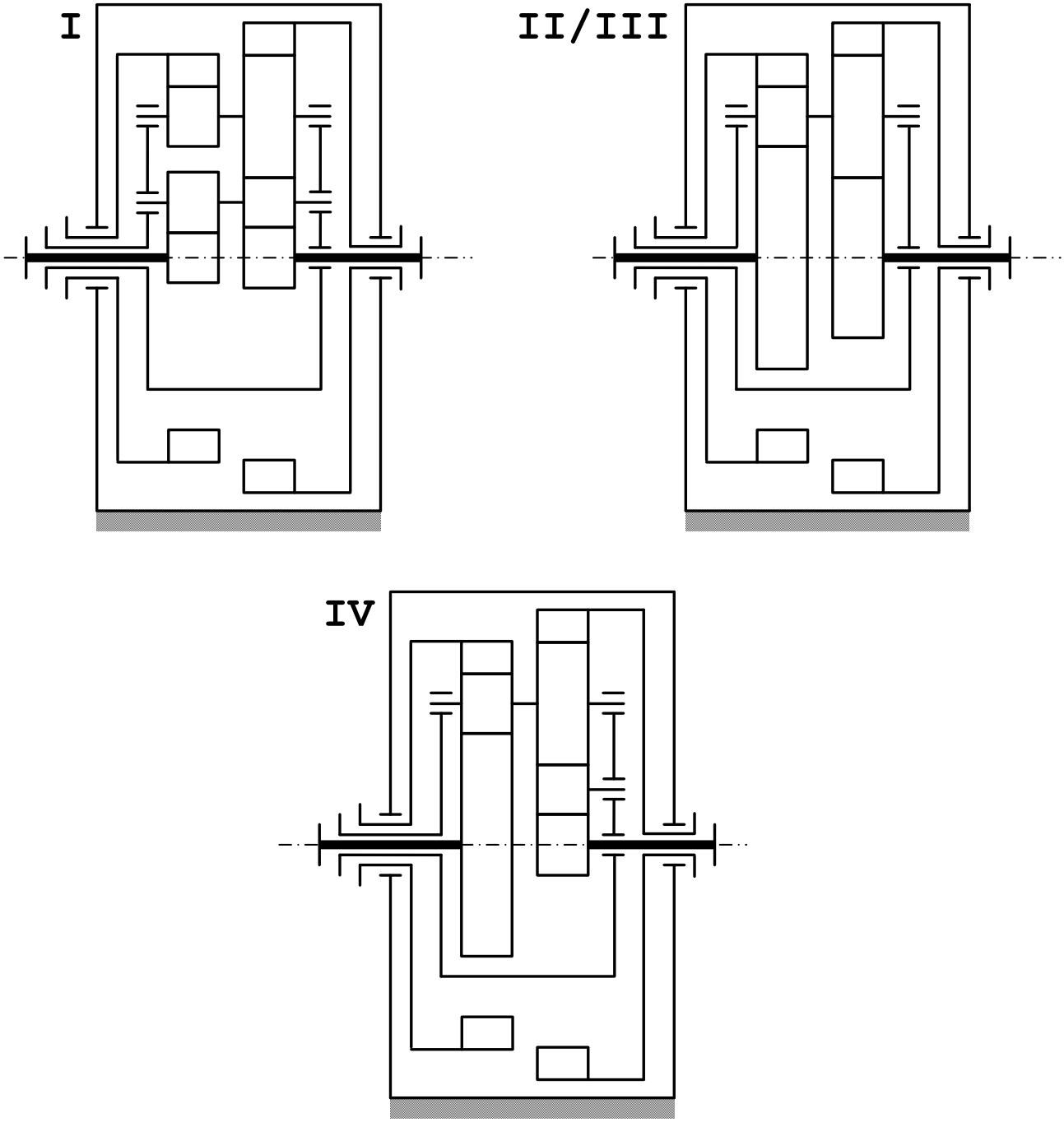

Figure 4-33: Example 5-shaft CCPGTs corresponding to Figure 4-32

As for two meshing power sources and two sinks, four different virtual subgraphs are feasible depending on the quantities of meshing power (**Figure 4-36**). The basic structure of the corresponding substitution figure is invariant (**Figure 4-37**). For this operating condition, the representation by substitution figures is not necessarily definite. As a function of the design of the CCPGT, several substitution figures can be functionally-equivalent at the same time (cf. Sections 4.2.3.3 and 4.2.3.4).

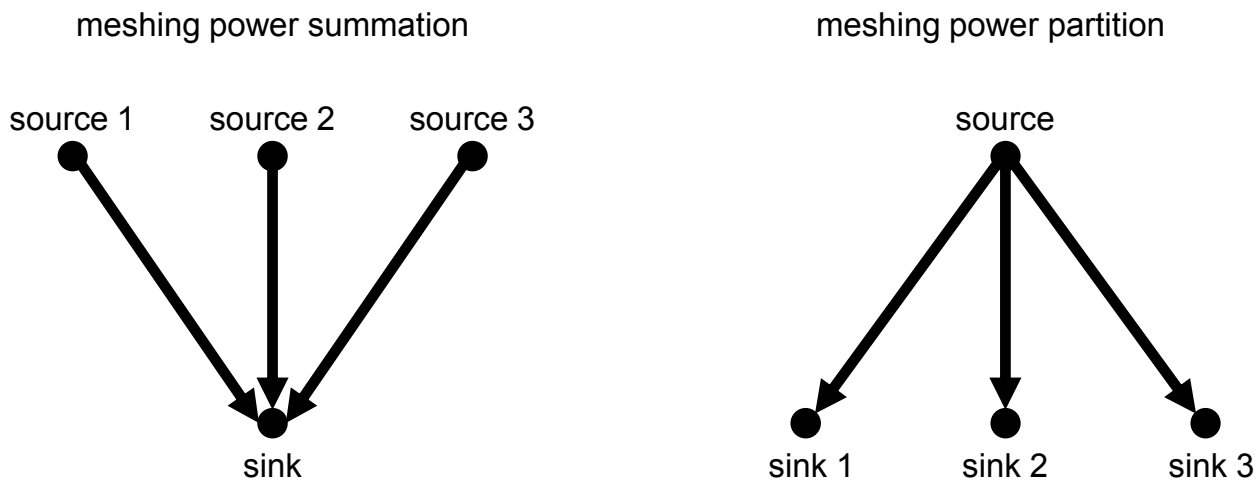

Figure 4-34: Virtual subgraphs of substitution figures for 5-shaft CCPGTs with four loaded central gear shafts (one source and three sinks or one sink and three sources)

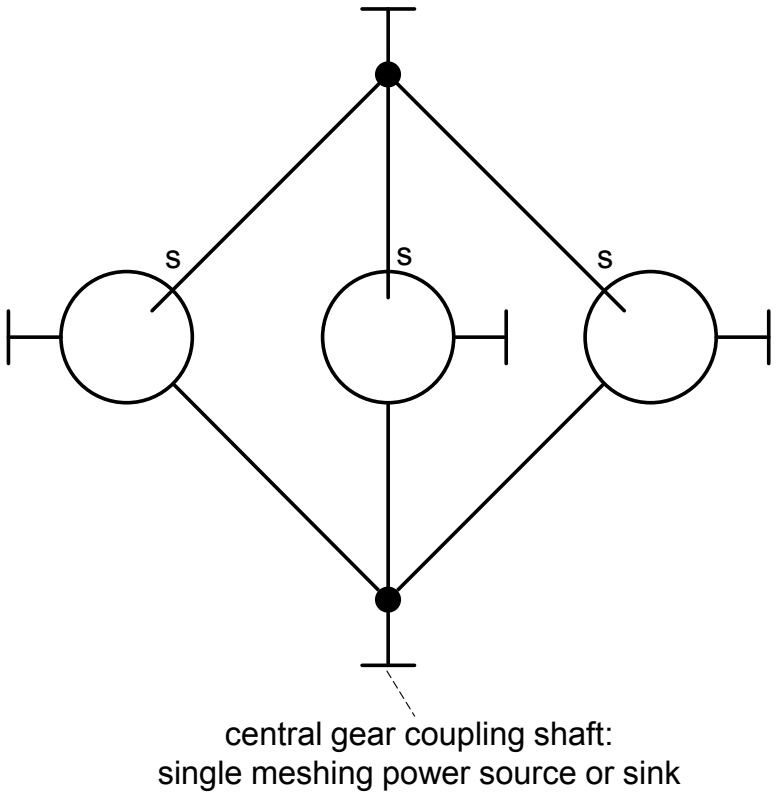

Figure 4-35: Substitution figure for 5-shaft CCPGTs with four loaded central gear shafts and single meshing power source or sink

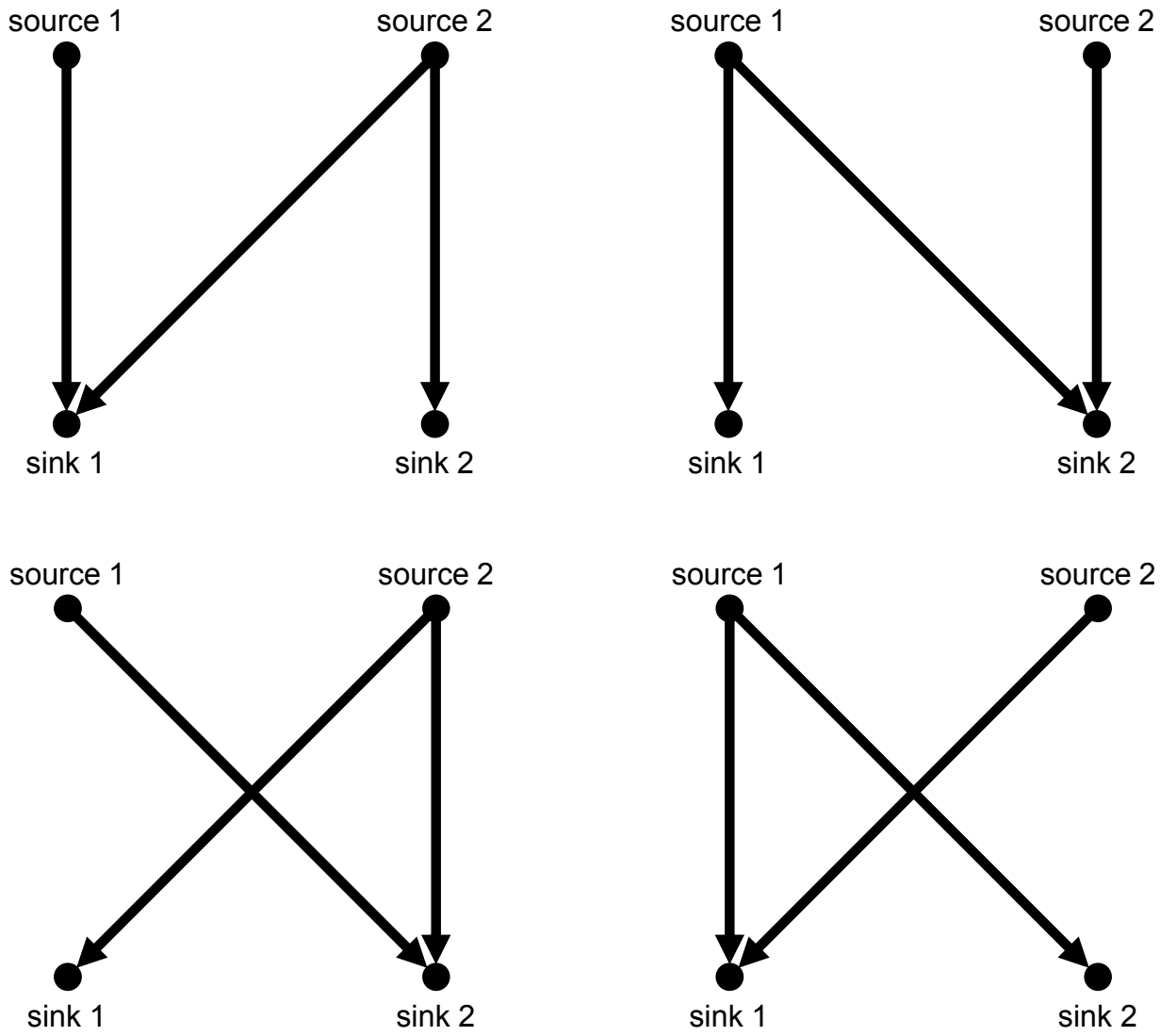

Figure 4-36: Virtual subgraphs of substitution figures for 5-shaft CCPGTs with four loaded central gear shafts (two sources and two sinks)

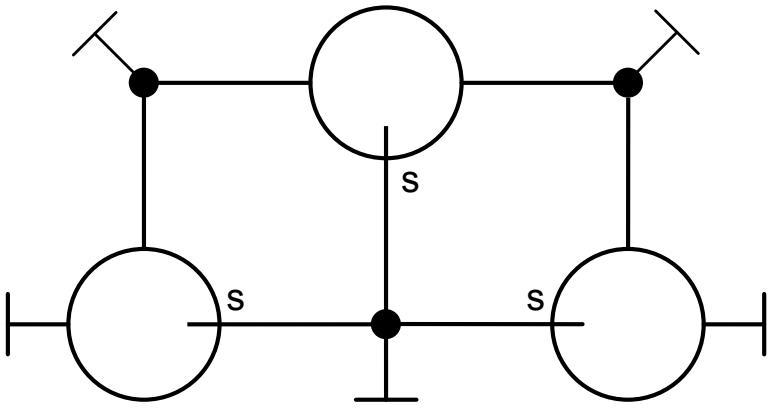

Figure 4-37: Substitution figures for 5-shaft CCPGTs with four loaded central gear shafts and two meshing power sources and sinks

4.3 An approximate calculation of efficiency

The methods presented in the Sections 4.1 and 4.2 allow a precise efficiency calculation within their underlying boundaries and assumptions. For it, a fairly detailed modeling of the transmission geometry is necessary and the modeling effort is rather high. In addition, the single calculation steps are complex. Instead of that, a simple and fast alternative method that requires only limited information about the PGT is desired. This is permitted by establishing further simplifying assumptions at the price of an efficiency approximation in place of an exact solution.

4.3.1 Simplified statics system of equations

It is stated in Section 4.2.2.2 that any kinematically-equivalent substitution figure is adequate for a statics analysis for loss-free operating conditions. On the basis of this analysis functionally-equivalent substitution figures are derived by means of grouping the central gears into meshing power sources and sinks and establishing bipartite trees (Section 4.2.3.4). Functionally-equivalent substitution figures feature at least two Wolf symbols and basic trains respectively having different basic train efficiencies in general. Thus, the overall power loss is:

$$|P_L| = \left|\Sigma\left(P_{m,in,g} \cdot (1-\eta_{0,g})\right)\right| = \left|\Sigma\left(T_{i,x,g} \cdot \omega_{m,x} \cdot (1-\eta_{0,g})\right)\right| \quad \text{for} \quad \left(T_{i,x,g} \cdot \omega_{m,x}\right) < 0 \qquad (4.40)$$

P_L	[W]	overall power loss	$T_{i,x,g}$	[Nm]	internal torque of central gear x in basic train g
$P_{m,in,g}$	[W]	input meshing power to basic train g	$\omega_{m,x}$	[rad/s]	meshing speed of central gear x
$\eta_{0,g}$	[-]	basic efficiency of basic train g			

If it is assumed that every basic train features the same basic efficiency factor, the partial meshing power terms from above only differ due to divergent internal torques. Hence, the terms corresponding to one central gear can be merged. For this purpose, a global basic train efficiency factor is introduced:

$$\left|P_{L,approx}\right| = \left|\Sigma\left(T_x \cdot \omega_{m,x} \cdot (1-\eta_{0,glob})\right)\right| \quad \text{for} \quad \left(T_x \cdot \omega_{m,x}\right) > 0 \qquad (4.41)$$

$P_{L,approx}$	[W]	approximated overall power loss	T_x	[Nm]	external torque of central gear x
$\eta_{0,glob}$	[-]	global basic train efficiency	$\omega_{m,x}$	[rad/s]	meshing speed of central gear x

Likewise, the meshing power terms must equal zero in sum:

$$\Sigma\left(T_x \cdot \omega_{m,x} \cdot \eta_{0,glob}\right) + \Sigma\left(T_y \cdot \omega_{m,y}\right) = 0 \quad \text{for} \quad \left(T_x \cdot \omega_{m,x}\right) > 0 \;\; and \;\; \left(T_y \cdot \omega_{m,y}\right) < 0 \qquad (4.42)$$

$\eta_{0,glob}$	[-]	global basic train efficiency	$T_{x/y}$	[Nm]	external torque of central gear x/y
			$\omega_{m,x/y}$	[rad/s]	meshing speed of central gear x/y

Additionally, the sum of external torques must equal zero, too:

$$\Sigma T_x + T_s = 0 \qquad (4.43)$$

T_x	[Nm]	external torque of central gear x	T_s	[Nm]	external torque of carrier shaft s

Consequently, two conditional equations are available for determining all external torques and a simplified basic statics system of equations can be set up:

$$\begin{pmatrix} (\omega_1-\omega_s)\cdot\eta_{0,glob}^{w1,x} & \cdots & (\omega_x-\omega_s)\cdot\eta_{0,glob}^{w1,x} & \cdots & (\omega_X-\omega_s)\cdot\eta_{0,glob}^{w1,x} & 0 \\ 1 & & 1 & & 1 & 1 \end{pmatrix} \begin{bmatrix} T_1 \\ \vdots \\ T_x \\ \vdots \\ T_X \\ T_s \end{bmatrix} = \begin{pmatrix} 0 \\ 0 \end{pmatrix} \qquad (4.44)$$

$$\text{with} \quad w1,x = \begin{cases} +1 & \text{if } T_x \cdot (\omega_x - \omega_s) > 0 \\ 0 & \text{else} \end{cases}$$

T_x	[Nm]	external torque of central gear x	ω_x	[rad/s]	angular speed of central gear x
T_s	[Nm]	external torque of carrier shaft s	ω_s	[rad/s]	angular speed of carrier s
$\eta_{0,glob}$	[-]	global basic train efficiency	X	[-]	total number of central gears
w1,x	[-]	efficiency exponent of central gear x			

Inserting preset values for all given torques, the simplified statics system of equations becomes quadratic and can be solved directly. This approach can be interpreted as a transformation of any gear pair subgraph or functionally-equivalent substitution figure into a simplified structure (**Figure 4-38**). It is not necessary to know the exact design of the CCPGT but only the kinematic relationships and basic ratios. Internal torques of Wolf symbols are not treated but only external torques. Besides the simplification regarding the basic train efficiency, no logical mistake in respect of the internal power flow has to be accepted. As only the meshing input power is impacted by the global basic train efficiency, the correct amount of meshing power leading to power losses is considered (cf. Section 4.2.3.2).

Another advantage of this approach is evident from the calculation time required. The dimension of the statics system of equations is as small as possible. In addition, only few iteration steps are needed in case of a meshing power direction change. According to the static DOF of a CCPGT, two external torques are to be calculated. This means that at maximum two efficiency exponents might change their value in equation (4.44) and four cases are to be distinguished. Thus, the calculation must converge after a maximum of four iteration steps. If not, it is about an impossible operating condition (cf. Section 4.4).

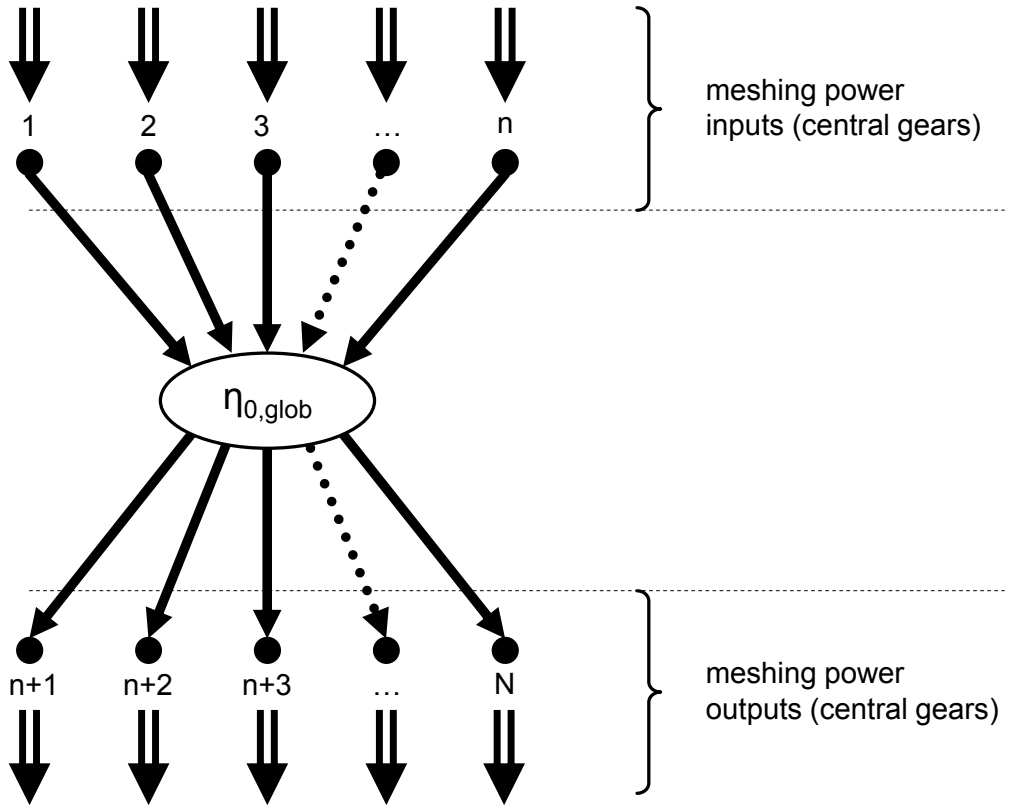

Figure 4-38: Simplified CCPGT structure for efficiency approximation

4.3.2 Approximation accuracy

The results of the exact efficiency calculation and the approximation deviate as the global basic efficiency has to be estimated if the final design of the CCPGT is not known. Also, the basic trains included in the CCPGT do not feature equal basic efficiency in general. Thus, the application of the approximation method as worst case calculation is most feasible. For this purpose, a reasonable global 'worst case' basic efficiency has to be selected. According to Section 3.1.4, an efficiency of 99% per external basic gearing and an efficiency of 99,5% per internal basic gearing is a realistic choice. Considering CCPGTs in use, included basic trains with unfavorable basic efficiency feature up to three external basic gearings (cf. **Figure 3-17**, **Figure 4-10**, **Figure 4-30** and **Figure 4-33**). Thus, a global basic train efficiency of 97% (~$0{,}99^3$) is proposed.

Furthermore, the extent of deviations between the results of different efficiency calculation methods depends not only on the design of the CCPGT but also on the present operating conditions. The operating DOF of a CCPGT equals its number of central shafts. The outcome of this is a multidimensional and theoretically unlimited operating range which complicates the quantification of deviations. A general expression of the overall efficiency is:

$$\eta = 1 - \frac{P_L}{P_{input}} = 1 - \frac{f(\eta_0, P_m)}{P_{input}} \qquad (4.45)$$

η	[-]	overall efficiency	P_L	[W]	overall power loss
η_0	[-]	basic gearing / basic train efficiency	P_{input}	[W]	overall input power
			P_m	[W]	meshing power

Herein, the overall power loss is a function of the basic gearing efficiency and the basic train efficiency as well as a function of the meshing power. Large deviations in the overall efficiency for different basic efficiency factors can only occur if the meshing power is large in comparison to the input power. The following examples shall demonstrate deviations for selected designs and operating points.

4.3.2.1 Example 3-shaft PGTs

In order to capture the whole efficiency range of a 3-shaft PGT, a description similar to [4_LAR57] is chosen. As a 3-shaft PGT features a kinematic DOF of two, speed ratios, power ratios and the overall efficiency can be expressed as a function of one speed ratio:

$$\lambda = \frac{n_1}{n_2} \qquad (4.46)$$

λ	[-]	speed ratio	$n_{1/2}$	[-]	speed of central shaft 1/2

The torque ratios of a 3-shaft PGT are constant and defined by the basic ratio for loss-free operating condition. Considering power losses, only two cases are available: meshing power flows from central gear 1 to central gear 2 and the other way round (w1 = ±1).

The first example PGT is a negative-ratio drive shown in **Figure 4-39**. In the following, all relevant quantities are calculated depending on λ being varied from minus to plus infinity. It is evident from **Figure 4-40** that all speed ratios other than λ are varied from minus to plus infinity, too.

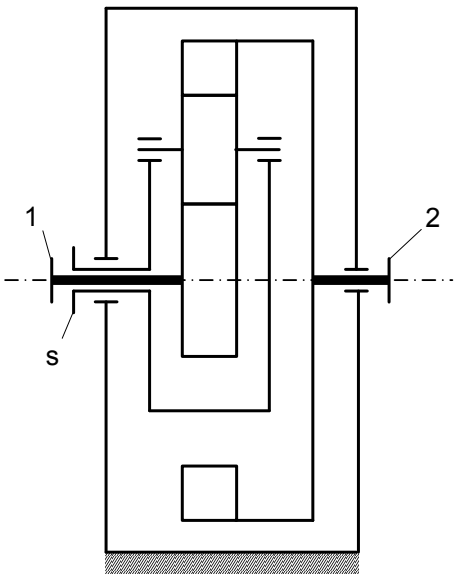

$$i_I = i_{12}^s = -3$$

$$\eta_{0,I} = 0{,}99 \cdot 0{,}995 \approx 0{,}985$$

$$(\eta_{0,glob} = 0{,}97)$$

Figure 4-39: Example negative-ratio drive for efficiency approximation

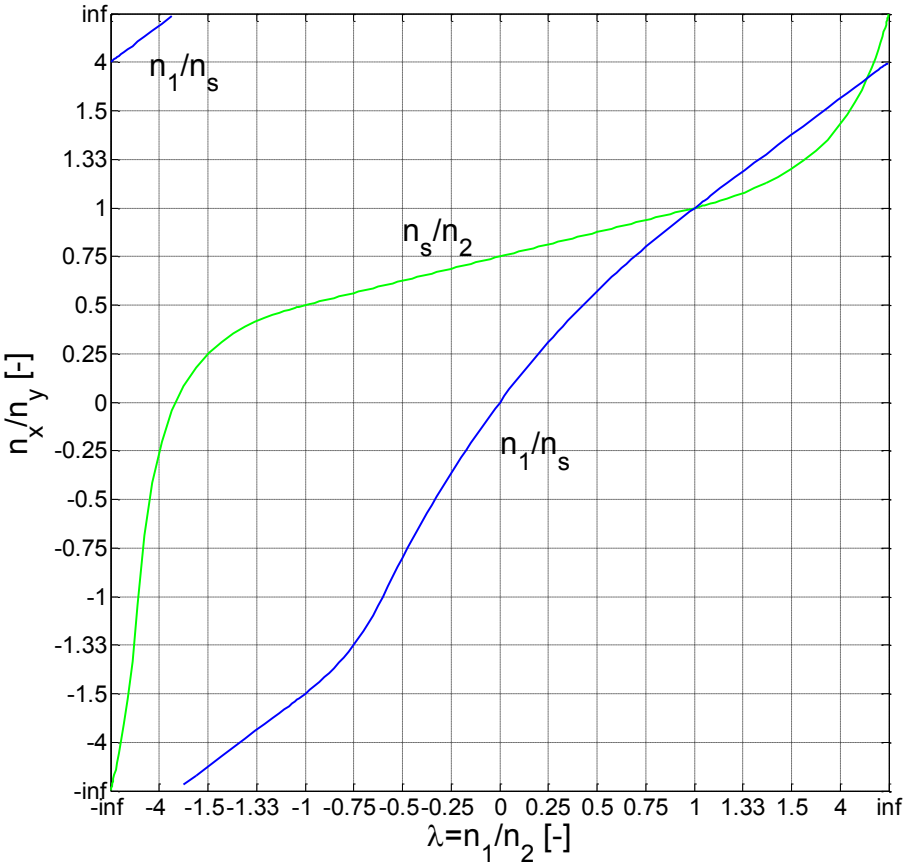

Figure 4-40: Speed ratios of 3-shaft PGT corresponding to Figure 4-39

For the efficiency calculation, two basic train efficiency values are estimated: a realistic one ($\eta_{0,l}$) and an (approximated) global one ($\eta_{0,glob}$). **Figure 4-41** shows the plots of the overall efficiency as a function of each basic efficiency. As a matter of fact, both plots are qualitatively comparable but small deviations exist.

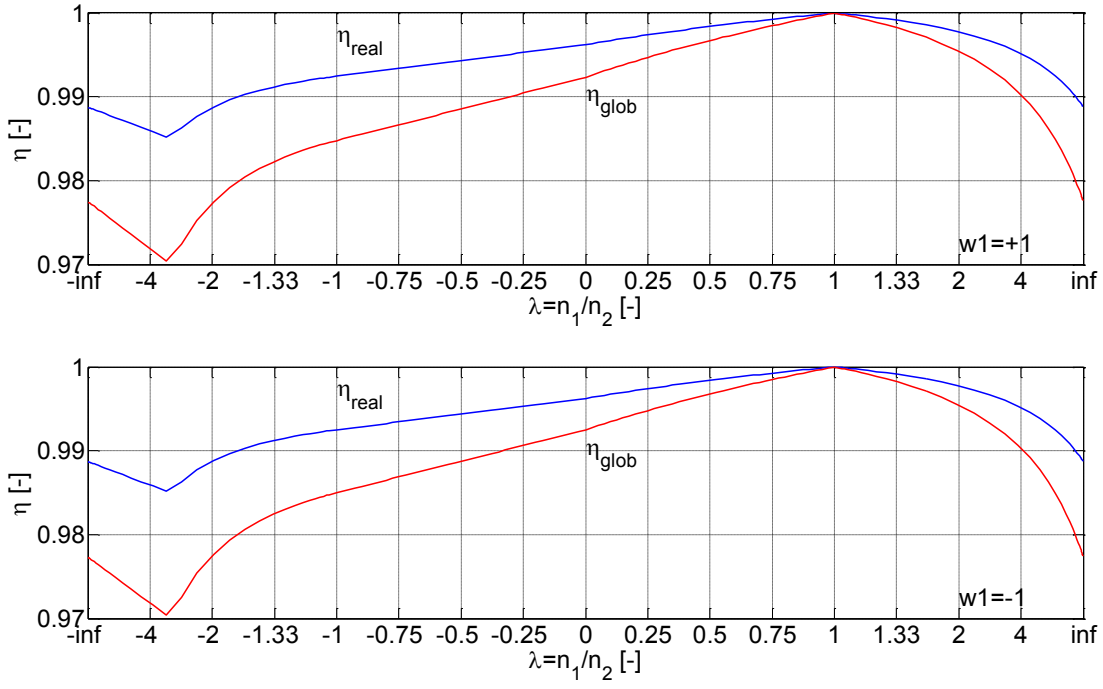

Figure 4-41: Realistic and approximated efficiency of 3-shaft PGT corresp. to Figure 4-40

The deviation between both efficiency plots is defined as:

$$\Delta\eta = \eta(\eta_{0,I}) - \eta(\eta_{0,glob}) \qquad (4.47)$$

$\Delta\eta$	[-]	efficiency deviation	$\eta_{0,I}$	[-]	realistic basic efficiency
η	[-]	overall efficiency	$\eta_{0,glob}$	[-]	global basic efficiency

According to equation (4.46), the ratio of input meshing power to absolute input power is decisive for the overall efficiency:

$$\theta = \frac{\Sigma P_{m,in}}{\Sigma P_{in}} \qquad (4.48)$$

θ	[-]	input power ratio	$\Sigma P_{m,in}$	[W]	(sum of) input meshing power
			ΣP_{in}	[W]	(sum of) absolute input power

Figure 4-42 and **Figure 4-43** disclose the strong correlation between θ and Δη. As the input meshing power of a negative-ratio drive cannot be larger than the absolute input power, the efficiency deviation is rather small meaning that the efficiency approximation is quite accurate.

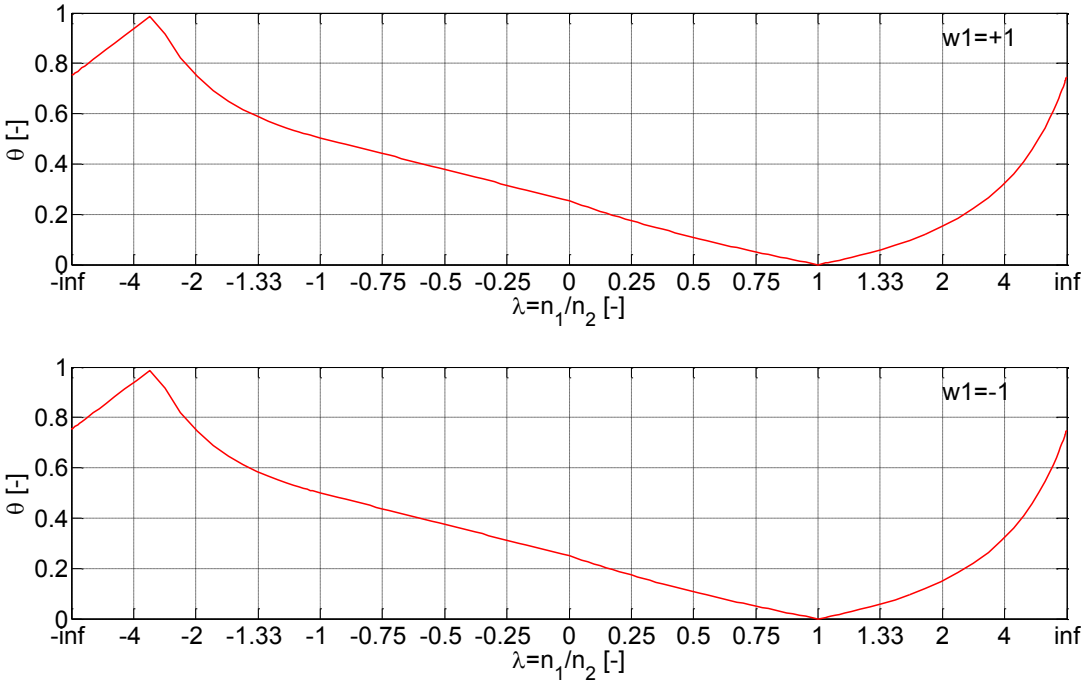

Figure 4-42: Input power ratio of 3-shaft PGT corresponding to Figure 4-40

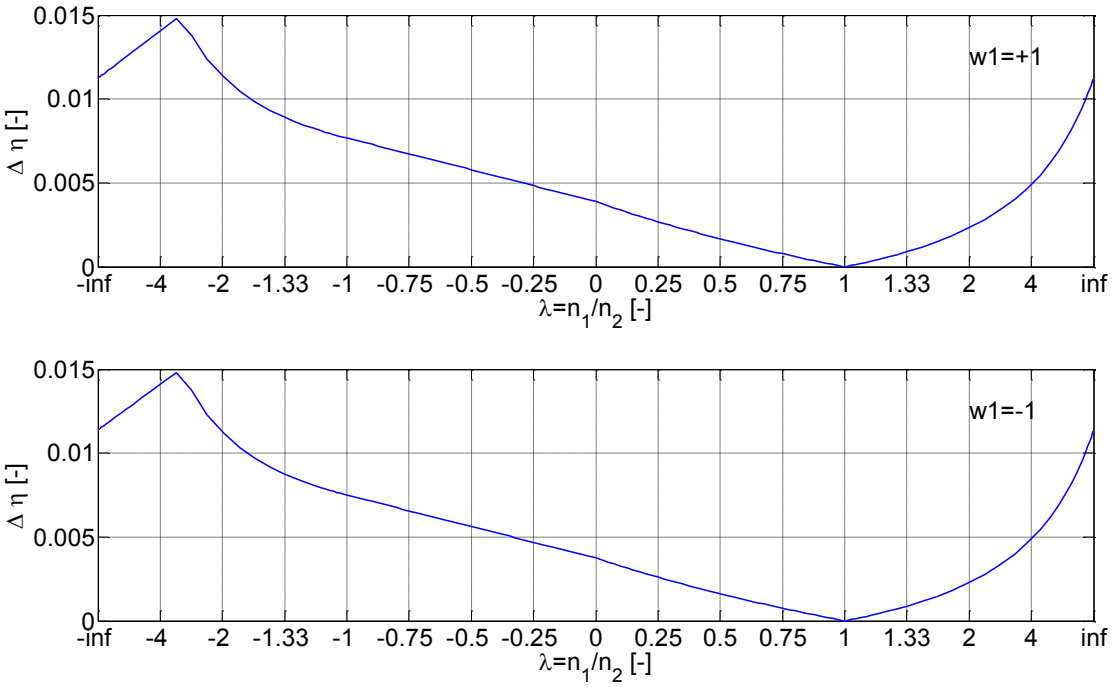

Figure 4-43: Efficiency deviation of 3-shaft PGT corresponding to Figure 4-40

The second example PGT is a positive-ratio drive with a basic ratio close to +1 (**Figure 4-44**). Thus, the input meshing power can be significantly larger the absolute input power. **Figure 4-45** shows the speed ratio plots as a function of λ.

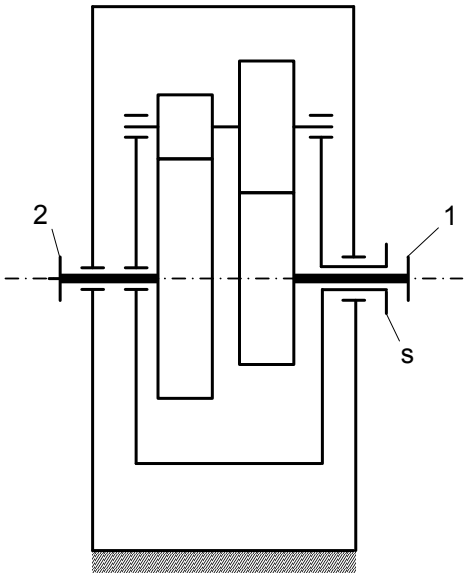

$$i_I = i_{12}^s = +1{,}1$$

$$\eta_{0,I} = 0{,}99^2 \approx 0{,}98$$

$$(\eta_{0,glob} = 0{,}97)$$

Figure 4-44: Example positive-ratio drive for efficiency approximation

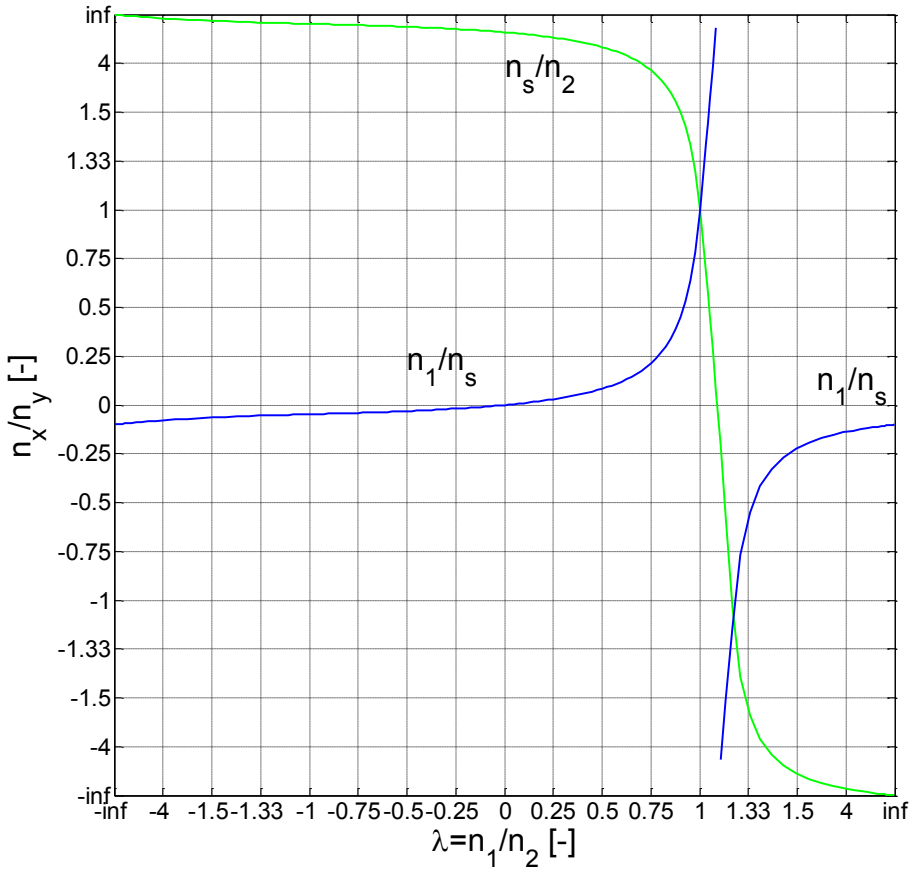

Figure 4-45: Speed ratios of 3-shaft PGT corresponding to Figure 4-44

The efficiency plots in **Figure 4-46** clearly differ from each other in part. Naturally, large differences are to be expected whenever the meshing input power is extensively larger than the absolute input power (**Figure 4-47** and **Figure 4-48**).

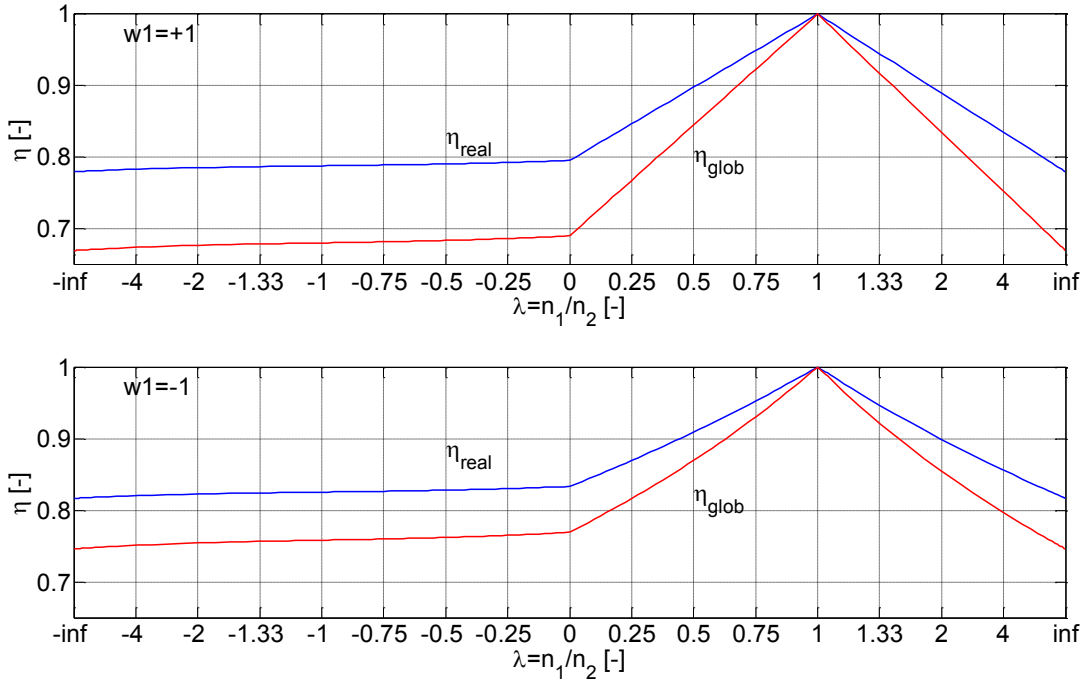

Figure 4-46: Realistic and approximated efficiency of 3-shaft PGT corresp. to Figure 4-44

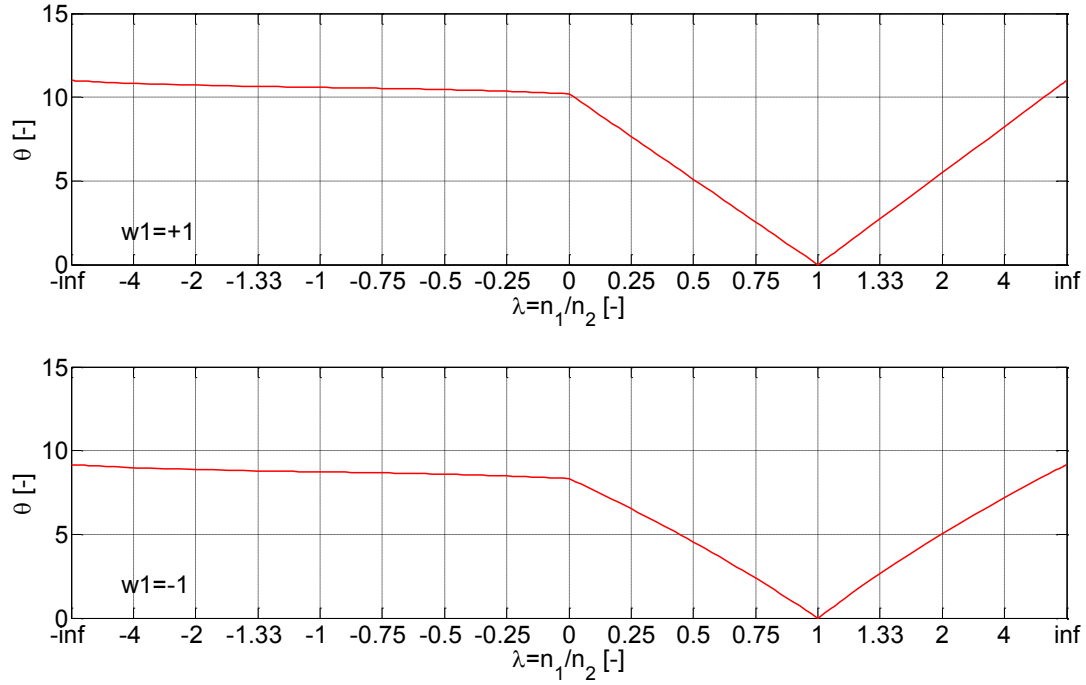

Figure 4-47: Input power ratio of 3-shaft PGT corresponding to Figure 4-44

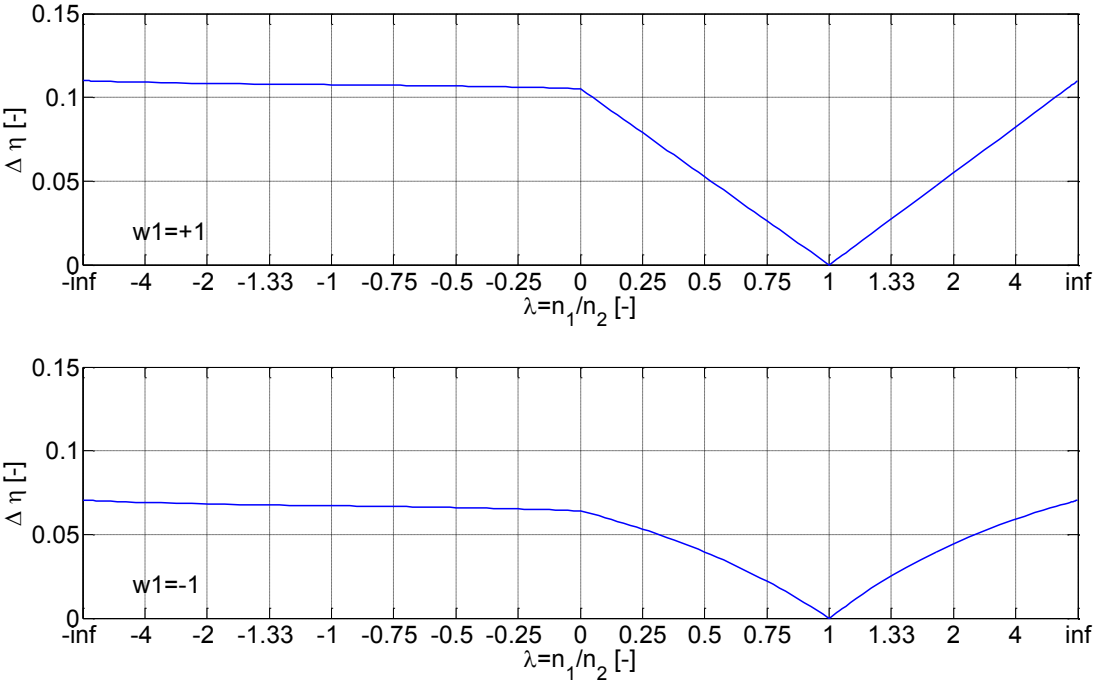

Figure 4-48: Efficiency deviation of 3-shaft PGT corresponding to Figure 4-44

4.3.2.2 Example 4-shaft CCPGTs

In contrast to a 3-shaft PGT, a 4-shaft CCPGT features an additional static DOF. Therefore, power ratios as well as the overall efficiency are not only a function of λ but also a function of an (arbitrary) torque ratio:

$$\nu = \frac{T_1}{T_2} \qquad (4.49)$$

ν	[-]	torque ratio	$T_{1/2}$	[-]	external torque of central shaft 1/2

Again, the meshing power sign of central gear 1 can be positive or negative (w1 = ±1). All other torques result from these parameters.

As a first example, a Ravigneaux set is taken into account (**Figure 4-49**). **Figure 4-50** provides an overview of the speed ratios depending on λ, **Figure 4-51** shows the torque ratios as a function of v for loss-free operating conditions.

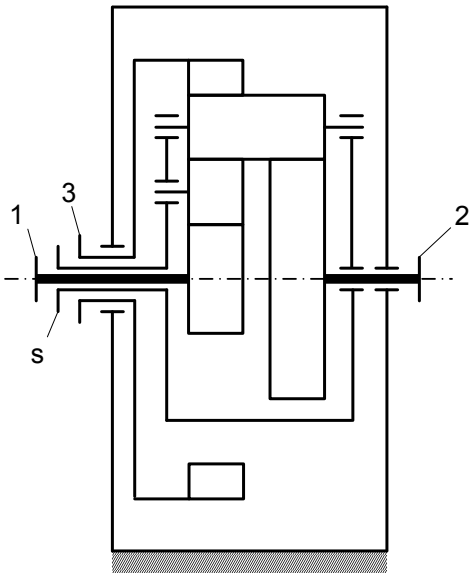

$$i_I = i_{12}^s = -2$$
$$i_{II} = i_{13}^s = +6$$
$$i_{III} = i_{23}^s = -3$$

$$\eta_{0,I} = 0{,}99^3 \approx 0{,}97$$
$$\eta_{0,II} = 0{,}99^2 \cdot 0{,}995 \approx 0{,}975$$
$$\eta_{0,III} = 0{,}99 \cdot 0{,}995 \approx 0{,}985$$

$$(\eta_{0,glob} = 0{,}97)$$

Figure 4-49: Example Ravigneaux set for efficiency approximation

The efficiency deviation is defined analogical to equation (4.47):

$$\Delta\eta = \eta(\eta_{0,I}, \eta_{0,II}, \eta_{0,III}) - \eta(\eta_{0,glob}) \qquad (4.50)$$

$\Delta\eta$	[-]	efficiency deviation	$\eta_{0,I/II/III}$	[-]	realistic basic efficiency
η	[-]	overall efficiency	$\eta_{0,glob}$	[-]	global basic efficiency

The efficiency plot depending on λ and v is a 3-dimensional field shown in **Figure 4-52**. As before, the efficiency deviation (**Figure 4-54**) is rather small up to 1,5% as the input power ratio (**Figure 4-53**) does not exceed values beyond 1,2.

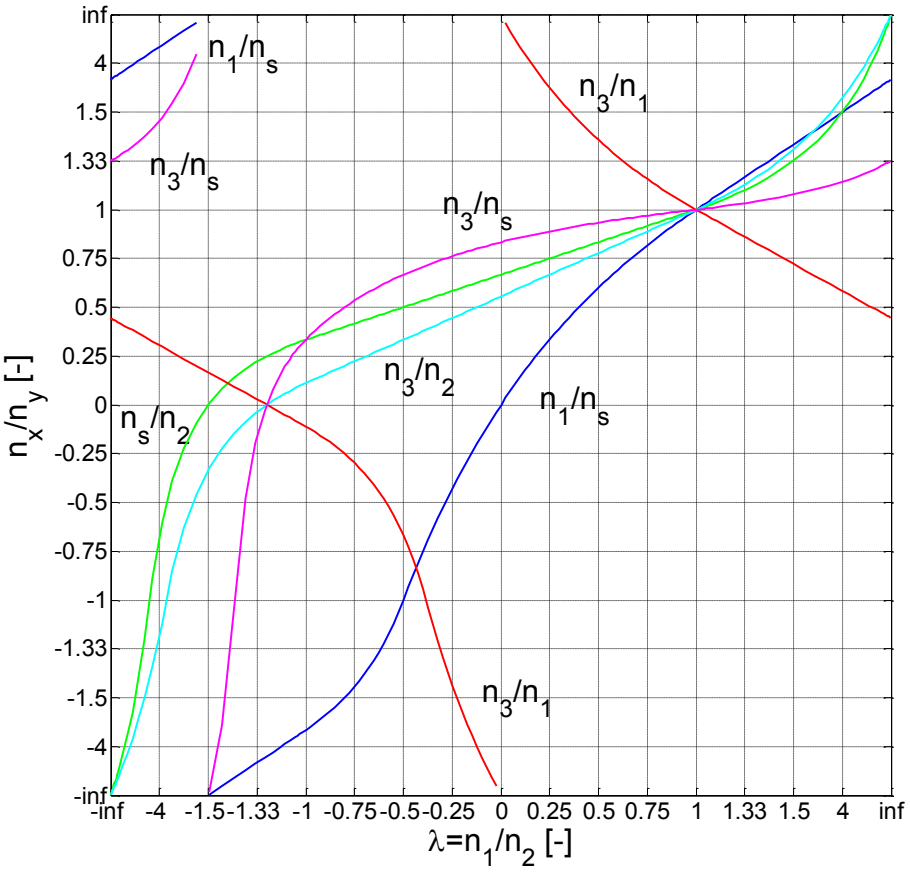

Figure 4-50: Speed ratios of 4-shaft CCPGT corresponding to Figure 4-49

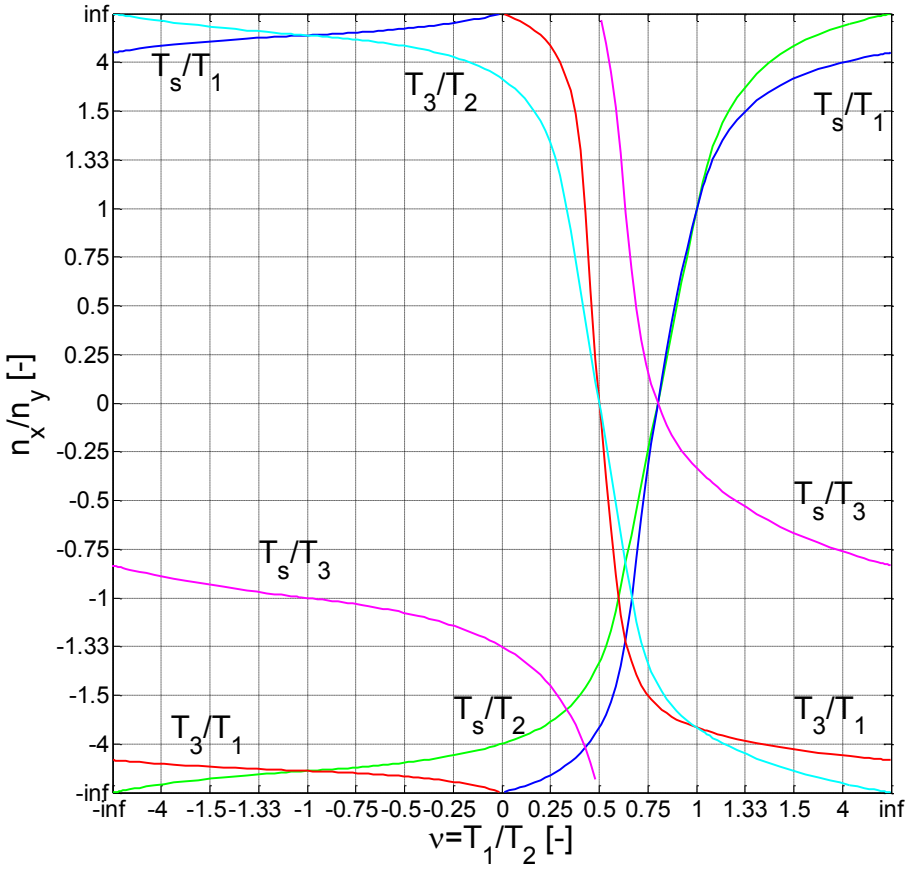

Figure 4-51: Loss-free torque ratios of 4-shaft CCPGT corresponding to Figure 4-49

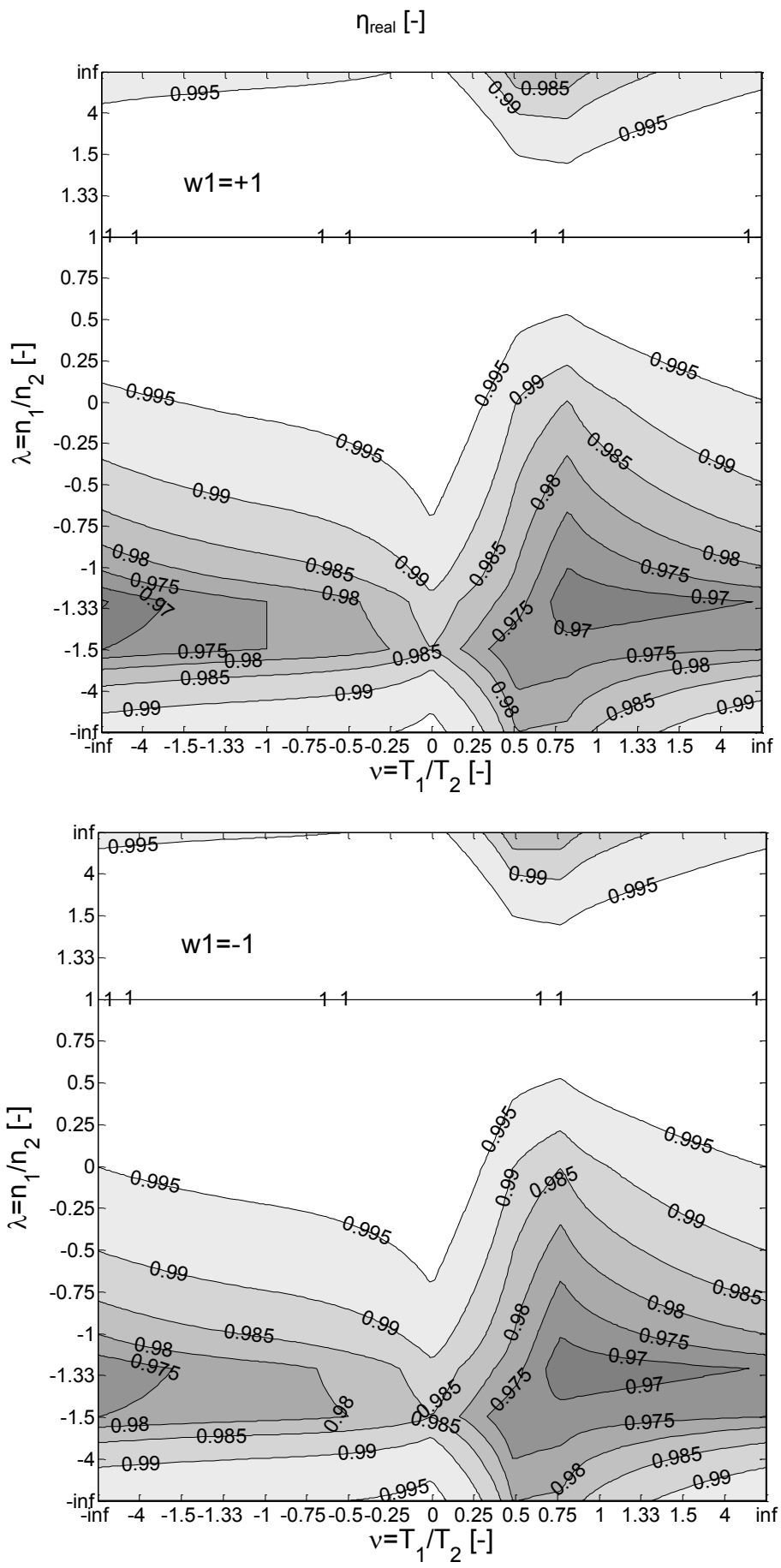

Figure 4-52: Realistic efficiency of 4-shaft CCPGT corresponding to Figure 4-49

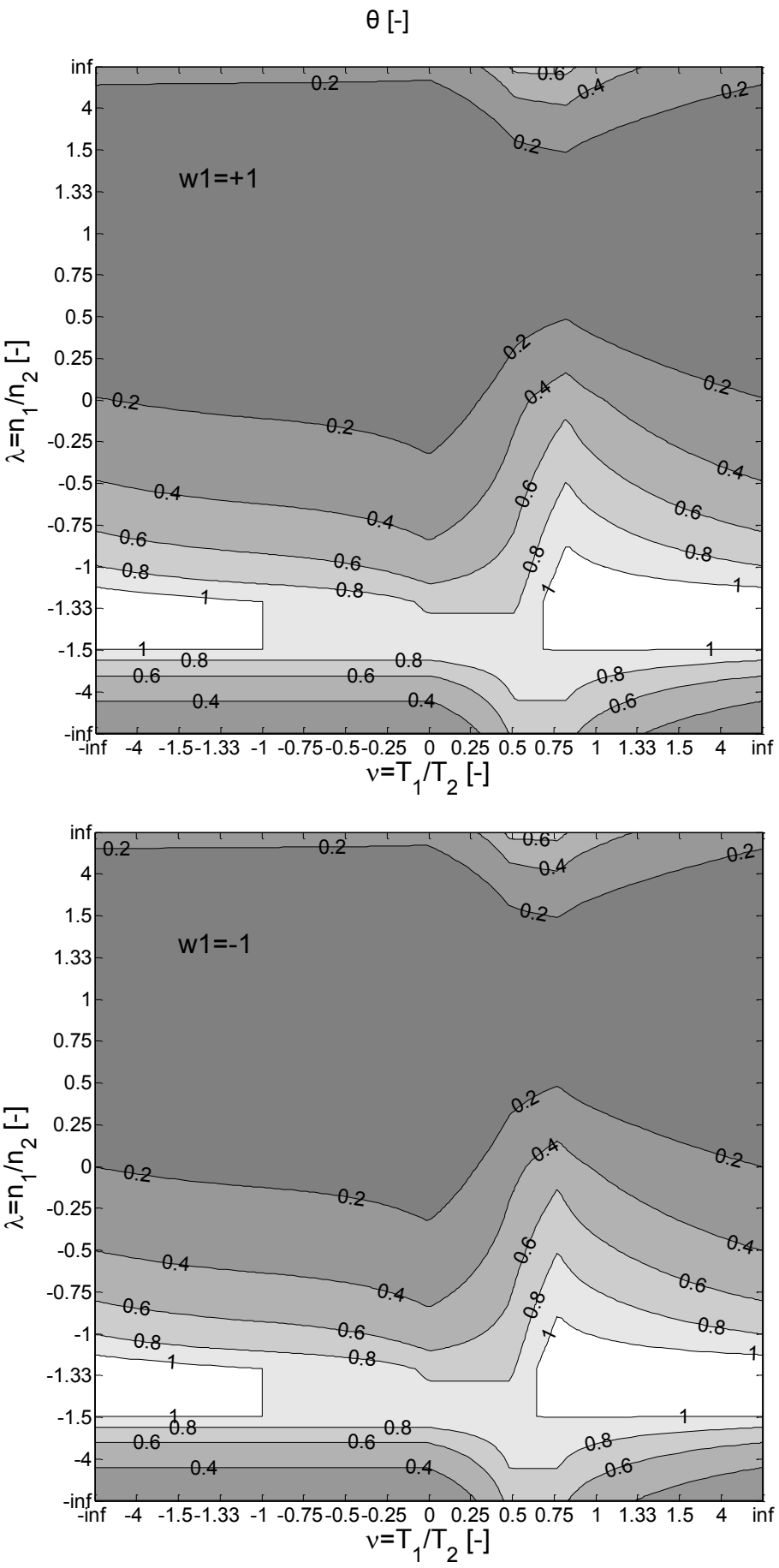

Figure 4-53: Input power ratio of 4-shaft CCPGT corresponding to Figure 4-49

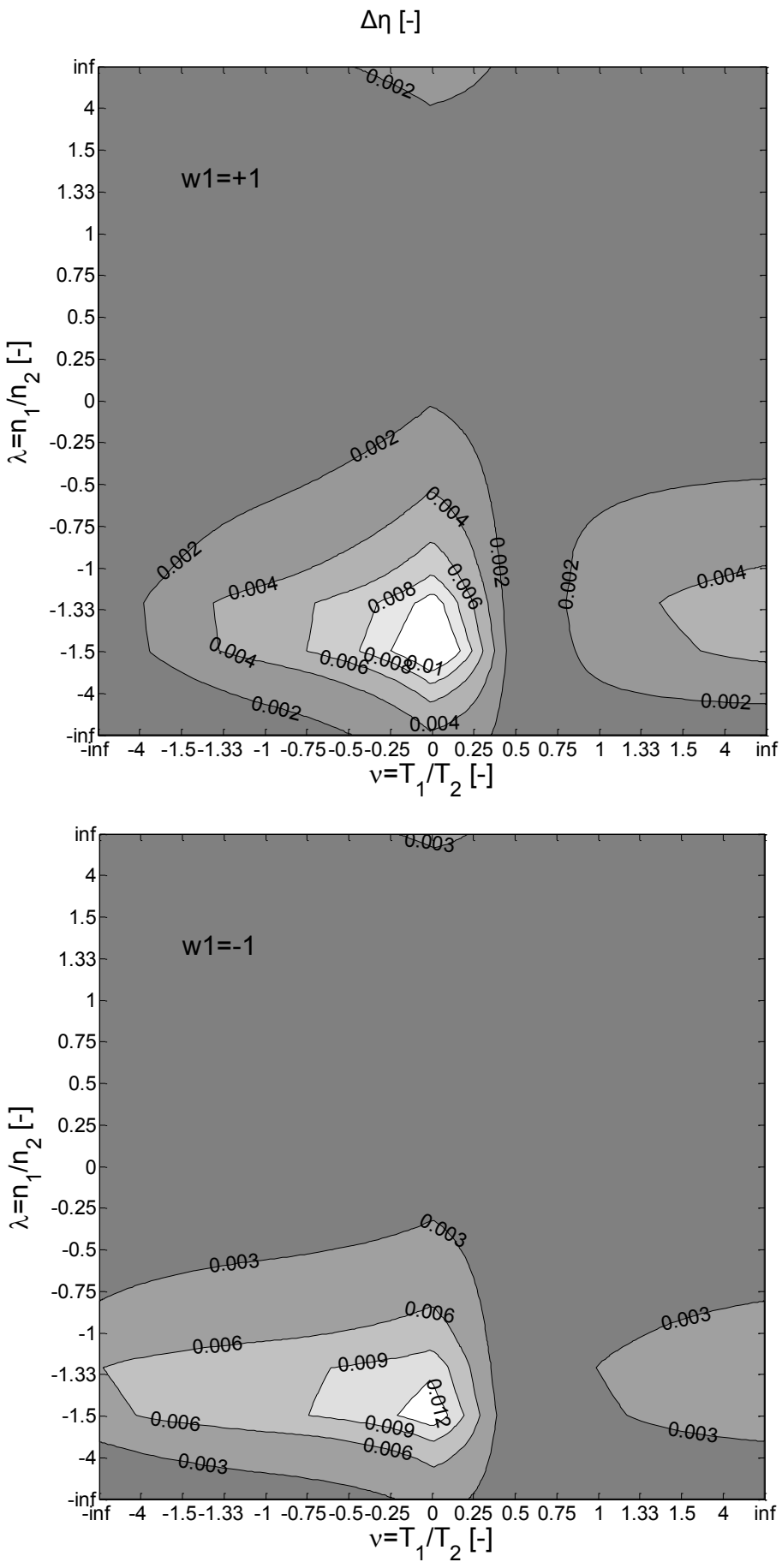

Figure 4-54: Efficiency deviation of 4-shaft CCPGT corresponding to Figure 4-49

Figure 4-55 shows the structure of the second example 4-shaft CCPGT. All basic ratios included are near +1.

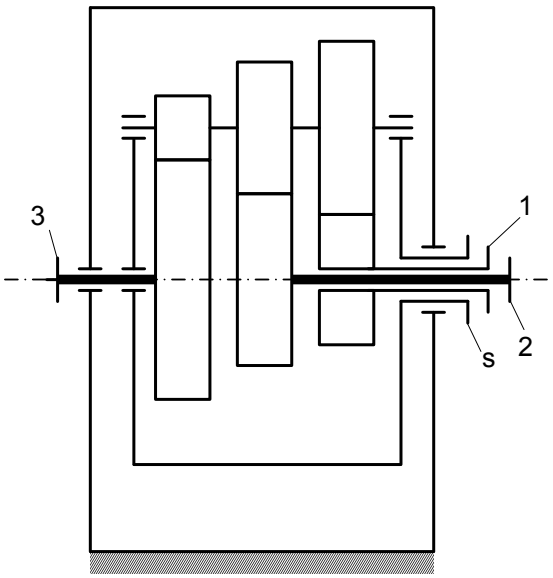

$$i_I = i_{12}^s = +1{,}1$$
$$i_{II} = i_{13}^s = +1{,}32$$
$$i_{III} = i_{23}^s = +1{,}2$$

$$\eta_{0,I} = 0{,}99^2 \approx 0{,}98$$
$$\eta_{0,II} = 0{,}99^2 \approx 0{,}98$$
$$\eta_{0,III} = 0{,}99^2 \approx 0{,}98$$

$$(\eta_{0,glob} = 0{,}97)$$

Figure 4-55: Example 4-shaft CCPGT composed of positive-ratio drives for efficiency approximation

Varying λ and ν from minus to plus infinity, all speed and torque ratios run through the same range (**Figure 4-56** and **Figure 4-57**). The plot of the realistic overall efficiency is shown in **Figure 4-58**. As the input power ratio (**Figure 4-59**) exceeds values of 14 at the margin, efficiency deviations (**Figure 4-60**) of up to 15% occur.

In conclusion, the presented efficiency approximation method for CCPGTs is appropriate for qualitative efficiency comparisons. Quantitative statements should only be used if the input meshing power is smaller than or close to the absolute input power. For a worst case approximation, a low global basic efficiency of about 97% is to be considered.

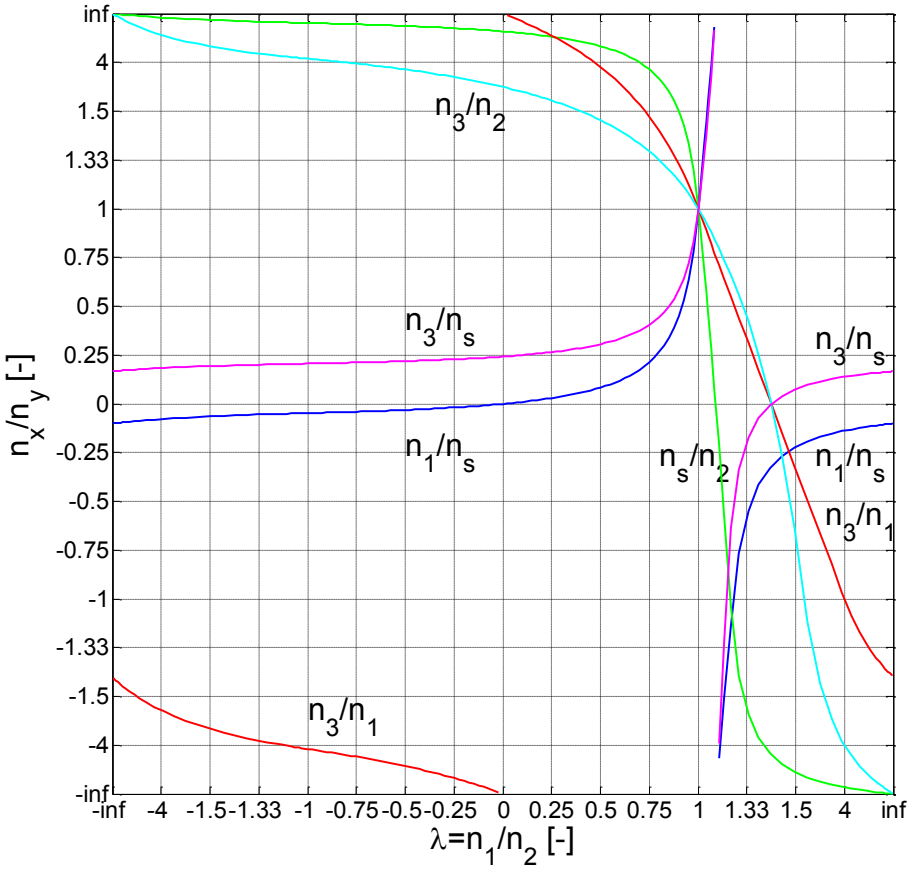

Figure 4-56: Speed ratios of 4-shaft CCPGT corresponding to Figure 4-55

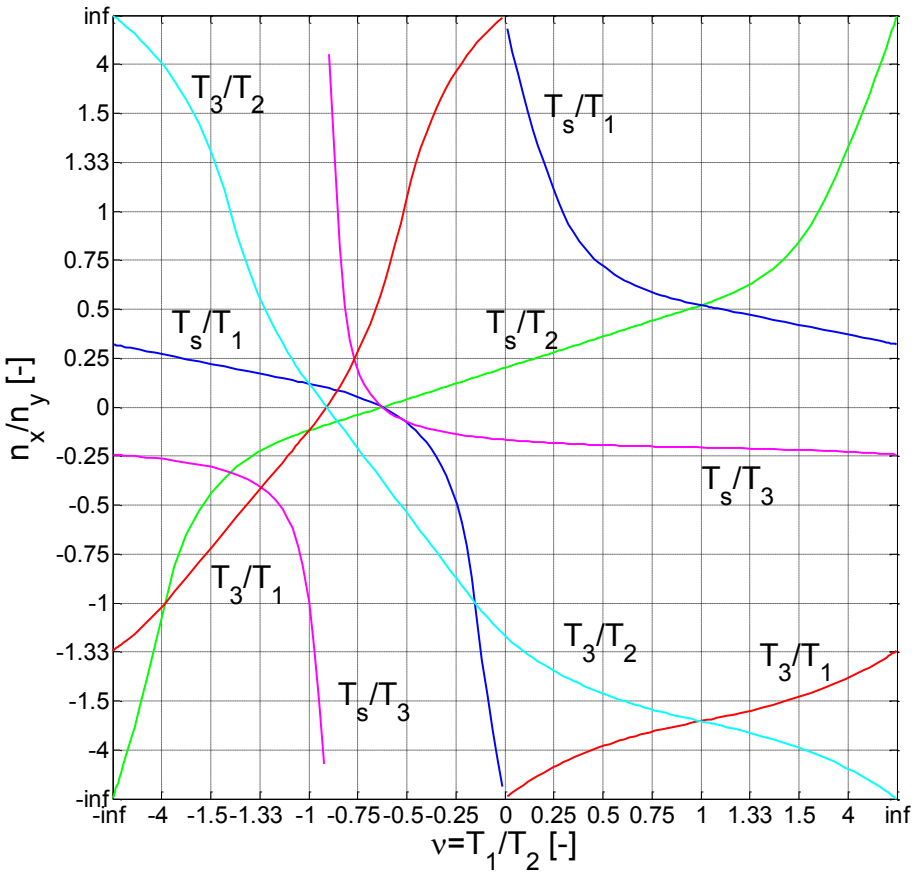

Figure 4-57: Loss-free torque ratios of 4-shaft CCPGT corresponding to Figure 4-55

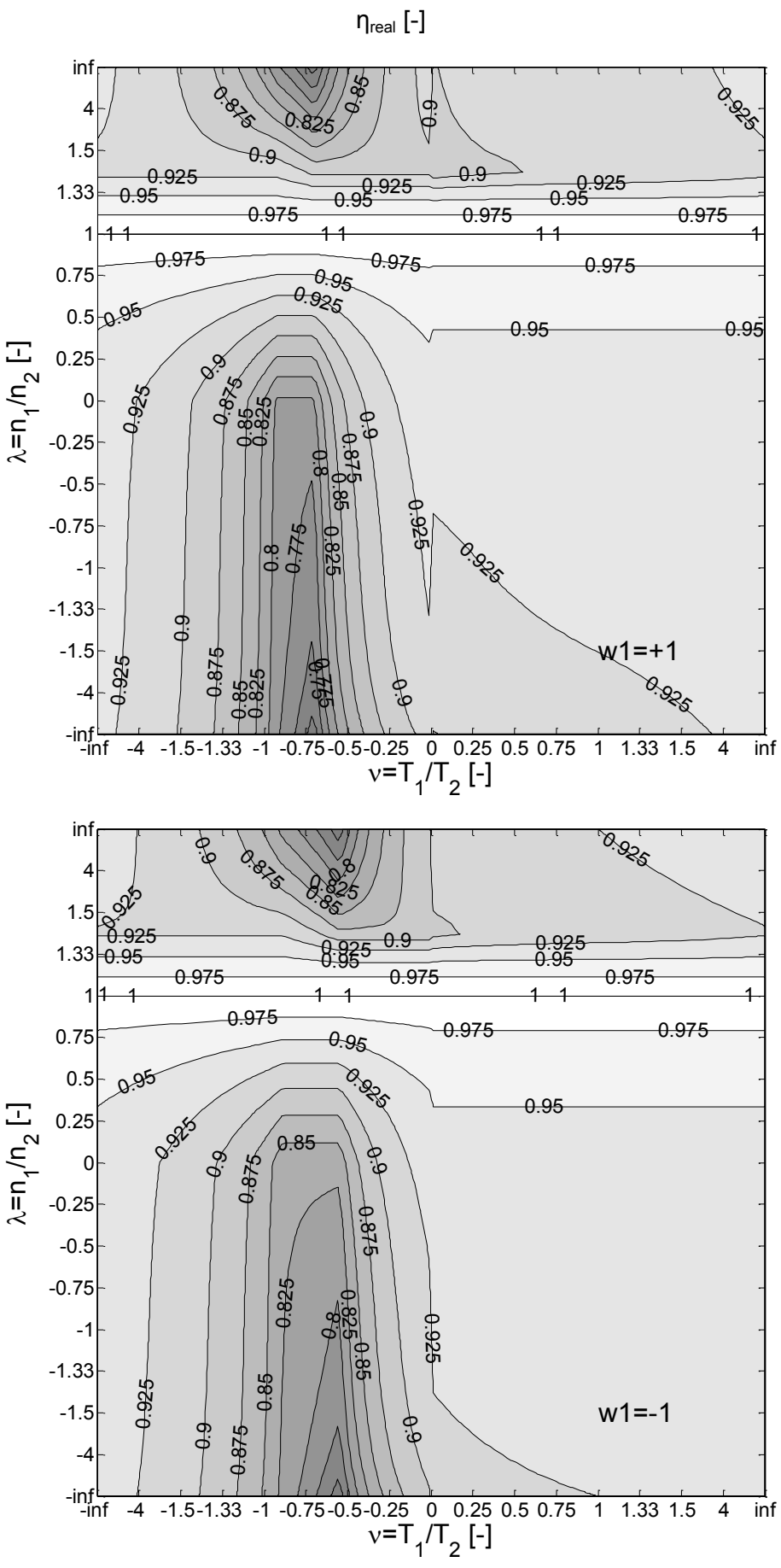

Figure 4-58: Realistic efficiency of 4-shaft CCPGT corresponding to Figure 4-55

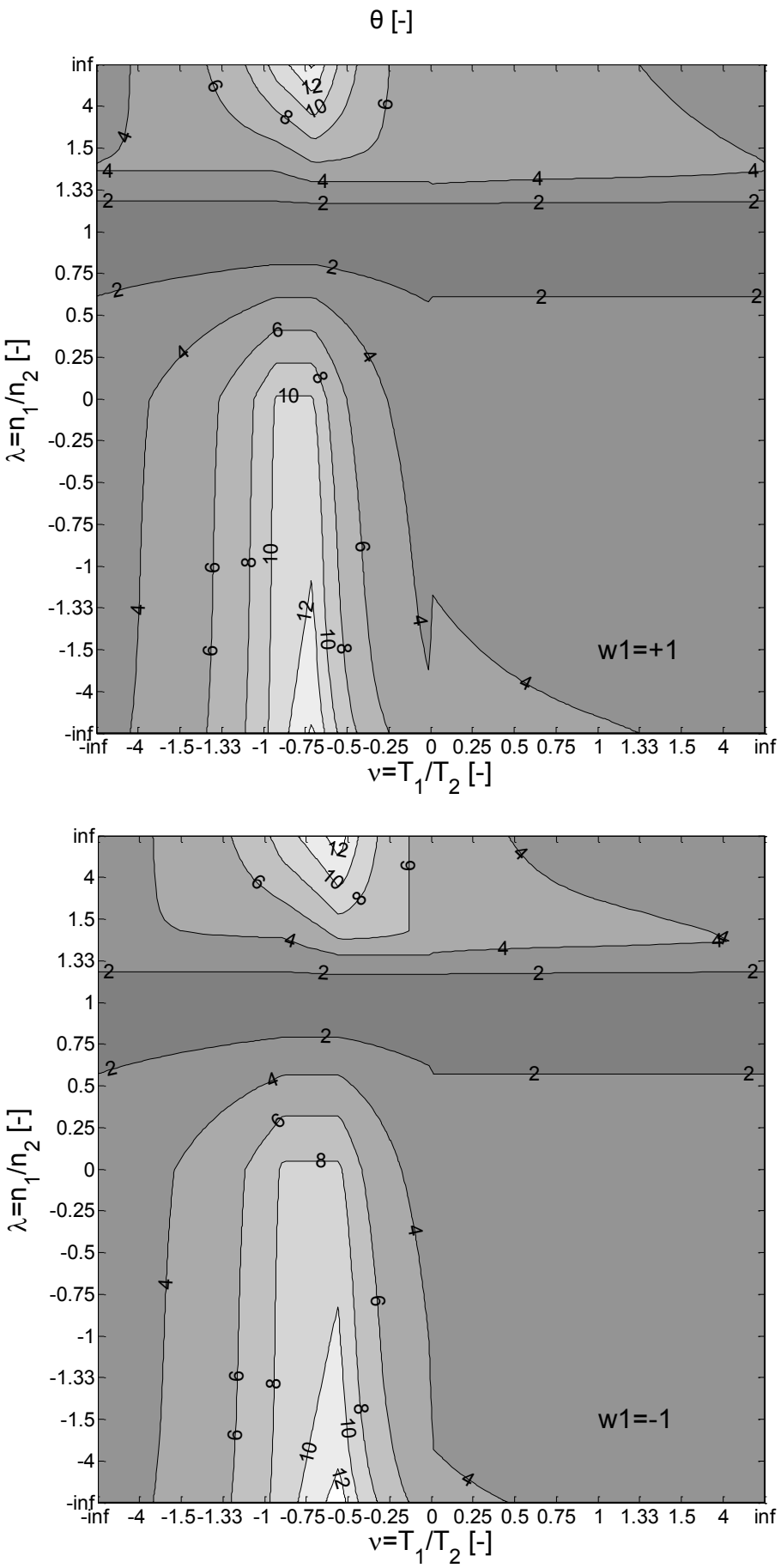

Figure 4-59: Input power ratio of 4-shaft CCPGT corresponding to Figure 4-55

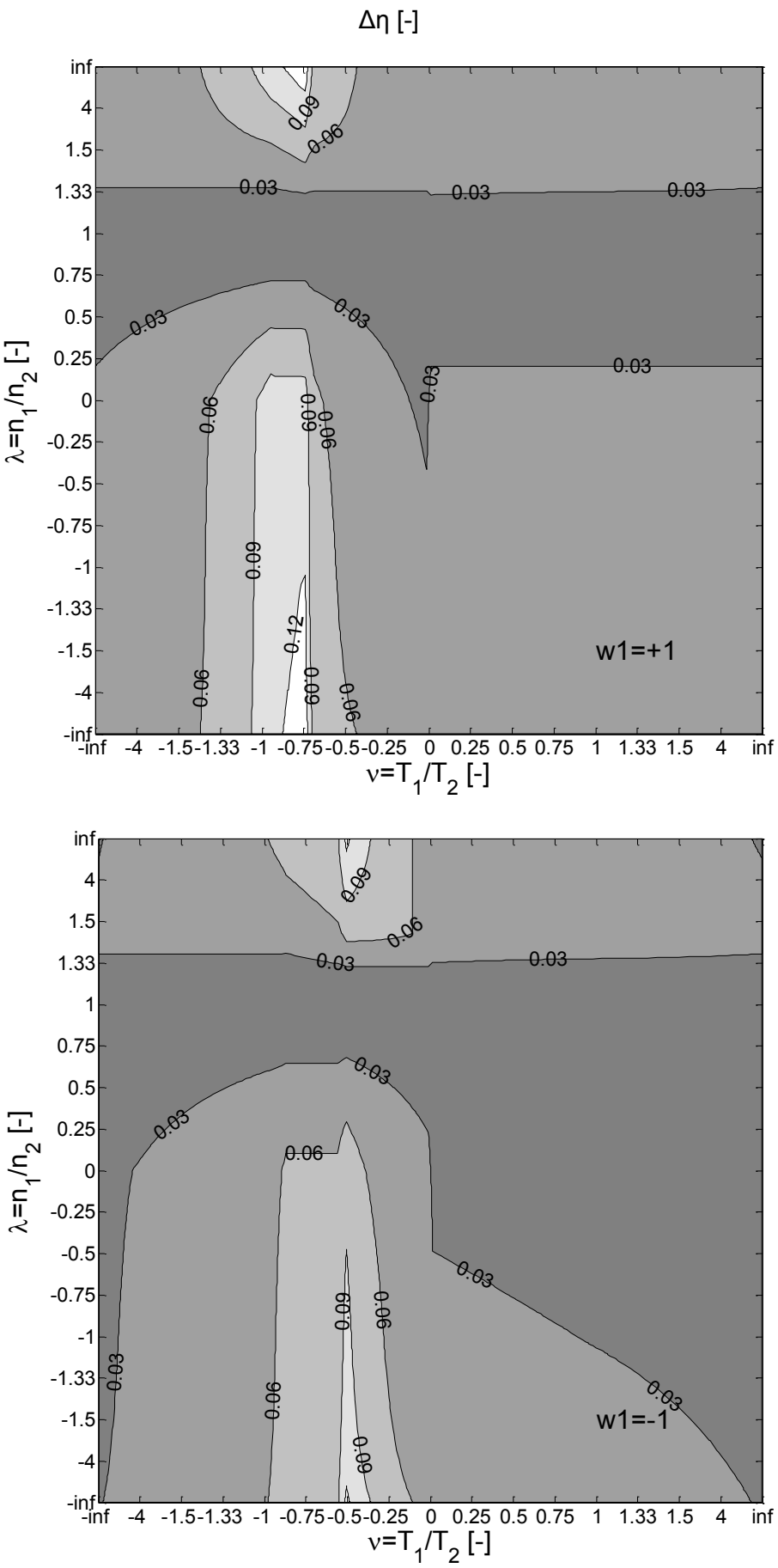

Figure 4-60: Efficiency deviation of 4-shaft CCPGT corresponding to Figure 4-55

4.4 Special operating conditions and self-locking

PGTs can feature locking and self-locking effects as already mentioned in Section 3.5. These effects arise if a change of direction of the power flow of a central shaft is observed when power losses are taken into account. Power losses can force an actual output shaft to become an input shaft if the remaining input power cannot cover the overall power demand. It is also possible that the iteration described in Sections 4.1.5 and 4.2.3.4 does not converge at all. Then, an impossible operating condition is on hand. In this section, locking and self-locking effects for basic trains, single PGTs and CCPGTs are discussed.

4.4.1 Locking effects for basic trains

Initially, only basic trains with fixed carrier are considered (**Figure 4-61**). As for the basic train of an ordinary single PGT it is feasible to assume a basic efficiency larger than 95%. According to equation (3.9) the torque ratio of the central gears is influenced in contrast to the loss-free case but the sign of the output torque cannot change since the basic efficiency factor is positive. No matter how small the input power or the basic efficiency is assumed, output power must be existent. The basic train of a single PGT cannot feature two (central gear) input shafts at the same time.

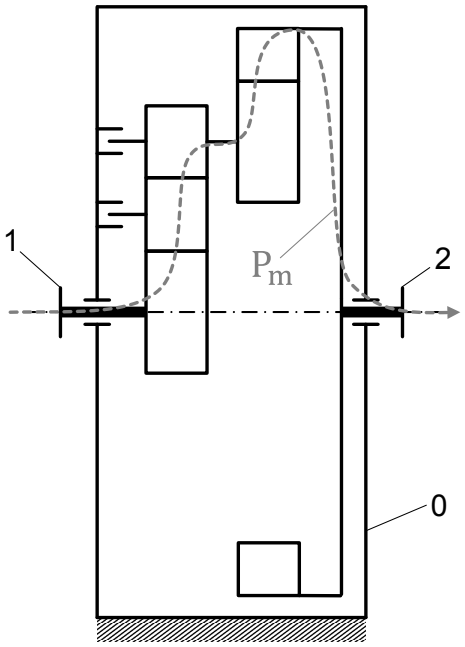

Figure 4-61: Example basic train of a single PGT

The basic train(s) of a CCPGT can feature multiple inputs and outputs. The question of which torque ratio is influenced by considering power losses depends on which inputs and outputs are predefined. **Figure 4-62** shows the basic train structure of a 4-shaft CCPGT with fixed carrier. The input power of central gear 1 is given as well as the output power of central gear 2 (superscript asterisk). The external power of central gear 3 results from the meshing power balance. The torque of the carrier and housing result from the torque balance. One can imagine that central gear 3 is an output if the input power of central gear 1 is larger than the output power of central gear 2 for loss-free operating conditions. If power losses occur and the input power of central gear 1 multiplied by the related basic efficiency is not enough to satisfy the power demand of central gear 2, central gear 3 has to assume the role of an input shaft. In order to enable this operating condition, central gear 3 must be connected to an appropriate drive unit. Otherwise, the transmission is locking as the output power is larger than the available input power in a mathematical sense.

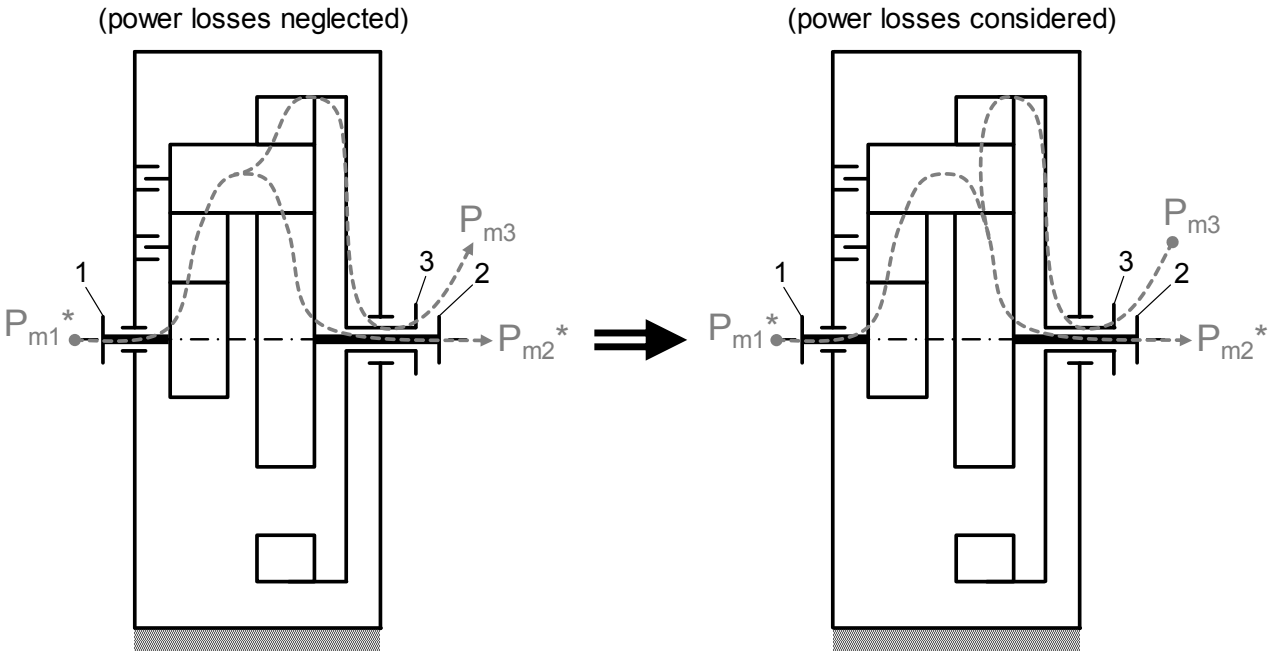

Figure 4-62: Example basic train structure of a 4-shaft CCPGT

This operating condition can also be compared to a driven shaft being braked (**Figure 4-63**). The shaft won't start to turn unless the input torque is larger than the maximum brake torque. Neglecting the material strength, it is always possible to overcome the locking effect by increasing the input power and input torque respectively as long as the brake torque is not increasing simultaneously.

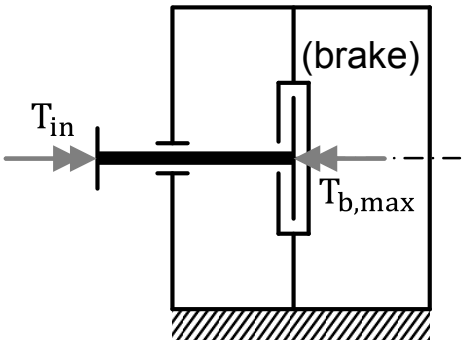

Figure 4-63: Shaft with brake

4.4.2 Single planetary gear transmissions and self-locking

In contrast to basic trains with fixed carrier, single PGTs can show self-locking only for the carrier shaft. **Self-locking means that a shaft switches to an input shaft considering power losses, which cannot be reversed by increasing the input power of another shaft.** In case of self-locking, power losses increase proportionally with the input power increasing. Thus self-locking of a (single) PGT can only be overcome by driving the locked shaft directly. The basic equations for the torque of the carrier shaft depending as a function of a central gear torque read as follows:

$$T_s = (i_{1\,2}^{s} \cdot \eta_0^{w1} - 1) \cdot T_1$$
$$T_s = \left(\frac{1}{i_{1\,2}^{s} \cdot \eta_0^{w1}} - 1\right) \cdot T_2 \qquad (4.51)$$

η_0	[-]	basic train efficiency	w1	[-]	efficiency exponent
$i_{1\,2}^{s}$	[-]	basic ratio	$T_{1/2/s}$	[Nm]	external torque of central gear 1/2 or carrier shaft s

Obviously, the sign of the carrier shaft torque switches in comparison to loss-free conditions for one of the following two cases:

1. $i_{1\,2}^{s} > 1 \;\; and \;\; \eta_0 < \frac{1}{i_{1\,2}^{s}}$ and $w1 = +1$
2. $0 < i_{1\,2}^{s} < 1 \;\; and \;\; \eta_0 < i_{1\,2}^{s}$ and $w1 = -1$ (4.52)

η_0	[-]	basic train efficiency	w1	[-]	efficiency exponent
$i_{1\,2}^{s}$	[-]	basic ratio			

The sign of w1 is a function of given speeds and torques, but it is not relevant whether the single PGT features two or three running shafts. If only two shafts are running, namely one central gear shaft and the carrier shaft, self-locking can be identified by calculating the overall efficiency. If the overall efficiency is equal to zero, self-locking is on hand. In order to keep the PGT running, it is necessary to drive the carrier shaft directly. Some authors, e.g. Mueller [2_MUL01], also indicate negative overall efficiency values as the carrier shaft is still interpreted as an output shaft.

In case of three running shafts, it is not sufficient only to consider the overall efficiency. The following example shows that the overall efficiency can still be larger than zero with a self-locking carrier shaft. The parameters of the given positive-ratio drive are:

$$i_{1\,2}^{s} = 1{,}02$$
$$\eta_0 = 0{,}95 \qquad (4.53)$$

$i_{1\,2}^{s}$	[-]	basic ratio	η_0	[-]	basic train efficiency

The kinematics of the PGT is predefined as follows:

$$n_1 = +200\ \text{rpm} \;;\; n_2 = +100\ \text{rpm} \;\Rightarrow\; n_s = -4900\ \text{rpm} \qquad (4.54)$$

$n_{1/2/s}$	[rpm]	absolute speed of central shaft 1/2/s

The torques of central shafts 2 and s result from the torque of central shaft 1, which is supposed to be preset (loss-free operating conditions):

$$T_1 = +100\ \text{Nm} \;\Rightarrow\; T_2 = -102\ \text{Nm} \;;\; T_s = +2\ \text{Nm}$$
$$(P_1 = +2094\ \text{W} \;\Rightarrow\; P_2 = -1068\ \text{W} \;;\; P_s = -1026\ \text{W}) \qquad (4.55)$$

$T_{1/2/s}$	[Nm]	external torque of central shaft 1/2/s	$P_{1/2/s}$	[W]	external power of central shaft 1/2/s

Hence, central shaft 1 is an input shaft while central shaft 2 is an output shaft as well as the carrier shaft s. The efficiency exponent w1 equals +1.

Now, power losses are taken into account. The resulting torques of central shafts 2 and s are influenced:

$$T_1 = +100\,\mathrm{Nm} \;\Rightarrow\; T_2 = -96{,}9\,\mathrm{Nm}\;;\; T_s \overset{!}{=} -3{,}1\,\mathrm{Nm}$$
$$(P_1 = +2094\,\mathrm{W} \;\Rightarrow\; P_2 = -1015\,\mathrm{W}\;;\; P_s \overset{!}{=} +1591\,\mathrm{W}) \qquad (4.56)$$

$T_{1/2/s}$	[Nm]	external torque of central shaft 1/2/s	$P_{1/2/s}$	[W]	external power of central shaft 1/2/s

As a matter of fact, the sign of the torque of the carrier shaft switches and the carrier turns into an input shaft. Consequently, central shaft s has to be driven to maintain the predefined conditions. In contrast, central shaft 2 is still an output. Thus, the overall efficiency is larger than zero:

$$\eta = -\frac{P_{out}}{P_{in}} \approx 27{,}5\% \qquad (4.57)$$

η	[-]	overall efficiency	P_{in}	[W]	overall (absolute) input power
			P_{out}	[W]	overall (absolute) output power

Expressing the power of central shaft s and the power loss as a function of the input power, it can easily be seen that central shaft s cannot be turned into an output shaft by increasing the input power and power losses are linearly depending on the input power:

$$P_s = 2\cdot\pi\cdot T_s\cdot n_s = 2\cdot\pi\cdot(i_{1\,2}^{s}\cdot\eta_0 - 1)\cdot T_1\cdot\frac{n_s}{n_1}\cdot n_1 = \underbrace{(i_{1\,2}^{s}\cdot\eta_0 - 1)\cdot\frac{n_s}{n_1}}_{>0}\cdot P_1 == \underbrace{\text{const.}}_{>0}\cdot P_1$$

$$P_L = -(1-\eta_0)\cdot P_{m1} = -2\cdot\pi\cdot(1-\eta_0)\cdot T_1\cdot(n_1 - n_s) = \underbrace{-(1-\eta_0)\cdot\frac{n_1 - n_s}{n_1}}_{<0}\cdot P_1 = \qquad (4.58)$$
$$= \underbrace{\text{const.}}_{<0}\cdot P_1$$

$i_{1\,2}^{s}$	[-]	basic ratio	$T_{1/s}$	[Nm]	external torque of central shaft 1/s
η_0	[-]	basic train efficiency	$P_{1/s}$	[W]	absolute power of central shaft 1/s
$n_{1/s}$	[rpm]	absolute speed of central shaft 1/s	P_{m1}	[W]	meshing power of central shaft 1
			P_L	[W]	absolute power loss

4.4.3 Complex-compound planetary gear transmissions, locking and self-locking

It was shown in Section 4.4.1 that self-locking is not possible for central gears of CCPGTs with fixed carrier. The locking effect can always be overcome by increasing the input meshing power. Anyhow, self-locking can occur for centrals gears of CCPGTs with rotating carrier. A common example is the Wolfrom type CCPGT working as speed increaser with one internal gear being fixed, the other internal gear as input and the sun gear as output (**Figure 4-64**). The carrier is without external load.

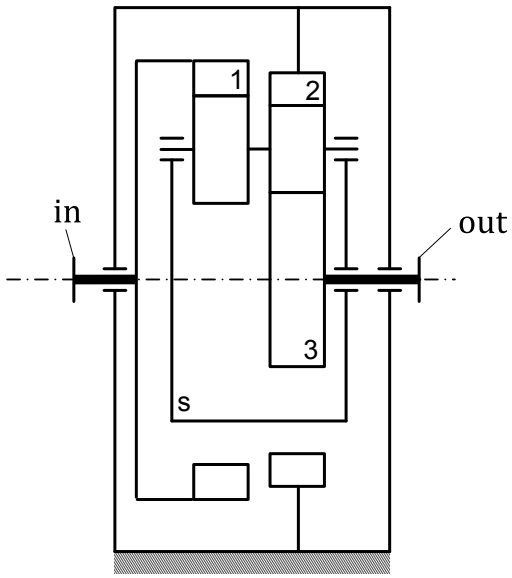

$$i_I = i_{12}^s = +\frac{101}{100}$$
$$i_{II} = i_{23}^s = -\frac{1}{3}$$
$$i_{III} = i_{13}^s = -\frac{101}{300}$$

$$\eta_{0,I} = \eta_{1\,2}^s = \eta_{2\,1}^s = 0{,}995^2 \approx 0{,}99$$
$$\eta_{0,II} = \eta_{2\,3}^s = \eta_{3\,2}^s = 0{,}995 \cdot 0{,}99 \approx 0{,}985$$
$$\eta_{0,III} = \eta_{1\,3}^s = \eta_{3\,1}^s = 0{,}995 \cdot 0{,}99 \approx 0{,}985$$

Figure 4-64: Wolfrom type CCPGT working as speed increaser

The overall transmission ratio results from equation (2.7):

$$i_t = \frac{n_1}{n_3} = i_{1\,3}^2 = \frac{1 - i_{1\,2}^s}{1 - i_{3\,2}^s} = -\frac{1}{400} \qquad (4.59)$$

i_t	[-]	overall transmission ratio	i_{xy}^z	[-]	compound ratio
i_{xy}^s	[-]	basic ratio			

As central gear 1 is supposed to be a power input, its speed and external torque are positive. Carrying out a kinematics and statics analysis for loss-free operating conditions leads to the functionally equivalent substitution figure (**Figure 4-65**). It is valid as long as the external torque of central gear 3 is greater than zero.

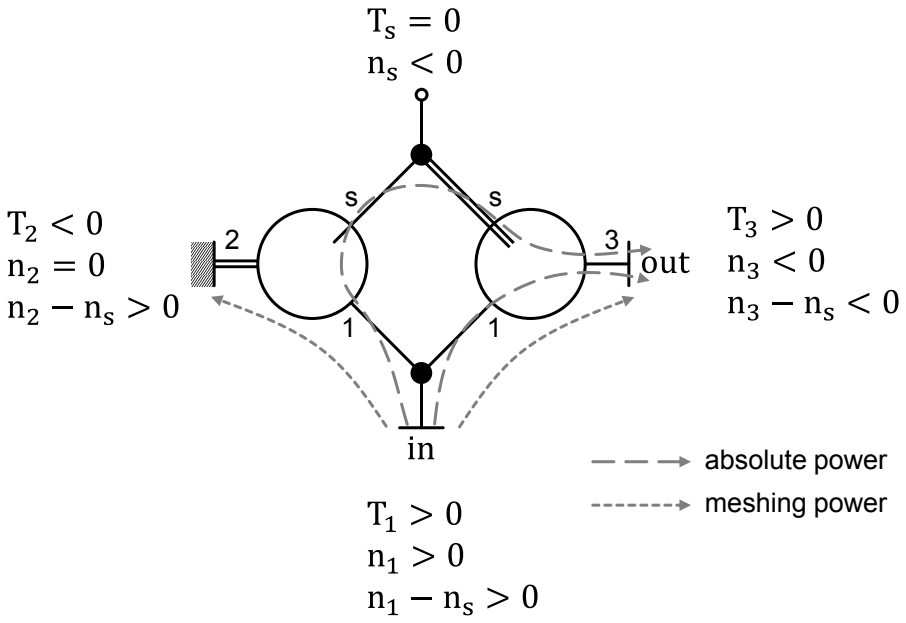

Figure 4-65: Functionally-equivalent substitution figure corresponding to Figure 4-64 for operating conditions without self-locking

The meshing power of central gear 1 is partitioned to central gear 2 and 3. Thus the meshing power balance with power losses included reads:

$$P_{m1} + \frac{P_{m2}}{\eta^s_{1\,2}} + \frac{P_{m3}}{\eta^s_{1\,3}} = 0$$
$$\Rightarrow \; T_1 \cdot (n_1 - n_s) + \frac{T_2 \cdot (n_2 - n_s)}{\eta^s_{1\,2}} + \frac{T_3 \cdot (n_3 - n_s)}{\eta^s_{1\,3}} = 0 \qquad (4.60)$$

P_{mx}	[W]	meshing power of central gear x	T_x	[Nm]	external torque of central gear x
$n_{x/s}$	[rpm]	absolute speed of central gear x / carrier s	$\eta^s_{x\,y}$	[-]	basic efficiency

Additionally, the sum of torques must equal zero:

$$T_1 + T_2 + T_3 + \underbrace{T_s}_{=0} = 0 \qquad (4.61)$$

$T_{x/s}$	[Nm]	external torque of central gear x / carrier s

Substituting equations (4.59) and (4.61) into (4.60) leads to the power ratio between central gear 3 and 1:

$$\frac{P_3}{P_1} = \frac{T_3 \cdot n_3}{T_1 \cdot n_1} = \frac{(1 - i^s_{1\,2} \cdot \eta^s_{1\,2}) \cdot \overbrace{(i^s_{1\,2} \cdot i^s_{1\,3} \cdot \eta^s_{1\,2} \cdot \eta^s_{1\,3})}^{<0}}{\underbrace{(i^s_{1\,2} \cdot \eta^s_{1\,2})}_{>0} \cdot \underbrace{(i^s_{1\,2} \cdot \eta^s_{1\,2} - i^s_{1\,3} \cdot \eta^s_{1\,3})}_{>0}} \cdot \underbrace{\frac{1}{i_t}}_{<0} < 0 \quad for \;\; i^s_{1\,2} > 1/\eta^s_{1\,2} \qquad (4.62)$$

P_x	[W]	absolute power of central gear x	T_x	[Nm]	external torque of central gear x
n_x	[rpm]	absolute speed of central gear x	$i^s_{x\,y}$	[-]	basic ratio
i_t	[-]	overall transmission ratio	$\eta^s_{x\,y}$	[-]	basic efficiency

As for the limit case, the numerator and the power of central gear 3 can become zero for:

$$1 - i^s_{1\,2} \cdot \eta^s_{1\,2} = 0$$
$$\Rightarrow \; i^s_{1\,2} = \frac{1}{\eta^s_{1\,2}} \qquad (4.63)$$

$i^s_{x\,y}$	[-]	basic ratio	$\eta^s_{x\,y}$	[-]	basic efficiency

Then, self-locking occurs for central gear 3 and its external torque equals zero. Beyond this limit case, power has to be supplied to central gear 3 and the external torque of central gear 3 has to be less than zero. Thus, the substitution figure is to be modified in order to be functionally-equivalent (**Figure 4-66**).

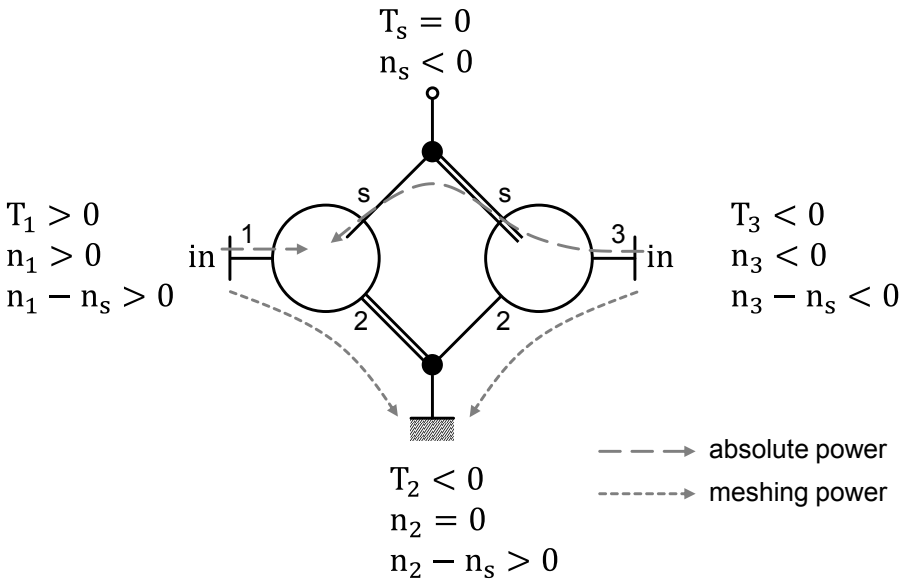

Figure 4-66: Functionally-equivalent substitution figure corresponding to Figure 4-64 for operating conditions with self-locking

Now, the meshing power balance reads:

$$\eta^s_{1\,2} \cdot P_{m1} + P_{m2} + \eta^s_{2\,3} \cdot P_{m3} = 0$$
$$\Rightarrow \quad \eta^s_{1\,2} \cdot T_1 \cdot (n_1 - n_s) + T_2 \cdot (n_2 - n_s) + \eta^s_{2\,3} \cdot T_3 \cdot (n_3 - n_s) = 0 \qquad (4.64)$$

P_{mx}	[W]	meshing power of central gear x	T_x	[Nm]	external torque of central gear x
$n_{x/s}$	[rpm]	absolute speed of central gear x / carrier s	$\eta^s_{x\,y}$	[-]	basic efficiency

Substituting equations (4.59) and (4.61) into (4.64) leads to the new power ratio between central gear 3 and 1, which is positive:

$$\frac{P_3}{P_1} = \frac{T_3 \cdot n_3}{T_1 \cdot n_1} = \frac{(1 - i^s_{1\,2} \cdot \eta^s_{1\,2}) \cdot \overbrace{i^s_{1\,3}}^{<0}}{\underbrace{\eta^s_{2\,3} \cdot i^s_{1\,2} - i^s_{1\,3}}_{>0}} \cdot \frac{1}{\underbrace{i_t}_{<0}} > 0 \quad for \;\; i^s_{1\,2} < 1/\eta^s_{1\,2} \qquad (4.65)$$

P_x	[W]	absolute power of central gear x	T_x	[Nm]	external torque of central gear x
n_x	[rpm]	absolute speed of central gear x	$i^s_{x\,y}$	[-]	basic ratio
i_t	[-]	overall transmission ratio	$\eta^s_{x\,y}$	[-]	basic efficiency

Hence, increasing the absolute input power and/or the input meshing power of central gear 1 does not cause central gear 3 to become an output again like for loss-free operating conditions. However, the phenomenon of self-locking is not induced by central gear 3 itself but by the carrier. Imagining central gear 3 to be unloaded and carrier s to be the actual output shaft leads to a single positive-ratio drive featuring two internal gears (**Figure 4-67**).

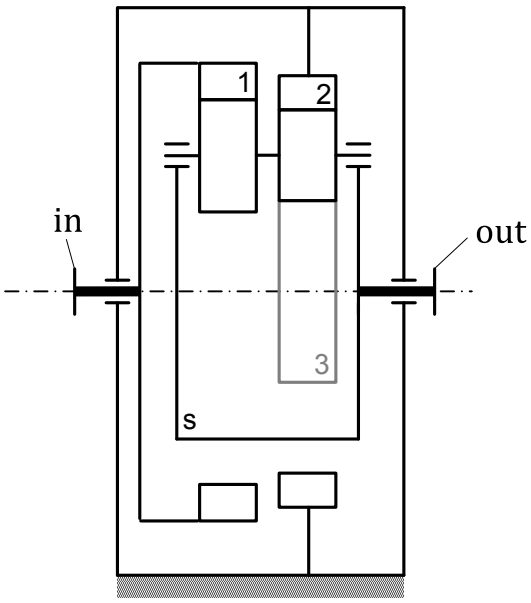

$$i_I = i_{12}^s = +\frac{101}{100}$$

$$\eta_{0,I} = \eta_{1\,2}^s = \eta_{2\,1}^s = 0{,}995^2 \approx 0{,}99$$

Figure 4-67: Positive-ratio drive derived from Figure 4-64 working as speed increaser

The power ratio between the output shaft s and the input shaft 1 is:

$$\frac{P_s}{P_1} = \frac{T_s \cdot n_s}{T_1 \cdot n_1} = \frac{1 - i_{1\,2}^s \cdot \eta_{1\,2}^s}{\underbrace{i_{1\,2}^s - 1}_{>0}} \quad \begin{cases} < 0 & for \;\; i_{1\,2}^s > 1/\eta_{1\,2}^s \\ > 0 & for \;\; i_{1\,2}^s < 1/\eta_{1\,2}^s \end{cases} \qquad (4.66)$$

$P_{x/s}$	[W]	absolute power of central gear x / carrier s	$T_{x/s}$	[Nm]	external torque of central gear x / carrier s
$n_{x/s}$	[rpm]	absolute speed of central gear x / carrier s			
$i_{x\,y}^s$	[-]	basic ratio	$\eta_{x\,y}^s$	[-]	basic efficiency

Obviously, the self-locking limit case is identical to equation (4.63). The existence or absence of central gear 3 does not influence self-locking of the given CCPGT. Thus, self-locking is also possible for central gears in presence of a self-locking carrier.

In the following, it is assumed that an additional external input is applied to the carrier shaft in **Figure 4-64**. Hence, all four shafts are loaded. The input of the carrier shall be rather small such that input power is still needed to be supplied to central shaft 3 in order to keep the transmission in motion. **Figure 4-68** shows the functionally-equivalent substitution figure for this operating condition. The external power of central shaft can be expressed as a function of the external power of central shaft 1 and carrier shaft s:

$$P_3 = 2 \cdot \pi \cdot T_3 \cdot n_3 = \underbrace{\frac{\overbrace{2 \cdot \pi \cdot i_{1\,3}^s}^{<0}}{\underbrace{\eta_{2\,3}^s \cdot i_{1\,2}^s - i_{1\,3}^s}_{>0}}}_{} \cdot \left(\underbrace{(1 - i_{1\,2}^s \cdot \eta_{1\,2}^s)}_{>0 \; for \; i_{1\,2}^s < 1/\eta_{1\,2}^s} \cdot \underbrace{\frac{1}{i_t}}_{<0} \cdot \underbrace{P_1}_{>0} + \underbrace{\frac{n_3}{n_s}}_{>0} \cdot \underbrace{P_s}_{>0} \right) \qquad (4.67)$$

$P_{x/s}$	[W]	absolute power of central gear x / carrier s	T_x	[Nm]	external torque of central gear x
$n_{x/s}$	[rpm]	absolute speed of central gear x / carrier s	$i_{x\,y}^s$	[-]	basic ratio
i_t	[-]	overall transmission ratio	$\eta_{x\,y}^s$	[-]	basic efficiency

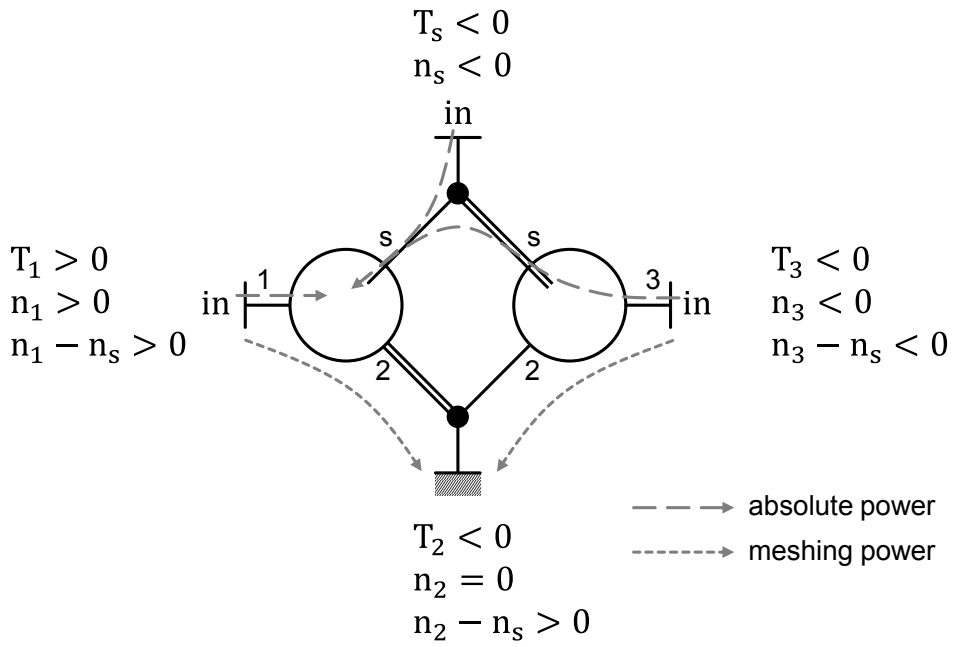

Figure 4-68: Functionally-equivalent substitution figure corresponding to Figure 4-64 for operating conditions with self-locking with additional input at the carrier shaft

Equation (4.67) reveals that it is possible to turn central shaft 3 into an output shaft by increasing the input power at the carrier s but not at central shaft 1. Thus, central shaft 3 is self-locking in respect of central shaft 1 that can be overcome by driving the carrier s. Self-locking depends on which shafts are driven and on the superposition of power flow in case of CCPGTs with multiple static DOFs.

4.4.4 General self-locking criterion

In order to check whether or not self-locking does occur for a given PGT with its operating condition, the following steps are to be carried out. First, it is to be monitored if an actual output shaft turns into an input shaft by considering power losses. In case power cannot be supplied to this shaft, the intended operating condition cannot be achieved. Anyhow, it can be tested if the ‘lack of power’ can be handled by increasing the input power and decreasing the output power respectively of another shaft if available. For this purpose, the partial derivative of the power of the ‘locked’ shaft with respect to the power of another shaft must be negative to turn it back into an output shaft. In this context speeds are interpreted as constants:

$$\frac{\partial P_{\mathrm{locked}}}{\partial P_{\mathrm{in/out}}} < 0 \qquad (4.68)$$

P_{locked}	[W]	absolute power of the ‘locked’ shaft	$P_{\mathrm{in/out}}$	[W]	absolute power of another in-/output shaft

Consequently, if no task helps overcome the locking effect the intended operating condition has to be modified by setting the power of the ‘locked’ shaft to zero. Unloaded, ‘dragged’ central gears are not of further relevance for self-locking. In the end, it is only

relevant if it is possible to keep the carrier shaft in motion. Hence, it must be possible to generate output power at the carrier shaft (cf. Sections 4.4.2 and 4.4.3). In case this does not succeed, self-locking is existent.

4.4.5 Impossible operating conditions

Besides self-locking, impossible operating conditions can theoretically be created by choosing unfavorable set point values. Impossible operating conditions appear if the amount of output power demanded cannot be provided due to too low efficiency and locking effects. For the example single PGT given in Section 4.4.2, which features self-locking for the carrier shaft, it is impossible to demand output power from the carrier shaft. In any case, as the single PGT offers two kinematic and one static DOF, output power can theoretically be demanded by selecting predefined speeds and torques. If so, the iteration procedure for solving torques under power loss conditions (cf. Sections 4.1.5 and 4.2.3.4) does not converge. As already mentioned, the number of iteration steps is very limited as only two central gear torques at maximum are unknown. It is necessary to monitor repetitive iteration steps to identify impossible operating conditions and to avoid infinite loops.

5 Synthesis by means of Helfer diagrams and equivalent lever models

The efficiency calculation methods discussed in the previous chapter are useful for analyzing given CCPGTs. A synthesis method is needed to find a suitable transmission concept corresponding to a predefined task and operating condition respectively. As mentioned in Section 3.6, existing synthesis methods are often aimed at finding transmissions for specific applications, e.g. automated transmissions, at which CCPGTs are excluded by the majority. Only very few references concentrate on the synthesis of CCPGTs.

In general, the problem of PGT synthesis implicates a huge and frequently unmanageable solution space. Therefore, authors focus on limiting the solution space by imposing constraints in respect of designs, applications and operating conditions. Almost exclusively, systematic combinatorics is used to produce variants considering predefined constraints. Afterwards, it is checked if the variants meet the demands of the intended task. Naturally, procedures like these cannot be efficient as many variants will not even comply with the demands. Furthermore, variants generated are too complex in regard to the design and thus not practicable.

Within the scope of this chapter, a synthesis method for basic CCPGT structures is discussed. It features two main modules (**Figure 5-1**). On the one hand, an abstract model is generated from predefined, desired operating conditions. The model is based on the Kutzbach and Helfer diagram and on an equivalent lever (cf. Section 3.2.2). It is independent from a specific CCPGT structure, and therefore, does not limit the solution space to specific designs. In addition, it allows one to define arbitrary operating conditions matching the DOF of a CCPGT. On the other hand, CCPGT structures are derived from the equivalent lever model as well as from a reference CCPGT, which contains all feasible CCPGT structures regarding the design complexity. Thereby, those and only those solutions which are able to perform the predefined demands and which are reasonable in principle from a designer's point of view are created. Hence, the generated solution space is kept small while featuring all relevant CCPGT structures.

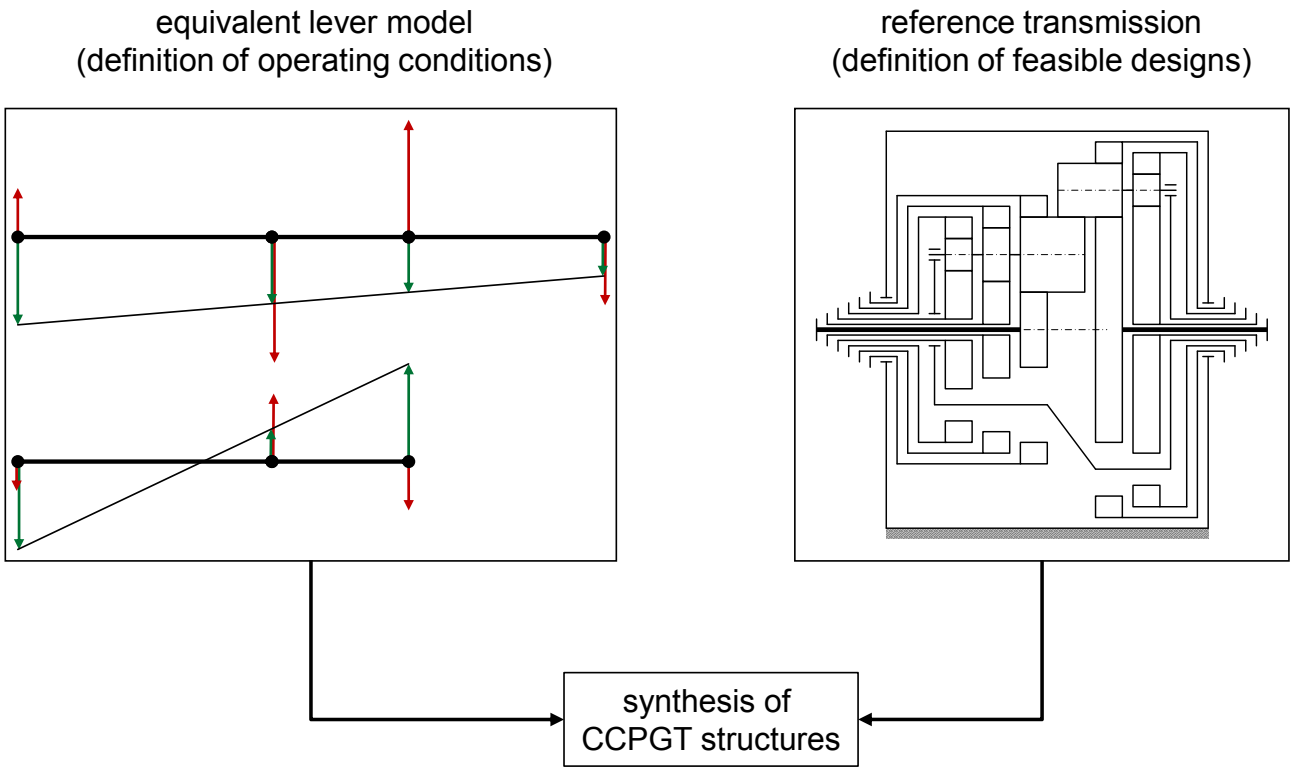

Figure 5-1: Basic principle of proposed CCPGT synthesis method

5.1 Basics of the equivalent lever model

By means of the Helfer diagram a CCGT is transformed into an equivalent lever model. This transformation is definite. Every CCPGT corresponds to a definite lever model. The other way round, a particular lever model corresponds to all kinematically-equivalent CCPGTs. In the following, the most important details are mentioned.

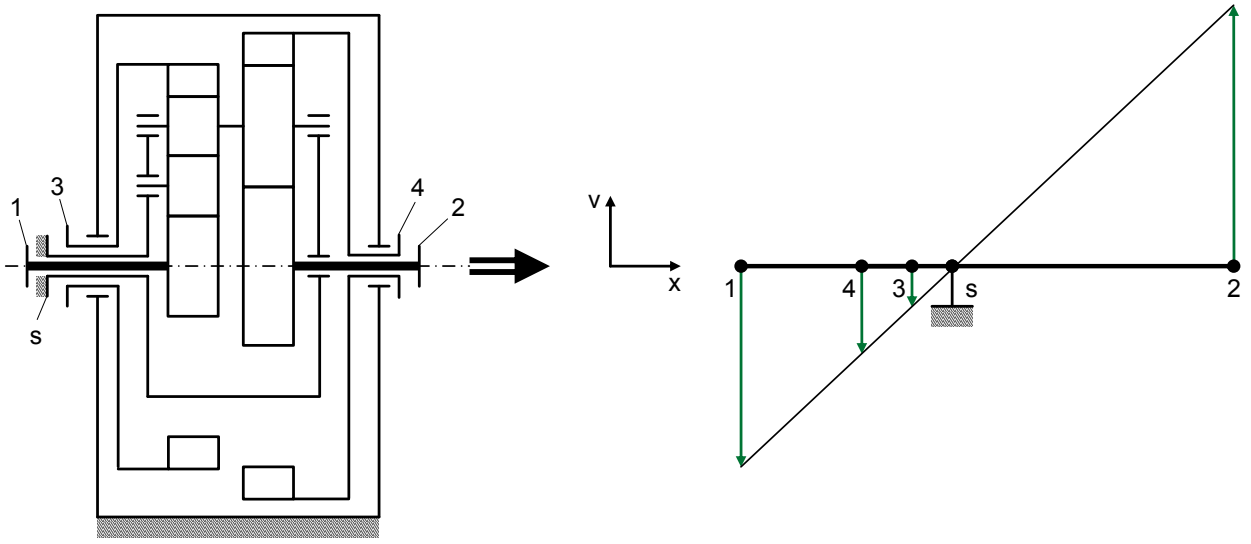

Figure 5-2: Example lever model of a 5-shaft CCPGT with speeds

Figure 5-2 shows a lever model corresponding to a 5-shaft CCPGT. The lever model is arranged such that rotational speeds of the CCPGT correspond to translational speeds v of the lever in case of pure vertical movement. The central shafts are represented by nodes on the lever being characterized by a coordinate x. The lever is to be interpreted as being rigid, i.e. no bending or deformations are allowed to occur. The lever features two kinematic DOF. It can accomplish a translational and a rotational movement. Two predefined speeds determine the speeds of all other nodes. One can imagine that the speed ratios of the central gears with the carrier being fixed are a function of the basic ratios of the CCPGT. If node s is fixed and all other nodes are rotating around node s the speed ratios are functions of the leverages:

$$n_i \mathrel{\hat{=}} v_i$$

$$\Rightarrow \frac{n_i - n_s}{n_j - n_s} = i_{ij}^{s} = \frac{v_i - v_s}{v_j - v_s} = \frac{x_i - x_s}{x_j - x_s} \qquad (5.1)$$

$n_{i/j}$	[rpm]	rotational speed of central shaft i/j	$v_{i/j}$	[m/s]	translational speed of node i/j
n_s	[rpm]	rotational speed of carrier s	v_s	[m/s]	translational speed of node s
i_{ij}^{s}	[-]	basic ratio	$x_{i/j}$	[m]	coordinate of node i/j
			x_s	[m]	coordinate of node s

Thus, the (relative) coordinates x are defined by the basic ratios of the CCPGT. A pure rotation of the lever around s matches the meshing case of the CCPGT, a pure translation matches the coupling case.

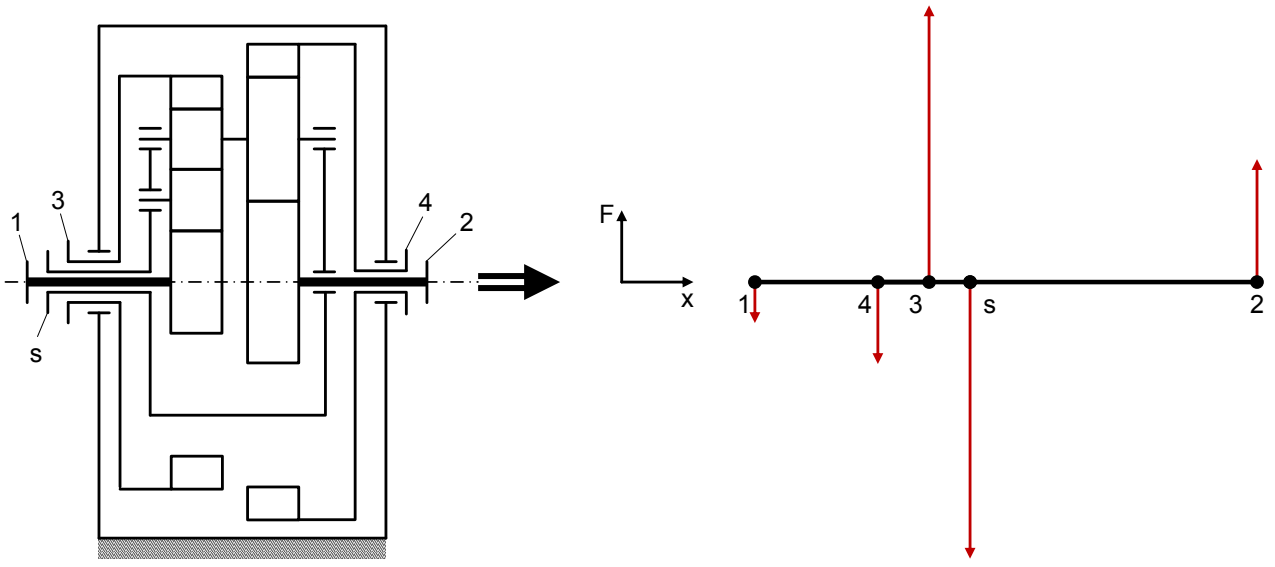

Figure 5-3: Example lever model of a 5-shaft CCPGT with forces

Further, if the lever is loaded with vertical forces at the nodes, the force, torque and power balance respectively must be satisfied for static operating conditions (**Figure 5-3**). This is true for the transmission as well as for the lever:

$T_i \mathrel{\widehat{=}} F_i$

$$\Sigma T_i = 0 \;\Leftrightarrow\; \Sigma F_i = 0 \qquad (5.2)$$

$$\Sigma T_i \cdot n_i = 0 \;\Leftrightarrow\; \Sigma F_i \cdot x_i = 0 \;\Rightarrow\; \Sigma F_i \cdot v_i = 0$$

T_i	[Nm]	external torque at central shaft i	F_i	[N]	(vertical) force at node i
n_i	[rpm]	rotational speed of central shaft i	v_i	[m/s]	translational speed of node i
n_s	[rpm]	rotational speed of carrier s	x_i	[m]	coordinate of node i

A 3-node lever features one static DOF as one force determines the other two forces via the force and torque balance. Every additional node increases the static DOF by one. Hence, the kinematic and static DOF of an equivalent lever is identical to the kinematic and static DOF of the CCPGT. The lever as well as the CCPGT can feature multiple in- and outputs.

In conclusion, the lever model is suitable for the complete representation and illustration of speeds and torques of a CCPGT. It offers a clear view on the speed and torque ratios irrespective of the CCPGT geometry. For synthesis purposes it is useful to define a lever via one or multiple operating conditions without focusing on a specific PGT layout. It 'contains' all kinematically-equivalent CCPGTs which are able to match the intended operating conditions basically. Then, an adequate CCPGT can be found.

It is worth mentioning that the lever model is also suitable for analyzing coupled PGTs as long as its basic structure features a kinematic DOF of two. Helfer [4_HEL67] provides a descriptive example including a 3-speed automatic transmission (**Figure 5-4**). The single PGTs forming the gear train are coupled twice with each other such that they can be interpreted as a single rigid lever.

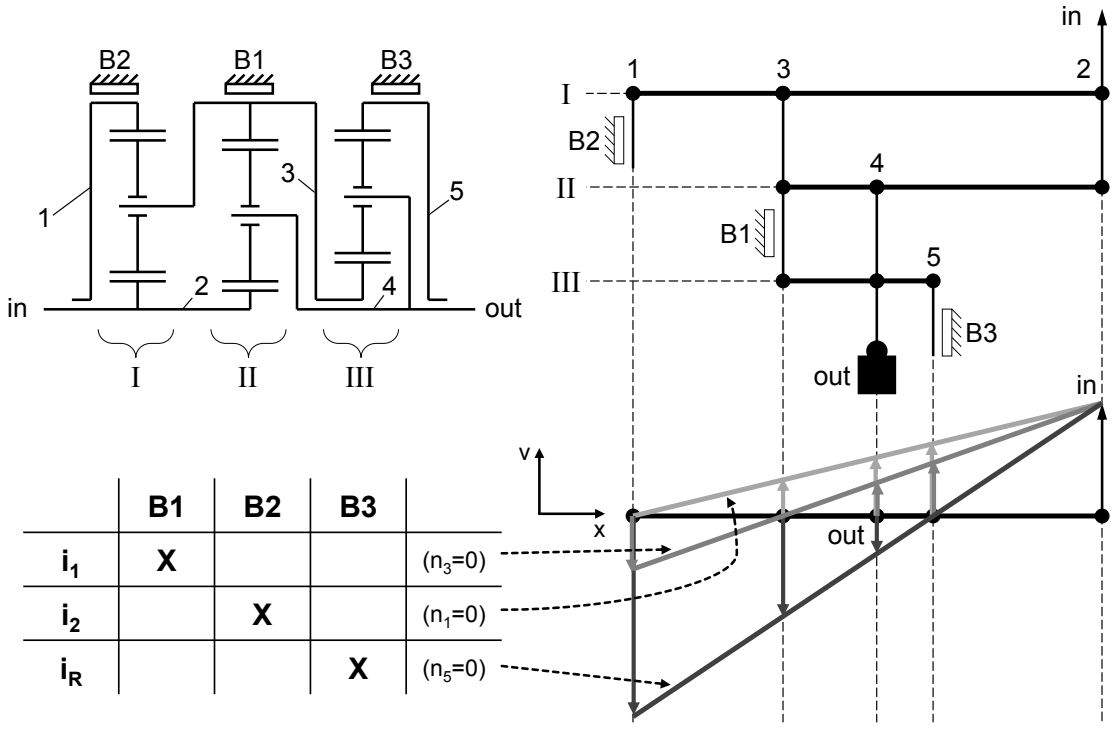

Figure 5-4: DIWA transmission 501 JSR with corresponding lever model [4_HEL67]

5.2 Generation of an equivalent lever model for one operating condition

A variety of possibilities for the definition of a lever model is thinkable. The leverages depend on coordinates x, transmission ratios, speeds, torques and power. For a proper characterization of an operating condition it is useful to provide speeds and torques. Hereby, efficiency analysis can be carried out later.

In order to choose a nomenclature independent from design aspects, lever nodes are assigned capital letters. As a PGT or CCPGT features minimum three central shafts, three lever nodes are to be defined at least. Without loss of generality, nodes A and B are always activated. As only ratios are of relevance but no absolute coordinates, the coordinate of node A is set to zero, the coordinate of node B equals one:

$$x_A = 0$$
$$x_B = 1 \qquad (5.3)$$

$x_{A/B}$	[m]	coordinate of node A/B

By presetting all desired speeds, equation (5.2) is used to find the coordinate of every additional node. In this regard, no two nodes should feature identical speeds as they would overlay each other and result in redundant central shafts and central gears with identical kinematic characteristics:

$$\frac{x_i - x_A}{x_B - x_A} = \frac{n_i - n_A}{n_B - n_A}$$
$$\Rightarrow \quad x_i = \frac{n_i - n_A}{n_B - n_A} \cdot x_B \qquad (5.4)$$

$x_{i/A/B}$	[m]	coordinate of node i/A/B	$n_{i/A/B}$	[rpm]	speed of node i/A/B

Next, the operating condition torques are to be defined. Two torques have to remain as unknowns according to the static DOF of the lever. They are determined by using the force and torque balance from equation (5.2). Since torques at central shafts directly correspond to forces at the nodes of the lever model, it is possible to write:

$$\Sigma T_i = 0$$
$$\Sigma T_i \cdot x_i = 0 \qquad (5.5)$$

T_i	[Nm]	external torque (force) at node i	x_i	[m]	coordinate of node i

Carrying out this procedure, an overall lever model for one operating condition is established. Alternatively, one speed of a node can remain unknown if an additional torque preset is available. If so, the missing coordinate is derived from equation (5.5). Afterwards, the missing speed is determined using equation (5.4). In case the coordinate of node A or B is missing the resulting coordinate must not equal zero and one respectively. A subsequent linear stretch or strain helps being consistent with (5.3).

A special case exists if three nodes in total are to be defined. For this case, three torque presets are sufficient to determine all coordinates as two coordinates are already defined by (5.3) and the third coordinate is gained from (5.5). If more than three nodes are needed, it is not possible to determine all coordinates only by defining desired torques as the number of conditional equations is insufficient.

5.3 Definition of multiple operating conditions

A CCPGT is able to satisfy multiple operating conditions. Multiple partial levers corresponding to different operating conditions may be collapsed into a single lever representing the final CCPGT. Hence, the partial levers must be assembled in such a manner that the final overall lever is rigid and consistent with the DOF of the CCPGT. A definite overall lever is generated if at least two nodes of a novel partial lever are identical with the existing final overall lever (**Figure 5-5**). Here, the vertical links are interpreted as jointed rods analogical to **Figure 5-4**. If only one node was identical, the two levers would be freely scalable independent of each other such that no definite overall lever could be assembled.

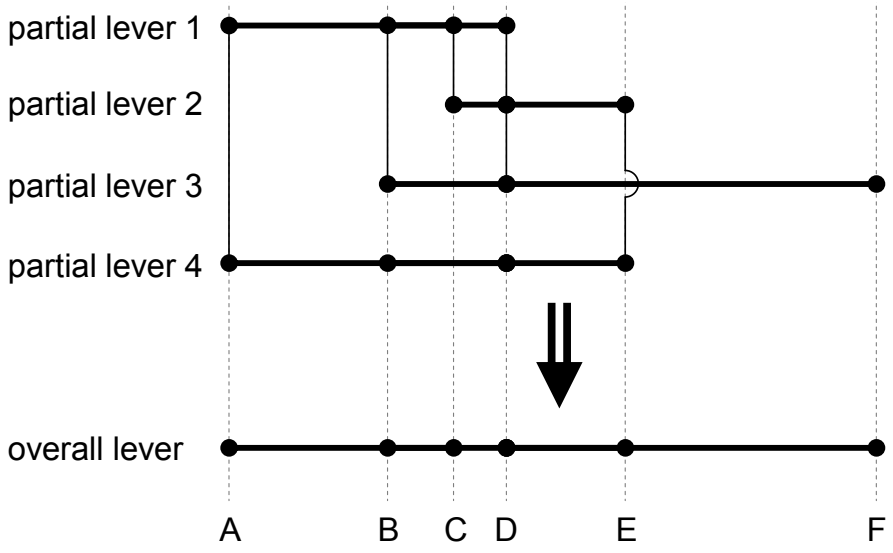

Figure 5-5: Example definition of multiple operating conditions

The definition of novel partial levers is carried out in accordance with Section 5.2. If only two nodes are identical with those of the existing overall lever, speed and torques are freely presettable. If more than two nodes are already defined, the speed of a third, already defined node k results from the speeds of two other already defined nodes i and j as:

$$n_k = \frac{x_k - x_i}{x_j - x_i} \cdot \left(n_j - n_i\right) + n_i \qquad (5.6)$$

n_k	[rpm]	unknown speed of defined node k	$x_{i/j/k}$	[m]	coordinates of nodes i/j/k
$n_{i/j}$	[rpm]	known speeds of defined nodes i/j			

When integrating novel partial levers into the overall lever, two exceptions should be watched. One is that novel nodes coincide with existing nodes. As stated in Section 5.2, this case would lead to central shafts with identical kinematic characteristic and should be avoided for the benefit of simplicity of the resulting CCPGT. The other is that the novel lever or at least parts of it are already contained within the existing overall lever. If so, it might be possible to match desired operating conditions with existing nodes and central shafts respectively and thus to simplify the CCPGT.

In order to check a correlation between two levers, the characteristic leverages are to be compared. A 3-node lever features one characteristic leverage (**Figure 5-6**). The segment between the middle node and an end node is referred to the overall length of the lever:

$$l_{BA} = \frac{x_B - x_A}{x_C - x_A} \qquad (5.7)$$

l_{BA}	[-]	characteristic leverage of 3-node lever	$x_{A/B/C}$	[m]	coordinates of nodes A/B/C

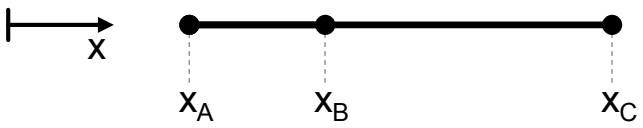

Figure 5-6: 3-node lever

Every additional node leads to an additional characteristic leverage. Hence an n-node lever features n-2 characteristic leverages. For instance, a 4-node lever (**Figure 5-7**) has:

$$l_{BA} = \frac{x_B - x_A}{x_D - x_A}$$
$$l_{CA} = \frac{x_C - x_A}{x_D - x_A} \qquad (5.8)$$

l_{BA}	[-]	first characteristic leverage of 4-node lever	$x_{A/B/C/D}$	[m]	coordinates of nodes A/B/C/D
l_{CA}	[-]	second characteristic leverage of 4-node lever			

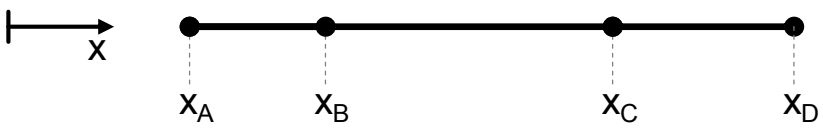

Figure 5-7: 4-node lever

In general, segments could also be related to other arbitrary segments. The ratio of the lengths of segments to the overall length of the lever implicates the advantage that characteristic leverages do not reach extremely high values. For a systematic correlation check, parts of the novel lever and the existing lever are compared starting with a maximum number of nodes and finishing with a minimum number of three nodes. For this purpose, the same number of nodes is picked from each lever:

$$a_{lever,overall} = \binom{CS_{overall}}{a}$$

$$a_{lever,novel} = \binom{CS_{novel}}{a} \qquad (5.9)$$

$$\text{with} \quad \max(CS_{overall}, CS_{partial}) \leq a \leq 3$$

$a_{lever,overall}$	[-]	number of levers contained in the overall lever	$CS_{overall}$	[-]	number of nodes of the overall lever
$a_{lever,novel}$	[-]	number of levers contained in the novel lever	$CS_{partial}$	[-]	number of nodes of the novel lever
a	[-]	number of nodes picked for comparison			

Further, a coordinate vector is formed both for the part of the overall and the novel lever with the coordinates in ascending order:

$$\vec{x}_{overall} = \begin{bmatrix} x_{overall,1} \\ x_{overall,2} \\ \vdots \\ x_{overall,a} \end{bmatrix}$$

$$\vec{x}_{novel} = \begin{bmatrix} x_{novel,1} \\ x_{novel,2} \\ \vdots \\ x_{novel,a} \end{bmatrix} \qquad (5.10)$$

$\vec{x}_{overall}$	[m]	coordinate vector for the overall lever part	$x_{overall,i}$	[m]	coordinate of node i of the overall lever part
$\vec{x}_{novel}$	[m]	coordinate vector for the novel lever part	$x_{novel,i}$	[m]	coordinate of node i of the novel lever part
a	[-]	number of nodes picked for comparison			

Hereby, the vectors of characteristic leverages are built as:

$$\vec{l}_{overall} = \begin{bmatrix} l_{overall,1} \\ l_{overall,2} \\ \vdots \\ l_{overall,a-2} \end{bmatrix} = \begin{bmatrix} \frac{x_{overall,2} - x_{overall,1}}{x_{overall,a} - x_{overall,1}} \\ \frac{x_{overall,3} - x_{overall,1}}{x_{overall,a} - x_{overall,1}} \\ \vdots \\ \frac{x_{overall,a-1} - x_{overall,1}}{x_{overall,a} - x_{overall,1}} \end{bmatrix}$$

$$\vec{l}_{novel} = \begin{bmatrix} l_{novel,1} \\ l_{novel,2} \\ \vdots \\ l_{novel,a-2} \end{bmatrix} = \begin{bmatrix} \frac{x_{novel,2} - x_{novel,1}}{x_{novel,a} - x_{novel,1}} \\ \frac{x_{novel,3} - x_{novel,1}}{x_{novel,a} - x_{novel,1}} \\ \vdots \\ \frac{x_{novel,a-1} - x_{novel,1}}{x_{novel,a} - x_{novel,1}} \end{bmatrix} \qquad (5.11)$$

$\vec{l}_{overall}$	[-]	leverage vector for the overall lever part	$l_{overall,i}$	[-]	char. leverage l of the overall lever part
$\vec{l}_{novel}$	[-]	leverage vector for the novel lever part	$l_{novel,i}$	[-]	char. leverage l of the novel lever part
a	[-]	number of nodes picked for comparison	$x_{overall,i}$	[m]	coordinate of node i of the overall lever part
			$x_{novel,i}$	[m]	coordinate of node i of the novel lever part

In order to prove if the reversed novel lever part matches the overall lever part as well, a second, reversed vector of characteristic leverages is calculated:

$$\vec{l}_{novel,rev} = \begin{bmatrix} l_{novel,rev,1} \\ l_{novel,rev,2} \\ \vdots \\ l_{novel,rev,a-2} \end{bmatrix} = \begin{bmatrix} \frac{x_{novel,a} - x_{novel,2}}{x_{novel,a} - x_{novel,1}} \\ \frac{x_{novel,a} - x_{novel,3}}{x_{novel,a} - x_{novel,1}} \\ \vdots \\ \frac{x_{novel,a} - x_{novel,a-1}}{x_{novel,a} - x_{novel,1}} \end{bmatrix} = \begin{bmatrix} 1 - \frac{x_{novel,2} - x_{novel,1}}{x_{novel,a} - x_{novel,1}} \\ 1 - \frac{x_{novel,3} - x_{novel,1}}{x_{novel,a} - x_{novel,1}} \\ \vdots \\ 1 - \frac{x_{novel,a-1} - x_{novel,1}}{x_{novel,a} - x_{novel,1}} \end{bmatrix} = 1 - \vec{l}_{novel} \qquad (5.12)$$

$\vec{l}_{novel,rev}$	[-]	rev. leverage vector for the novel lever part	$l_{novel,rev,i}$	[-]	rev. char. leverage l of the novel lever part
$\vec{l}_{novel}$	[-]	leverage vector for the novel lever part	$x_{novel,i}$	[m]	coordinate of node i of the novel lever part
a	[-]	number of nodes picked for comparison			

Now, the characteristic leverages can be compared by pairs:

$$d_i = \left| \frac{l_{overall,i} - l_{novel,i}}{l_{overall,i}} \right|$$

$$d_{rev,i} = \left| \frac{l_{overall,i} - l_{novel,rev,i}}{l_{overall,i}} \right| \qquad (5.13)$$

$$\text{for } i = 1, \dots, a-2$$

d_i	[-]	deviation of leverages	$l_{overall,i}$	[-]	char. leverage l of the overall lever part
$d_{rev,i}$	[-]	deviation of leverages (reversed)	$l_{novel,i}$	[-]	char. leverage l of the novel lever part
a	[-]	number of nodes picked for comparison	$l_{novel,rev,i}$	[-]	rev. char. leverage l of the novel lever part

If all deviations d equal zero, both parts of the levers match each other exactly, which seldom occurs. The correlation is detected up to a certain limit value defined by the designer (say 1%). Whether or not a correlation is detected, different cases are to be distinguished.

No correlation means that, by definition, two nodes match and no further nodes overlay each other (**Figure 5-8**). It is reasonable to integrate the novel lever into the existing overall lever. For this, the novel lever is scaled such that matching nodes are aligned.

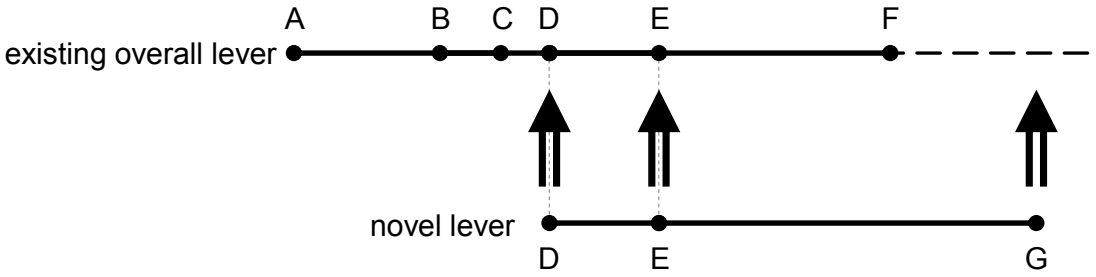

Figure 5-8: Integration of novel lever into existing overall lever without correlation

If a correlation is detected, two or more identical nodes exist and further nodes with different indices match each other, the selection of nodes and indices respectively should be changed (**Figure 5-9**). Otherwise, kinematic redundancies occur and the resulting CCPGT tends to be more complex than necessary.

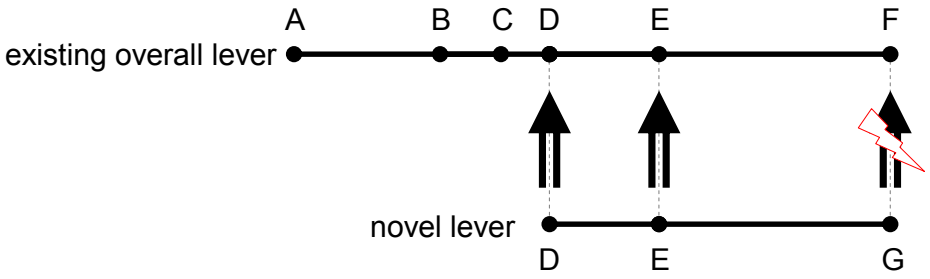

Figure 5-9: Useless correlation of novel and existing overall lever

In the event of a correlation detection with matching nodes whose indices are not identical, it is to be evaluated by the designer whether a permutation of connections is acceptable for the benefit of reducing the number of central shafts or not (**Figure 5-10**). If so, the selection of nodes for the novel lever can be modified.

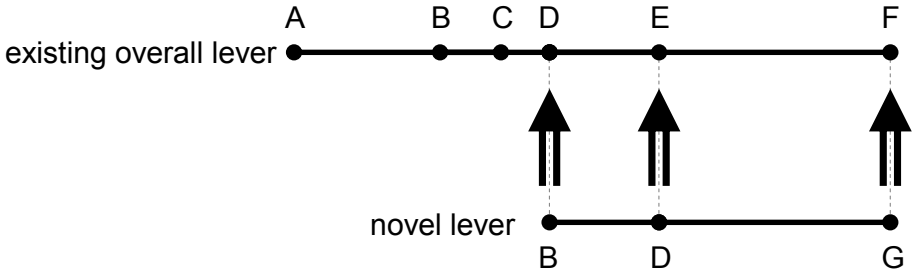

Figure 5-10: Reasonable correlation of novel and existing overall lever

5.4 Efficiency approximation and carrier node localization

So far, the abstract nodes of the overall lever model represent central shafts of a corresponding CCPGT. The concrete type of a node in terms of sun gears, internal gears or carrier is unknown. In respect of the localization of the carrier, two cases may be distinguished. The carrier node can either be identical to an existing node of the overall lever or be an additional node. **Figure 5-11** shows an example for the first case, **Figure 5-12** shows an example for the second. If the carrier node is an additional node, then it has no external load as it is not connected to the periphery for any of the defined operating conditions. Logically, it is useless to define additional, unused central gear nodes.

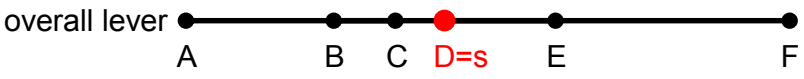

Figure 5-11: Overall lever with carrier node being identical to existing node

Figure 5-12: Overall lever with additional carrier node

In theory, there are infinite possibilities for the position of the carrier node. The position of the carrier node strongly influences the design of the CCPGT as it has impact on the basic ratios. Hence, infinite designs of CCPGTs can be found which all satisfy the desired operating conditions in terms of kinematics and statics without power loss.

Furthermore, the position of the carrier node affects the efficiency of the CCPGT drastically. Indeed, the basic efficiency of a gearing is a function of its design (external, internal gearing and parameters) but the meshing speed of a central gear node and its meshing power are dependent on the position of its node relative to the carrier node. The meshing power of a central node is given as:

$$P_{m,i} = 2 \cdot \pi \cdot T_i \cdot (n_i - n_s) \qquad (5.14)$$

$P_{m,i}$	[W]	meshing power of central gear node i	n_i	[1/s]	speed of central gear node i
T_i	[Nm]	external torque of central gear node i	n_s	[1/s]	speed of carrier node s

The speed of the carrier node is a function of its position. Also, the question of whether the meshing power of a central gear node is positive or negative is up to the sign of its torque on the one hand and up to its relative position to the carrier on the other hand. In case, a central gear node and the carrier node overlay each other, the meshing power of this central gear node equals zero.

Although the finalized design of the CCPGT is unknown yet, its efficiency can be approximated using the method presented in Section 4.3. For this purpose, speeds, external loads and a global, approximated basic efficiency are required disregarding information about the CCPGT design parameters. The outcome of this is the efficiency depending on the position/coordinate of the carrier node for every operating condition. By means of this approximation, a statement can be made about where to place the carrier node for the best efficiency performance. Hence, the solution space of adequate CCPGTs can be reduced reasonably and remarkably.

A typical characteristic of the approximated overall efficiency for an example operating condition of a lever as a function of the carrier node position is shown in **Figure 5-13**. Values marked with an asterisk are used to define the lever model and the operating condition respectively. The torque values are valid for the loss-free case. The overall efficiency is high if the transferred meshing power is small. Thus, high efficiency is expected for the carrier node being located close to the existing nodes. The farther away the carrier node is located compared to the other nodes, the smaller the efficiency becomes as the relative (meshing) speed as well as the meshing power with power loss increases.

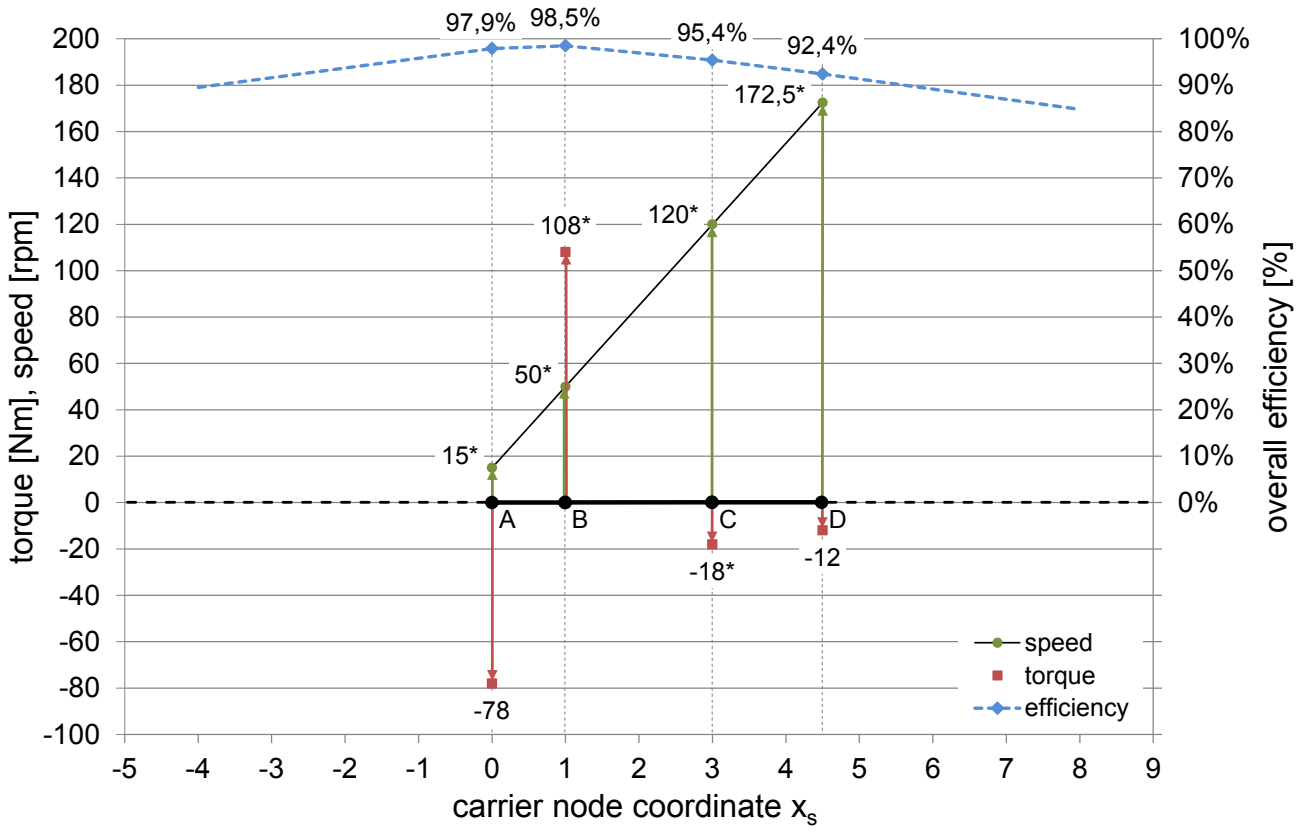

Figure 5-13: Characteristic of the approximated overall efficiency of a lever model for an example operating condition

To find an appropriate position for the carrier node in case of multiple operating conditions, it is useful to weight their efficiency values:

$$\bar{\eta} = \sum_i q_i \cdot \eta_i \quad \text{with} \quad \sum_i q_i = 1 \qquad (5.15)$$

$\bar{\eta}$	[-]	weighted overall efficiency	q_i	[-]	weighting factor for operating condition i
η_i	[-]	efficiency for operating condition i			

The weighting factors can be chosen, for instance, according to the importance or the time slice of an operating condition. Alternatively, the sum of power losses multiplied by the time slice helps evaluate the carrier node position for a minimum overall loss of energy:

$$\sum_i E_i = \sum_i (1 - \eta_i) \cdot P_{in,i} \cdot t_i \qquad (5.16)$$

E_i	[J]	loss of energy of operating condition i	$P_{in,i}$	[W]	input power of operating condition i
η_i	[-]	efficiency for operating condition i	t_i	[s]	time slice of operating condition i

If an appropriate position is found for the carrier node, a grouping of the remaining nodes is possible. The nodes to the left and to the right of the carrier node feature different directions of rotation with respect to the speed to the carrier node. Thus, the directions of rotation of all central gears of a corresponding CCPGT must be consistent with the specification of the lever model. **Figure 5-14** shows an example.

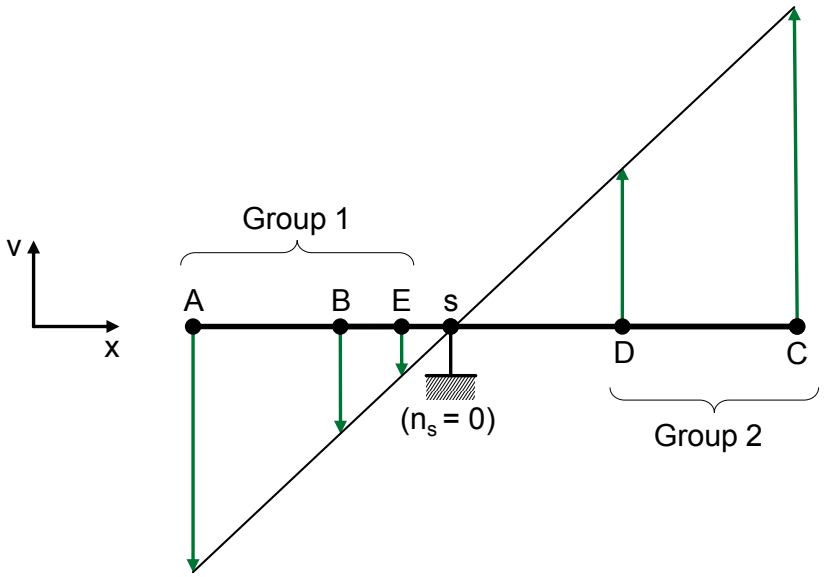

Figure 5-14: Example grouping of central gear nodes with defined carrier node

5.5 Generation of CCPGT structures

In this section, the final generation of CCPGT structures is presented. Introducing different synthesis possibilities, the most favorable one is identified and discussed in detail.

5.5.1 Principles of structure synthesis

There are several possibilities for generating CCPGT structures on the basis of a lever model. The easiest but most computationally intensive one is the incremental variation of the geometry of a reference CCPGT in combination with a comparison to the predefined lever model. The variants of the reference CCPGT are transformed into single 'local' lever models. Afterwards, it is checked if a 'local' lever model matches the predefined one. A reference CCPGT may look like in **Figure 5-15**. It consists of two meshing planet assemblies, five planes of action (I to V), five sun gears (SG_I to SG_V), five internal gears (IG_I to IG_V) and five planet gears (PG_I to PG_V) and eleven central shafts including the carrier s. It is defined by two center distances (cd_1 and cd_2) as well as the diameters of the central gears and the planet gears, respectively. If the planet assemblies are in extended position, the angle α indicates their relative position. Defining two center distances and five planet gear diameters the whole transmission with its basic ratios is specified in principle. The reference CCPGT shown contains common designs of single PGTs and CCPGTs with up to two meshing planets and a maximum of three planet gears per planet assembly. If it is transformed into an 11-node lever, at least parts of it may match the predefined lever. Nodes and central gears that are not matching any node of the predefined lever are removed.

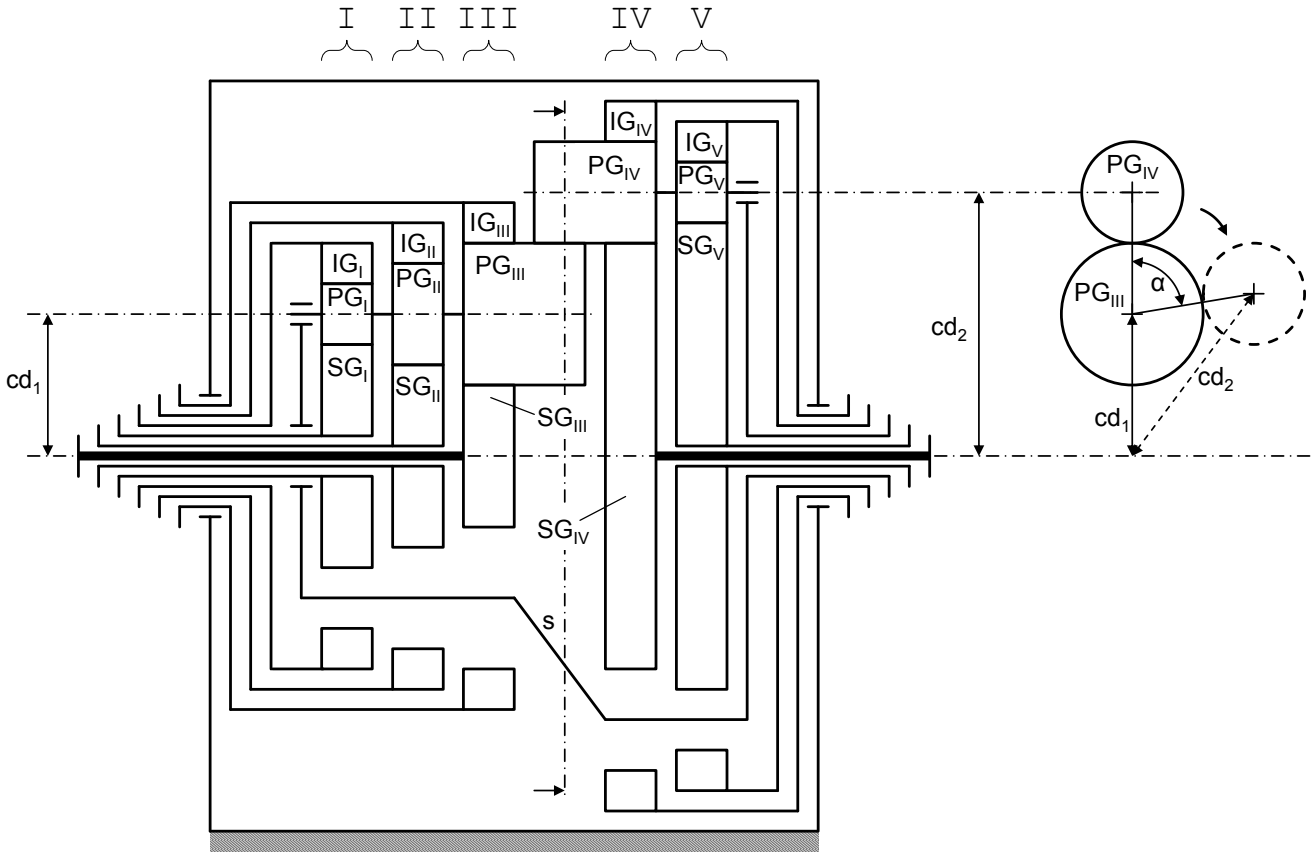

Figure 5-15: Example reference CCPGT

The basic problem of this procedure is the huge diversity of generated structures. For a maximum of only ten incremental steps per one of the seven needed parameters, ten million CCPGT variants are created. Due to the incremental breakdown, the local levers will not match the predefined lever exactly. Also, a very large set of redundant variants is created. Next, it is not sure if matching variants are jumped over as a result of too large incremental steps.

A further synthesis possibility is to fractionalize the predefined lever into connected 3-node levers, to look for single PGTs matching the 3-node levers and to check if the reassembly of a CCPGT out of the single PGTs is possible. This procedure is related to the approach of many authors such as Mueller [2_MUL01] who attempted to find common components of jointed single PGTs in order to ‘reduce’ them into a CCPGT. Analogical to **Figure 5-4**, the 3-node levers of the fractionized overall lever must be coupled twice to keep the kinematic DOF of two. Also, the 3-node levers must feature a common carrier node s (**Figure 5-16**). Multiple fractionations exist. The generation of fractionized levers is totally equivalent to the generation of kinematically-equivalent substitution figures in principle (cf. Section 4.2.1). Hence, **Table 4-3** is valid for the number of fractionized levers, too. By way of example, 16 ‘kinematically-equivalent’ fractionations are available for a 5-node lever.

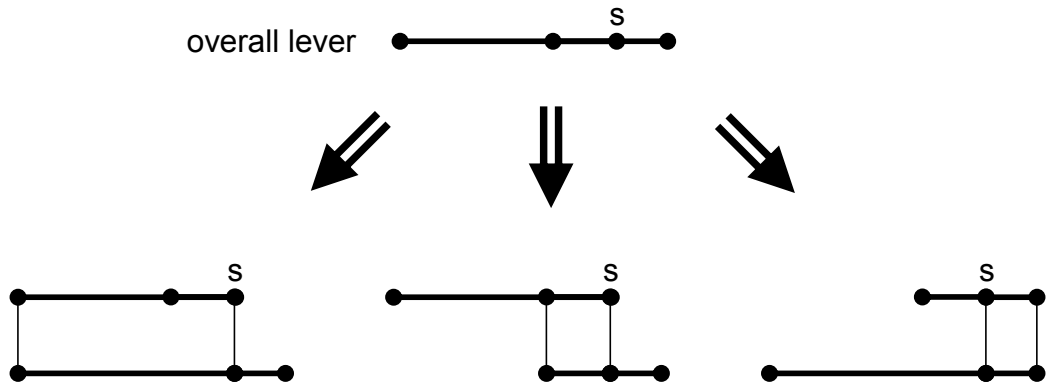

Figure 5-16: Example fractionation of a 4-node lever into connected 3-node levers

Each 3-node lever corresponds to a single PGT. Gibson and Kramer [5_GIB84] list 22 single PGTs to be distinguished whereof at least eight PGTs can be indicated as being conventional. Thus, it is to be checked if any combination of single PGTs corresponding to the 3-node levers leads to a CCPGT. For this purpose, the possible basic train ratio of a focused single PGT has to match the characteristic leverage and basic ratio of the 3-node lever. Additionally, the central gears of jointed central gear nodes have to be of the same type (external or internal gear). Furthermore, the central gears have to mesh with adequate planets. A total of two or three planet assemblies is acceptable. Obviously, the combination of single PGTs will not result in CCPGTs for most cases. However, a huge number of variants has to be checked. Considering a 5-node lever with 16 feasible fractionations, three 3-node levers per fractionation and eight possible single PGTs per 3-node lever, the number of variants is 384. Besides, a systematic and computerized check is difficult to realize due to the geometric diversity.

Another synthesis method, which will be pursued from now on, features a direct determination of central and planet gear diameters on basis of the predefined lever. For it, a reference CCPGT of **Figure 5-15** is needed, which demonstrates the most complicated CCPGT to be considered. The reference CCPGT is transformed into a reference lever whose number of nodes is larger than or equal to the number of nodes of the predefined lever. Afterwards, nodes of both levers are combinatorially assigned by pairs. Here, unused nodes of the reference lever are discarded. The ‘remaining’ structure of the reference CCPGT is analyzed in regard to the feasibility of predefined lever. Thereby, diameters of the central and planet gears are calculated as a function of the characteristic leverages of the predefined lever and structures with inapplicable diameters are omitted again. Finally, a small number of potential CCPGT structures is filtered out.

5.5.2 Reference CCPGT and characteristics

In order to generate feasible CCPGT structures, it is necessary to analyze the reference CCPGT in detail. The essential parameters of the reference CCPGT model shown in **Figure 5-15** are slightly simplified in comparison to a real CCPGT. The specified diameters are to be interpreted as pitch diameters. However, in reality a planet gear features multiple

and different pitch diameters due to addendum modification if meshing with multiple mating gears. These pitch diameters differ marginally and impact the relationship between the basic ratio and the center distance(s) of a basic train. Anyhow, deviations in respect of the target basic ratios have to be accepted as it is not possible in general to find numbers of teeth resulting in the desired basic ratios intimately. Numbers of teeth can only be integer, installation conditions must be met and numbers of teeth are to chosen considering load carrying capacity aspects last but not least.

The reference CCPGT features eleven central shafts. A maximum of two meshing planet assemblies is regarded as being reasonable from a designer's view. The corresponding lever model is shown in **Figure 5-17**. It features two groups of central gear nodes in analogy with **Figure 5-14**. Apparently, five nodes are located to the right and to the left of the carrier node s. Predefined levers featuring more than five nodes per group cannot match the reference CCPGT and its lever respectively.

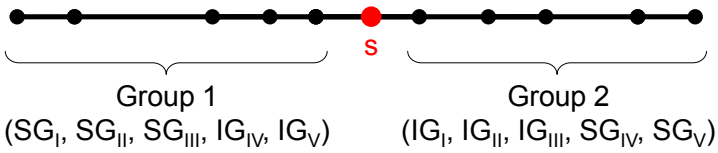

Figure 5-17: Lever model corresponding to the reference CCPGT of Figure 5-15

Frequently, if the predefined lever is comparatively small, it is useful to 'deactivate' certain central gears of the reference CCPGT from the beginning and not to allow all PGT structures included in the model in order to avoid unfavorable designs. If so, the corresponding lever model is reduced accordingly.

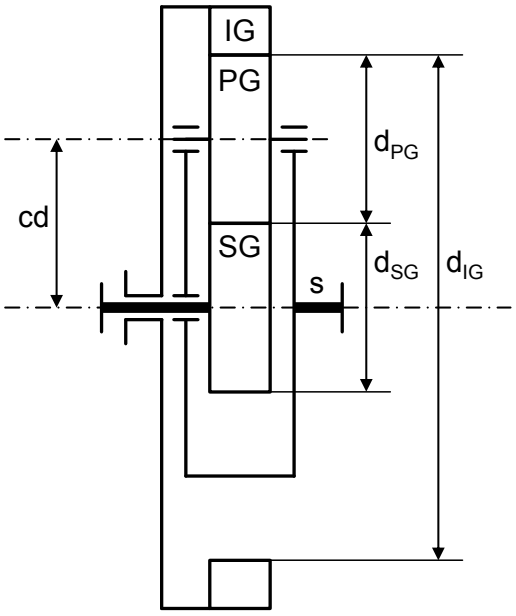

Figure 5-18: Isolated negative-ratio drive derived from reference CCPGT in Figure 5-15

Isolating components and assembly groups of the reference CCPGT, the geometric characteristics become clear. A single negative-ratio basic train containing one sun gear, one planet and one internal gear is defined by two geometric parameters e.g. the center distance and one diameter ratio. All other diameters can be calculated depending on these parameters (**Figure 5-18**). The center distance can be interpreted as a scaling factor. Its absolute value is not of relevance for the structure in principle. Further, the diameter ratio of the internal gear to the sun gear is a function of the basic ratio:

$$\frac{d_{IG}}{d_{SG}} = i^{s}_{SG,IG} = \frac{-2 \cdot cd - d_{PG}}{2 \cdot cd - d_{PG}}$$

$$\Rightarrow \quad d_{PG} = 2 \cdot cd \cdot \frac{i^{s}_{SG,IG} + 1}{i^{s}_{SG,IG} - 1} \qquad (5.17)$$

$$\Rightarrow \quad d_{SG} = 2 \cdot cd - d_{PG}$$

$$\Rightarrow \quad d_{IG} = -2 \cdot cd - d_{PG}$$

$i^{s}_{SG,IG}$	[-]	basic ratio of central gears SG and IG	d_{SG}	[m]	diameter of sun gear SG
cd	[m]	center distance	d_{PG}	[m]	diameter of planet gear PG
			d_{IG}	[m]	diameter of internal gear IG

Choosing an adequate scaling factor, the system is determined by one parameter, the basic ratio. Adding further basic gearings each consisting of one connected planet and one central gear, the system is still determined if one more basic ratio per basic gearing is available (**Figure 5-19**).

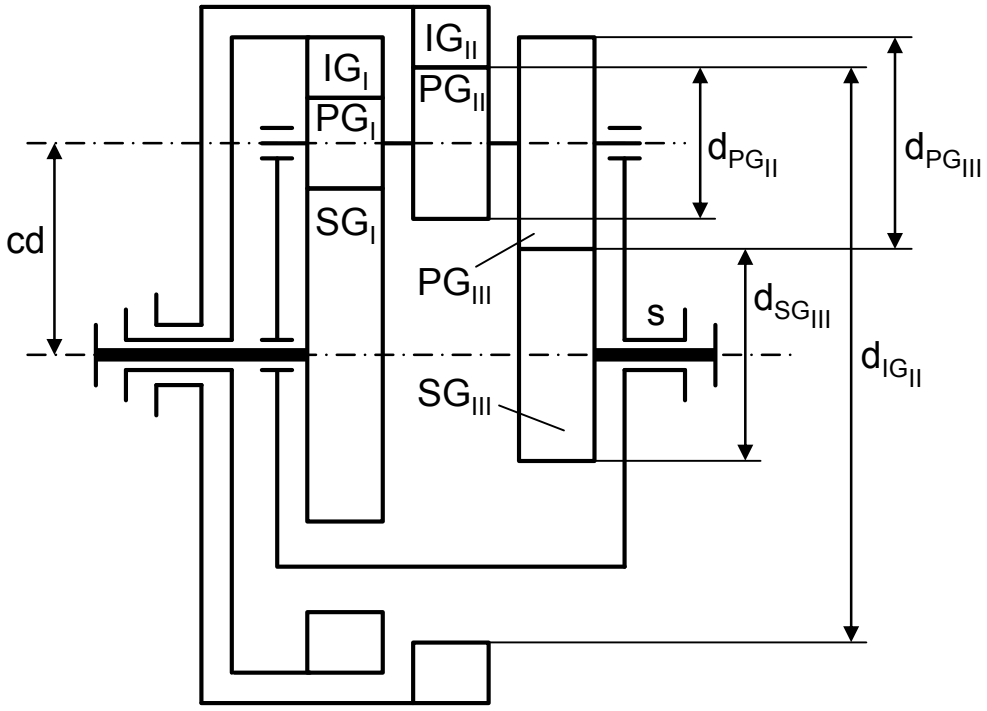

Figure 5-19: Determined CCPGT system derived from reference CCPGT in Figure 5-15

After the gear diameters of plane I are calculated using equation (5.17), the remaining diameters are derived as follows:

$$d_{PG_{II}} = \frac{2 \cdot cd \cdot d_{PG_I}}{i_{SG_I,IG_{II}} \cdot (d_{PG_I} - cd) - d_{PG_I}}$$

$$\Rightarrow \quad d_{IG_{II}} = -2 \cdot cd - d_{PG_{II}} \qquad (5.18)$$

$$d_{PG_{III}} = \frac{-2 \cdot cd \cdot d_{PG_I}}{i_{SG_I,SG_{III}} \cdot (d_{PG_I} - cd) - d_{PG_I}}$$

$$\Rightarrow \quad d_{SG_{III}} = 2 \cdot cd - d_{PG_{III}}$$

$i^s_{SG_I,IG_{II}}$	[-]	basic ratio of central gears SG_I and IG_{II}	$d_{SG_{I/III}}$	[m]	diameter of sun gear $SG_{I/III}$
$i^s_{SG_I,SG_{III}}$	[-]	basic ratio of central gears SG_I and SG_{III}	$d_{PG_{I/II/III}}$	[m]	diameter of planet gear $PG_{I/II/III}$
cd	[m]	center distance	$d_{IG_{II}}$	[m]	diameter of internal gear IG_{II}

An over-determined system is in hand if one planet assembly features more than one negative-ratio drive like in **Figure 5-18**. Generally, it is not possible to meet all basic ratio requirements of the predefined lever exactly with an over-determined CCPGT structure. **Figure 5-20** shows such a system. One can imagine that the diameters of all gears except sun gear SG_{II} are calculated analogical to **Figure 5-19**. If so, the diameter of sun gear SG_{II} results from the others as there is no further degree of freedom for the geometry design. In contrast, the corresponding node within the lever can be moved freely with respect to the remaining nodes.

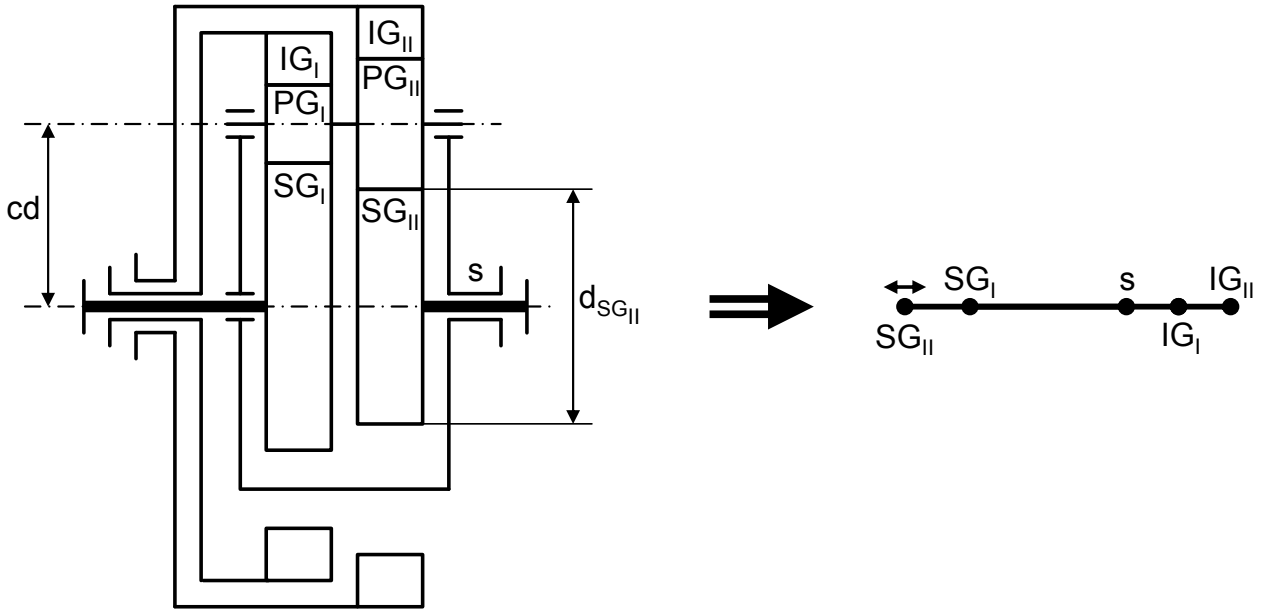

Figure 5-20: Over-determined CCPGT system derived from reference CCPGT in Figure 5-15

The structure of **Figure 5-20** is one time over-determined. Adding a further negative-ratio drive, the system is twice over-determined. In order design a structure being as close to the requirements as possible, a quality criterion is to be set up. The structure is designed such that the deviations between desired and performed basic ratios are minimized. For it, the planet diameters are varied. All basic ratios of the over-determined system are considered.

The most complicated system is the under-determined system, which occurs in the absence of negative-ratio drives analogical to **Figure 5-18**. Besides the center distance, one more diameter ratio can be selected freely (**Figure 5-21**). Other diameter ratios result from the desired basic ratios and the diameter ratio, which was selected first according to equation (5.18).

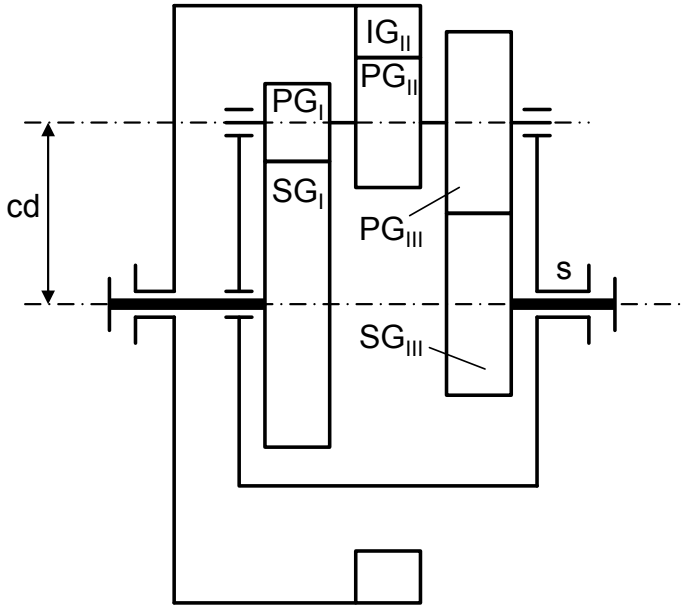

Figure 5-21: One time under-determined CCPGT system derived from reference CCPGT in Figure 5-15

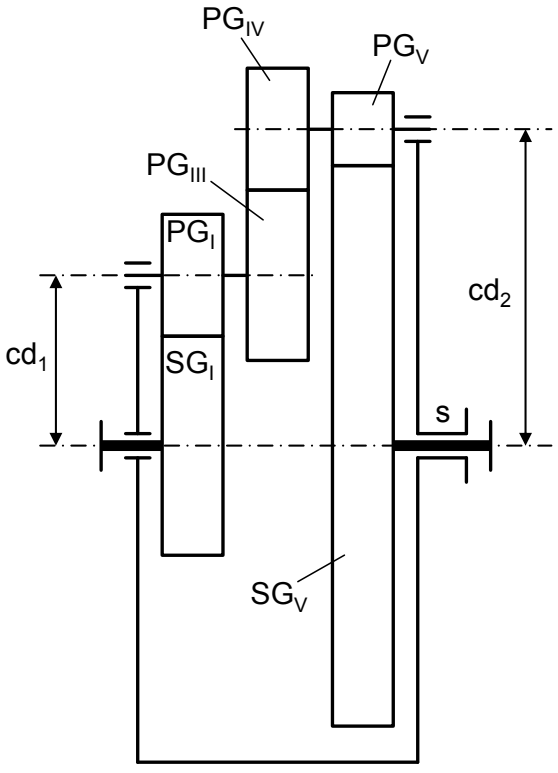

Figure 5-22: Four times under-determined CCPGT system derived from reference CCPGT in Figure 5-15

A meshing planet pair increases the degree of under-determinacy by one. Further, if no central gears are in mesh with the planet gear pair, additional degrees of freedom regarding the structure geometry are available. **Figure 5-22** shows a CCPGT structure featuring the maximum degree of under-determinacy of four. All planet gear diameters are independently selectable. With one center distance as scaling factor, the other center distance, the relative position of the planet assemblies (angle α in **Figure 5-15**) and the central gear diameters result from the desired basic ratio and the planet gear diameters. A high degree of under-determinacy occurs above all if explicitly more central shafts of the reference CCPGT are 'activated' than nodes of the predefined lever exist. These solutions are often not of relevance as the structures are more complex than they have to be.

For each degree of under-determinacy one diameter ratio can be optimized e.g. with reference to the following aims:

1. low design space or outer diameter
2. avoidance of extreme gear ratios
3. generation of same parts
4. avoidance of interferences of planets
5. avoidance of stepping of planet assemblies in favor of short overall length and easy manufacturing

Depending on the requirements, an adequate solution is to found for this optimization problem. For a first preliminary structure design, the diameters can be chosen as follows if possible:

$$\mathrm{d_{PG_{I/II}}} = \mathrm{cd_1}$$

$$\mathrm{d_{PG_V}} = \mathrm{cd_2}$$

$$\mathrm{d_{PG_{III}}} = \frac{\mathrm{cd_1}}{4} \qquad (5.19)$$

$$\mathrm{d_{PG_{IV}}} = \frac{\mathrm{cd_2}}{4}$$

$\mathrm{d_{PG_x}}$	[m]	diameter of planet gear $\mathrm{PG_x}$	$\mathrm{cd_{1/2}}$	[m]	center distance 1/2

Hereby, interference of planets $\mathrm{PG_{III}}$ and $\mathrm{PG_{IV}}$ are avoided and the size of all other planets is identical to size of their mating sun gears.

It is reasonable to define freely selectable diameter ratios in a certain order. First, the gear diameters of internal gearings are to be defined, subsequently the gear diameters of external gearings (**Figure 5-23**). The theoretical range of an internal gearing ratio is limited as the planet gear can only be of the same size of the internal gear at maximum. The range of an external gearing ratio is not limited as the diameters of the planet gear and the sun gear do not restrict each other. Hence, every basic ratio can be generated if this procedure is followed and no basically working structure is excluded due to unfavorably chosen planet diameters.

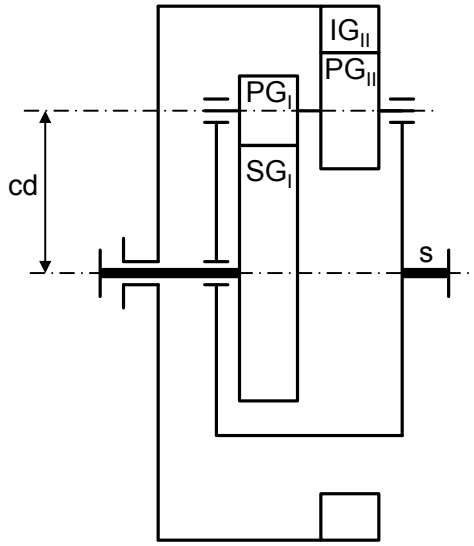

$$-\infty < i^{s}_{SG_I,PG_I} < 0$$

$$1 < i^{s}_{PG_{II},IG_{II}} < \infty$$

Figure 5-23: Ratio range of internal and external gearings

5.5.3 Synthesis by systematic matching of lever model and reference CCPGT

For the final synthesis of CCPGT structures, the ‘activated’ central gears of the reference are combinatorially assigned to the central gear nodes of the predefined lever. Naturally, at least as many central gears have to be activated per group as central gear nodes exist (cf. **Figure 5-14** and **Figure 5-17**). Considering one group, the appropriate number of central gears is picked out of the activated ones. Every permutation of an assortment of these central gears constitutes a possible assignment:

$$a_{VAR,GRxy} = \binom{a_{CG,ref,GRx}}{a_{CG,lever,GRy}} \cdot a_{CG,lever,GRy}! = \frac{a_{CG,ref,GRx}!}{(a_{CG,ref,GRx} - a_{CG,lever,GRy})!} \quad (5.20)$$

$a_{VAR,GRxy}$	[-]	number of assignment variants with group x of the reference CCPGT and group y of the predefined lever	$a_{CG,ref,GRx}$	[-]	number of central gears of the reference CCPGT in group x
			$a_{CG,lever,GRy}$	[-]	number of central gear nodes of the predefined lever in group y

Table 5-1 lists the resulting number of variants. In case of up to three activated central gears the number of potential structure variants is very limited. Only for very complex CCPGTs with more than four central gears per group, a high number of variants is to be expected. The total number of variants results from equation (5.21). At maximum, if every group assignment features 120 variants and if the groups are switched in addition, the total number of variants equals 28800. Assuming that only three central gears are activated per group of the reference CCPGT and only two nodes are located to the left and to the right of the predefined lever (5-node lever), a total number of potential structures of only 72 results.

$a_{VAR,GRxy}$		$a_{CG,ref,GRx}$				
		1	**2**	**3**	**4**	**5**
$a_{CG,lever,GRy}$	**1**	1	2	3	4	5
	2		2	6	12	20
	3			6	24	60
	4				24	120
	5					120

$a_{VAR,GRxy}$	[-]	number of assignment variants with group x of the reference CCPGT and group y of the predefined lever	$a_{CG,ref,GRx}$	[-]	number of central gears of the reference CCPGT in group x
			$a_{CG,lever,GRy}$	[-]	number of central gear nodes of the predefined lever in group y

Table 5-1: Number of assignment variants of central gears of group x of the reference CCPGT to nodes of group y of the predefined lever

$$a_{VAR,total} = \frac{a_{CG,ref,GR1}!}{(a_{CG,ref,GR1} - a_{CG,lever,GR1})!} \cdot \frac{a_{CG,ref,GR2}!}{(a_{CG,ref,GR2} - a_{CG,lever,GR2})!} + \frac{a_{CG,ref,GR1}!}{(a_{CG,ref,GR1} - a_{CG,lever,GR2})!} \cdot \frac{a_{CG,ref,GR2}!}{(a_{CG,ref,GR2} - a_{CG,lever,GR1})!} \quad (5.21)$$

$a_{VAR,total}$	[-]	total number of assignment variants for every group assignment possible	$a_{CG,ref,GR1/2}$	[-]	number of central gears of the reference CCPGT in group 1/2
			$a_{CG,lever,GR1/2}$	[-]	number of central gear nodes of the predefined lever in group 1/2

Among the potential structure variants it is to be checked which ones lead to feasible CCPGT structures. A calculation of resulting gear diameters using equations (5.17) and (5.18) reveals if a structure is feasible or not. Detecting any geometrical violation such as negative planet or sun gear diameters, positive internal gear diameters, negative center distances or non-meshing planet pairs, the structure is dismissed. In general, the number of feasible structures is significantly smaller than the number of potential structures for this reason.

In order to design structures that are as close to the requirements as possible, the synthesis is performed considering the following order:

1. Geometry calculation for over-determined (sub-) structures
2. Geometry calculation for determined (sub-) structures
3. Geometry calculation for under-determined (sub-) structures

According to Section 5.5.2, the number of isolated negative-ratio drives per planet assembly like in Figure 5-18 is decisive for a structure or substructure being determined or over-

or under-determined. If the structure or a part of it is over-determined, the diameters of relevant planets of negative-ratio drives are varied incrementally to find an approximate solution. The desired basic ratios are gained from the leverages of the predefined lever:

$$i^{s}_{CG1,CG2} = \frac{x_{CG1} - x_{s}}{x_{CG2} - x_{s}} \qquad (5.22)$$

$i^{s}_{CG1,CG2}$	[-]	basic ratio of central gears CG1 and CG2	$x_{CG1/2}$	[m]	coordinate of central gear node CG1/2
			x_{s}	[m]	coordinate of carrier node s

As quality criterion the method of least-squares can be applied. Every basic ratio included in the over-determined structure is considered:

$$d = \sum_{k} \left(\frac{i^{s}_{struct,k} - i^{s}_{lever,k}}{i_{lever,k}} \right)^{2} \qquad (5.23)$$

d	[-]	error square of basic ratios of over-determined structure including k basic ratios	$i^{s}_{struct,k}$	[-]	k-th basic ratio of potential structure
			$i^{s}_{lever,k}$	[-]	k-th basic ratio of predefined lever

After an appropriate geometry for the over-determined structure is found, the determined (sub-) structure is designed followed by the under-determined (sub-) structure. The ratios of these (sub-) structures correspond exactly to those of the predefined lever.

The number of remaining structures depends on the concrete configuration of the predefined lever and the activated central gears of the reference CCPGT. For instance, taking into account a predefined 5-node lever shown in **Figure 5-24** and a reference CCPGT with only six central gears activated like in **Figure 5-25**, the number of potential structures is 72. After the geometry calculation, only four determined, one over-determined and ten under-determined structures are left. Examples in Chapter 6 demonstrate the practical application of the presented synthesis method.

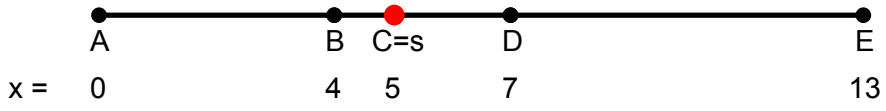

Figure 5-24: Example lever model for structure synthesis

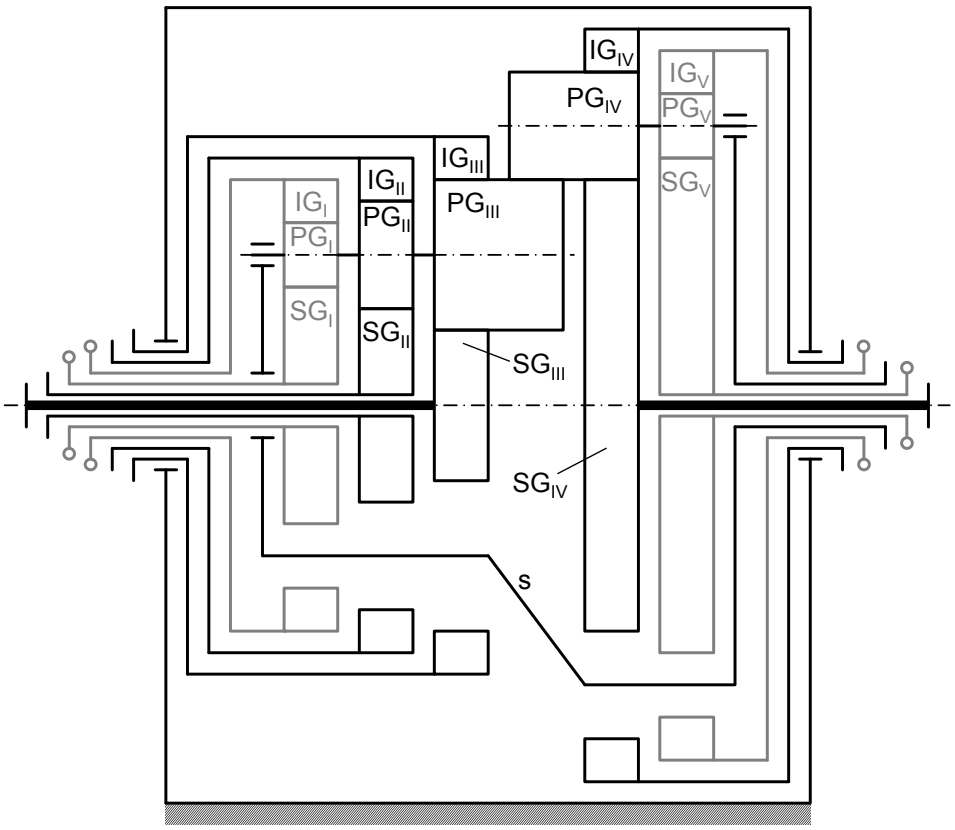

Figure 5-25: Reference CCPGT with reduced number of activated central gears

6 Application examples

Some application examples are presented in this chapter to demonstrate the use of the methods presented in the previous chapters. These application examples consist of three automotive devices.

6.1 Active Differential and electric vehicle MUTE

The electric vehicle ‘MUTE’ was developed by TU München and presented at the International Motor Show (IAA) in 2011 (**Figure 6-1**). It is a small, rear-driven two-seater with a limited drive power of 15 kW and a net mass of 400 kg without energy storage. It is equipped with a rechargeable lithium-ion-battery with a capacity of approx. 10 kWh and a second, scalable and recyclable ‘range-extender-battery’ guaranteeing a range of at least 100 km in combination. Further details can be found in [6_HOH11].

Figure 6-1: Design of the electric vehicle MUTE

For the benefit of efficiency, driving dynamics, safety, traction and comfort, MUTE features a torque vectoring system allowing a controllable redistribution of torque from one wheel to the other. The applied torque vectoring system is fully electrically driven. Its structure is shown in **Figure 6-2**. It contains an electric drive machine, an axle drive, a spur gear differential and a superimposing unit with a superimposing gear and electric machine. The combination of spur gear differential and superimposing gear is called ‘Active Differential’.

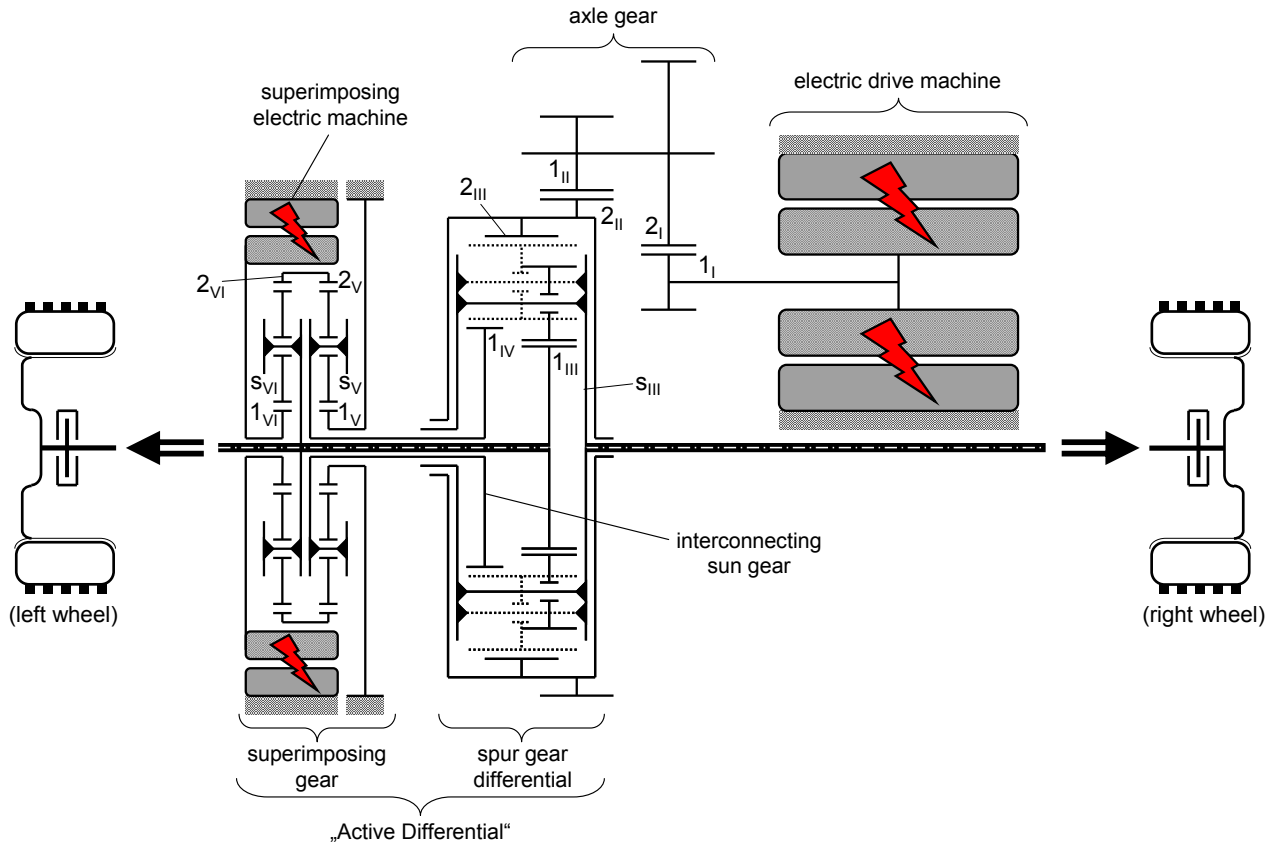

Figure 6-2: Structure of the MUTE power train [6_HOH11]

Only the electric drive machine provides drive power. Its torque is converted by the axle gear and distributed to the output shafts by the spur gear differential. The basic torque distribution ratio of the differential is 50:50 in normal operating mode when torque vectoring is deactivated and the superimposing electric machine as well as the superimposing gear is without any load. If torque vectoring is be activated, the superimposing electric machine works as an actuator for the superimposing gear and generates torque, which is converted by the superimposing gear. The unit interacts with the interconnecting sun gear, changing the basic torque distribution ratio continuously within the differential. It is also worth mentioning that the superimposing electric machine does not rotate if both wheels are running at the same speed.

A kinematic configuration that is equivalent to this system and the corresponding lever model are shown in **Figure 6-3**. The spur gear differential in combination with the interconnecting sun gear constitutes a CCPGT. It is intended to find alternative structures in the following. Four operating conditions are defined (**Figure 6-4**): two conventional differential modes and two torque vectoring modes (left turn / right turn). As the conventional differential modes are the most important and most frequently used ones, they are weighted each with 40%, the others are weighted each with 10%. Approximated efficiency values with a global basic efficiency of 97% show that nodes B, C or D are favorable to choose as the carrier node.

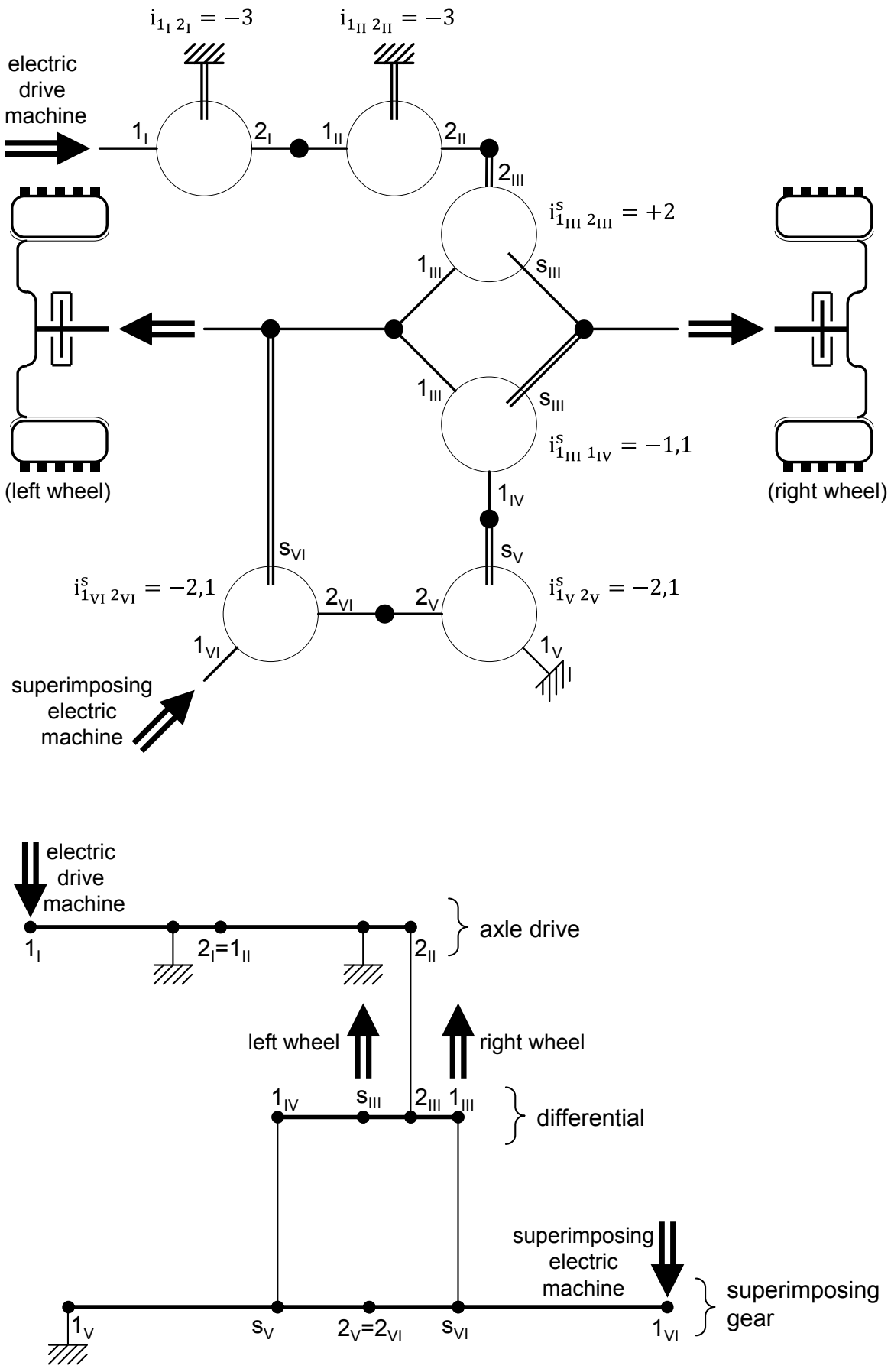

Figure 6-3: Kinematic configuration that is equivalent to Figure 6-2 and the corresponding lever model

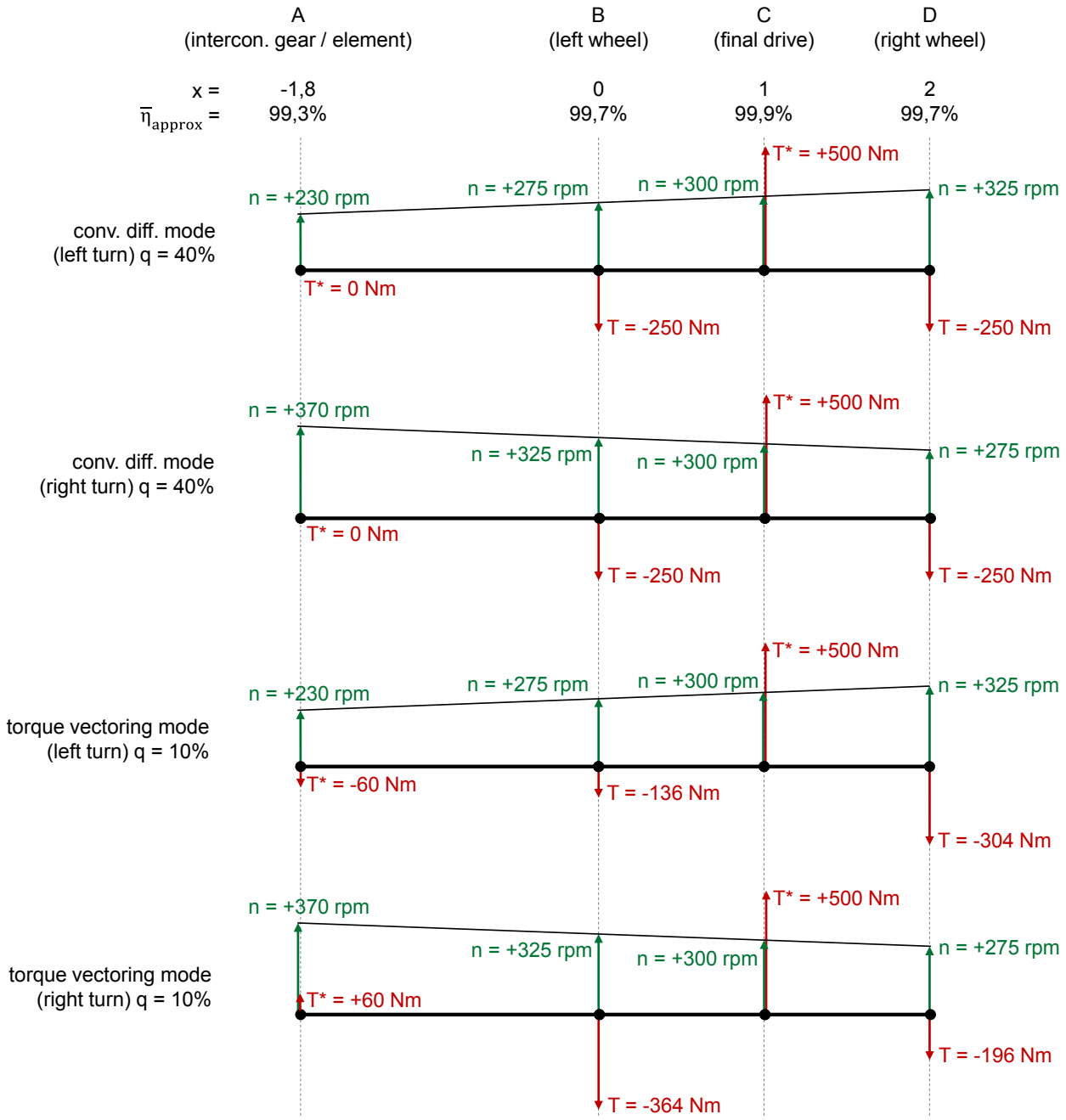

Figure 6-4: Operating conditions and lever definition for MUTE differential

As the differential is supposed not to be too complex with regard to the robustness and the manufacturing costs, structures without stepped planets are of special interest. Therefore, a simple reference CCPGT is considered featuring only two sun gears and two internal gears (**Figure 6-5**). As there are only two central gear nodes available per group for this reference CCPGT, node D cannot be taken as the carrier node. Carrying out the synthesis procedure of Section 5.5.3 indicates that only two basic, under-determined structures are capable of satisfying the predefined requirements. One of them is the known, current configuration that is installed in MUTE (**Figure 6-6** left). The other one is somewhat more complex in comparison, as one more internal gear is required (**Figure 6-6** right). A more accurate efficiency calculation assuming a basic efficiency of 99% per external gearing

and 99,5% per internal gearing discloses that the second solution is slightly more advantageous in terms of its power loss.

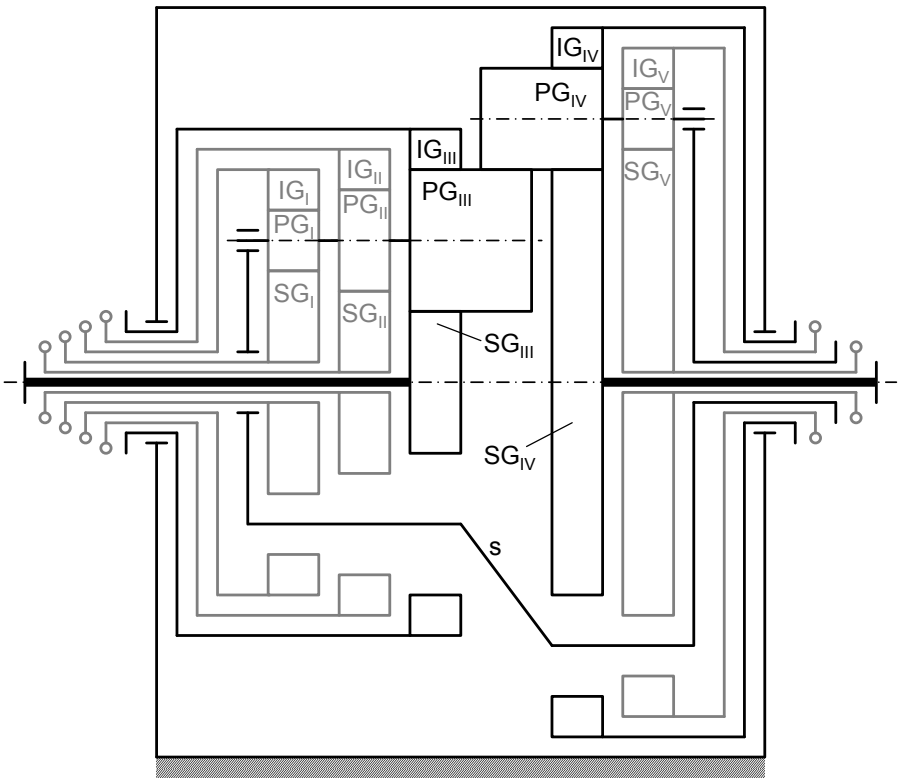

Figure 6-5: Reference CCPGT considered for MUTE differential

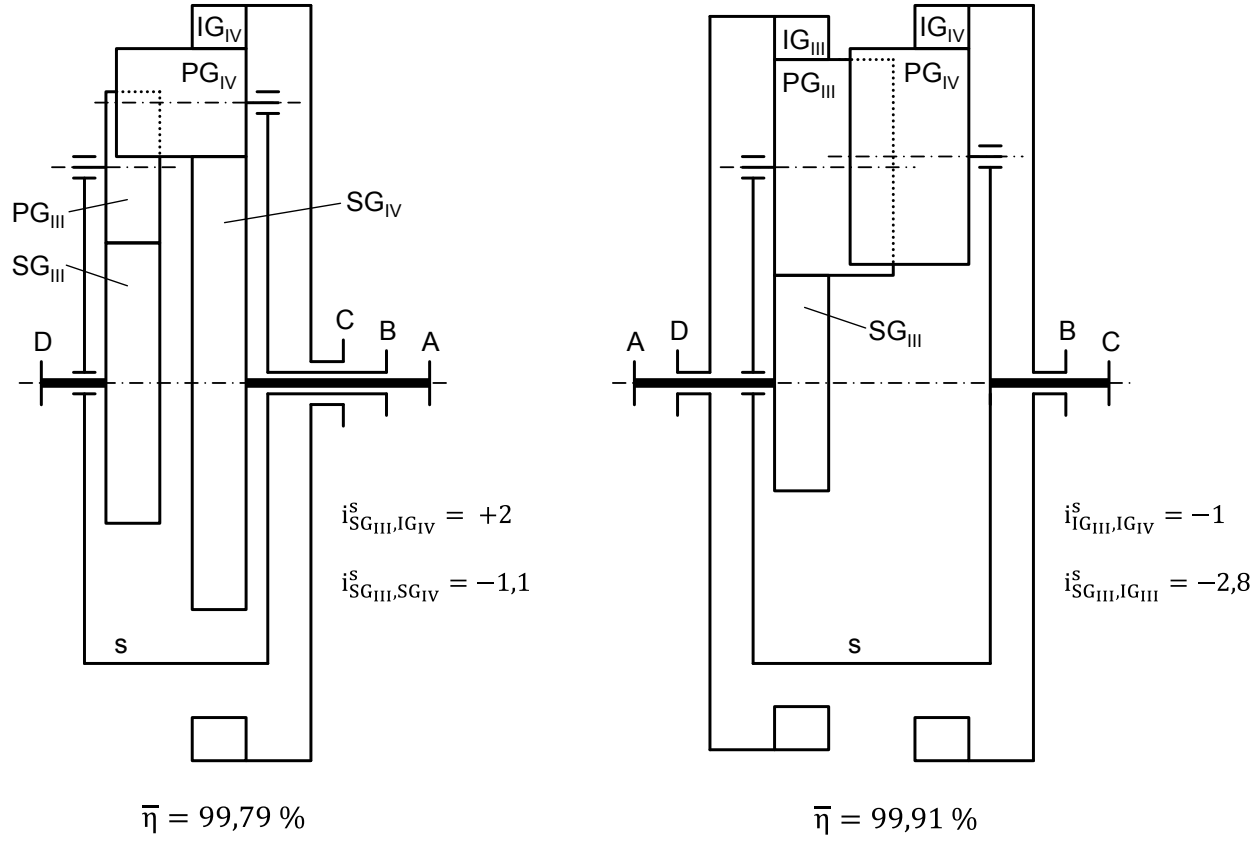

Figure 6-6: Synthesis solutions for MUTE differential

6.2 Electrified continuously variable transmission

Electrified continuously variable transmissions (E-CVT) provides several advantages compared to conventional CVTs due to their hybrid functionalities. Well-known representatives are the Toyota Prius and the BMW X6 Active Hybrid / Mercedes-Benz ML 450 Hybrid. A study was completed to investigate if similar transmission concepts are useful for compact cars. A sample car was considered featuring front-wheel drive and a net mass of 1070 kg. The car is equipped with a 3-cylinder Diesel-ICE having a maximum power of 70 kW and a maximum torque of 210 Nm. Thus, the maximum speed is limited to about 180 km/h.

Two electric machines are applied to the transmission. These machines are required to be small to keep the required torque and power as small as possible as well. Hence, a maximum torque of 65 Nm and a maximum power of 36 kW are allowed. The basic scheme is shown in **Figure 6-7**.

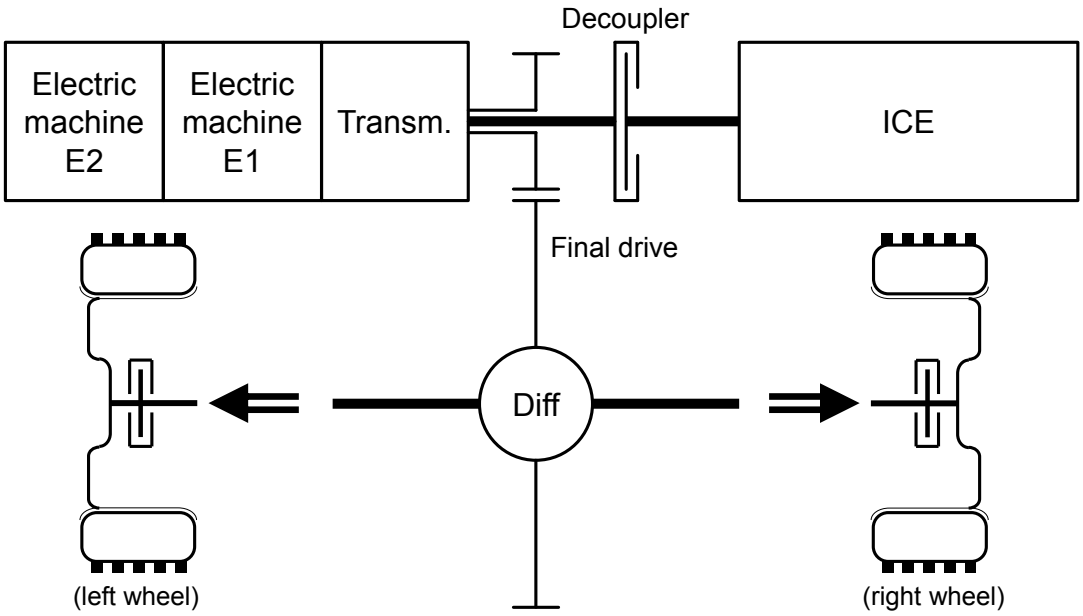

Figure 6-7: Scheme of the E-CVT power train

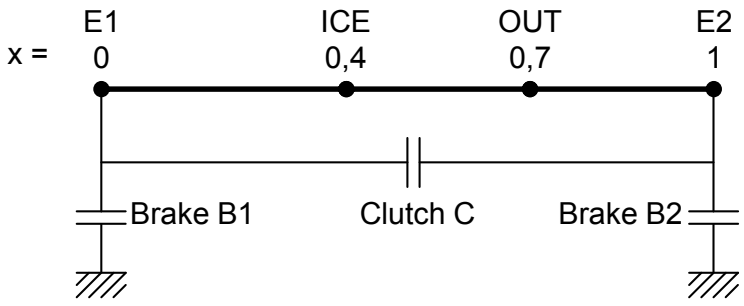

Figure 6-8: Lever configuration for E-CVT transmission

Considering a 4-shaft CCPGT for the transmission, Hein proved that a lever configuration shown in **Figure 6-8** is the most feasible one. This lever features a kinematic and static

DOF of two. The torque provided by the ICE is converted by the electric machines why the torque at the output / final drive is variable. Here, the torque of one electric machine is ‘free’ to choose. Also, the speeds of the ICE and the output are independent. Therefore, the transmission ratio is continuous and variable:

$$i_t = \frac{n_{ICE}}{n_{OUT}} \qquad (6.1)$$

i_t	[-]	E-CVT transmission ratio	n_{ICE}	[rpm]	speed of ICE
			n_{OUT}	[rpm]	speed of transmission output

For the steady state operating condition, the (mechanical) power of one electric machine must balance the other. In addition, a ratio of the power of one electric machine relative to the power of the ICE is defined:

$$P_{E1} = -P_{E2}$$
$$\varepsilon = \frac{P_{E1}}{P_{ICE}} \qquad (6.2)$$

ε	[-]	power ratio	$P_{E1/2}$	[W]	mechanical power of electric machine E1/2
P_{ICE}	[W]	power of ICE			

The power ratio is a function of the lever configuration and the transmission ratio:

$$\varepsilon = \frac{(i_t-1)^2}{i_t} \cdot \frac{(x_{ICE}-x_{E1}) \cdot (x_{E2}-x_{OUT})}{(x_{OUT}-x_{ICE}) \cdot (x_{E2}-x_{E1})} - \frac{i_t-1}{i_t} \cdot \frac{(x_{ICE}-x_{E1})}{(x_{E2}-x_{E1})} + \cdot \frac{(x_{E2}-x_{OUT})}{(x_{E2}-x_{E1})} - \frac{(x_{OUT}-x_{ICE})}{(x_{E2}-x_{E1})} + (i_t-1) \qquad (6.3)$$

ε	[-]	power ratio	$x_{ICE/OUT}$	[m]	node coordinates of output/ICE
i_t	[-]	E-CVT transmission ratio	$x_{E1/2}$	[m]	node coordinates of E1/2

By means of the proposed lever configuration, it is possible to limit the power ratio within a range of ±30% if the transmission ratio is kept within a range of approx. 0,4 to 2,6. This corresponds to a spread of 6,5 (**Figure 6-9**). Definite transmission ratios can easily be generated by applying brakes at the electric machine nodes (for one electric machine standing still) or by applying a clutch C for the coupling case. Choosing a final drive ratio of 2,5, the coupling case corresponds to the maximum speed gear (i_t = 1). Engaging brake B1 provides an overdrive gear (i_t = 0,6) while engaging brake B2 results in a definite gear for low speeds (i_t = 2).

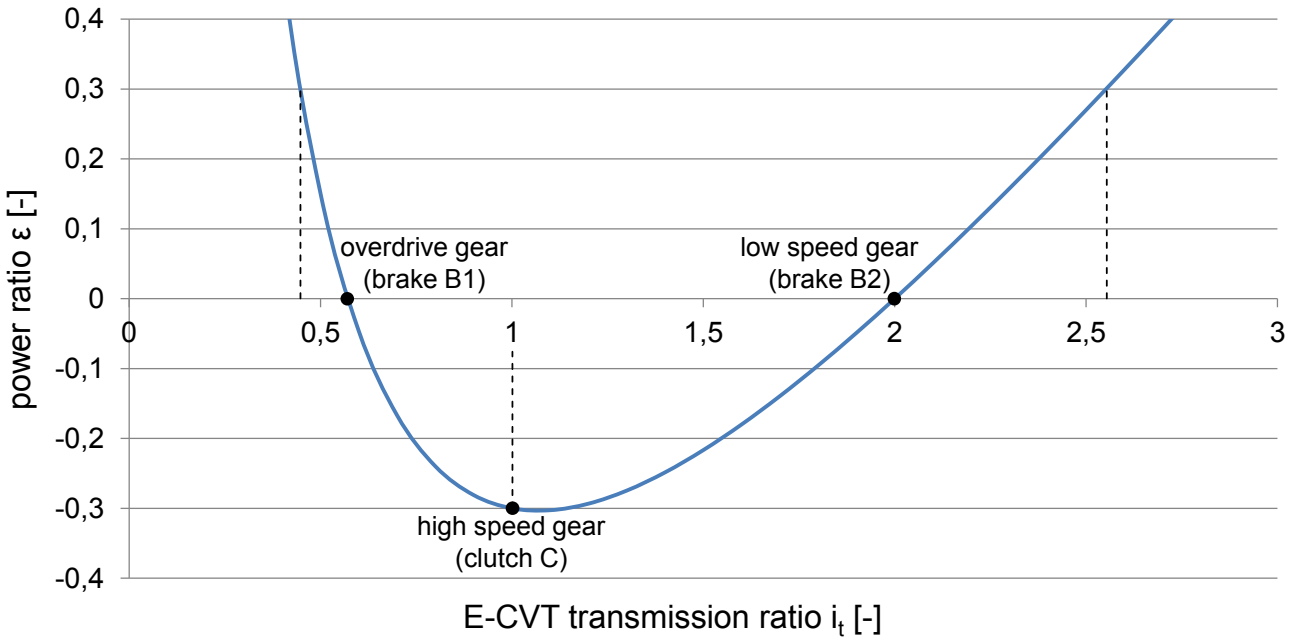

Figure 6-9: Power ratio ε depending on the E-CVT transmission ratio i_t

The main disadvantage of the presented 4-node lever design is that the driveaway torque at the beginning is low. Assuming that all three machines are driving, the maximum axle torque equals approx. 550 Nm. The driveaway torque can easily be increased by adding another node to the lever being fixed by brake B3 (**Figure 6-10**). This node functions as support and supplies an additional static DOF to allow independent machine torques.

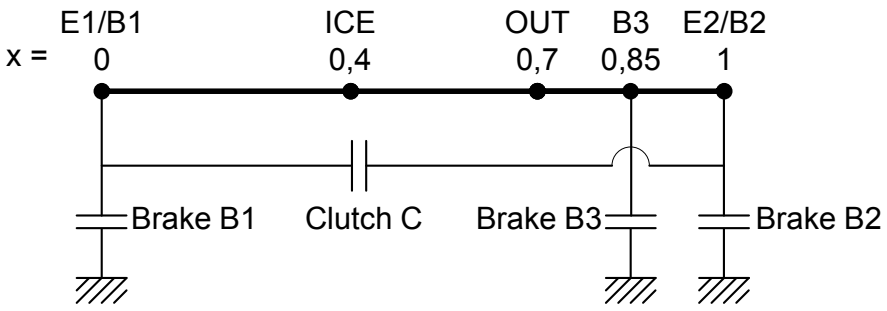

Figure 6-10: Improved lever configuration for E-CVT transmission with additional brake

Five example operating conditions shown in **Figure 6-11** are used to define the lever model. The calculation of approximated efficiencies (97% global basic efficiency) shows that nodes ICE, OUT and B3 are qualified best as carrier node. Taking into account a reference CCPGT of medium complexity such as the one shown in **Figure 5-25** the synthesis yields a total of 28 under-determined and 4 over-determined structures. Among these structures, only the most desirable one with best overall efficiency is presented here (**Figure 6-12**). Assuming a basic gearing efficiency of 99,5% per internal gearing and 99% per external gearing leads to a weighted overall efficiency of 99,54%.

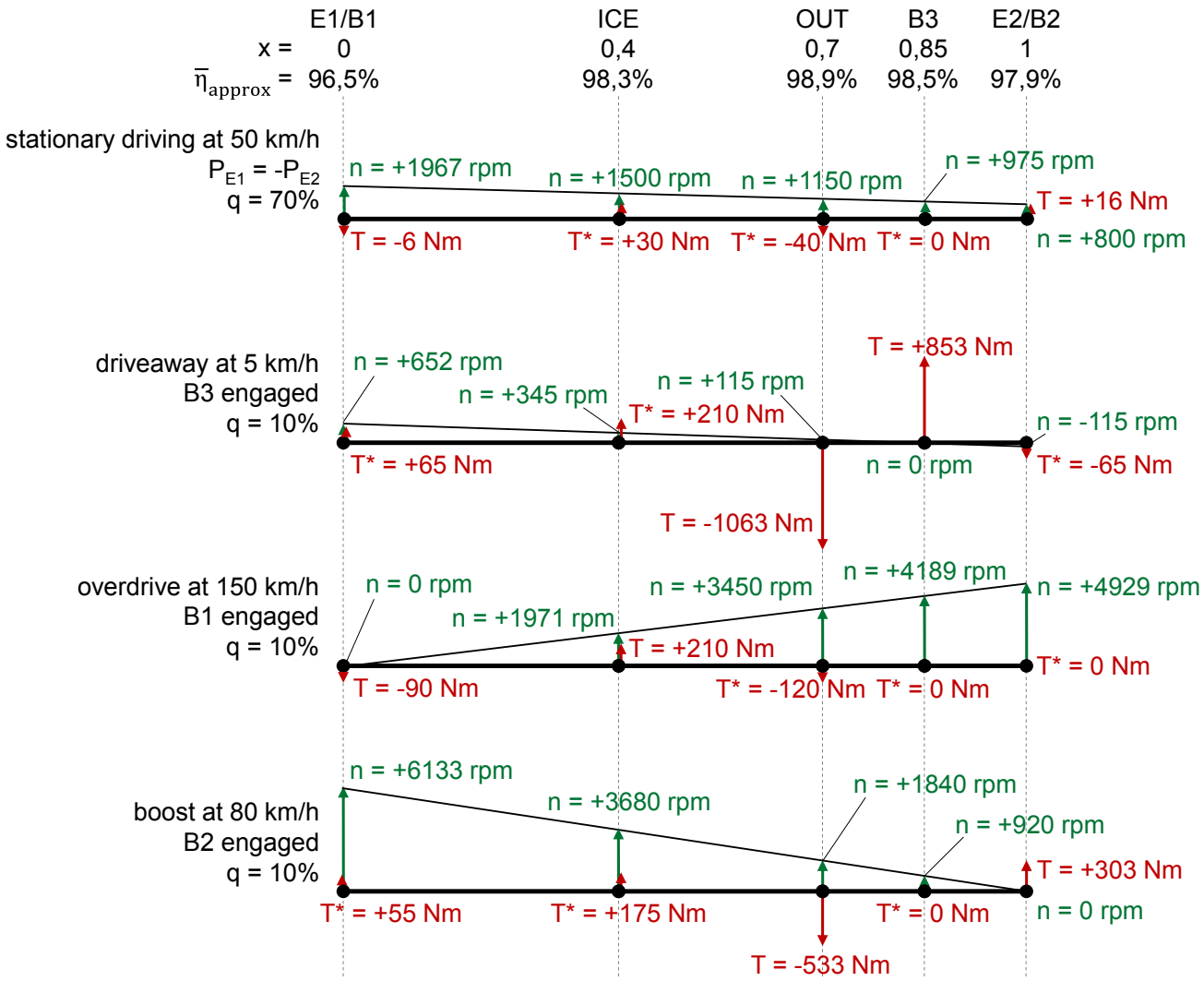

Figure 6-11: Operating conditions and lever definition for E-CVT transmission

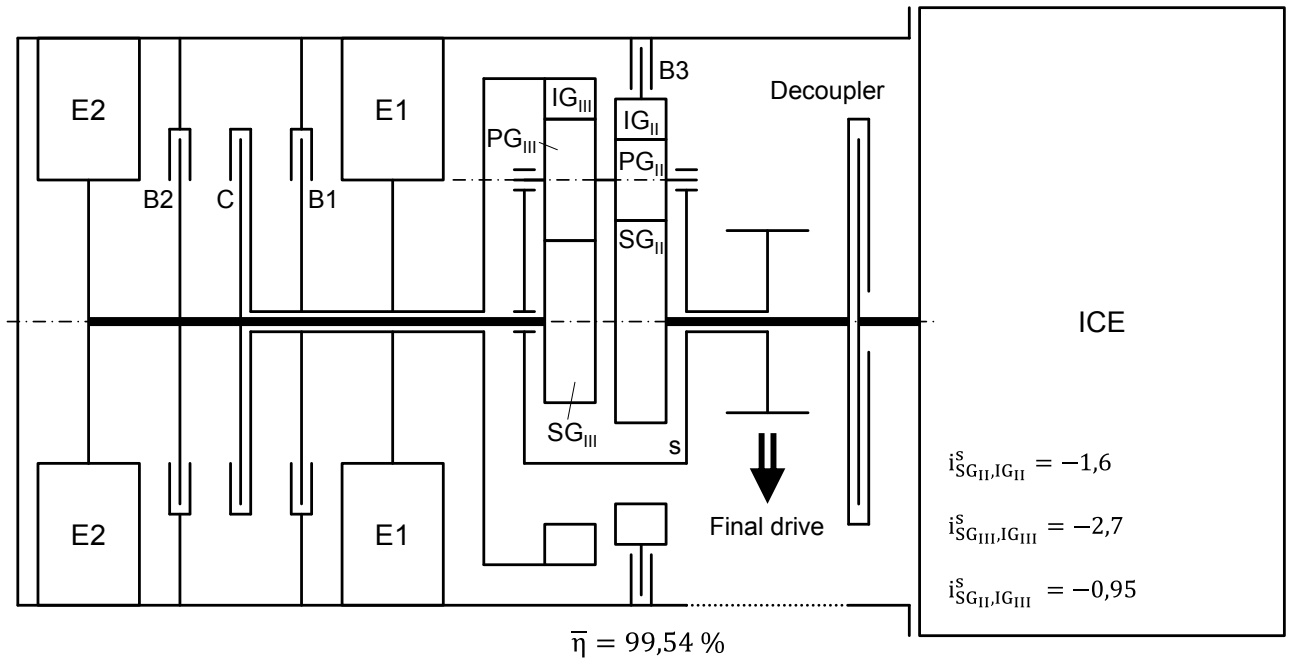

Figure 6-12: The most desirable synthesis solution for E-CVT transmission

6.3 TVhybrid axle

The ‘TVhybrid axle’ is a drive unit for parallel hybrid vehicles which was published first by Höhn, Wirth and Kurth [6_HOH10]. It is to be installed at the rear axle of a car with the front axle being driven by the ICE. The TVhybrid axle features a hybrid mode at which both wheels of the rear axle are driven with equal torque. A second torque vectoring mode is used to generate opposite torque at the rear wheels in order to cause a yaw momentum. A single electric machine works as actuator and drive machine. In addition, a shifting device is needed to switch between both modes. **Figure 6-13** shows a workable structure.

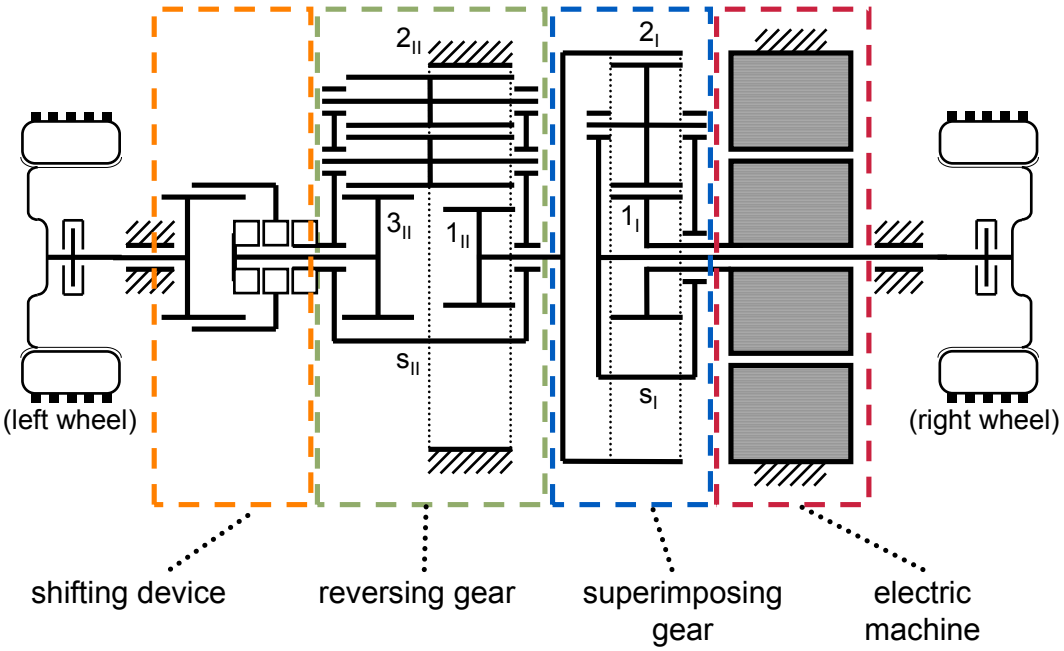

Figure 6-13: Structure of the TVhybrid axle [6_HOH10]

The transmission of the TVhybrid axle can be subdivided into a superimposing gear working as ‘differential with speed reduction’ and a reverse gear adjusting the torque direction of the left wheel. An equivalent kinematic configuration is provided in **Figure 6-14**.

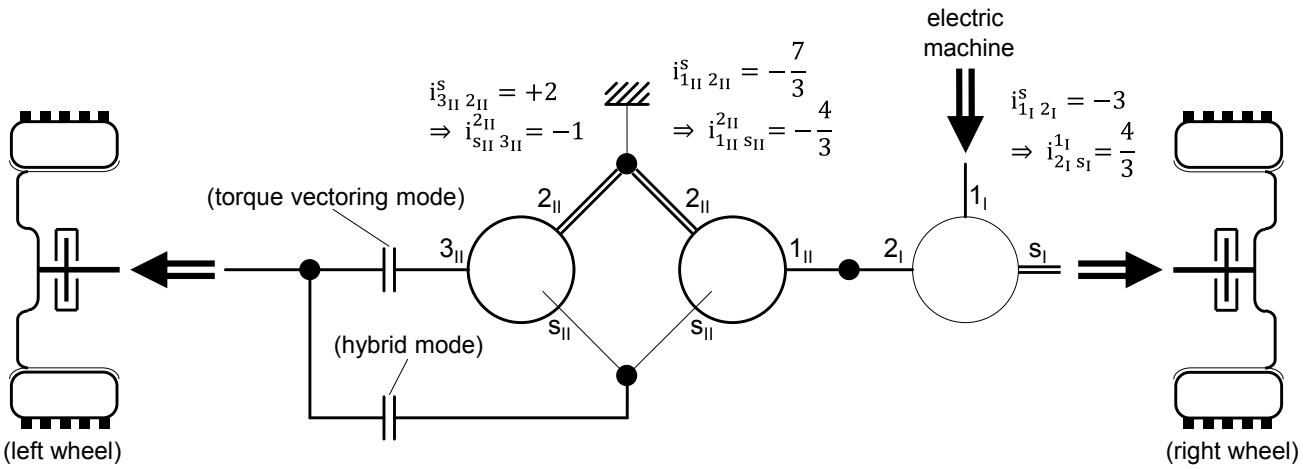

Figure 6-14: An equivalent kinematic configuration corresponding to Figure 6-13

The transmission ratios are chosen such that an overall transmission ratio of 8 is generated for the hybrid mode. Thus, the hybrid mode can be used for vehicle speeds up to about 120 km/h until the maximum electric machine speed reaches 8000 rpm. Switching to the torque vectoring mode, the electric machine is standing still if both wheels are running with equal speeds. Hence, the torque vectoring mode can be activated regardless of the vehicle speed (maximum vehicle speed ~ 250 km/h). The electric machine is assumed to deliver a maximum torque of 125 Nm and a maximum power of 30 kW.

Depending on the superimposing gear basic ratio, the reverse gear is supposed to function as a 2-speed transmission with definite ratios of ±4/3, which can be achieved by means of a 4-shaft CCPGT. Three different lever configurations are thinkable: alternating fixed shafts (**Figure 6-15**), alternating input shafts (**Figure 6-16**) or alternating output shafts (**Figure 6-17**). Each mode is considered for straight-ahead driving at its maximum vehicle speed in order to identify fast turning elements. For every lever configuration the node being fixed in hybrid mode fits best as carrier node. Considering the reference CCPGT shown in **Figure 5-25**, the synthesis produces a total of 8 determined and 39 underdetermined structures. Among these structures, the one featuring the best overall weighted efficiency of 98,60% is shown in **Figure 6-18**. In contrast, the reverse gear contained in **Figure 6-13** results in an overall weighted efficiency of only 95,69% for identical operating conditions but much simpler design.

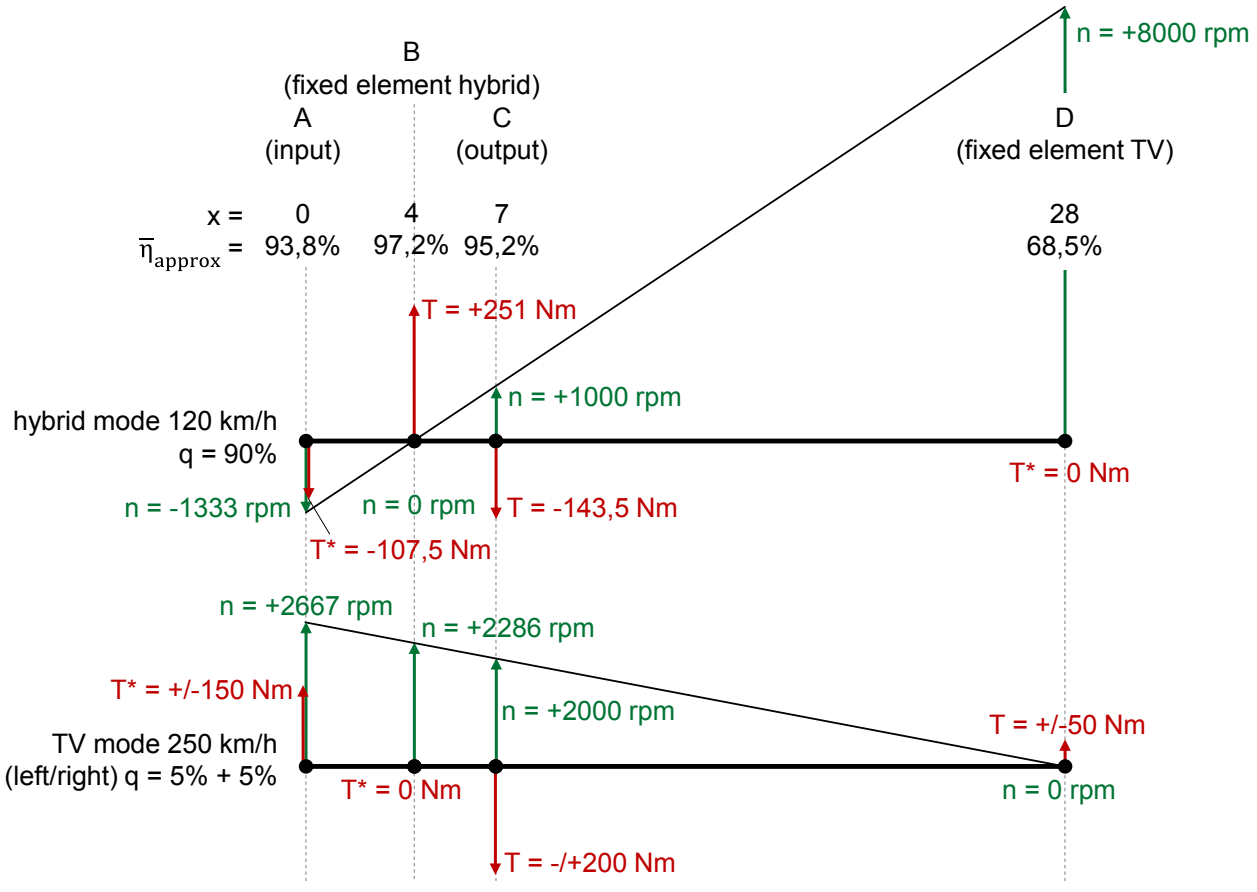

Figure 6-15: Operating conditions and lever definition for TVhybrid reverse gear with alternating fixed shafts

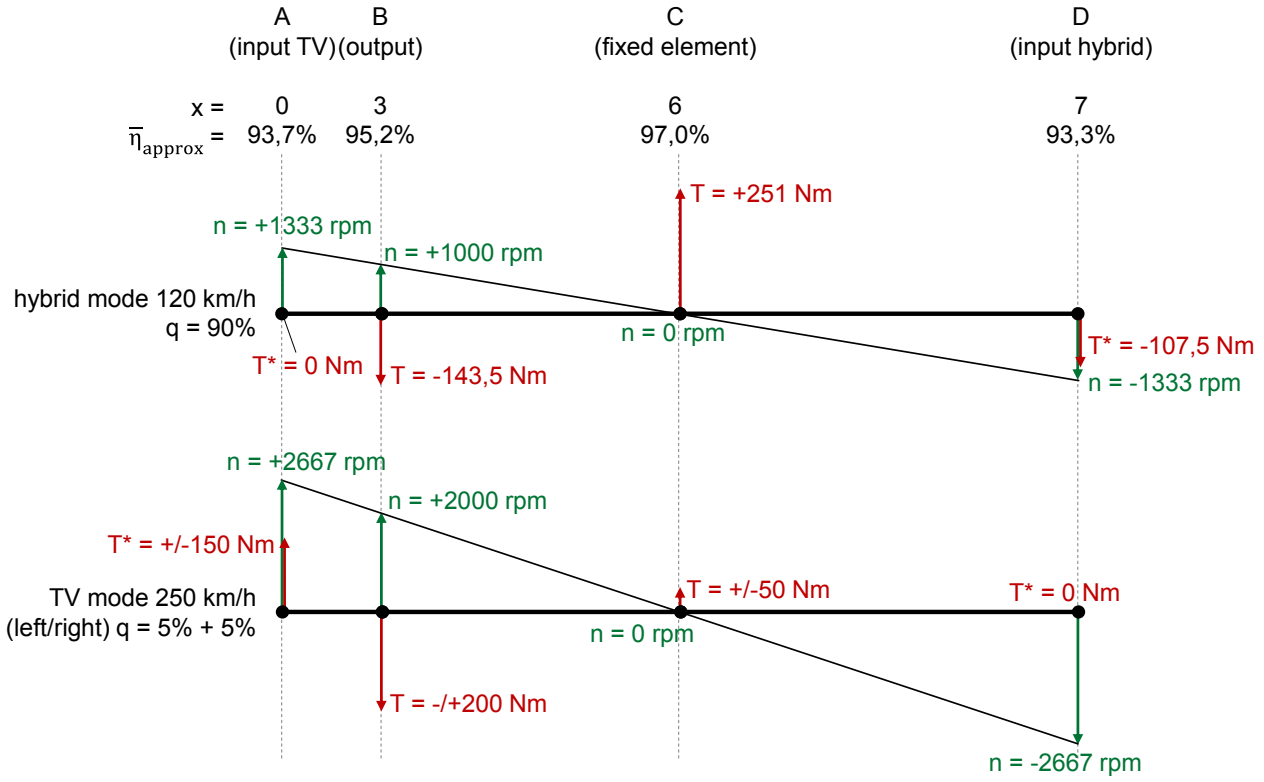

Figure 6-16: Operating conditions and lever definition for TVhybrid reverse gear with alternating input shafts

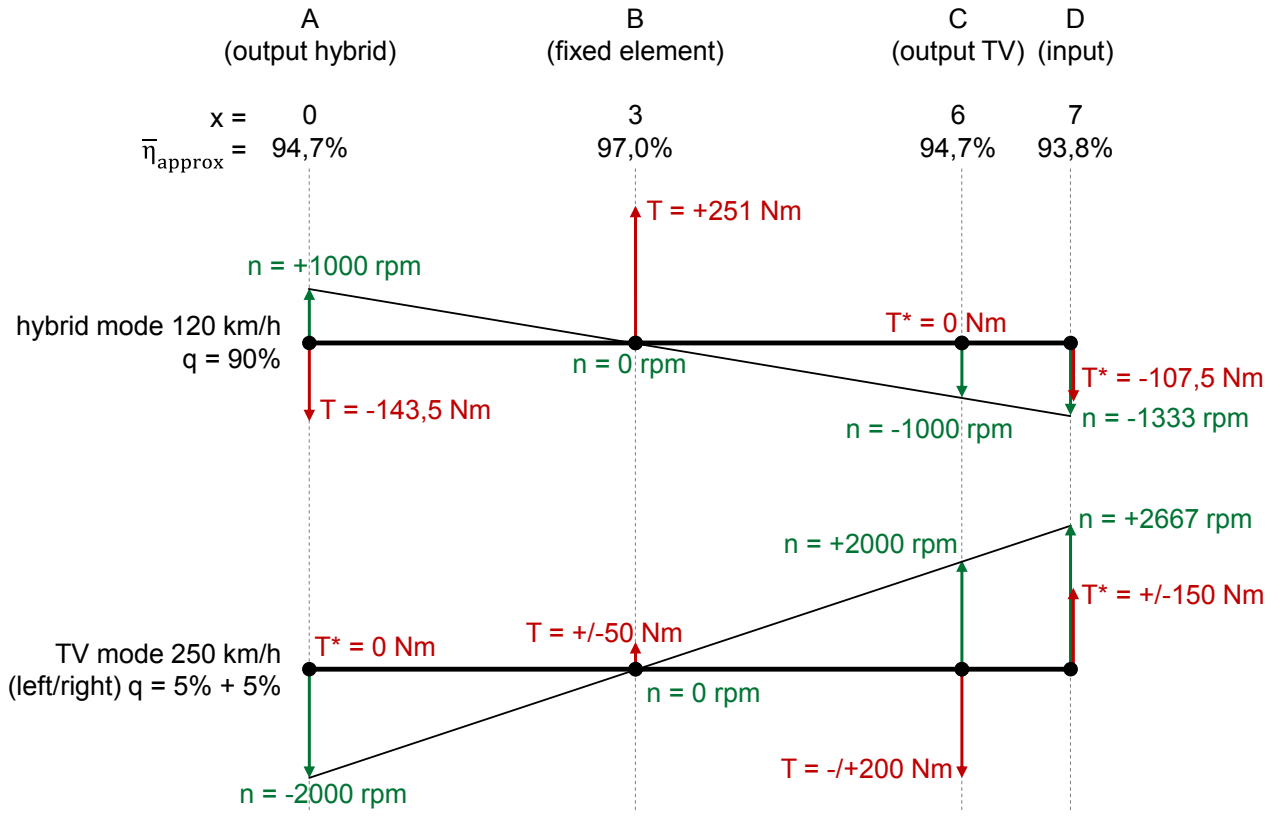

Figure 6-17: Operating conditions and lever definition for TVhybrid reverse gear with alternating output shafts

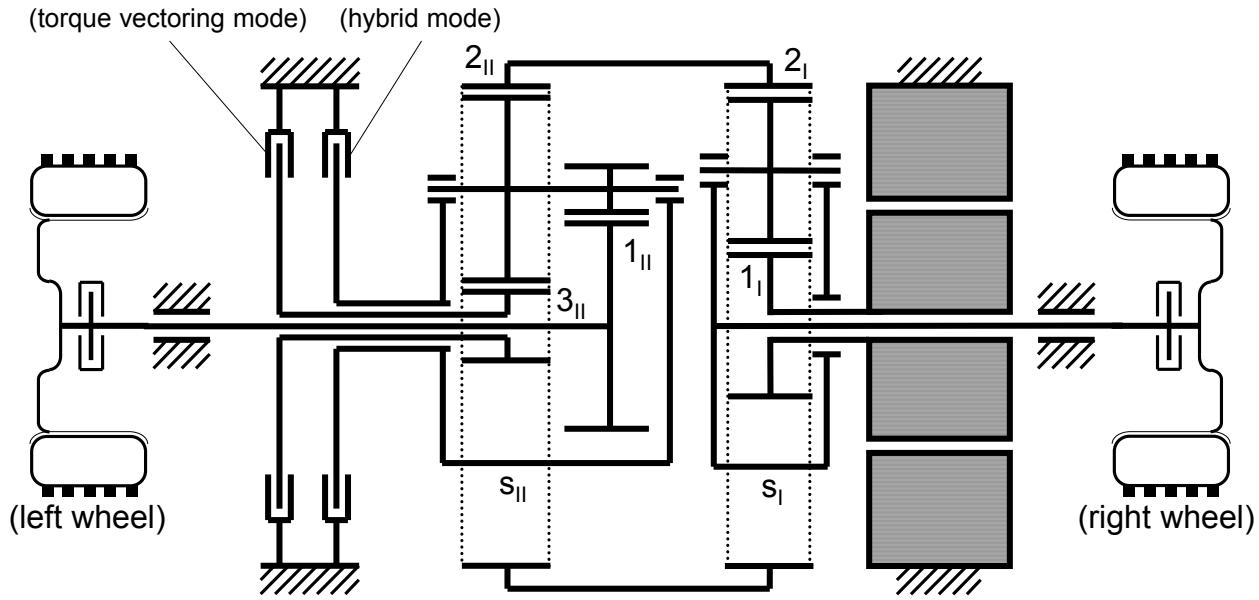

$$i^{s}_{3_{II}\,2_{II}} = -6 \quad i^{s}_{1_{II}\,2_{II}} = -\frac{3}{4} \quad i^{s}_{1_{I}\,2_{I}} = -3 \qquad \overline{\eta} = 98{,}60\ \%$$

$$\Rightarrow i^{3_{II}}_{1_{II}\,2_{II}} = +\frac{3}{4} \qquad \Rightarrow i^{1_{I}}_{2_{I}\,s_{I}} = \frac{4}{3}$$

Figure 6-18: Synthesis solution with the best overall efficiency for TVhybrid reverse gear

7 Conclusions and outlook

Complex-compound planetary gear transmissions can feature particular and significant advantages in comparison to standard planetary gears or spur gear trains. However, analysis and synthesis of complex-compound planetary gear transmissions are rather complex. Hence, the question of which structure matches an intended application the best and how this structure behaves in terms of its power loss performance is difficult to answer. This study is dedicated to the calculation of kinematics and statics for loss-free conditions and operating conditions with power losses as well as to the structure synthesis of complex-compound planetary gears during the early design phases.

Planetary gear transmissions can be represented by graphs. Graphs are abstract models containing the main information needed to facilitate required analyses. Relevant components in the gear train are mapped to nodes, the physical interrelationships such as gearing or bearing correlations are represented by edges connecting nodes. Once a graph is assembled, an automated derivation of kinematics and statics systems of equations is possible. The graph representation also helps understand the internal power flow. As meshing power can only be transferred via gear pair edges and all gear pair edges of a complex-compound planetary gear set form a tree, the flow of meshing power is without circuits and can be compared to network flow problems. Powerful mathematical algorithms like the simplex algorithm are suitable to solve these problems. For this purpose, the efficiency of single gearings is to be taken as a constant in order to maintain linearity. Further boundary conditions are needed depending on the system's degree of freedom.

It is shown that another well-established representation method known as 'Wolf symbols' can also be used for efficiency computations. By means of Wolf symbols, planetary gears are converted into substitution figures. Feasible substitution figures are either kinematically-equivalent or functionally-equivalent. Kinematically-equivalent substitution figures allow a correct determination of speeds and torques for loss-free operating conditions. Moreover, functionally-equivalent substitution figures feature correct torques in consideration of power losses. Substitution figures offer a clear view of the transmission structure while reducing the number of parameters to be determined. However, the Wolf symbol representation is not unique for complex-compound planetary gear sets. In general, multiple functionally-equivalent substation figures are available as a function of the given structure and the present operating conditions. With the aid of a classification of central gears to meshing power sources or sinks, the number of substitution figures to be analyzed is reduced significantly making the Wolf symbol method appropriate for complex-compound planetary gear transmission with up to five central shafts.

An efficiency approximation method is derived. Only limited information about the transmission is needed by taking into account a global basic train efficiency instead of individual values for each basic train. Without knowledge of the exact structure, the efficiency is approximated quite accurately with regard to a structure synthesis.

Planetary gear transmissions can feature very high as well as very low efficiency values. Self-locking is an extreme case occurring for special designs and operating conditions. As for complex-compound planetary gear transmissions, self-locking can also occur only apparently for unfavorably chosen boundary conditions. A procedure is proposed revealing if an operating condition and central shaft respectively is self-locking or not.

Planetary gear synthesis is a major problem in the face of the diversity of available structures and possible combinations. For this reason, synthesis methods being confined to specific designs and applications are prevalently suggested. Many developers build all solutions within a certain range by means of combinatorics and check their applicability subsequently. At this, useless solutions are also produced. A universal structure synthesis method for complex-compound planetary gear transmissions is proposed within this study. This method takes advantage of a lever analogy, which is detached from design aspects and used to define desired operating conditions. These operating conditions can be of any kind, even having multiple inputs and outputs. A simple and clear lever model is derived from these operating conditions. The lever is specified furthermore by means of the efficiency approximation method mentioned above in order to diminish the number of resulting solutions in advance. In addition, a reference transmission structure is to be defined indicating the most complicated structure to be considered. Hereby, the number of solutions is likewise decreased and impractical solutions are avoided. A systematic matching process combining the lever model and the reference transmission generates definite transmission structures. In sum, only feasible structures satisfying the desired operating conditions are created. The number of these structures is explicitly limited. Examples of use show that the synthesis method is well-suited for finding new transmission concepts containing complex-compound planetary gears.

The proposed synthesis method can be refined by adding further design steps. An automated dimensioning considering loads of the predefined operating conditions is feasible. A value benefit analysis considering weight, designed space, manufacturing costs and so on would help decrease the number of structures even more. The lever analogy being used is qualified for transmissions with a basic structure featuring a kinematic degree of freedom of two. For the synthesis of more complex structures a more general approach is required. Numerous examples of systems being composed with the aid of graph theory can be found. For this purpose, the requirements regarding a new transmission application are to be formulated as (linear) target functions and edge conditions limiting the solution space. Then, an efficient algorithm can be used to generate solutions without combinatorics. This author believes that this approach would present the most promising potential for an as universal as possible synthesis method.

8 References

[1] Standard gearing technology works

[**1_DUD94**] Dudley, D. W.: *Gear Handbook: The Design, Manufacture, and Application of Gears;* Cleveland: CRC Press (1994)

[**1_JEN91**] Jensen, P. W.: *Classical and Modern Mechanisms for Engineers and Inventors;* New York: Marcel Dekker (1991)

[**1_KLE05**] Klement, W.: *Fahrzeuggetriebe;* München: Hanser Verlag (2005)

[**1_LEC94**] Lechner, G.; Naunheimer, H.: *Fahrzeuggetriebe;* Berlin: Springer-Verlag (1994)

[**1_LIN96**] Linke, H.: *Stirnradverzahnung;* München: Hanser Verlag (1996)

[**1_LOO96**] Looman, J.: *Zahnradgetriebe: Grundlagen, Konstruktion, Anwendung in Fahrzeugen;* Berlin: Springer-Verlag (1996)

[**1_MER46**] Merrit, H. E.: *Gears: A Book of Reference for Engineers Concerned with the Design, Manufacture Application or Maintenance of Gear Drives*; 2nd edn; London: Sir Isaac Pitman & Sons; Ltd. (1946)

[**1_NIE03**] Niemann, G.; Winter, H.: *Maschinenelemente, Band 2: Getriebe allgemein, Zahnradgetriebe - Grundlagen, Stirnradgetriebe*; vol. 2; Berlin: Springer-Verlag (2003)

[**1_NIE04**] Niemann, G.; Winter, H.: *Maschinenelemente, Band 3: Schraubrad-, Kegelrad-, Schnecken-, Ketten-, Riemen-, Reibradgetriebe, Kupplungen, Bremsen, Freiläufe*; vol. 3; Berlin: Springer-Verlag (2004)

[**1_NIE05**] Niemann, G.; Winter, H.; Höhn, B.-R.: *Maschinenelemente, Band 1: Konstruktion und Berechnung von Verbindungen, Lagern, Wellen*; vol. 1; Berlin: Springer-Verlag (2005)

[**1_TUL62**] Tulpin, W. A.: *Gear Design;* London: The Machinery Publishing Co.; Ltd (1962)

[2] Standard planetary gearing works

[**2_BOG80**] Böge, A.: *Die Mechanik der Planetengetriebe;* Vieweg (1980)

[**2_KLE62**] Klein, H.: *Die Planetenrad Umlaufrädergetriebe;* München: Hanser Verlag (1962)

[**2_KUD77**] Kudrjawzew, W. N.; Kirdjaschew J. N.: *Planetengetriebe;* Leningrad (1977)

[**2_LEI87**] Leistner F.; Lörsch, G.; Wilhelm O.: *Umlaufrädergetriebe;* Berlin: VEB Verlag Technik (1987)

[**2_MUL01**] Müller, H. W.: *Die Umlaufgetriebe;* Berlin: Spinger-Verlag (2001)

[**2_PIC81**] Pickard, J.: *Planetengetriebe in der Praxis: Auslegung, Konstruktion, Fertigung, Anwendung, Betriebserfahrungen*; 2nd edn; Grafenau: Lexika-Verlag (1981)

[**2_POP49**] Poppinga, R.: *Stirnrad-Planetengetriebe;* Stuttgart: Franckh'sche Verlagshandlung (1949)

[**2_STR50**] Strauch, H.: *Die Umlaufrädergetriebe;* München: Hanser Verlag (1950)

[**2_STR70**] Strauch, H.: *Theorie und Praxis der Planetengetriebe;* Krausskopf (1970)

[**2_TER74**] Terplan, Z.: *Dimensionierungsfragen der Zahnrad-Planetengetriebe;* Budapest: Akademia Kiado (1974)

[**2_VOL90**] Volmer, J.: *Umlaufrädergetriebe;* Berlin: Verlag Technik (1990)

[**2_WOL58**] Wolf, A.: *Die Grundlagen der Umlaufgetriebe: Die Grundgesetze der Umlaufgetriebe;* Braunschweig: Vieweg & Sohn (1958)

[3] Power losses and efficiency of transmissions and components

[**3_AND80a**] Anderson, N. E.; Loewenthal, S. H. (Eds.): *Effect of geometry and operating conditions on spur gear system power loss;* ASME; Third International Power Transmissions and Gearing Conference; San Francisco, California (1980)

[**3_AND81**] Anderson, N. E.; Loewenthal, S. H. (Eds.): *Design of Spur Gear for Improved Efficiency;* ASME; Design Engineering Conference; Chicago (1981)

[**3_AND80b**] Anderson, N. E.; Loewenthal, S. H.: *Spur Gear Efficiency at Part and Full Load;* NASA Technical Memorandum (1980)

[**3_AND83**] Anderson, N. E.; Loewenthal, S. H.: *Comparison of spur gear efficiency prediction methods;* US Government Reports (1983)

[**3_BAR97**] Barnes, J. P.: *Non-Dimensional Characterization of Gear Geometry, Mesh Loss and Windage;* AGMA technical paper (1997)

[**3_BON89**] Boness, R. J. (Ed.): *Churning Losses of Discs and Gears Running Partially Submerged in Oil;* ASME; Fifth International Power Transmission and Gearing Conference; Chicago (1989)

[**3_BRA95**] Brändlein; Eschmann; Hasbargen; Weigand: *Die Wälzlagerpraxis: Handbuch für die Berechnung und Gestaltung von Lagerungen*, 3rd edn; Mainz: Vereinigte Fachverlage GmbH (1995)

[**3_BUT89**] Butsch, M.: *Hydraulische Verluste schnelllaufender Stirnradgetriebe;* Dissertation; Universität Stuttgart (1989)

[**3_CHA07**] Changenet, C.; Velex, P. (Eds.): *Housing influence on churning losses in geared transmissions;* International Design Engineering Technical Conferences & Computers and Information in Engineering Conference; Las Vegas (2007)

[**3_CHA06**] Changenet, C.; Velex, P.: *A Model for the Prediction of Churning Losses in Geared Transmissions - Preliminary Results;* Journal of Mechanical Design; 129 (1); pp. 128–133 (2006)

[**3_DAH94**] Dahlke, H.: *Handbuch Wälzlagertechnik: Bauarten, Gestaltung, Betrieb:* Vieweg & Sohn (1994)

[**3_DAW84**] Dawson, P. H. (Ed.): *Windage Loss in Larger High-Speed Gears*, Proceedings of the Institution of Mechanical Engineers (1984)

[**3_DAW88**] Dawson, P. H.: *High Speed Gear Windage;* GEC Review; 4 (3); pp. 51–59 (1988)

[**3_DIA04**] Diab, Y.; Ville, F.; Velex, P.: *Windage Losses in High Speed Gears - Preliminary Experimental and Theoretical Results;* Journal of Mechanical Design; 126; pp. 903–908 (2004)

[**3_DOL02**] Doleschel, A.: *Wirkungsgradberechnung von Zahnradgetrieben in Abhängigkeit vom Schmierstoff*; Dissertation; TU München (2002)

[**3_DUD71**] Duda, M.: *Der geometrische Verlustbeiwert und die Verlustunsymmetrie bei geradverzahnten Evolventen-Stirnrädern;* Forschung im Ingenieurwesen 37 (2) (1971)

[**3_EAS08**] Eastwick, C. N.; Johnson, G.: *Gear Windage: A Review;* Journal of Mechanical Design (130) (2008)

[**3_EIS66**] Eiselt, H.: *Beitrag zur experimentellen und rechnerischen Bestimmung der Freßtragfähigkeit von Zahnradgetrieben unter Berücksichtigung der Zahnflankenreibung*; Dissertation; TU Dresden (1966)

[**3_FAG99**] FAG: *Wälzlager: Kugellager, Rollenlager, Gehäuse, Zubehör*; 41st edn (1999)

[**3_FAG08**] FAG: *Wälzlager: Kugellager, Rollenlager, Nadellager, Laufrollen, Lager für Gewindetreiber, Spannlager, Gehäuseeinheiten, Lagergehäuse, Zubehör*; 1st edn: Schäffler Gruppe (2008)

[**3_FOR84**] Forschungsvereinigung Antriebstechnik (Ed.): *Wärmeabführung: Wärmeabführung bei Getrieben*; Forschungsvorhaben Nr. 69/I (1984)

[**3_FUN87**] Funck, G.: *Wärmeabführung: EDV-Programm zur Berechnung von Wärmehaushaltes von Zahnradgetrieben; Benutzeranleitung und Programmbeschreibung*; Forschungsvorhaben Nr. 69 I u. II; München (1987)

[**3_GAC68**] Gackstetter, G.: *Verlustarme Zahnräder: Einfluss von Kopfkürzung und Eingriffswinkel, Zähnezahl und Flankenrücknahme auf Zahnverlustleistung und Tragfähigkeit, Verschleiss und Geräusch bei schrägverzahnten Stirnrädern*; Dissertation; TU München (1968)

[**3_GRA99**] Gratz, M.: *Numerische Simulation der Strömung in schnellaufenden Zahnradgetrieben*; Dissertation; Universität Stuttgart (1999)

[**3_GRE90**] Greiner, J.: *Untersuchungen zur Schmierung und Kühlung einspritzgeschmierter Stirnradgetriebe*; Dissertation; Universität Stuttgart (1990)

[**3_HAR01**] Harris, T. A.: *Rolling Bearing Analysis*; 4th edn: John Wiley & Sons; Inc (2001)

[**3_HOH07**] Höhn, B.-R.; Michaelis, K.; Otto, H.-P. (Eds.): *Minimised gear lubrication by a minimum oil/air flow rate;* ASME; International Design Engineering Technical Conferences & Computers and Information in Engineering Conference; Las Vegas (2007)

[**3_ISO01a**] ISO 14179-1: *Gears - Thermal capacity - Part 1: Rating gear drives with thermal equilibrium at 95°C sump temperature* (2001)

[**3_ISO01b**] ISO 14179-2: *Gears - Thermal capacity - Part 2: Thermal load-carrying capacity* (2001)

[**3_JAU94a**] Jaufmann, C.: *Zur Tauchschmierung schnellaufender Fahrzeuggetriebe*; Dissertation; Universität Stuttgart (1994)

[**3_KAH07**] Kahraman, A.; Xu, H.: *Prediction of Mechanical Efficiency of Parallel-Axis Gear Pairs;* Journal of Mechanical Design (129) (2007)

[**3_KUR08**] Kurth, F.; Michaelis, K.; Stangl, M.: *FVA-EDV Programm: WTplus – Benutzeranleitung*; Forschungsvorhaben Nr. 69 IV; München (2008)

[**3_KUR09**] Höhn, B.-R.; Michaelis, K.; Kurth, F.: *Efficiency and Power Flow Analysis of Multi-Speed Transmissions*; Power Transmissions Conference; Kallithea, Greece (2009)

[**3_MAR09**] Marchesse, Y.; Changenet, C.; Ville, F.; Velex, P. (Eds.): *Investigations on CFD Simulation for Predicting Windage Power Losses in Spur Gears;* 3rd International Conference on Integrity, Reliability and Failure; Porto, Portugal (2009)

[**3_MAU94**] Maurer, J.: *Lastunabhängige Verzahnungsverluste schnellaufender Stirnradgetriebe;* Dissertation; Universität Stuttgart (1994)

[**3_MAU85**] Mauz, W.: *Hydraulische Verluste bei Tauch- und Einspritzschmierung von Zahnradgetrieben;* Forschungsvereinigung Antriebstechnik e.V. (1985)

[**3_MAU87**] Mauz, W.: *Hydraulische Verluste von Stirnradgetrieben bei Umlaufgeschwindigkeiten bis 60 m/s;* Dissertation; Universität Stuttgart (1987)

[**3_MIC88**] Michaelis, K.: *Die Integraltemperatur zur Beurteilung der Freßtragfähigkeit von Stirnradgetrieben*; Dissertation; TU München (1988)

[**3_MIH02**] Mihalidis, A.; Bakolas, V.; Panagiotidis, K.; Drivakos, N.: *Prediction of the Friction Coefficient of Spur Gear Pairs;* VDI-Berichte (1665); pp. 705–719 (2002)

[**3_MIZ89**] Mizutani, H.; Isikawa, Y.; Townsend, D. P. (Eds.): *Effects of Lubrication on the Performance of High Speed Spur Gears;* NASA Technical Memorandum; Fifth International Power Transmission and Gearing Conference; Chicago (1989)

[**3_NAR86**] Naruse, C.; Haizuka, S.; Nemoto, R.; Kurokawa, K.: *Studies on Frictional Loss, Temperature Rise and Limiting Load for Scoring of Spur Gears;* Bulletin of JSME (29); pp. 600–608 (1986)

[**3_OHL58**] Ohlendorf, A.: *Verlustleistung und Erwärmung von Stirnrädern*; Dissertation; TU München (1958)

[**3_OTT09**] Otto, H.-P.: *Flank Load Carrying Capacity and Power Loss Reduction by Minimised Lubrication*; Dissertation; TU München (2009)

[**3_PAL56**] Palmgren, A.: *Neuere Untersuchungen über Energieverluste in Wälzlagern;* Konstruktion 8 (11); pp. 467–468 (1956)

[**3_PAL59**] Palmgren, A.: *Ball and Roller Bearing Engineering*; 3rd edn; New York: John Wiley & Sons Inc. (1959)

[**3_PET07**] Petry-Johnson, T. T.; Chase, D. R.; Kahraman, A.; Anderson, N. E. (Eds.): *Experimental Investigation of Spur Gear Efficiency;* ASME; International Design Engineering Technical Conferences & Computers and Information in Engineering Conference; Las Vegas (2007)

[**3_ROS08**] Rosander, P.; Bednarek, G.; Seetharaman, S.; Kahraman, A.: *Entwicklung eines Wirkungsgradmodells für Schaltgetriebe;* ATZ; 110 (4); pp. 346–357 (2008)

[**3_SCH95**] Schlenk, L.: *Untersuchungen zur Fresstragfähigkeit von Großzahnrädern*; Dissertation; TU München (1995)

[**3_SEE09a**] Seetharaman, S.: *An Investigation of Load-Independent Power Losses of Geared Systems*; PhD thesis; Ohio State University; Columbus (2009)

[**3_SEE09b**] Seetharaman, S.; Kahraman, A.; Moorhead, M. D.; Petry-Johnson, T. T.: *Oil Churning Power Losses of a Gear Pair: Experiments and Model Validation;* Journal of Tribology (2009)

[**3_SKF94**] SKF: *Hauptkatalog: Das Wälzlager-Handbuch* (1994)

[**3_SKF04**] SKF: *Hauptkatalog: Das Wälzlager-Handbuch für Studenten* (2004)

[**3_STR05**] Strasser, D.: *Einfluss des Zahnflanken- und Zahnkopfspieles auf die Leerlaufverlustleistung von Zahnradgetrieben;* Dissertation; Ruhr-Universität Bochum (2005)

[**3_WAL82**] Walter, P.: *Anwendungsgrenzen für die Tauchschmierung von Zahnradgetrieben Plansch- und Quetschverluste bei Tauchschmierung;* Forschungsvereinigung Antriebstechnik e.V.; Forschungsvorhaben Nr. 44/I; Stuttgart (1982)

[**3_WIM06**] Wimmer, J. A.: *Lastverluste von Stirnradverzahnungen: Konstruktive Einflüsse, Wirkungsgradmaximierung, Tribologie;* Dissertation; TU München (2006)

[4] Structural analyses, power flow and efficiency of planetary gears

[**4_ARN96**] Arnaudow, K.: *Einfaches Verfahren zur Ermittlung des Übersetzungsverhältnisses zusammengesetzter Planetengetriebe;* VDI-Berichte (1230) (1996)

[**4_ARN04**] Arnaudow, K.; Karaivanov, D.: *Die Blindleistung in Planetengetrieben;* Proceedings of the Conference on Research and Development of Machine Elements and Systems IMRES'04; Kragujevac (16. i 2004)

[**4_ARN87**] Arnaudow, K.; Karaivanov, D.: *Zusammengesetzte Planetengetriebe: Zweisteggetriebe und ihre kinematische und Kraft-Analyse.* Intern. Symposium "Planetengetriebe '87"; Pernik (1987)

[**4_ARN01**] Arnaudow, K.; Karaivanov, D.: *Engineering analysis of the coupled two-carrier planetary gearing through the lever analogy.* Proceedings of the International Conference on Mechanical Transmissions; Chongqing, China (2001)

[**4_BOT69**] Böttcher, S.; Sierig, G.: *Selbsthemmung an Zahnradgetrieben;* Konstruktion 21 (11); pp. 421–427 (1969)

[**4_BOU88**] Bouche, B.: *Selbsthemmende Planetengetriebe;* VDI-Berichte (672); pp. 141–161 (1988)

[**4_BRA29**] Brandenberger, H.: *Wirkungsgrad und Aufbau einfacher und zusammengesetzter Umlaufgetriebe;* Maschinenbau Betrieb (Nr. 8 u. 9); pp. 249/253 u. 290/294 (1929)

[**4_BUC70**] Buchsbaum, F.; Freudenstein, F.: *Synthesis of Kinematic Structure of Geared Kinematic Chains and other Mechanisms;* Journal of Mechanisms (5); pp. 357–392 (1970)

[**4_CHE07**] Chen, C.; Angeles, J.: *Virtual-Power Flow and Mechanical Gear-Mesh Power Losses of Epicyclic Gear Trains;* Journal of Mechanical Design (129) (2007)

[**4_CHE08**] Chen, D.-Z.; Shieh, W.-B.; Yeh, Y.-C.: *Kinematic Characteristics and Classification of Geared Mechanisms Using the Concept of Kinematic Fractionation;* Journal of Mechanical Design (130) (2008)

[**4_DEL00**] del Castillo, J. M.: *Symbolic Computation of Planetary Gear Train Efficiency;* European Congress on Computational Methods in Applied Sciences and Engineering; Barcelona; Spain (11-14 September, 2000)

[**4_DEL02b**] del Castillo, J. M.: *The Analytical Expression of the Efficiency of Planetary Gear Trains;* Mechanism and Machine Theory (37); pp. 197–214 (2002)

[**4_DIA94a**] Diaconescu, D.; Duditza, F.: *Wirkungsgradberechnung von zwangläufigen Planetengerieben*; Teil 1: Entwicklung einer neuen Methode; Antriebstechnik 33 (10); pp. 70–74 (1994)

[**4_DIA94b**] Diaconescu, D.; Duditza, F.: *Wirkungsgradberechnung von zwangläufigen Planetengerieben*; Teil 2: Weitere Beispielrechnungen und Vorteile; Antriebstechnik 33 (11); pp. 61–63 (1994)

[**4_DUA01**] Duan, Q.; Yang, S.: *A study on power-flow and efficiency of 3k type planetary gear trains;* Proceedings of the International Conference on Mechanical Transmissions; Chongqing, China (2001)

[**4_FOR69**] Förster, H. J.: *Zur Berechnung des Wirkungsgrades von Planetengetrieben;* Konstruktion 21 (5); pp. 165–178 (1969)

[**4_FRE72**] Freudenstein, F.: *Kinematics and Statics of a Coupled Epicyclic Spur Gear Train;* Mechanism and Machine Theory (7); pp. 263–275 (1972)

[**4_GLO65**] Glover J. H.: *Efficiency and Speed-Ratio Formulas for Planetary Systems;* Product Engineering; (36) (19) (1965)

[**4_HAR60**] Hardy, H. W.: *Planetary Gearing: Design and Efficiecy:* The Machinery Publishing Co.; Ltd (1960)

[**4_HED88**] Hedman, A.: *Mechanical Transmission Systems: a General Computer-based Method of Analysis*; Dissertation; Göteborg, Sweden (1988)

[**4_HED93**] Hedman, A.: *Transmission analysis: automatic derivation of relationships;* Journal of Mechanical Design; 115; pp. 1031–1037 (1993)

[**4_HEL66**] Helfer, F.: *Ein einfaches Verfahren zur Untersuchung von Planetengetrieben;* Voith-Forschung und Konstruktion (14); pp. 11–16 (1966)

[**4_HEL67**] Helfer, F.: *Ein Analogieverfahren zur Untersuchung von Planetengetrieben;* ATZ; 69 (5); pp. 149–152 (1967)

[**4_HOC65**] Hock, J.: *Beitrag zur Ermittlung des Wirkungsgrades einfacher und gekoppelter Umlaufgetriebe;* VDI-Z. (Reihe 1, Nr. 3) (1965)

[**4_HSI96b**] Hsieh, L. C.; Tsai, L. W.: *Kinematic Analysis of Epicyclic-type Transmission Mechanisms Using the Concept of Fundamental Geared Entities;* Journal of Mechanical Design (118); pp. 294–299 (1996)

[**4_IKE09**] Ikejo, K.; Nagamura, K.; Yada, T.; Kagari, Y.: *Self-Locking of 2S-C Type Planetary Gear Train Composed of External Gears.* Proceedings of the ASME 2009 International Design Engineering Technical Conference & Computers

and Information in Engineering Conference; San Diego; California; USA (2009)

[**4_JAK60**] Jakobsson, B.: *Torque distribution, power flow and zero output conditions of epicyclic gear trains*; Report Nr. 10; Chalmers University of Technology; Gothenburg, Sweden (1960)

[**4_JAK66**] Jakobsson, B.: *Efficiency of epicyclic gears considering the influence of the number of teeth*; Report Nr. 27; Chalmers University of Technology; Gothenburg, Sweden (1966)

[**4_JAR67a**] Jarchow, F.: *Leistungsverzweigung im Getriebe;* VDI-Nachrichten (49) (1967)

[**4_JEN68**] Jensen, P. W.: *Kinematic space requirements and efficiency of coupled planetary gear systems;* ASME Paper (68-Mech-45) (1968)

[**4_JEN69**] Jensen, P. W.: *Raumbedarf und Wirkungsgrad zusammengesetzter Planetenrädergetriebe mit einstufigem Planetenrad;* Konstruktion 21 (5); pp. 178-184 (1969)

[**4_KET01**] Kettler, J.: *Planetengetriebe-Sumpftemperatur: Ölsumpftemperatur von Planetengetrieben*; AiF; Forschungsvorhaben Nr. 313 (2001)

[**4_KLE82**] Klein, B.: *Theoretische Grundlagen zum Auslegen von Wolfromkoppelgetrieben;* Maschinenmarkt (88) (1982)

[**4_KRA61**] Krause, R.: *Kritische Untersuchung der Wirkungsgrad-Berechnung einfacher Planetengetriebe;* Maschinenmarkt (90); pp. 25–28 (1961)

[**4_KRE43**] Kreines, M. A.: *Zur Berechnung der Wirkungsgrades von Zahnradgetrieben*; t. XLI; Nr. 8 (1943)

[**4_KRE47**] Kreines, M. A.: *Wirkungsgrad und Übersetzungsverhältnis von Zahnradgetrieben*; Tr. Sem. TMM; vol. 1; Moskau (1947)

[**4_KRE65**] Kreines, M. A.; Rosowski, M. S.: *Zahnradgetriebe;* Universität Moskau (1965)

[**4_KRJ55**] Krjukov A. D.: *Experimentelle Untersuchung der Wirkungsgrade von Umlaufgetrieben mit Innen- und Außeneingriff;* Vestnik maschinostroeniya (9); pp. 14–19 (1955)

[**4_KUT27**] Kutzbach, K.: *Mehrgliedrige Radgetriebe und ihre Gesetze*; Maschinenbau 6 (22); pp. 1080/1083 (1927)

[**4_LAR57**] Larsson, H.; Carlsson, B.; Jakobsson, B.: *Wirkungsgrad und Selbsthemmung einfacher Umlaufgetriebe;* Chalmers University of Technology; Göteborg, Sweden (1957)

[**4_LE11**] Le Xiang, C.; Zhang, Y. Y.; Liu, H.; Ciu, M.: *The Research on General Modeling Methods of the Complicated Transmission Based on Hypergraph Theory;* Applied Mechanics and Materials; 86; pp. 704–708 (2011)

[**4_LIU00**] Liu, C.-P.; Chen, D.-Z.: *On the Embedded Kinematic Fractionation of Epicyclic Gear Trains;* Journal of Mechanical Design; 122; pp. 479–483 (2000)

[**4_LIU04**] Liu, C.-P.; Chen, D.-Z.; Chang, Y.-T.: *Kinematic analysis of geared mechanisms using the concept of kinematic fractionation;* Mechanism and Machine Theory; 39; pp. 1207–1221 (2004)

[**4_LOO66**] Looman, J.: *Leistungsverzweigung - positiv oder negativ?;* VDI-Z.; 108 (6); pp. 221–226 (1966)

[**4_LOO88**] Looman, J.: *Planetengetriebe: Eine leistungsfähige Komponente der Antriebstechnik;* VDI-Berichte (672) (1988)

[**4_LOO99**] Looman, J.: *Berechnung reduzierter Planetengetriebe*; Zahnradgetriebe '99; VDI-Berichte (1460); pp. 23–36 (1999)

[**4_MAG74**] Mägi, M.: *On efficiencies of mechanical coplanar shaft power transmissions*; Dissertation; Chalmers University of Technology; Göteborg, Sweden (1974)

[**4_MAT98**] Mathis, R.: *Une theorie de l'invention et de l'optimisation des concepts de trains planétaires épicyloideaux;* Université Strasbourg (1998)

[**4_MAT99**] Mathis, R.; Remond, Y.: *A new approach to solving the inverse problem for compound gear trains;* Journal of Mechanical Design; 121 (1999)

[**4_MAT02**] Mathis, R.; Remond, Y.: *Solving the Kinematic Inverse Problem for Epicyclic Gear Trains;* VDI-Berichte (1665); pp. 479–489 (2002)

[**4_MAT09**] Mathis, R.; Remond, Y.: *Kinematic and dynamic simulation of epicyclic gear trains;* Mechanism and Machine Theory; 44; pp. 412–424 (2009)

[**4_MUL79**] Müller, H. W.: *Zur Einordnung der Umlaufgetriebe in die Systematik der Getriebe;* Konstruktion 31 (11); pp. 449–450 (1979)

[**4_MUL87**] Müller, H. W.: *Zum Mechanismus der Selbsthemmung;* Konstruktion 39 (3); pp. 93–100 (1987)

[**4_NEU62**] Neussel, P.: *Untersuchung von rückkehrenden Umlaufgetrieben mit und ohne Selbsthemmung unter besonderer Berücksichtigung von Koppelgetrieben;* Dissertation; TH Darmstadt (1962)

[**4_NIK53**] Nikitin A. A.: *Die Bestimmung des Wirkungsgrades von Differentialgetrieben nach der Methode des Kräfteaustausches;* Maschinenbautechnik; 2 (3); pp. 116–119 (1953)

[**4_NIK61**] Nikolaus, H.: *Graphische Darstellung der Drehzahl-, Momenten- und Leistungsverteilung in einfach rückkehrenden Planetengetrieben;* Maschinenmarkt (90); pp. 29–39 (1961)

[**4_OLS91**] Olson, D. G.; Erdman, A. G.; Riley, D. R.: *Topological Analysis of Single-Degree-of-Freedom Planetary Gear Trains;* Journal of Mechanical Design; 113; pp. 10–16 (1991)

[**4_ORN63**] Örnhagen, L.: *On self-locking transmissions*; Report Nr. 24; Chalmers University of Technology; Gothenburg, Sweden (1963)

[**4_PAS94**] Pasquier, M.; Foucher, P.: *An analytical method for the calculation of the efficiency of planetary gears;* AGMA technical paper (1994)

[**4_PEN93a**] Pennestri, E.; Freudenstein, F.: *A Systematic Approach to Power Flow and Static-Force Analysis in Epicyclic Spur-Gear Trains;* Journal of Mechanical Design (115); pp. 639–644 (1993)

[**4_PEN93b**] Pennestri, E.; Freudenstein, F.: *The Mechanical Efficiency of Epicyclic Gear Trains;* Journal of Mechanical Design (115); pp. 645–651 (1993)

[**4_PEN03a**] Pennestri, E.; Mantriota, G.: *Theoretical and Experimental Efficiency Analysis of Multi-Degrees-of-Freedom Epicyclic Gear Trains;* Multibody System Dynamics; 9; pp. 389–408 (2003)

[**4_PEN03b**] Pennestri, E.; Valentini, P. P.: *A Review of Formulas for the Mechanical Efficiency Analysis of Two Degrees-of-Freedom Epicyclic Gear Trains;* Journal of Mechanical Design; 125; pp. 602–608 (2003)

[**4_PIC75**] Pickard, J.: *Berechnungsgrundlagen einfacher und zusammengesetzter Planetengetriebe;* Antriebstechnik 14 (1); pp. 28–34 (1975)

[**4_POP51**] Poppinga, R.: *Der Wirkungsgrad der Planetengetriebe;* VDI-Z. (93/9); pp. 250–252 (1951)

[**4_PRA99**] Prahasto, T.; Andrews, G. C.: *Analysis of planetary gear trains using vector network theory;* Graphs & Mechanics; Gliwice, Poland (10-12 October; 1999)

[**4_PRI70**] Prins, G.; Aberkrom, P.: *Leistungsflüsse in Umlaufgetrieben;* Fördern und Heben; 20 (2); pp. 85–92 (1970)

[**4_RAD56**] Radzimowsky E.: *A Simplified Approach for Determining Powerlosses and Efficiency of Planetary Gear Devices;* Machine Design (28); pp. 101–110 (1956)

[**4_RAD59**] Radzimowsky E.: *How to find Efficiency and Power in Planetary Gear Drives;* Machine Design; 31 (vom 11. Juni); pp. 144–153 (1959)

[**4_ROE63**] Roessner W.: *Die Leistungsübertragung durch Umlaufrädergetriebe;* Das Industrieblatt; 63 (6); pp. 354–359 (1963)

[**4_SAN75**] Sanger, D. J.: *Matrix methods in the analysis and synthesis of coupled differentials and differential mechanisms*; University of Salford, U.K. (1975)

[**4_SCH85**] Schoo, A.: *Verzahnungsverlustleistung in Planetenradgetrieben;* Dissertation; Ruhr-Universität Bochum (1985)

[**4_SEE64**] Seeliger, K.: *Das Leistungsverhalten von Getriebekombinationen;* VDI-Z. (106 Nr. 6); pp. 206–211 (1964)

[**4_SIE68**] Sierig, G.: *Untersuchung von Wirkungsgrad, Verzahnungsverlust, Selbsthemmung und Lastverteilung am Umlaufgetriebe unter besonderer Berücksichtigung des Wolfromgetriebes;* Dissertation; TU Berlin (1968)

[**4_STA07**] Stangl, M.: *Methodik zur kinematischen und kinetischen Berechnung mehrwelliger Planeten-Koppelgetriebe*; Dissertation; TU München (2007)

[**4_STR60**] Strömblad, J.: *Beschleunigungsverlauf und Gleichgewichtsdrehzahlen einfacher Planetenegetriebe nebst Selbsthemmungsversuche;* Chalmers University of Technology; Göteborg, Sweden (1960)

[**4_TAL12**] Talbot, D.; Kahraman, A.; Singh, A.: *An Experimental Investigation of the Efficiency of Planetary Gear Sets;* Journal of Mechanical Design; 134 (2012)

[**4_TER75**] Terplan, Z.: *One of the comparison possibilities of epicyclic gears*; Technical University of Heavy Industry; Miskolc, Hungary (1975)

[**4_TIA97**] Tian, L.; Li-qiao, l.: *Matrix system for the analysis of planetary transmissions;* Journal of Mechanical Design; 119; pp. 333–337 (1997)

[**4_VDI78**] VDI Richtlinien: *VDI 2157, Planetengetriebe: Begriffe, Symbole, Berechnungsgrundlagen* (1978)

[**4_WIL41**] Willis, R.: *Principles of Mechanism;* John W. Parker (1841)

[**4_WOJ75**] Wojnarowski, J.; Lidwin, A.: *The Application of Signal Flow Graphs - the Kinematic Analysis of Planetary Gear Trains;* Mechanism and Machine Theory; 10; pp. 17–31 (1975)

[**4_WOL49**] Wolf, A.: *Die Umlaufgetriebe und ihre Berechnung;* VDI-Z. (91/22); pp. 597–603 (1949)

[**4_WOL12**] Wolfrom, U.: *Der Wirkungsgrad von Planetenrädergetrieben;* Werkstattstechnik; VI. (1912)

[**4_ZAJ39**] Zajonz, R.: *Die zeichnerische und rechnerische Untersuchung von Stirnrad-Umlaufgetrieben*, Dissertation; TH Dresden 1938; (ATZ (IV. Beiheft) (1939))

[5] Design and synthesis of planetary gears

[**5_ALT27a**] Altmann, F.: *Antrieb von Hebezeugen durch hochübersetzende, raumsparende Stirnradgetriebe;* Maschinenbau; 6 (22) (1927)

[**5_ALT27b**] Altmann, F.: *Die Baurformen gleichachsiger Stirnradumformer;* Maschinenbau; 6 (22) (1927)

[**5_ALT50**] Altmann: *Koppelgetriebe für gleichförmige Übersetzung;* VDI Sonderdruck (Bd. 92 Nr. 33); pp. 909–916 (1950)

[**5_AN01**] An, P.; Fang, L.: *Innovative Synthesis of Epicyclic Gear Trains Based on Kinematic Chain with Single Joints;* Machine Design and Research; 17 (1); pp. 44–46 (2001)

[**5_ARN03**] Arnaudow, K.; Karaivanov, D.: *Coupled Multi-Carrier Planetary Gears, Their Systematics, Properties and Abilities;* International Conference "Power Transmissions"; pp. 52–59 (2003)

[**5_ARN05a**] Arnaudow, K.; Karaivanov, D.: *Einfache Bestimmung: Systematik, Eigenschaften und Möglichkeiten von Zusammengesetzten Mehrsteg-Planetengetrieben;* Antriebstechnik (5); pp. 58–65 (2005)

[**5_ARN05b**] Arnaudow, K.; Karaivanov, D.: *Higher Compound Planetary Gears Trains;* VDI-Berichte (1904); pp. 327–344 (2005)

[**5_ARN10**] Arnaudow, K.; Karaivanov, D.: *The Complex Compound Multi-Carrier Planetary Gear Trains - a Simple Study;* VDI-Berichte (2108); pp. 673–684 (2010)

[**5_CHA65**] Chang, C. T.: *Multi-Stage Planetary Gear Trains;* Design News (June 23); pp. 138–145 (1965)

[**5_CHA94**] Chatterjee, G.; Tsai, L. W.: *Enumeration of Epicyclic-type Automatic Transmission Gear Trains;* SAE Technical Paper (941012) (1994)

[**5_CHA96**] Chatterjee, G.; Tsai, L. W.: *Computer-Aided Sketching of Epicyclic-Type Automatic Transmission Gear Trains;* Journal of Mechanical Design; 118; pp. 405–411 (1996)

[**5_CHE99**] Chen, D.-Z.; Liu, C.-P.: *A Hierarchical Decomposition Scheme for the Topological Synthesis of Articulated Gear Mechanisms;* Journal of Mechanical Design; 121; pp. 256–263 (1999)

[**5_CHR99**] Christ, M.: *Rechnersoftware für die integrierte Gestaltung und Berechnung von Planetengetrieben;* Dissertation; Ruhr-Universität Bochum (1999)

[**5_DEL02a**] del Castillo, J. M.: *Enumeration of 1-DOF Planetary Gear Train Graphs Based on Functional Constraints;* Journal of Mechanical Design (124); pp. 723–732 (2002)

[**5_DEL05**] del Castillo, J. M.; Salgado, D. R.: *A method for detecting degenerate structures in planetary gear trains;* Mechanism and Machine Theory; 40; pp. 948–962 (2005)

[**5_DOM01**] Domian, H.-J.: *Systematische Synthese von Getriebestrukturen der Vorgelegebauart*; Dissertation; TU München (2001)

[**5_DRE83**] Dreher, K.: *Rechnergestützte Optimierung von Planetenkoppelgetrieben;* Dissertation; TH Darmstadt (1983)

[**5_FRE71**] Freudenstein, F.: *An application of Boolean algebra to the motion of epicyclic drives;* ASME Journal of Engineering for Industry (93, Series B); pp. 176–182 (1971)

[**5_GAC65**] Gackstetter, G.: *Auswahl von Planetengetrieben zur Leistungsverzweigung für Regelgetriebe;* Konstruktion 17 (9) (1965)

[**5_GAU50**] Gaunitz, A.: *Planetengetriebe mit großer Übersetzung;* VDI-Z. (92/33); pp. 956 (1950)

[**5_GIB84**] Gibson, D.; Kramer, S.: *Symbolic Notation and Kinematic Equations of Motion of the Twenty-Two Basic Spur Planetary Gear Trains;* Journal of Me-

chanisms, Transmissions and Automation in Design (106); pp. 333–340 (1984)

[**5_GRU86**] Grüschow, G.: *Optimierung von Planetengetrieben;* Dissertation; TU Braunschweig (1986)

[**5_GUM06**] Gumpoltsberger, G.: *Systematische Synthese und Bewertung von mehrgängigen Planetengetrieben;* Dissertation; TU Chemnitz (2006)

[**5_HAI43**] Hain, K.: *Addier- und Subtrahiergetriebe;* Die Meßtechnik; 12 (10); pp. 207–210 (1943)

[**5_HSI96a**] Hsieh, H.-I.: *Enumeration and Selection of Clutching Sequences Associated with Epicyclic-Type Transmissions Mechanism;* University of Maryland (1996)

[**5_HSI99**] Hsieh, L. C.: *Method for the Kinematic Design of Multi-Speed Automatic Transmissions;* Proceedings of the Tenth World Congress on the Theory of Machine and Mechanism (5); pp. 2374–2379 (1999)

[**5_HSU94a**] Hsu, C.-H.: *Displacement isomorphism of planetary gear trains;* Mechanism and Machine Theory (29); pp. 513–523 (1994)

[**5_HSU94b**] Hsu, C.-H.; Lin, Y. L.: *Automatic identification of redundant links in planetary gear trains;* Mathematical and Computer Modeling (19); pp. 67–81 (1994)

[**5_HSU97**] Hsu, C.-H.; Wu, Y. C.: *Automatic Detection of Embedded Structure in Planetary Gear Trains;* Journal of Mechanical Design (119); pp. 315–318 (1997)

[**5_HSU99**] Hsu, C.-H.: *Systematic enumeration of epicyclic gear mechanisms for automotives;* JSME International Journal (42, series C); pp. 225–233 (1999)

[**5_HSU00**] Hsu, C.-H.: *Epicyclic Gear Mechanisms for Multi-Speed Automotive Automatic Transmissions;* Proc. Natl. Sci. Counc. ROC(A) (Vol. 25 Nr. 1); pp. 63–69 (2000)

[**5_HSU02**] Hsu, C.-H.: *An Analytic Methodology for the Kinematic Synthesis of Epicyclic Gear Mechanisms;* Journal of Mechanical Design (Vol. 124); pp. 574–576 (2002)

[**5_HSU09**] Hsu, C.-H.; Huang, R. H.: *Systematic Design of Six-Speed Automatic Transmissions With an Eight-Link Two-DOF Ravigneaux Gear Mechanism;* Journal of Mechanical Design; 131 (1) (2009)

[**5_HYL92**] Hylander, M.: *Synthese und Optimierung von Planetengetrieben (On Synthesis in Epicyclic Transmissions Design);* VDI-Berichte (1007); pp. 121-134 (Machine and Vehicle Design Report Nr. 1993-02-26) (1992)

[**5_JAR64**] Jarchow, F.: *Leistungsverzweigte Getriebe;* VDI-Z. (106/6); pp. 196/205 (1964)

[**5_JAR67b**] Jarchow, F.; Langenbeck, K.; Benthake, H.: *Planeten- und Überlagerungsgetriebe;* Antriebstechnik 6 (10); pp. 343-348 (1967)

[**5_KAH04**] Kahraman, A.: *A kinematics and power flow analysis methodology for automatic transmission planetary gear trains;* Journal of Mechanical Design (Vol. 126) (2004)

[**5_KAP11**] Kapelevich, A. L.; Ananiev, V. M. (Eds.): *Gear Transmission Density Maximization;* ASME; International Design Engineering Technical Conferences & Computers and Information in Engineering Conference; Washington, DC, USA (2011)

[**5_KUN95**] Kuntz, P.: *Rechnerunterstützte Synthese und Variantenkonstruktion von Planetengetrieben;* Dissertation; TU Braunschweig (1995)

[**5_LEV68**] Levai, Z.: *Structure and Analysis of planetary gear trains;* Journal of Mechanisms (3); pp. 131–148 (1968)

[**5_LI93**] Li, X.: *Systematische Synthese mehrgängiger Planetengetriebe;* Dissertation; RWTH Aachen (1993)

[**5_LI04**] Li, X.; Schmidt, L.: *Grammar-Based Designer Assistance Tool for Epicyclic Gear Trains;* Journal of Mechanical Design; 126 (5); pp. 895–901 (2004)

[**5_LOR67**] Lörsch, G.: *Umlaufrädergetriebe für hohe Übersetzungen;* Maschinenbautechnik (16); pp. 15–18 (1967)

[**5_MAN68**] Manolescu N. I.; Antonescu P.: *Structural synthesis of planetary mechanisms used in automatic transmissions;* ASME Paper (68-Mech-44) (1968)

[**5_MUL81**] Müller, H. W.; Dreher, K.: *Computer Aided Design and Optimisation of Compound Planetary Gears;* Symposium on Gearing & Power Transmissions; Tokyo (1981)

[**5_MUL09**] Mulzer, F.: *Systematik hoch übersetzender koaxialer Getriebe*; Dissertation; TU München (2009)

[**5_NIT83**] Nitescu, G.: *Analyse und Synthese der Planetengetriebe;* Antriebstechnik 22 (4); pp. 62–68 (1983)

[**5_NIT86**] Nitescu, G.; Heidemeyer, P.: *Mehrstufige Planetengetriebe für Kraftfahrzeuge;* Antriebstechnik 25 (3); pp. 67–73 (1986)

[**5_OTT68**] Ott, A.: *Zur systematischen Synthese mehrgängiger Umlaufräder-Schaltgetriebe;* ATZ (70 Nr. 1, 3, 4); pp. 1-6, 104-108, 131-134 (1968)

[**5_PIC76**] Pickard, J.; Köpf, P.: *Synthese von Mehrgang-Koppelgetrieben in Planetenbauweise;* Antriebstechnik 15 (6); pp. 330–333 (1976)

[**5_RAV85**] Ravisankar, R.: *Computerized Synthesis of the Structure of Geared Kinematic Chains;* Mechanism and Machine Theory; 20 (5); pp. 367–387 (1985)

[**5_ROS91**] Ross, C. S.; Route, W. D.: *A Method for Selecting Parallel Connected Planetary Gear Trains for Automotive Automatic Transmissions;* SAE Paper (911941) (1991)

[**5_SCH10**] Schneider, E.; Müller, J.; Leesch, M.; Resch, R.: *Synthese eines Achtgang-Automatikgetriebes für Hybridantriebe;* ATZ; 112 (12); pp. 908–915 (2010)

[**5_SCH71**] Schnetz, K.: *Optimierung zusammengesetzter Planetengetriebe;* VDI-Z. (Reihe 1, Nr. 30) (1971)

[**5_SCH76**] Schnetz, K.: *Reduzierte Planeten-Koppelgetriebe;* Dissertation; TH Darmstadt (1976)

[**5_SEE63**] Seeliger, K.: *Das Mehrsteg-Getriebe;* Desch Antriebstechnik (5); pp. 9–16 (1963)

[**5_SHI93**] Shin, J. K.; Krishnamurty, S.: *Standard code technique in the enumeration of epicyclic gear trains;* Mechanism and Machine Theory; 28 (3); pp. 347–355 (1993)

[**5_TSA87**] Tsai, L. W.: *An Application of the Linkage Characteristic Polynomial to the topological Synthesis of Epicyclic Gear Trains*, Transmissions and Automation in Design; ASME Journal of Mechanism (Vol. 109 Nr. 3); pp. 329–336 (1987)

[**5_TSA01**] Tsai, L. W.: *Mechanism Design - Enumeration of Kinematic Strutures According to Function;* Boca Raton: CRC Press (2001)

[**5_TSA88**] Tsai, L. W.; Maki, E. R.; Lui, T.; Kapil, N. G.: *The Categorization of Planetary Gear Trains for Automatic Transmissions According to Kinematic Topology;* SAE Technical Paper (885062) (1988)

[**5_TUP57**] Tuplin, W. A.: *Konstruktion von zusammengesetzten Planetengetrieben;* Machine Design (29); pp. 100 (1957)

[**5_WOH01**] Wohlenberg, P.: *Auslegung von Koppelgetrieben mit wiederholtem Durchlauf interaktiv erstellter Bearbeitungsstrategien;* VDI Fortschritt-Berichte; Band 337; Hannover (2001)

[**5_WOJ06**] Wojnarowski, J.; Kopec, J.; Zawislak, S.: *Gears and Graphs;* Journal of theoretical and applied mechanics (44); pp. 139–162 (2006)

[**5_ZAW07**] Zawislak, S.: *Artificial intelligence aided design of gears based on graph-theoretical models;* 12th IFToMM World Congress; Besancon, France (2007)

[6] Application examples of planetary gears

[**6_APR03**] Apró, F.: *The place of the Wolfrom (3K) planetary gear drive among connected drives;* International Conference "Power Transmissions '03" (2003)

[**6_ARN09**] Arnaudow, K.; Karaivanov, D.: *The Wolfrom Gear Train - A Case of Highest-Complexity Related Modifications of the Tooth Meshing.* Proceedings of the ASME 2009 International Design Engineering Technical Conference & Computers and Information in Engineering Conference; San Diego, California, USA (2009)

[**6_BRE06**] Breitfeld, C.; Müller, A.; Burger, A.; Mischnick, M.; Bauchrowitz, E.; Schröder, J.: *Die weiterentwickelten Sechsgang-Automatikgetriebe von BMW;* ATZ; 108; pp. 820–831 (2006)

[**6_CSO**] Csobán, A.; Kozma, M.: *Influence of the Power Flow and the Inner Gear Ratios on the Efficiency of Heavy-Duty Differential Planetary Gears*; Budapest University of Technilogy and Economics; Hungary

[**6_DAC01**] Dach, H.; Köpf, P.; Gruhle, W.-D.: *Pkw-Automatgetriebe;* Die Bibliothek der Technik (88) (2001)

[**6_FOR90**] Förster, H. J.: *Automatische Fahrzeuggetriebe;* Berlin: Springer-Verlag (1991)

[**6_GAC66**] Gackstetter, G.: *Leistungsverzweigung bei der stufenlosen Drehzahlregeglung mit Vierwellen-Planetengetrieben;* VDI-Z. (108/6); pp. 210–214 (1966)

[**6_GOT91**] Gott, P. G.: *Changing Gears: The development of the Automotive Transmission;* Society of Automotive Engineers, Inc.; Warrendale (1991)

[**6_GRE03**] Greiner, J.: *Siebengang-Automatikgetriebe von Mercedes-Benz;* ATZ; 105 (10); pp. 920–930 (2003)

[**6_GRE99**] Greiner, J.; Riedl, K.; Gansloser P.: *Stand und Zukunft der Pkw-Automatgetriebe mit Planetenradsätzen bei Mercedes-Benz*; Planetengetriebe; VDI-Berichte (1460); pp. 231–255 (1999)

[**6_HOH10**] Höhn, B.-R.; Wirth, C.; Kurth, F.: *Elektrischer Achsantrieb mit Torque-Vectoring-Funktion;* VDI Getriebekongress; Friedrichshafen (2010)

[**6_HOH11**] Höhn, B.-R.; Wirth, C.; Kurth, F.; Wiesbeck, F.: *Der elektromechanische Antriebsstrang mit Torque-Vectoring-Funktion des E-Fahrzeugs MUTE der TU München;* VDI Getriebekongress; Friedrichshafen (2011)

[**6_HUS86**] Hustede, J.: *PLANUREX-Planetengetriebe;* VDI-Z.; 128 (7); pp. 233–234 (1986)

[**6_JAR67c**] Jarchow, F.: *Überlagerungsgetriebe für stufenlose Drehzahl- und Drehmomentwandlung in Kraftfahrzeugen;* VDI-Berichte (105); pp. 69–78 (1967)

[**6_JAR87**] Jarchow, F.: *Stufenlos wirkendes hydrostatisches Lastschaltgetriebe für Kraftfahrzeuge;* VDI-Z.; pp. 38–46 (1987)

[**6_LEH84**] Lehmann, M.: *Bestimmung des Wirkungsgrades von Zykloiden-Kurvenscheiben-Getrieben;* Antriebstechnik 23 (12) (1984)

[**6_LEP90**] Lepelletier, P. A. G. EP 0.434.525 B1: *Transmission Automatique multivitesses pour véhicule automobile* (1990)

[**6_LLO10**] Lloyd, R. A.: *6-Ratio Planetary Shift Transmission Controlled by 4 External Brakes, and Design Method*, Getriebe in Fahrzeugen 2010; VDI-Berichte (2081); pp. 247–260 (2010)

[**6_LOO90**] Looman, J.: *Planetengetriebe, das Kernstück automatischer Fahrzeuggetriebe;* Maschinenbautechnik (39); pp. 451-455 M11 (1990)

[**6_NIT87**] Nitescu, G.: *Stufenlos verstellbares meachnisches Leistungsverzweigungsgetriebe für KFZ;* Konstruktion 39 (4); pp. 139–145 (1987)

[**6_PER57**] Perret, W.: *Wechselgetriebe mit Umlaufrädern;* Forsch. Ing.-Wes. (23/3); pp. 102–106 (1957)

[**6_PER58**] Perret, W.: *Aus Hohlradgetrieben aufgebaute Wechselgetriebe;* VDI-Z. (100/11); pp. 434/436 (1958)

[**6_PIC79**] Pickard, J.: *Planetengetriebe in automatischen Fahrzeuggetrieben;* Automobil-Industrie (4); pp. 41–49 (1979)

[**6_POL76**] Polak, J. C. Patent US 4.070.927: *Planetary Gearing Arrangement for a Transmission* (1976)

[**6_RAV38**] Ravigneaux, P. (11) CA 378043: *Speed-Changing Device* (1938)

[**6_RIE67**] Rieseler, H.: *Zur Entwicklung automatischer Fahrzeuggetriebe;* ATZ; 69 (5) (1967)

[**6_SCH97**] Schlecht, B.: *Planetengetriebe als Überlastsicherung in Sonderantrieben;* Antriebstechnik 36 (10); pp. 28–34 (1997)

[**6_SEE59**] Seeliger, K.: *Planetengetriebe in drehzahlveränderlichen Antrieben;* VDI-Z. (101/6); pp. 217/224 (1959)

[**6_SEH05**] Seherr-Thoss, H. C. G. v.: *The Construction of Planetary Gears and Advances Made by Wilhelm STOECKICHT;* VDI-Berichte (1904); pp. 373–383 (2005)

[**6_STA09**] Stahl, K.; Mulzer, F.: *Auslegung und Berechnung des Duo-Planetengetriebes;* Konstruktion pp. 54–58 (6 Juni, 2009)

[**6_TEN99a**] Tenberge, P.; Hofmann, W.: *Elektromechanisches Hybridgetriebe;* VDI-Berichte (1459); pp. 307–330 (1999)

[**6_TEN99b**] Tenberge, P.: *Doppelkupplungsgetriebe in Planetenradbauweise*, Getriebestrukturen zwischen Automatik- und Doppelkupplungsgetrieben; VDI-Berichte (2006); pp. 97–120 (1999)

[**6_WAG07**] Wagner, G.; Naunheimer, H.; Scherer, H.; Dick, A.: *Achtgang-Automatikgetriebe zur Reduzierung des Kraftstoffverbrauchs;* ATZ; 109 (6); pp. 512–519 (2007)

[7] Mathematical works and studies

[**7_AHU93**] Ahuja, K. R.; Magnanti, L. T.; Orlin, B. J.: *Network Flows: Theory, Algorithms, and Applications;* Upper Saddle River; New Jersey: Prentice Hall (1993)

[**7_AIG10**] Aigner, M.; Ziegler, G.: *Das Buch der Beweise*; 3rd edn; Berlin: Springer-Verlag (2010)

[**7_DEO01**] Deo, N.; Micikevicius, P.: *Prüfer-Like Codes for Labeled Trees*; University of Central Florida; USA (2001)

[**7_HAJ10**] Hajiaghaei-Keshteli, M.; Molla-Alizadeh-Zavardehi, S.; Tavakkoli-Moghaddam, R.: *Addressing a nonlinear fixed-charge transportation problem using a spanning tree-based genetic algorithm;* Computers & Industrial Engineering; 59; pp. 259–271 (2010)

[**7_PAU04**] Paulden, T.; Smith, K. D.: *The Rainbow Code: A Superior Genetic Algorithm Represantation for Layered Trees.* Proceedings of the 34th International Conference on Computers & Industrial Engineering (2004)

[**7_PRU18**] Prüfer, H.: *Neuer Beweis eines Satzes über Permutationen;* Archiv der Mathematik und Physik; 27; pp. 742–744 (1918)

[**7_SCH00**] Schrijver, A.: *Theory of Linear and Integer Programming*; 2nd edn; England: John Wiley & Sons; Inc (2000)

[**7_VAN97**] Vanderbei, J. R.: *Linear Programming: Foundations and Extensions*; 3rd edn; Boston/London/Dordrecht: Kluwer Academic Publishers (2000)

[**7_WAN97**] Wang, Y.-L.; Chen, H.-C.; Liu, W.-K.: *A Parallel Algorithm for Construction a Labeled Tree;* IEEE Transactions on Parallel and Distributed Systems; 8 (12); pp. 1236–1240 (1997)

[8] Supervised student research projects

In the context of this dissertation, the following student research projects were carried out at FZG from 2010 till 2012 by means of the technical and scientifical supervision of this author. Relevant results were achieved and partially integrated into this work. The author thanks all students for their commitment and assistance.

- Gwinner, P.: *Verifikation verschiedener Wirkungsgradberechnungsverfahren für reduzierte Planetekoppelgetriebe mit C++;* diploma thesis; FZG, TU München, submitted 10/2011; integrated into Chapter 4
- Hein, M.: *Konzeption und Entwurf eines leistungverzweigten Antriebsstrangs mit Planetengetrieben für hybride Anwendungen;* semester thesis; FZG, TU München, submitted 07/2011; integrated into Chapter 6
- Sing, A.: *Synthese von reduzierten Planetenkoppelgetrieben mit Hilfe der Balkenanalogiemethode;* diploma thesis; FZG, TU München, submitted 01/2012; integrated into Chapter 5
- Staab, T.: *Untersuchung der Selbsthemmungsfähigkeit einfacher und zusammengesetzter Planetengetriebe;* semester thesis; FZG, TU München, submitted 09/2011; integrated into Chapter 4

FZG Dissertations

No.	Author	Titel
1	PERRET, H.	Übertragung konstanter Leistung durch stufenlos mechanische Regeltriebe. TH Braunschweig 1935.
2	BELLMANN, H.	Beiträge zur Prüfung von Bremsbelägen. TH Braunschweig 1939.
3	HIERSIG, H.M.	Der Zusammenhang von Gestaltung und Beanspruchung bei Schneckengetrieben mit Evolventenverzahnung. TH Braunschweig 1943.
4	HELBIG, F.	Walzenfestigkeit und Grübchenbildung von Zahnrad- und Wälzlagerwerkstoffen. TH Braunschweig 1943.
5	ARF, D.	Pendelrollenlager mit symmetrischen und unsymmetrischen Rollen. TH Braunschweig 1944.
6	OESMANN, W.	Entwicklung einer Stahlsand-Schalt- und Regelkupplung. TH Braunschweig 1945.
7	RUBO, E.	Ermittlung der Achsfehler-Empfindlichkeit verschiedener Zylinder-Schneckengetriebe mit Hilfe des Einlauf-Abschliffvolumens. TH Braunschweig 1948.
8	GLAUBITZ, H.	Drehmomentmessungen zum Wendevorgang bei Raupenfahrwerken. TH Braunschweig 1948.
9	TALKE, H.	Beiträge zur hydrodynamischen Schmiertheorie des ebenen Gleitschuhes auf ebener Fläche. TH Braunschweig 1948.
10	CRAMER, H.	Über die Reibung und Schmierung feinmechanischer Geräte. TH Braunschweig 1949.
11	THOMAS, W.	Reibscheiben-Regelgetriebe mit Linienberührung. TH Braunschweig 1949.
12	MAUSHAKE, W.	Theoretische Untersuchung von Schneckengetrieben mit Globoidschnecke und Stirnrad. TH Braunschweig 1950.
13	KRAUPNER, K.W.	Das plastische Verhalten umlaufender Stahlrollen bei Punktberührung. TH Braunschweig 1951.
14	BANASCHEK, K.	Die Gleitreibung geschmierter Flächen kleiner Schmiegung. Einfluß von Werkstoffpaarung, Krümmung, Oberfläche und Schmierstoff. TH Braunschweig 1951.
15	HEYER, E.	Versuche mit Zylinderschneckentrieben. Einfluß von Zahnform, Modul, Durchmesser und Schmierstoff auf Verlustleistung und Tragfähigkeit. TH München 1952.
16	HENTSCHEL, G.	Der Hochleistungswälztrieb. Entwicklungsstand und Entwicklungsmöglichkeiten. TH München 1952.
17	WINTER, H.	Tragfähigste Evolventengeradverzahnung. TH München 1954.
18	ROY, A.K.	Spannungsoptische Untersuchung eines schrägverzahnten Stirnrades. TH München 1957.
19	RETTIG, H.	Dynamische Zahnkraft. TH München 1957.
20	OHLENDORF, H.	Verlustleistung und Erwärmung von Stirnrädern. TH München 1958.
21	UNTERBERGER, M.	Geräuschuntersuchungen an geradverzahnten Zahnrädern. TH München 1958.

No.	Author	Titel
22	LOOMAN, J.	Das Abrichten von profilierten Schleifscheiben zum Schleifen von schrägverzahnten Stirnrädern. TH München 1959.
23	JARCHOW, F.	Versuche an Stirnrad-Globoidschneckentrieben. TH München 1960.
24	POPOVIC, L.	Einfluß von Zahnform und Bearbeitung auf die Zahnfußfestigkeit. TH München 1960.
25	EHRLENSPIEL, K.	Die Festkörperreibung von geschmierten und ungeschmierten Metallpaarungen mit Linienberührung. TH München 1962.
26	PITTROFF, H.	Riffelbildung infolge Stillstandserschütterungen bei Wälzlagern. TH München 1962.
27	SCHREIBER, H.	Zur Auswertung von Lebensdauerversuchen an Wälzlagern. TH München 1962.
28	ROTH, K.	Untersuchungen über die Eignung der Evolventenzahnform für eine allgemein verwendbare feinwerktechnische Normverzahnung. TH München 1963.
29	NARUSE, Ch.	Verschleiß, Tragfähigkeit und Verlustleistung bei Schraubenradgetrieben. TH München 1964.
30	GARTNER, F.	Die Mischreibung bei Linienberührung. TH München 1964.
31	ASSMANN, H.	Vergleichende Untersuchung von Getriebeölen im FZG-Stirnrad- und Esso-Hypoidprüfstand. TH München.
32	REISTER, D.	Einseitiges Breitentragen bei Stirnrädern. TH München 1965.
33	KORRENN, H.	Gleitreibung in den Kontaktstellen zwischen den Wälzkörpern und den Laufbahnen der Ringe von Wälzlagern. TH München 1965.
34	HÖSEL, Th.	Geräuschuntersuchungen an schrägverzahnten Stirnrädern mit Evolventenverzahnung. TH München 1965.
35	LANGENBECK, K.	Die Verschleiß- und Freßgrenzlast der Hypoidgetriebe. TH München 1966.
36	MEMMEL, M.	Untersuchungen über die Tragfähigkeit und Gebrauchsdauer von Gelenklagern. TH München 1966.
37	BÖTSCH, H.	Der Einfluß der Oberflächenbearbeitung und -behandlung auf die Flankenfestigkeit von Stirnrädern aus Vergütungsstahl. TH München 1966.
38	LECHNER, G.	Die Freßlastgrenze bei Stirnrädern aus Stahl. TH München 1966.
39	LANGE, S.	Untersuchungen von Helicon- und Spiroidgetrieben mit abwickelbaren Schneckenflanken nach der hydrodynamischen und nach der Hertzschen Theorie. TH München 1967.
40	SCHWÄGERL, D.	Untersuchung von Helicon- und Spiroidgetrieben mit trapezförmigem Schneckenprofil nach der Hertzschen und nach der hydrodynamischen Theorie. TH München 1967.
41	MICHELS, K.	Schneckengetriebe mit Werkstoffpaarung Stahl/Grauguß. TH München 1968.
42	GACKSTETTER, G.	Verlustarme Verzahnung. TH München 1968.
43	GEUPEL, H.	Flüssigkeitsreibung bei Punktberührung. TH München 1969.
44	GREKOUSSIS, R.	Vergleichende Untersuchungen zur Freßtragfähigkeit von Hypoid- und Stirnrädern. TH München 1969.

No.	Author	Titel
45	BAETHGE, J.	Zahnfederhärte, Drehwegfehler und Geräusch bei Stirnrädern. TH München 1969.
46	SCHULZ, H.D.	Untersuchung über Tragfähigkeiten und Verlustleistung von Schneckengetrieben mit trapezförmigem Schneckenprofil und kegeliger Schnecke. TH München 1969.
47	STÖLZLE, K.	Leistungsübertragung in Planetengetrieben bei statischem und dynamischem Betrieb. Berechnung, Optimierung und Versuchsergebnisse. TH München 1970.
48	SEITZINGER, K.	Die Erwärmung einsatzgehärteter Zahnräder als Kennwert für ihre Freßtragfähigkeit. TU München 1971.
49	STÖSSEL, K.	Reibungszahlen unter elasto-hydrodynamischen Bedingungen. TU München 1971.
50	SCHMIDT, G.	Berechnung der Wälzpressung schrägverzahnter Stirnräder unter Berücksichtigung der Lastverteilung. TU München 1972.
51	HIRT, M.	Einfluß der Zahnfußausrundung auf Spannung und Festigkeit von Geradstirnrädern. TU München 1974.
52	WILKESMANN, H.	Berechnung von Schneckengetrieben mit unterschiedlichen Zahnprofilformen (Tragfähigkeits- und Verlustleistung für Hohlkreis-, Evolventen- und Geradlinienprofil). TU München 1974.
53	RICHTER, M.	Der Verzahnungswirkungsgrad und die Freßtragfähigkeit von Hypoid- und Schraubenradgetrieben - Versuchsergebnisse und Berechnungsmethoden. TU München 1976.
54	RÖSCH, H.	Untersuchungen zur Wälzfestigkeit von Rollen - Einfluß von Werkstoff, Wärmebehandlung und Schlupf. TU München 1976.
55	GAGGERMEIER, H.	Untersuchungen zur Reibkraftübertragung in Regel-Reibradgetrieben im Bereich elasto-hydrodynamischer Schmierung. TU München 1977.
56	KÄSER, W.	Beitrag zur Grübchenbildung an gehärteten Zahnrädern. Einfluß von Härtetiefe und Schmierstoff auf die Flankentragfähigkeit. TU München 1977.
57	KNABEL, W.	Geräusche und Schwingungen an Stirnradgetrieben. Untersuchungen geometrischer Einflüsse bei hohen Drehzahlen und Belastungen. TU München 1977.
58	WIRTH, X.	Über den Einfluß von Schleifkerben auf die Zahnfußtragfähigkeit und das Schädigungsverhalten oberflächengehärteter Zahnräder. TU München 1977.
59	HUBER, G.	Zylinderschneckengetriebe, ein Beitrag zur Berechnung von Grübchen- und Gleitverschleiß und Angaben zum Wirkungsgradverhalten aus Versuchen. TU München 1978.
60	BROSSMANN, U.	Über den Einfluß der Zahnfußausrundung und des Schrägungswinkels auf Beanspruchung und Festigkeit schrägverzahnter Stirnräder. TU München 1979.
61	PLEWE, H.-J.	Untersuchungen über den Abriebverschleiß von geschmierten, langsam laufenden Zahnrädern. TU München 1980.
62	FRESEN, G.	Untersuchungen über die Tragfähigkeit von Hypoid- und Kegelradgetrieben (Grübchen, Ridging, Rippling, Graufleckigkeit und Zahnbruch). TU München 1981.
63	OSTER, P.	Beanspruchung der Zahnflanken unter Bedingungen der Elastohydrodynamik. TU München 1982.

No.	Author	Titel
64	HORNUNG, K.	Zahnräder aus Bainitischem Gusseisen mit Kugelgraphit. TU München 1983.
65	WEISS, T.	Zum Festigkeits- und Verzugsverhalten von randschichtgehärteten Zahnrädern. TU München 1983.
66	VOJACEK, H.	Das Reibungsverhalten von Fluiden unter elastohydrodynamischen Bedingungen. Einfluß der chem. Struktur des Fluides, der Werkstoffe und der Makro- und Mikrogeometrie der Gleit/Wälzkörper. TU München 1984.
67	SCHÖNNENBECK, G.	Einfluß der Schmierstoffe auf die Zahnflankenermüdung (Graufleckigkeit und Grübchenbildung) hauptsächlich im Umfangsgeschwindigkeitsbereich 1...9 m/s. TU München 1984.
68	WIENER, H.	Untersuchung der Rollenkinematik im Axial-Pendelrollenlager. TU München 1984.
69	MATHIAK, D.	Untersuchungen über Flankentragfähigkeit, Zahnfußtragfähigkeit und Wirkungsgrad von Zylinderschneckengetrieben. TU München 1984.
70	STRASSER, H.	Einflüsse von Verzahnungsgeometrie, Werkstoff und Wärmebehandlung auf die Zahnfußtragfähigkeit. TU München 1984.
71	JOACHIM, F.-J.	Untersuchungen zur Grübchenbildung an vergüteten und normalisierten Zahnrädern (Einfluß von Werkstoffpaarung, Oberflächen- und Eigenspannungszustand). TU München 1984.
72	GERBER, H.	Innere dynamische Zusatzkräfte bei Stirnradgetrieben - Modellbildung, innere Anregung und Dämpfung. TU München 1984.
73	SIMON, M.	Messung von elasto-hydrodynamischen Parametern und ihre Auswirkung auf die Grübchentragfähigkeit vergüteter Scheiben und Zahnräder. TU München 1984.
74	SCHMIDT, W.	Untersuchungen zur Grübchen- und zur Zahnfußtragfähigkeit geradverzahnter evolventischer Innenstirnräder. TU München 1984.
75	FUNCK, G.	Wärmeabführung bei Getrieben unter quasistationären Betriebsbedingungen. TU München 1985.
76	PAUL, M.	Einfluß von Balligkeit und Lageabweichungen auf die Zahnfußbeanspruchung spiralverzahnter Kegelräder. TU München 1986.
77	HOPPE, F.	Das Abschalt- und Betriebsverhalten von mechanischen Sicherheitskupplungen. TU München 1986.
78	MICHAELIS, K.	Die Integraltemperatur zur Beurteilung der Freßtragfähigkeit von Stirnradgetrieben. TU München 1987.
79	WECH, L.	Untersuchungen zum Wirkungsgrad von Kegelrad- und Hypoidgetrieben. TU München 1987.
80	KNAUER, G.	Zur Grübchentragfähigkeit einsatzgehärteter Zahnräder - Einfluß von Werkstoff, Schmierstoff und Betriebstemperatur. TU München 1988.
81	PLACZEK, T.	Lastverteilung und Flankenkorrektur in gerad- und schrägverzahnten Stirnradstufen. TU München 1988.
82	PFLAUM, H.	Das Reibungsverhalten ölgeschmierter Kegelreibkupplungen in Synchronisationseinrichtungen von Kraftfahrzeug-Schaltgetrieben. TU München 1988.
83	BRINCK, P.	Zahnfußtragfähigkeit oberflächengehärteter Stirnräder bei Lastrichtungsumkehr. TU München 1989.
84		entfallen

No.	Author	Titel
85	NEUPERT, K.	Verschleißtragfähigkeit und Wirkungsgrad von Zylinder-Schneckengetrieben. TU München 1990.
86	PREXLER, F.	Einfluß der Wälzflächenrauheit auf die Grübchenbildung vergüteter Scheiben im EHD-Kontakt. TU München 1990.
87	SCHALLER, K.-V.	Betriebsfestigkeitsuntersuchungen zur Grübchenbildung an einsatzgehärteten Stirnradflanken. TU München 1990.
88	COLLENBERG, H.-F.	Untersuchungen zur Freßtragfähigkeit schnellaufender Stirnradgetriebe. TU München 1991.
89	MÜLLER, R.	Schwingungs- und Geräuschanregung bei Stirnradgetrieben. TU München 1991.
90	ANZINGER, M.	Werkstoff- und Fertigungseinflüsse auf die Zahnfußtragfähigkeit, insbesondere im hohen Zeitfestigkeitsgebiet. TU München 1991.
91	KAGERER, E.	Messung von elastohydrodynamischen Parametern im hochbelasteten Scheiben- und Zahnkontakt. TU München 1991.
92	HASLINGER, K.	Untersuchungen zur Grübchentragfähigkeit profilkorrigierter Zahnräder. TU München 1991.
93	VOLLHÜTER, F.	Einfluß der Achsversetzung auf die Grübchen- und Zahnfußtragfähigkeit von spiralverzahnten Kegelrädern. TU München 1992.
94	PINNEKAMP, B.	Das Schaltverhalten von PKW-Getriebesynchronisierungen. TU München 1992.
95	SCHUBERT, M.	Einfluß der Befestigungsart und Radkranzdicke auf die Zahntragfähigkeit von Innenstirnrädern. TU München 1993.
96	STEINGRÖVER, K.	Untersuchung zu Verschleiß, Verlustgrad und Fressen bei Zylinder-Schneckengetrieben. TU München 1993.
97	ELSTORPFF, M.-G.	Einflüsse auf die Grübchentragfähigkeit einsatzgehärteter Zahnräder bis in das höchste Zeitfestigkeitsgebiet. TU München 1993.
98	EMMERT, S.	Untersuchungen zur Zahnflankenermüdung (Graufleckigkeit, Grübchenbildung) schnellaufender Stirnradgetriebe. TU München 1994.
99	SUCHANDT, Th.	Betriebsfestigkeitsuntersuchungen zur Zahnfußtragfähigkeit einsatzgehärteter Zahnräder und zur Bruchfestigkeit vergüteter Laschenketten. TU München 1994.
100	HÄMMERL, B.	Lebensdauer- und Temperaturverhalten ölgekühlter Lamellenkupplungen bei Lastkollektivbeanspruchung. TU München 1994.
101	WEISS, R.	Einfluß der Ölalterung auf die Zahnflankentragfähigkeit. TU München 1994.
102	SCHLENK, L.	Untersuchungen zur Freßtragfähigkeit von Großzahnrädern. TU München 1995.
103	MANN, U.	Schmierfilmbildung in elastohydrodynamischen Kontakten, Einfluß verschiedener Grundöle und Viskositäts-Index-Verbesserer. TU München 1995.
104	RUDZEWSKI, S.	Systemtechnische Verknüpfung eingeführter Getriebeberechnungsprogramme. TU München 1995.
105	RANK, R.	Untersuchungen zur Lebensdauerprüfung von Synchronisierungen. TU München 1995.

No.	Author	Titel
106	EBERSPÄCHER, C.	Reihenfolgeeffekte bei der Grübchen-Betriebsfestigkeit einsatzgehärteter Zahnräder. TU München 1995.
107	RANK, B.	Untersuchungen zur Grübchenbildung bei Zylinder-Schneckengetrieben. TU München 1996.
108	SATTELBERGER, K.	Schwingungs- und Geräuschanregung bei ein- und mehrstufigen Stirnradgetrieben. TU München 1997.
109	HIRSCHMANN, V.	Tragfähigkeitsuntersuchungen an stufenlosen Umschlingungsgetrieben. TU München 1997.
110	THOMAS, J.	Flankentragfähigkeit und Laufverhalten von hartfeinbearbeiteten Kegelrädern. TU München 1998.
111	WIKIDAL, F.	Berechnung der Flankenpressung gerad- und schrägverzahnter Stirnräder für last- und fertigungsbedingte Abweichungen. TU München 1998.
112	PERPONCHER, V., CH.	Einflüsse von Reibflächentopographie und Beanspruchungen auf das Reibungs- und Verschleißverhalten von Synchronisierungen. TU München 1998.
113	SCHEDL, U.	Einfluß des Schmierstoffs auf die Grübchenlebensdauer einsatzgehärteter Zahnräder. TU München 1998.
114	VOLLMER, T.	Methodik zur Entwicklung einer Fahrstrategie für Fahrzeuge, ausgeführt am Beispiel des Autarken Hybrids. TU München 1998.
115	HEITMANN, A.	Entwicklung des i²-Getriebes für den Autarken Hybrid-Antriebsstrang. TU München 1998.
116	PFLEGER, F.	Schalt- und Lebensdauerverhalten von Lamellenkupplungen. TU München 1998.
117	KERSCHL, S.	Der Autarke Hybrid - Optimierung des Antriebsstrangs hinsichtlich Energieverbrauch und Bestimmung des Einsparpotentials,TU München 1998.
118	DÖBEREINER, R.	Tragfähigkeit von Hochverzahnungen geringer Schwingungsanregung,TU München 1998.
119	WEIGAND, U.	Werkstoff- und Wärmebehandlungseinflüsse auf die Zahnfußtragfähigkeit,TU München 1999.
120	SCHRADE, U.	Einfluß von Verzahnungsgeometrie und Betriebsbedingungen auf die Graufleckentragfähigkeit von Zahnradgetrieben,TU München 2000.
121	KÖLL, J.	Konstruktion des Getriebes für ein Pkw-Hybridantriebssystem,TU München 2000.
122	FÖRSTER, W.	Der Lastschaltvorgang beim stufenlosen i²-Getriebe des Autarken Hybrid-Antriebsstrangs,TU München 1999.
123	LANGE, N.	Hoch fresstragfähige Schneckengetriebe mit Rädern aus Sphaeroguß,TU München 2000.
124	LUTZ, M.	Methoden zur rechnerischen Ermittlung und Optimierung von Tragbildern an Schneckengetrieben,TU München 2000.
125	KOPATSCH, F.	Wirksamkeit von Viskositätsindex-Verbesserern im EHD-Zahnradkontakt,TU München 2000.
126	BAYERDÖRFER, I.	Einfluß von betriebsbedingten Schmierstoffveränderungen auf die Flankentragfähigkeit einsatzgehärteter Stirnräder,TU München 2000.
126e	DOMIAN, H.-J.	Systematische Synthese von Getriebestrukturen der Vorgelegebauart. TU München 2001.

No.	Author	Titel
127	TOBIE, T.	Zur Grübchen- und Zahnfußtragfähigkeit einsatzgehärteter Zahnräder,TU München 2001.
128	STAHL, K.	Grübchentragfähigkeit einsatzgehärteter Gerad- und Schrägverzahnungen unter besonderer Berücksichtigung der Pressungsverteilung,TU München 2001.
129	NEUMÜLLER, M.	Einfluß der Ölalterung auf Reibungs- und Verschleißverhalten von Synchronisierungen,TU München 2001.
130	MOSBACH, C.	Das Reibungs- und Reibschwing-Verhalten nasslaufender Lamellenkupplungen,TU München 2002.
131	DYLA, A.	Modell einer durchgängig rechnerbasierten Produktentwicklung,TU München 2002.
132	GRASWALD, C.	Reibung im elastohydrodynamischen Kontakt von Reibradgetrieben,TU München 2002.
133	GEISER, H..	Grundlagen zur Beurteilung des Schwingungsverhaltens von Stirnrädern,TU München 2002.
134	SCHINAGL, S.	Zahnfußtragfähigkeit schrägverzahnter Stirnräder unter Berücksichtigung der Lastverteilung,TU München 2002.
135	DOLESCHEL, A.	Wirkungsgradberechnung von Zahnradgetrieben in Abhängigkeit vom Schmierstoff,TU München 2003.
136	ANNAST, R.	Kegelrad-Flankenbruch, TU München 2003
137	SÜSSMUTH, J.-F.	Eignungsbeurteilung von Schmierstoffen für stufenlose Umschlingungsgetriebe, TU München 2003.
138	MATTEN, D.	Methode zur Entwicklung ingenieurwissenschaftlicher Berechnungsprogramme, TU München 2003.
139	GEIER, N.	Untersuchung des Reibungs- und Verschleißverhaltens nasslaufender Kupplungen in Abhängigkeit ihrer Reibflächentopographie, TU München 2003
140	HERTTER, T.	Rechnerischer Festigkeitsnachweis der Ermüdungstragfähigkeit vergüteter und einsatzgehärteter Stirnräder, TU München 2003.
141	KRIEGER, H.	Alterung von Schmierstoffen im Zahnradprüfstand und in Praxisgetrieben, TU München 2004.
142	STEUTZGER, M.	Einfluß der Baugröße auf die Zahnfußtragfähigkeit einsatzgehärteter Stirnräder, TU München 2004.
143	SCHMIDBAUER, T.	Aufbau und Erprobung des Autarken Hybrid-Antriebsstrangs im Versuchsfahrzeug. TU München 2004.
144	LIU, W.	Einfluss verschiedener Fertigungsverfahren auf die Graufleckentragfähigkeit von Zahnradgetrieben. TU München 2004.
145	FEHLING, R.	Höhere Tragfähigkeit bei Zahnradflanken durch eine nichtevolventische Profilmodifikation. TU München 2004.
146	GUTTENBERG, P.	Der autarke Hybrid am Prüfstand - Funktion, Kraftstoffverbrauch und energetische Analyse. TU München 2004.
147	WIMMER, T.	Einflüsse auf das Lastübernahmeverhalten von nasslaufenden Lamellenkupplungen. TU München 2004.

No.	Author	Titel
148	RADEV, T.	Einfluss des Schmierstoffes auf die Grübchentragfähigkeit einsatzgehärteter Zahnräder - Entwicklung des Praxisnahen Pittingtests. TU München 2005.
149	KRASTEV, I.	Optimierung des Lastschaltvorgangs im i²-Getriebe. TU München 2005.
150	HEILEMANN, J.	Tragfähigkeit und Wirkungsgrad bei unterschiedlichen Schnecken-Zahnflankenformen unter Berücksichtigung der Oberflächenhärte und Härtetiefe. TU München 2005.
151	HEIZENRÖTHER, M.	Das Stirnraddifferenzial mit Innenverzahnung im Vergleich zum Kegelraddifferenzial inklusive einer Sperrwertanalyse. TU München 2005.
152	WIMMER, A.	Lastverluste von Stirnradverzahnungen - Konstruktive Einflüsse, Wirkungsgradmaximierung, Tribologie. TU München 2006.
153	BRUCKMEIER, S.	Flankenbruch bei Stirnradgetrieben. TU München 2006.
154	HAUSER, C.	Einfluss der Ölalterung auf Reibcharakteristik und Reibschwingverhalten von Lamellenkupplungen. TU München 2007.
155	GROSSL, A.	Einfluss von PVD-Beschichtungen auf die Flanken- und Fußtragfähigkeit einsatzgehärteter Stirnräder. TU München 2007.
156	STEINBERGER, G.	Optimale Grübchentragfähigkeit von Schrägverzahnungen. TU München 2007.
157	JAROS, M.	Integration des STEP-Produktmodells in den Getriebeentwicklungsprozess. TU München 2007.
158	RADEV, S.	Einfluss von Flankenkorrekturen auf das Anregungsverhalten gerad- und schrägverzahnter Stirnradpaarungen. TU München 2007.
159	BRAYKOFF, C.	Tragfähigkeit kleinmoduliger Zahnräder. TU München 2007.
160	STANGL, M.	Methodik zur kinematischen und kinetischen Berechnung mehrwelliger Planeten-Koppelgetriebe. TU München 2007.
161	STENICO, A.	Werkstoffmechanische Untersuchungen zur Zahnfußtragfähigkeit einsatzgehärteter Zahnräder. TU München 2007.
162	SCHWIENBACHER, S.	Einfluss von Schleifbrand auf die Flankentragfähigkeit einsatzgehärteter Zahnräder. TU München 2008.
163	WINKLER, J.	Tribologischer Schichtaufbau bei Synchronisierungen und sein Einfluss auf Reibung und Verschleiß. TU München 2008.
164	WIRTH, C.	Zur Tragfähigkeit von Kegelrad- und Hypoidgetrieben. TU München 2008.
165	KREIL, O.	Einfluss der Oberflächenstruktur auf Druckverteilung und Schmierfilmdicke im EHD-Kontakt. TU München 2009.
166	OTTO, H.-P.	Flank load carrying capacity and power loss reduction by minimised lubrication. TU München 2009.
167	OTTO, M.	Lastverteilung und Zahnradtragfähigkeit von schrägverzahnten Stirnrädern. TU München 2009.
168	TOMIC, D.	Zum Verschleiß von Kegelreibkupplungen - Einflüsse von Belastung und Schmierstoff auf Reibschichteigenschaften. TU München 2009.
169	WEISEL, C.	Schneckengetriebe mit lokal begrenztem Tragbild. TU München 2009.
170	WEITL, R.	Zur Tragfähigkeitsberechnung von Wälzlagern und Stirnrädern. TU München 2010.

No.	Author	Titel
171	MULZER, F.	Systematik hochübersetzender koaxialer Getriebe. TU München 2010.
172	SCHUDY, J.	Untersuchungen zur Flankentragfähigkeit von Außen- und Innenverzahnungen. TU München 2010.
173	BRETL, N.	Einflüsse auf die Zahnfußtragfähigkeit einsatzgehärteter Zahnräder im Bereich hoher Lastspielzahlen. TU München 2010.
174	GRIGGEL, T.	Einfluss der Fertigungsqualität auf die Schwingungsanregung von Stirnrädern. TU München 2010.
175	LAYHER, M.	Einfluss der Schmierstoffadditivierung auf das Reibungsverhalten nasslaufender Reibschaltelemente. TU München 2011.
176	HOCHMANN, M.	Zahnradtragfähigkeit bei Schmierung mit Getriebefließfetten. TU München 2011.
177e	DETZEL, J.	Tribologische Untersuchungen an Achsgetrieben zur Verbesserung des Wirkungsgrads. TU München 2011.
178	ZIEGLER, A.	Zur verkürzten Systemlebensdauerprüfung von Zahnradgetrieben. TU München 2011.
179	THOMA, F.	Lastübertragung im verformten System Lager-Welle-Zahnrad. TU München 2012.
180	FRÜHE, T.	Berechnung und Minimierung der Zahnfußspannung von Standard- und LowLos-Verzahnungen. TU München 2012.
181	WITZIG, J.	Flankenbruch - Eine Grenze der Zahnradtragfähigkeit in der Werkstofftiefe. TU München 2012.
182	KLEIN, M.	Zur Fresstragfähigkeit von Kegelrad- und Hypoidgetrieben. TU München 2012.
183	KURTH, F.	Efficiency Determination and Synthesis of Complex-Compound Planetary Gear Transmissions. TU München 2012.
184	WOHLLEBER, F.	Thermischer Haushalt nasslaufender Lamellenkupplungen. TU München 2012.